Aggregation and conformation of alpha-synuclein: effects of ligand binding and phosphomimetics

PASKINS, Aimee Rebecca

Aggregation and Conformation of Alpha-Synuclein: Effects of Ligand Binding and Phosphomimetics

Aimee Rebecca Paskins

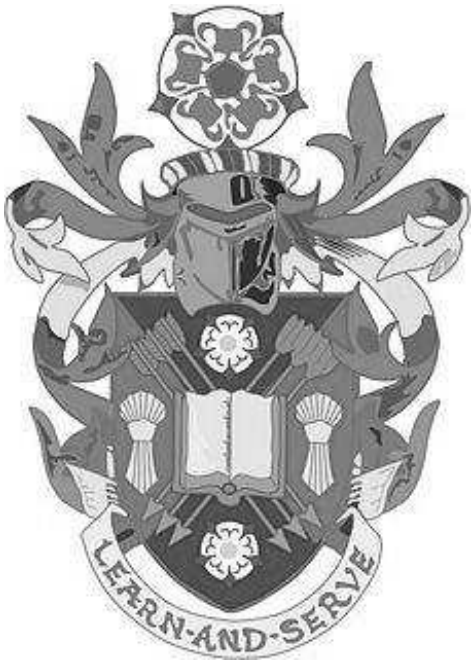

A thesis submitted in partial fulfilment of the requirements of Sheffield Hallam University for the Degree of Doctor of Philosophy in collaboration with The University of Leeds

Faculty of Health and Wellbeing

September 2017

Acknowledgements

First and foremost, I would like to extend my gratitude to Drs David Smith, Caroline Dalton and Catherine Duckett for supervising my PhD, and allowing me to work with and learn from them for the past four years. I would also like to thank Professor Nicola Woodroofe for the opportunity to gain my PhD at her wonderful Institution, and I would like to thank Professors Tom Smith and Christine Le Maitre, for their continued support and guidance throughout this process.

I would also like to thank the other PhD students in my research group and throughout the research centre, with particular thanks to Jodi Brookes, Nicola Wright, Karl Norris and Mootaz Salman. I couldn't have done it without you guys. Thanks for all the encouragement, laughs, nights out, and most of all the support when it was needed most. You're all awesome and I look forward to reminiscing about our PhD days for years to come.

I would also like to thank my mum Susan, dad Andy, brother Adam and my niece Ava for your continued love, support, guidance, and help with every aspect of my journey through this endeavour. Thanks for helping me become the scientist I always wanted to be!

Luke, I cannot thank you enough for everything you have done for me during this process. Thank you for all the encouraging words, cooking, computer help, and making me take time off when I really needed to. Your continued support, love

and understanding has kept me afloat through the hardest challenge of my life, so thank you so much with all my heart.

I would also like to thank all my friends for all the conversations, encouragement, beers, coming to my public engagement talks and most of all making me forget my worries occasionally. John Duffy, Katy Bakx and Louise Briggs, you've been through it with me the whole way, thank you so much for everything. I look forward to spending more time with you now!

Thank you so much everyone, it has been a long, difficult, but mostly exciting and rewarding journey, thank you all for accompanying me.

Abstract

Parkinson's disease (PD) affects 1 in 500 of the UK population. A critical step in disease aetiology is the formation of Lewy bodies (LBs), deposits of aggregated alpha-synuclein (αsyn) as amyloid inclusions, within surviving neurons. It is well established that αsyn within LBs has undergone a variety of post-translational modifications, including S129 phosphorylation, and LBs are known to be rich in metals such as copper. It has however, yet to be established how phosphorylation of αsyn and metal ions influence in the pathology of PD, and if the formation of LBs can be prevented by the use of small molecule inhibitors. Electrospray ionisation-ion mobility spectrometry- mass spectrometry (ESI-IMS-MS) was used to investigate the conformational changes to compact states of αsyn known to be linked to amyloid formation, for WT and two αsyn mutants mimicking phosphorylation at S87 and S129, in the presence of copper, and their aggregation was monitored by thioflavin-T assays. Results demonstrate that the conformational state of αsyn can be modulated by interactions with copper, causing an increase in the compact state, leading to an increased rate of aggregation. S129D αsyn showed the highest affinity for copper, and the fastest aggregation rates overall. SH-SY5Y cell culture models were used to investigate intracellular aggregation and phosphorylation state upon copper exposure. Increased copper concentration correlated with increased formation of unmodified and phosphorylated intracellular aggregates, an increase in apoptosis, and decreased cell viability. ESI-IMS-MS demonstrated curcumin and its derivatives were able to disrupt amyloid assembly, via prevention of autofragmentation and dissociation of low-order oligomers, thus preventing the aggregation of αsyn. In SH-SY5Y model used however, curcumins were unable to prevent the metal-induced intracellular aggregation of αsyn. Together, results support the hypothesis that phosphorylation has a key role in PD progression, and demonstrated that modified curcumins may be a potential therapeutic for PD.

Abbreviations

2 – Dimer

3 – Trimer

3D – Three Dimentional

4 - Tetramer

α-syn – Alpha-Synuclein

ε_0 – Empirical Permittivity of Vacuum

μM – Micromolar

Ω - Collisional Cross Section

Ω* – Reduced Collisional Cross Section

γ – Surface Tension

A – Correction Factor; Electric Field

Aβ – Amyloid Beta

AA – Ammonium Acetate

aa – Amino Acid

AD – Alzheimer's Disease

AFM – Atomic Force Microscopy

AR – Autosomal Recessive

ASD – Autosomal Dominant

ASR – Autosomal Recessive

ATD – Arrival Time Distribution

B – Correction Factor; Non-Linear Triwave Effects

CID – Collision Induced Association

CSD – Charge State Distribution

CSI – Charge State Ion

DAPI – 4,6-diamidine-2-phenylinodole dihydrochloride

DC – Direct Current

DLB – Dementia with Lewy Bodies

DMEM – Dubecco's Modified Eagle Media

DMSO – Dimethyl Sulfoxide

dt – Drift Time

dt_c – Corrected Drift Time

e – Charge of Electron

EDTA – Ethylenediaminetetra-acetic Acid

EGCG – Catechin Epillogallocatechin Gallate

EM – Electron Microscopy

ESI-IMS-MS – Electrospray Ionisation - Ion Mobility Spectrometry – Mass Spectrometry

ESI-MS – Electrospray Ionisation – Mass Spectrometry

FCS – Foetal Calf Serum

hrs - Hours

IAPP – Islet Amyloid Precursor Protein

IDP – Intrinsically Disordered Protein

IPTG – Isopropyl Ŧ-D-1-thiogalactopyranoside

K – Ion Mobility Constant

K_0 – Reduced Mobility

K_b – Boltzmann Constant

kDa - Kilodalton

L – Length

LB – Lewy Body

LuB – Luria Broth

LC-MS – Liquid Chromatography – Mass Spectrometry

L-DOPA - L-3,4-dihydroxyphenylalanine

m – Mass of Buffer Gas

M – Molar

M - Mass of Ion

mins – Minutes

mL/mls – Millileters

mM – Millimolar

ms – Millisecond

MSA – Multiple System Atrophy

MTT – 3-(4,5-dimethylthiaziazol-2-yl)-2,5-diphenyl-2H-tetrazolium Bromide

MW – Molecular Weight

m/z – Mass to Charge Ratio

N – Number Density of Buffer Gas

Nm – Nitrogen Mass

NAC – Non-Aβ Component

nESI-IMS-MS – Nano Electrospray Ionisation – Ion Mobility Spectrometry – Mass Spectrometry

NMR – Nuclear Magnetic Resonance

p – Buffer Gas Pressure

PBS – Phosphate Buffered Saline

PD – Parkinson's Disease

pm – Protein Mass

PMSF – Phenylmethylsulfonyl Fluoride

Q-TOF – Quadrupole Time-of-Flight

R – Radius of Droplet

r – reduced mass

RF – Radio Frequency

ROS – Reactive Oxygen Species

s - seconds

SD – Standard Deviation

SDS – Sodium Dodecyl Sulfate

SE – Size Exclusion

SEC – Size Exclusion Chromatography

SNPC – Substantia Nigra Pars Compacta

t – Time

TBS – Tris Buffered Saline

t_D – Drift Time

TEMED - tetrmethylethylendiamine

ThT – Thioflavin-T

v – Velocity

v_D – Drift Velocity

WT – Wild Type

ze – Absolute Charge

z_R – Calculated Charge of Protein

Contents

List of Tables

List of Figures

1. Introduction

1.1 Protein Misfolding and Disease

1.1.1 Protein Structure and Function

Proteins are biological polymers which tend to adopt a unique three-dimensional (3D) structure under native physiological conditions, and this unique structure determines the protein's native function (Wright and Dyson, 1999). This 3D shape is determined by the protein's primary amino acid (aa) sequence, as the different side chains of the amino acids interact with each other forming non-covalent bonds such as hydrogen bonds and ionic bonds. This coupled with Van der Waals forces and hydrophobic packaging determines the spatial arrangement of the individual amino acid residues and thus the protein's final conformation. The protein will fold into its minimal-energy configuration, to minimise the amount of free energy around itself, for example by shielding electrostatically charged side chains internally within the structure and folding is related to the thermodynamics of the protein (Eichner and Radford, 2011).

Failure of a protein to correctly form its native structure, if it has one, will render the protein unable to carry out its biological role, as it will no longer interact with its usual binding epitopes. This misfolding can also lead to proteins becoming pathogenic, and has been associated with the formation of aggregated protein complexes in a number of diseases, including Alzheimer's disease (AD), Parkinson's disease (PD) and diabetes (Sweeney *et al.*, 2017; Mukherjee *et al.*,

2015). Determining the structure and conformational arrangement of proteins and protein complexes therefore is essential to our understanding of both their biological function and roles within a range of diseases (Vendruscolo *et al.*, 2011; Walzthoeni *et al.*, 2013).

1.1.2 Intrinsically Disordered Proteins

Many proteins have no defined secondary structure, and these are universally termed intrinsically disordered proteins (IDPs). IDPs include proteins such as α-synuclein (αsyn), amyloid-β (Aβ) and p53, which are highly dynamic and have multiple conformational states to perform a variety of biological functions (Forman-Kay and Mittag, 2013). This intrinsic disorder may apply to the whole protein, or regions within them, and around a third of all eukaryotic proteins have now been shown to contain intrinsically disordered regions of over thirty residues in length (Babu *et al.*, 2011).

1.1.3 Protein Misfolding

Proteins are known to occasionally adopt partially unfolded, non-native conformations due to changes in their native environment or interactions with other molecules. Such interactions can lead to an accumulation of transient folding intermediates alongside the native protein. Normally these intermediates will be acted on by cellular quality control machinery, such as molecular

chaperones, and directed towards degradation or refolding (Chaudhuri and Paul, 2006; Gregersen *et al.*, 2006). Degradation and removal of these misfolded conformations must be tightly regulated, as incomplete or incorrect folding of some proteins can result in aggregation of these misfolded forms, leading to cellular toxicity and disease (Ecroyd and Carver, 2008). *In vivo* factors such as ageing, stress, environmental alterations or genetic mutations may affect this cellular quality control, shifting the protein's equilibrium towards the non-native, misfolded conformations, increasing a person's risk of developing these protein misfolding diseases (Natalello *et al.*, 2011).

1.2 Protein Misfolding Diseases

Over fifty diseases are known to result from the misfolding of proteins (Young *et al.*, 2015), collectively referred to as amyloid diseases or amyloidosis, due to the formation of so called amyloid material or amyloid deposits. Over thirty distinct proteins have been identified as amyloidogenic (Phillips *et al.*, 2015), but only a small number of these are known to cause disease in humans, some of which are outlined in table 1.1 (Uversky., 2008; Knowles *et al.*, 2014). The aggregation of some amyloid proteins however has been identified as functional, for example aggregated forms of Pmel17 play a role in the biosynthesis of melanin in humans, though these functional amyloids are much more commonly found in bacteria and fungi (Fowler *et al.*, 2007; Hammer *et al.*, 2008). Formation of amyloid material

may confer a cellular loss-of-function, a toxic gain-of-function, or in some cases a mixture of the two, dependent on the protein and disease (Winklhofer *et al.*, 2008; Vabulas and Hartl, 2011). Amyloid material has been identified in a variety of organs and tissue types, and these inclusions and plaques act as a hallmark for their relative diseases. Deposition can be widespread in the case of systemic amyloidoses such as primary systemic amyloidosis, or be confined to a specific location, such as the *Substantia Nigra Pars Compacta* (*SNPC*) of the brain in PD. The location of the inclusions often determines the symptoms, and consequently the clinical manifestations of amyloidosis are wide ranging (Uversky, 2008). Some amyloidogenic proteins can spread their toxic pathology from cell to cell, and therefore amyloid formation may be an acquired trait, such as in cases of the spongiform encephalopathies. These disease states are caused by exposure to a proteinaceous infectious particle, referred to as a prion protein (PrP) (Prusiner, 2012).

Amyloidogenic Protein	Protein Structure	Disease(s)
T-Synuclein	Natively Unfolded/IDP	PD, Diffuse Lewy Body Disease (DLBD), Multiple System Atrophy (MSA), Dementia with Lewy Bodies (DLB), Hallervoden-Spatz disease
T2-Microglobulin	T-sheet	Dialysis-related amyloidosis
Amyloid-T	Natively Unfolded/IDP	AD, Cardiovascular Amyloidosis, Congophillic Angiopathy
Amylin/ Islet Amyloid Polypeptide (IAPP)	Natively Unfolded/IDP	Type II Diabetes
Huntingtin	Unfolded Regions	Huntington茫Disease
Lysozyme	T-helical and T-sheet regions	Lysozyme Amyloidosis
Prion Protein	T-helical C-terminus	Creutzfelt-Jacob disease, Gertsmann-Straussler-Scheineker Syndrome, Bovine Spongiform Encelopathy (BSE), Scrapie
Transthyretin	T-sheet	Familial Amyloidotic Polyneuropathy

Table 1.1: Amyloid Proteins and Their Related Diseases.

Selection of the currently identified amyloid forming proteins and their related diseases. Adapted from Uversky, 2008 and Knowles *et al.*, 2014.

1.2.1 Amyloid Aggregation

Assembly into amyloid fibrils is initiated when the native protein becomes destabilised and unfolds, or in the case of intrinsically disordered amyloid proteins, such as Tsyn, naturally adopt a more partially folded, globule-like conformation, which, due to exposed hydrophobic patches, are highly prone to aggregation (Jahn and Radford, 2008). Self-assembly then begins, through a nucleation-dependent elongation mechanism, in a process referred to as aggregation, that eventually leads to the formation of mature fibrils. These fibrils are insoluble, non-branching, highly ordered structures, many ¾m in length and typically 5-15 nm in diameter under electron microscopy (Toyama and Weissman, 2011). They are defined by their distinct X-ray diffraction pattern, showing a characteristic cross-T structure, with T-sheets running perpendicular to the fibril axis (Eanes and Glenner, 1968; Eisenberg and Jucker, 2012). The fibrils are also protease resistant, insoluble in ionic detergents and can be recognised by the diagnostic indicator dye Congo Red (Wolfe and Cyr, 2011; Eisenberg and Jucker, 2012; Nilsson, 2004).

All amyloid proteins aggregate along a common pathway, outlined in figure 1.1, despite their often vast native structural differences (Wolfe and Cyr, 2011). *In vitro,* proteins may be directed onto the amyloid pathway by the presence of non-physiological conditions such as pH extremes, high temperature or pressure or the presence of metal ions or organic co-solvents (Rambaran and Serpell, 2008).

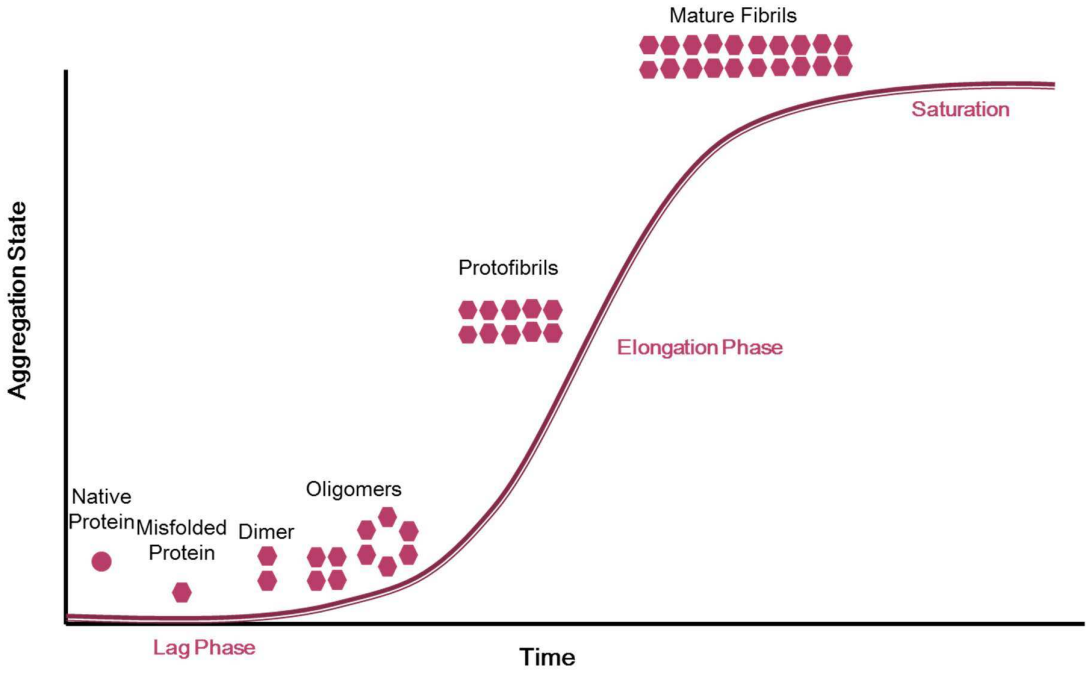

Figure 1.1: Amyloid Aggregation Pathway.

In the lag phase, the protein unfolds (if necessary), misfolds and then begins assembly into dimers, trimers and other low order oligomers. During the elongation phase, the oligomers form protofibrils, which mature into amyloid fibrils in the saturation stage.

In the case of IDPs, some monomeric conformations existing within the normal equilibrium have a higher propensity for aggregation, and aggregation in this case is triggered when the equilibrium is shifted in favour of these forms. Transition from these non-native partially folded structures to a pre-fibrillar conformation occurs via nucleated polymerisation, with the formation of oligomeric species during the lag phase of aggregation. Increasing evidence suggests these amyloidogenic, early oligomeric protein forms to be the toxic species involved

with disease, as opposed to the mature fibrils themselves (Ingelsson, 2016). These oligomeric species then further aggregate into larger oligomeric species during the elongation phase, forming protofibrils rich in ᵀ-sheets (Eisenberg and Jucker, 2012). These protofibrils then further entwine into the mature amyloid fibrils, which have been found deposited as plaques and inclusions in the various diseases. The number of protofibrils required to produce the mature fibrils varies between proteins and may also vary in number between fibres of the same protein (Rambaran and Serpell, 2008).

1.3 ᵀ-Synuclein and Parkinson's Disease

1.3.1 Parkinson's Disease

PD was first described in 1817 with the publication of James Parkinson's essay entitled "An essay of the shaking palsy", where he discussed the clinical symptoms of six patients, and laid the groundwork for the diagnosis and terminology of the disease (Parkinson, 2002). This disease is the second most common neurodegenerative disorder after AD, and affects ~1% of the world's population over the age of 65, with incident rates increasing to ~5% for individuals over the age of 85 (Marder *et al.*, 1996; de Lau *et al.*, 2006), making age the predominant risk factor for disease. Sporadic PD, which accounts for over 90% of patients, is the most prevalent form of the disease, however genetic factors have been identified in 5-10% of cases, which result in early-onset PD.

PD is an extremely debilitating disorder with clinical symptoms including, but not limited to, resting tremors on one or both sides of the body, muscle rigidity, slowness of movement referred to as bradykinesia, altered gait and balance and postural complications. There are also non-motor symptoms of the disease which include cognitive dysfunction, depression and sleep disorders (J ankovic, 2008).

Currently there is no cure or preventative measures to tackle the disease. Treatments such as Levodopa, a synthetic version of L-DOPA, the precursor to dopamine (DA), are currently utilised to manage the motor symptoms of the disease, but increasing our understanding of the causes and mechanisms of neuronal loss and amyloid fibre deposition is essential for future management and prevention of the disease.

1.3.2 Cellular Pathology of Parkinson表Disease

The main pathological hallmarks of PD are the deposition of amyloid fibres, composed primarily of -syn, in inclusions referred to as Lewy bodies (LB), and the gradual and selective degeneration of dopaminergic neurons in the *SNPC* of the brain, as discussed later in this chapter. The precise mechanisms behind neuronal cell death in PD are not however fully understood, as LBs are known to form within the surviving neurons as opposed to those which have lost their function (Natalello *et* al., 2011; Takahashi and Wakabayashi, 2001). It is now believed that oligomeric species formed during the lag phase of amyloid

formation, rather than mature amyloid fibrils or LBs, are responsible for the observed cell death (Ingelsson, 2016). Oligomeric species can create pores in the cell membrane, allowing for abnormal influx of ions such as calcium, leading to altered cellular homeostasis and apoptosis. It has also been suggested these oligomeric species may be able to pass their pathology from cell to cell, in a prion-like manner, leading to further disease progression (Ingelsson, 2016). Abnormal T syn deposits have also been observed within glial cells, such as oligodendrocytes and astrocytes, of PD patients. These occur most frequently within the dorsomedial portion of the *SNPC*, and their numbers have been shown to increase with disease progression, as is seen with LBs (Takahashi and Wakabayashi, 2001). The loss of neuronal function observed in PD, brought about by these abnormal deposits, leads to unregulated neurotransmitter release, resulting in the misfiring of neurons responsible for limb function and the motor symptoms of the disease.

1.3.3 Oxidative Stress and Parkinson表Disease

PD is also known to be related to oxidative stress, caused by the excess production of reactive oxygen species (ROS) in the brain (Blesa *et al.*, 2015; Manoharan *et al.*, 2016). ROS are continuously produced by all tissues *in vivo*, and have a variety of non-toxic functions such as cell signalling and homeostasis (Schieber and Chandel, 2014). However, when the balance between ROS

production and cellular antioxidant activity is uneven, and ROS are accumulated, oxidative stress can occur. In PD, oxidative stress is known to cause an imbalance in DA metabolism, further contributing to symptoms, and ROS mediated DNA damage is known to be a prominent feature in PD patients (Manoharan *et al.*, 2016). The primary causes of oxidative stress in PD include iron accumulation, enhanced DA metabolism, mitochondrial DNA mutations and the accumulation of hydroxyl radicals (Manoharan *et al.*, 2016).

1.3.4 T-Synuclein and Parkinson□Disease

As mentioned in the previous section, one of the hallmarks of PD is the deposition of intracellular inclusions, LBs, within the dopaminergic neurons of the *SNPC* in the brain (Natalello *et al.*, 2011; Lee *et al.*, 2014). LBs were first described in 1912 by Freidrich Henry Lewy as abnormal intracellular protein inclusions, which were later demonstrated to be composed of amyloid fibrils of Tsyn, stacked in a highly ordered and highly heterogeneous fashion (Spillantini *et al.*, 1997). LB formation occurs alongside the selective loss of dopaminergic neurons within the affected brain region (Natalello *et al.*, 2011; Lee *et al.*, 2014; Illes-Toth *et al.*, 2015) and both increase as disease progresses.

With the advancement in scientific technology, several other factors have since pointed to Tsyns association with PD, such as the point mutations A53T, A53E, A30P, H50Q, E46K and G15D in the *SNCA* gene encoding the protein being

identified as a cause of hereditary forms of the disease (Vargas *et al.*, 2017; Mason *et al.*, 2016). A number of these mutated forms of αsyn have also been shown to have a higher propensity for aggregation than wild-type (WT) αsyn *in vitro* (Uversky and Eliezer, 2009). Duplication and triplication of the *SNCA* gene have also been shown to result in early-onset PD and variations within the genes promotor region have been shown to cause an increase in susceptibility for disease development within some families (Lill, 2016; Konno *et al.*, 2016; Pankratz *et al.*, 2007; Vargas *et al.*, 2017).

PD may also be caused in a synergistic manner by genetic mutations in other genes, such as *LRRK2*, encoding the dardarin protein, *PRKN*, encoding parkin and *PINK1*, encoding PTEN Induced Putative Kinase 1, where point mutations, frameshift mutations, truncating mutations, exon rearrangements, deletions and duplications of the genes have all been observed to result in hereditary PD (Pankratz *et al.*, 2007; Lill, 2016).

1.3.5 Other Synucleinopathies

αSyn毒 disease causing properties are not limited to PD, and abnormal accumulation of αsyn aggregates can also result in Dementia with Lewy Bodies (DLB) or Multiple System Atrophy (MSA) and all three are collectively termed synucleinopathies (Spillantini and Godert, 2000). Due to the involvement of different cell types and brain regions between the three diseases, whilst there are

some similar symptoms, the clinical manifestation of the three diseases is varied (Yang and Yu, 2017). All three synucleinopathies manifest within the brain, but affect different cells and regions (Spillantini and Goedert, 2000).

PD symptoms are concurrent with the formation of αsyn inclusions within dopaminergic neurons of the *SNPC*. MSA however, results when αsyn accumulates within the glial cells, in particular the oligodendroglia, the cells responsible for making the myelin sheaths surrounding neurons (Laurens *et al.*, 2017). Sporadic disease is the most common form, as with PD, but hereditary forms associated with point mutations in the *SNCA* gene, such as rs3775444, rs3822086, rs1193107 and rs3857059 have also been reported (Al-Chalabi *et al.*, 2009; Scholz *et al.*, 2009).

DLB, like PD, results when αsyn accumulates into LBs within the *SNPC*. DLB patients however show fewer PD-like motor symptoms, and demonstrate increased cognitive decline in comparison to their PD patient counterparts (Elahi and Miller, 2017). Sporadic onset DLB is again the most common, however genetic factors have also been identified, such as variants in the *GBA* and *APOE* genes, encoding the proteins beta-glucocerebrosidase and apolipoprotein E, respectively (Vergouw *et al.*, 2017).

1.4 τ-Synuclein Structure and Function

1.4.1 Structure of τ-Synuclein

τSyn is an intrinsically disordered 14 kDa, 140 amino acid protein, predominantly found within the *SNPC* of the brain. It has no defined or permanent secondary structure, existing in an equilibrium of randomly disordered monomers of varying degrees of compactness and relative concentration. As shown in figure 1.2, the protein has three main domains; the N-terminal region (aa1-60) (Stefanis, 2012) consisting of imperfect, repetitive tandem motifs, which has been demonstrated to adopt amphipathic, τ-helical structures upon membrane binding (Uversky and Eliezer, 2009; Recchia *et al.*, 2004). The central hydrophobic domain (aa61-95) referred to as non-amyloid τ-component (NAC) (Stefanis, 2012), which has been associated with pathological brain lesions, inducing apoptotic cell death in culture (Lashuel *et al.*, 2013; El-Agnaf *et al.*, 1998) and has a natural tendency to form τ-structures. This region has also been demonstrated to be essential for the proteins aggregation (Lashuel *et al.,* 2013; Giasson *et al.*, 2001). The C-terminal region (aa96-140) is highly acidic, proline rich and prone to disorder (Meuvis *et al.*, 2010; Stefanis, 2012), and exists in a disordered conformation in monomeric, fibrillary and membrane-bound forms of the protein (Oueslati, 2016; Del Mar *et al.*, 2005). This region is known to be important for a variety of τsyn's functions, including interaction with metal ions (Oueslati, 2016; Brown, 2007; Paik *et al.*, 1999), DA (Oueslati, 2016), and other proteins such as Tau (Jensen *et al.*, 1999).

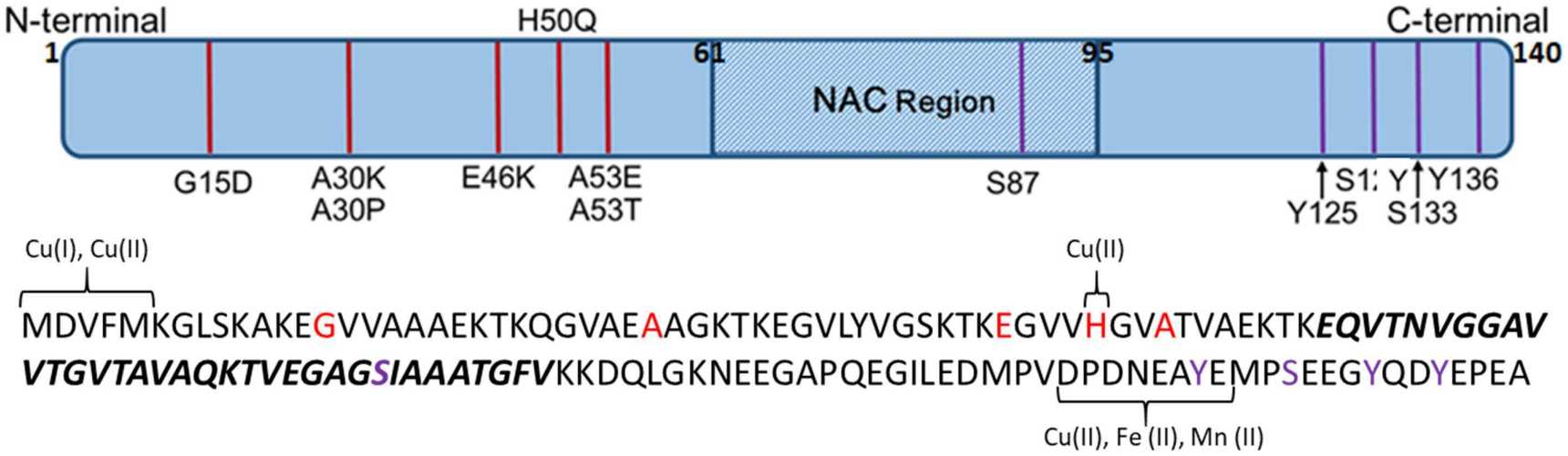

Figure 1.2: Simplified Structure and Amino Acid Sequence of α-Syn.

Simplified structure and amino acid sequence of α-syn, showing the NAC region highlighted in bold italic text, familial mutations with red lines and letters, phosphorylation sites with purple lines and letters and metal binding domains indicated on the sequence.

αSyn is known to exist in a range of conformations at any one time, due to its intrinsic disorder, and the conformational equilibrium of these conformations can be altered depending upon the environment (Illes-Toth *et al.,* 2015; Illes-Toth *et al.*, 2013). Extended conformations, consistent with an unfolded structure, are dominant under physiological conditions, whereas co-populated more compact structures, associated with increased aggregation and subsequent amyloid formation, are most prevalent under non-physiological conditions such as under extreme pH, or with the presence of co-factors such as metal ions, which will be discussed further in sections 1.6.1 and chapter 3.

Extended conformations of proteins have no secondary structure and exist as a worm-like chain of amino-acids, in a range of highly disordered, heterogeneous monomers. Compact conformations however have been suggested to exhibit small amounts of secondary structure, and representations of both forms of the protein are shown in figure 1.3. α-Helical structures are observed within the N-terminal region when αsyn is bound to membranes, and this is also known to contain a kink or break in the structure at aa43-44, as determined by molecular dynamics simulations coupled with Proteins with Atomic details on Course-grained Environment (PACE) modelling. These α-helices are also observed within the compact conformations of αsyn, along with β-hairpin folds in the region of aa36-56 (Yu *et al.*, 2015). These β-hairpin folds have been shown to be linked to the aggregation of the protein, as mutant forms of αsyn known to have a faster aggregation propensity, such as the A30P and A53T variants, form these β-

hairpin structures more quickly than the WT protein. The region containing the T -hairpin has also been demonstrated to interact with the C-terminal region of the protein, leading to further compaction (Yu *et al.*, 2015).

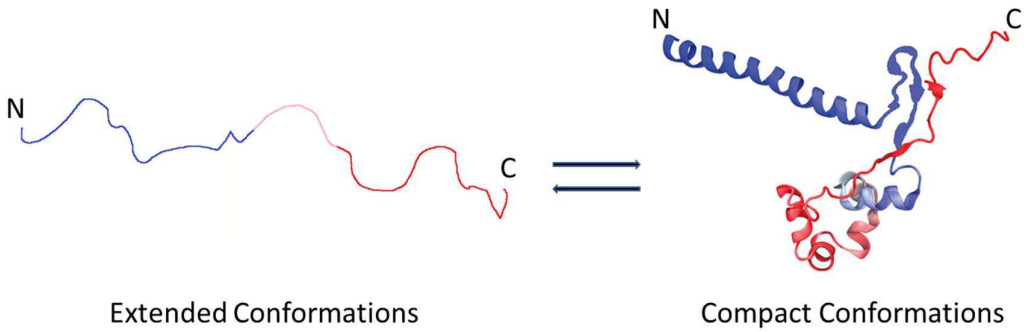

Figure 1.3: Representation of Extended and Compact □Syn Conformations. The N-terminal is highlighted in blue, the NAC region in pink and the C-terminal region in red. Adapted with permission from Yu *et al.*, 2015.

1.4.2 Physiological Role of ΠSyn

Currently, the exact physiological role of Tsyn is poorly understood, though evidence is mounting for its role in a number of cellular processes. It has been suggested to have a role in DA synthesis, via binding and inhibiting tyrosine hydroxylase, which is a rate limiting iron-dependent enzyme essential for DA biosynthesis (Perez *et al.,* 2002). It is also thought to have role in iron homeostasis, as its 5□promotor region is known to contain an iron response element (Rogers *et al.,* 2011). The protein itself is often found localised to membranes, suggesting there may be a role in endo and exocytosis of this

element (Baksi *et al.,* 2016; Snead and Eliezer, 2014). T-Syn is also known to have ferrireductase activity, and it has been demonstrated to bind to and utilise the redox cycling ability of copper ions to remove electrons from Fe(III), reducing it to Fe(II). This ferrireductase activity does not occur in the absence of copper ions, and a build-up of Fe(III) has been noted in the brains of PD patients, where a reduction in copper ions has also been observed (Dexter *et al.*, 1989; Davies *et al.*, 2011). Other suggested roles include modulation of synaptic vesicle size, and modulation of neurotransmitter storage and release (Nemani *et al.,* 2010; Lundblad *et al.,* 2012). It is also thought to act as a molecular chaperone for molecules such as the soluble N-ethylmaleimide-sensitive factor activating protein receptor (SNARE) proteins (Burrŭ *et al.*, 2010).

Attempts to further elucidate the functions of T-syn through knockout animal models have been attempted. However, knockout of the *SNCA* gene in mice models shows little physiological effect, with no alterations to synaptic plasticity, vesicle pools or DA uptake and release noted in any studies (Eriksen *et al.*, 2005; Chandra *et al.*, 2004).

1.5 Post-translational Modification of T-Synuclein

It has been well documented that T-syn found within the LBs of PD patients has undergone a variety of post-translational modifications (PTMs), which include phosphorylation of serine and tyrosine residues, acetylation of the N-terminus

and ubiquitination of lysine residues (Barrett and Greenamyre, 2015; Duce *et al.*, 2017; Oueslati., 2016; Fujiwara *et al.*, 2002; Popova *et al.*, 2015; Schmid *et al.*, 2013). The majority of PTM sites are also known to be located within the highly disordered C-terminal region of the protein. There are currently five known phosphorylation sites on T syn; two located at serine residues 87 and 129, and a further three located at tyrosines 125, 133 and 136 (Oueslati., 2016; Paleologou *et al.* 2010).

Phosphorylation at tyrosine residues appears to be predominantly associated with membrane binding, with phosphorylation at Y125 specifically playing an important role. It is suggested that this modification is important for the normal biological functions of T syn (Schreurs *et al.*, 2014). Data currently suggests that phosphorylation at S87, S129 or Y39 prevents the binding of T syn with biological membranes. It has also been suggested that phosphorylation at Y125 has a neuroprotective role and prevents the formation of neurotoxic oligomeric species (Chen *et al.*, 2009).

Phosphorylation at serine residues, and in particular S129, has been suggested to play a role in the pathogenicity of the protein, with 90% of T syn within LBs found to be phosphorylated at this amino acid residue. In its normal function, phosphorylation at S129 has been suggested to have a role in autophagy (Tenreiro *et al.*, 2014) and in cellular clearance of T syn via proteolytic degradation (Chau *et al.*, 2009; Machiya *et al.*, 2010).

Currently it is unclear exactly what the role of α-syn phosphorylation is in the pathogenesis of disease, and studies have yielded wildly contradictory results, but it is clear that phosphorylation at S129 plays an important role, due to its substantial increase within LBs isolated from PD patients.

1.6 Promotion and Prevention of α-Synuclein Aggregation via Ligand Binding

In vitro, the rapid formation of soluble oligomers and amyloid fibrils can be initiated by PTMs, metal binding and alterations to the protein's environment such as shifts in pH or temperature, incubation with denaturants such as sodium dodecyl sulphate (SDS), and vigorous agitation in solution. Increased aggregation propensity may also be induced via the introduction of destabilising mutations into the protein's primary sequence, such as the familial mutations A53T, A30P and E46K discussed earlier in the chapter (Wolfe and Cyr, 2011; Jahn and Radford, 2008; Uversky and Eliezer, 2009). The protein's conformational distribution is significantly dependent on the pH of the environment with acidic conditions resulting in the formation of the more compact species, and an observed increased in aggregation kinetics (Beveridge *et al.*, 2015; Morris and Finke, 2009). These compact conformations can also be induced by other external factors including temperature, organic solvents, salts,

pesticides, herbicides, heparin, polycations, methionine oxidation (Natalello *et al.*, 2011, Uversky and Eliezer, 2009, Brown, 2010).

The binding of ligands such as metal ions to αsyn has also been demonstrated to induce the formation of more compact conformations, and cause an increase in the aggregation rate of the protein (Mason *et al*, 2016; Uversky *et al*, 2001). In contrast, other ligands have been demonstrated to reduce the aggregation of αsyn *in vitro*, such as the presence of the natural polyphenolic compounds curcumin and Epigallocatechingallate (EGCG), which has also been demonstrated to increase the presence of the extended conformations of αsyn (Pandey *et al.*, 2008; Liu *et al.*, 2011). These aggregation promoting and preventing ligands will be discussed individually in this section.

1.6.1 Promotors of Aggregation

Ligands discussed within this section have been either shown to shift αsyn's conformational equilibrium towards the more compact, aggregation prone conformations, or increase the aggregation kinetics of the protein *in vitro*.

1.6.1.1 Metal Ions

Metal ions were first identified as a potentially important factor in PD progression as far back as 1924, when deposits of iron were identified, co-localised with LBs in the brains of PD patients (Lhermitte *et al.*, 1924). The link between heavy

metals and PD was then further solidified in the 1980s, when two separate studies identified increased levels of iron and zinc in the brains of PD patients (Dexter *et al.,* 1989; Riederer *et al.,* 1989). In contrast, copper levels in the *SNPC* were found to be reduced in comparison to control brains (Dexter *et al.*, 1989), however high levels of copper had also recently been identified in the cerebrospinal fluid of PD patients (Pall *et al.*, 1987). Increased levels of all three metals have since been found in the LBs of PD patients, and have also since been observed in and around amyloid plaques in AD patients (Lovell *et al.,* 1998; Miller *et al.*, 2006). Several epidemiological studies also noted that individuals with chronic industrial exposure to heavy metals, including copper, iron, manganese, zinc and aluminium, had an increased incidence rate of PD compared to the general population (Gorell *et al.*, 1999; Gorell *et al.*, 2004; Coon *et al.*, 2006), leading to increased interest in the role of metal homeostasis in the development and progression of PD and other neurodegenerative disorders.

The ability of metal ions, particularly copper to promote oligomerisation and increase amyloid fibril formation of -syn has been well established (Natalello *et al.*, 2011; Uversky and Eliezer, 2009; Brown, 2009; Uversky *et al.*, 2001). Incubation with copper has also demonstrated an increased population of the more compact, aggregation prone states of -syn, and this has been observed by a number of techniques, including nuclear magnetic resonance (NMR) (Binolfi *et al.*, 2008), circular dichroism (Binolfi *et al.*, 2008), electrospray ionisation 唖ion

mobility spectrometry 唖mass spectrometry (ESI-IMS-MS) (Natalello *et al.,* 2011; Mason *et al.,* 2016) and calorimetric titrations (Drew *et al.,* 2008).

Syn has been shown to have a high affinity for copper binding, and is known to have at least three specific binding motifs for the metal ion, as shown in figure 1.2 (Ahmad *et al.*, 2012). A high affinity binding site has been observed at the N-terminus, where the free nitrogen on the amino terminal anchors the metal ion. A second, lower affinity site has been observed at H50, anchored by the imidazole ring of the amino acid, and a third low affinity site was found within the C-terminus involving the residues D121, N122 and E123 (Binolfi *et al.,* 2012; Mason *et al.*, 2016; Binolfi *et al.*, 2006). The protein has been demonstrated to bind copper ions more readily than any other metal currently investigated (Binolfi *et al.*, 2006). Electron paramagnetic resonance (EPR) spectroscopy demonstrated the high affinity binding site, within the N-terminus, could bind the protein when present in the nanomole range (Ahmad *et al.*, 2012).

Iron has also been shown to increase the aggregation rate of syn *in vitro* (Binolfi *et al.*, 2006; Uversky *et al.*, 2001). Divalent iron has also been found to bind to the C-terminus of syn via 2D-NMR studies, and this metal also appears to be utilising D121 as an anchoring residue (Binolfi *et al.*, 2006; Peng *et al.,* 2010).

The interaction of syn with metal ions will be discussed further in chapter 3.

1.6.1.2 Spermine

Another extensively studied promotor of αsyn aggregation is spermine, a naturally present polyamine involved in both neuronal cell proliferation and differentiation, and in the modulation of ion channel receptors (Grabenauer *et al.*, 2008). It has the ability to complex with αsyn under native physiological conditions resulting in enhanced rates of fibrillation. Upon the binding of spermine, which is known to occur on the C-terminus of the protein, αsyn and its familial variants undergo a structural collapse, resulting in a reduction in cross sectional area (Grabenauer *et al.*, 2008; Illes-Toth *et al.*, 2013; Moree *et al.*, 2015).

1.6.2 Prevention of Aggregation

The prevention of oligomer and amyloid assembly through the use of small molecule inhibitors, that bind specifically to precursor protein conformations, is an important challenge. Small molecules can prevent fibril formation by binding to and stabilising non-amyloidogenic states. One strategy towards preventing aggregation is therefore to shift the population back to non-amyloidogenic conformations through stabilisation of the unfolded state. Identifying such inhibitors is problematic, due to the conformational heterogeneity of amyloid proteins, but several compounds have been demonstrated *in vitro* to reduce the

aggregation of Tsyn, which will be discussed in the following sections, and these could provide novel drug candidates for treating PD.

1.6.2.1 Polyphenolic Compounds

Polyphenolic compounds have been proving good novel candidates for anti-amyloid therapeutics for some time. Natural curcumin is of particular interest, as it appears to have a variety of medicinal properties *in vitro*, and has been utilised as medicine in eastern cultures for thousands of years (Witkin and Li, 2013).

In 2008, curcumin was demonstrated by both western blot and in an SH-SY5Y neuroblastoma cell model, to inhibit the aggregation of Tsyn (Pandey *et al.*, 2008). The molecule is also known to have antioxidant properties, which may be how it exerts its effects on amyloid aggregation. Increased oxidative stress is known to be initiated by overexpression of Tsyn, and is suggested to play a key role in PD development and progression, through the production of free radicals such as ROS (Jenner and Olanow, 1996; Dexter *et al.*, 1989). Phenolic antioxidants, including curcumin, act as hydrogen donors, inhibiting the propagation of free radical chain reactions (Venkateswarlu *et al.*, 2005), thereby reducing the damaging effect of these species. Inhibition of free-radical species may therefore be a possible mechanism for curcumin to prevent Tsyn aggregation.

Another natural polyphenol known to interact with amyloid proteins is EGCG; an antioxidant found in green tea, which has been demonstrated to prevent amyloid

formation *in vitro* via multiple techniques. Incubation of A53T mutant αsyn with EGCG prevented its aggregation into amyloid fibrils, as determined via thioflavin-t (ThT) assay, where aggregation was completely halted. The same study also determined binding to ECGC prevented the conformational shift towards the compact states, normally observed with A53T αsyn, as determined by ESI-IMS-MS (Liu *et al.*, 2011).

The interaction of αsyn with curcumin will be discussed further in chapter 4.

1.6.2.2 Dopamine

One of αsyn's natural and most important ligands, DA, has also been suggested to prevent the aggregation of αsyn upon binding to the protein. In the presence of DA, αsyn yields a diverse range of SDS resistant, non-amyloid oligomers (Leong *et al.*, 2009). It has been observed that the incremental uptake of DA pushes the equilibrium of αsyn towards the highly expanded states, which become fully populated upon the binding of three DA ligands to the protein, when compact states may no longer be observed. DA binds uniquely to the most expanded conformations of αsyn, as determined by ESI-IMS-MS, indicating that the ligand binding site in this instance requires an extended conformation (Illes-Toth *et al.*, 2013).

These observations demonstrate that modulation of amyloid assembly is possible, by either alteration to the co-populated precursor states, or by directly blocking

assembly via the use of inhibitors. With successful identification of appropriate ligands, targeting aggregation of T-syn via either targeting of the monomeric protein, or oligomeric species produced along the aggregation pathway, may be a promising potential therapeutic method for PD alleviation, and this will be further investigated in chapter 4.

1.7 ESI-IMS-MS as a Tool for Understanding Protein Conformation

Native mass spectrometry (ESI-MS) allows for highly sensitive and extremely rapid identification of proteins and protein complexes by simultaneously analysing all species present within a sample, through determination of their mass to charge ratio, or *m/z*. It can provide information on the aggregation properties of amyloid proteins by identification of all species within a sample, including monomeric proteins, oligomeric species, protofibrils and protein fragments, whilst also determining their relative intensities.

Further structural information on the conformation of monomeric and oligomeric species within a sample can be determined using ion mobility spectrometry, to separate co-populated conformations with the same *m/z*, appearing within the same spectral peak, which would not be distinguishable from one another with native ESI-MS. By calculation of the collisional cross sectional area (CCS or ┤) of each ion, overlapping species within the spectra, with the same CSI but different conformational properties, can be determined from one another and

therefore, information on the conformation of each protein species can be determined (Smith *et al.*, 2009; Ruotolo *et al.*, 2008).

1.7.1 ESI-IMS-MS and the Advantages of Ion Mobility

The addition of ion mobility drift cells to native mass spectrometry instrumentation has allowed for the characterisation of monomeric and oligomeric protein conformations, through determination of their CCS. During an ion mobility experiment, the time taken for an analyte of interest to travel through an ion mobility cell or drift tube containing a neutral gas, whilst under the influence of a weak electric field, is measured. As will be further discussed throughout this section, the mobility of an analyte through the drift cell is determined by its mass, conformation, and charge obtained during ionisation, with a physically larger analyte taking longer to transverse the drift cell, and an analyte with a smaller conformation travelling faster (Mason *et al.*, 2016; Smith *et al.*, 2009).

1.7.1.1 ESI-IMS-MS Instrumentation

An ESI-IMS-MS instrument, such as the Synapt G2 (Waters, Manchester) utilised in this project, consists of a nano-electrospray source, which may be an automated sampler such as the NanoMate (Advion, UK), externally mounted to the instrument to conduct ambient ionisation at atmospheric pressure. As shown in figure 1.4, this source is mounted near a sampling cone, which draws a

continuous beam of ions into the internal compartments of the instrument, which are kept under vacuum. Ions then travel through an ion guide towards and through the quadrupole mass analyser to the ion mobility chamber. Ions are then trapped, before being pulsed into the N_2 cell for mobility separation, before being halted again in the transfer. Ions then enter the vacuum of the time-of-flight (TOF) mass analyser, which determines their *m/z*, before arrival time distributions (ATD) are determined by the ion detection system

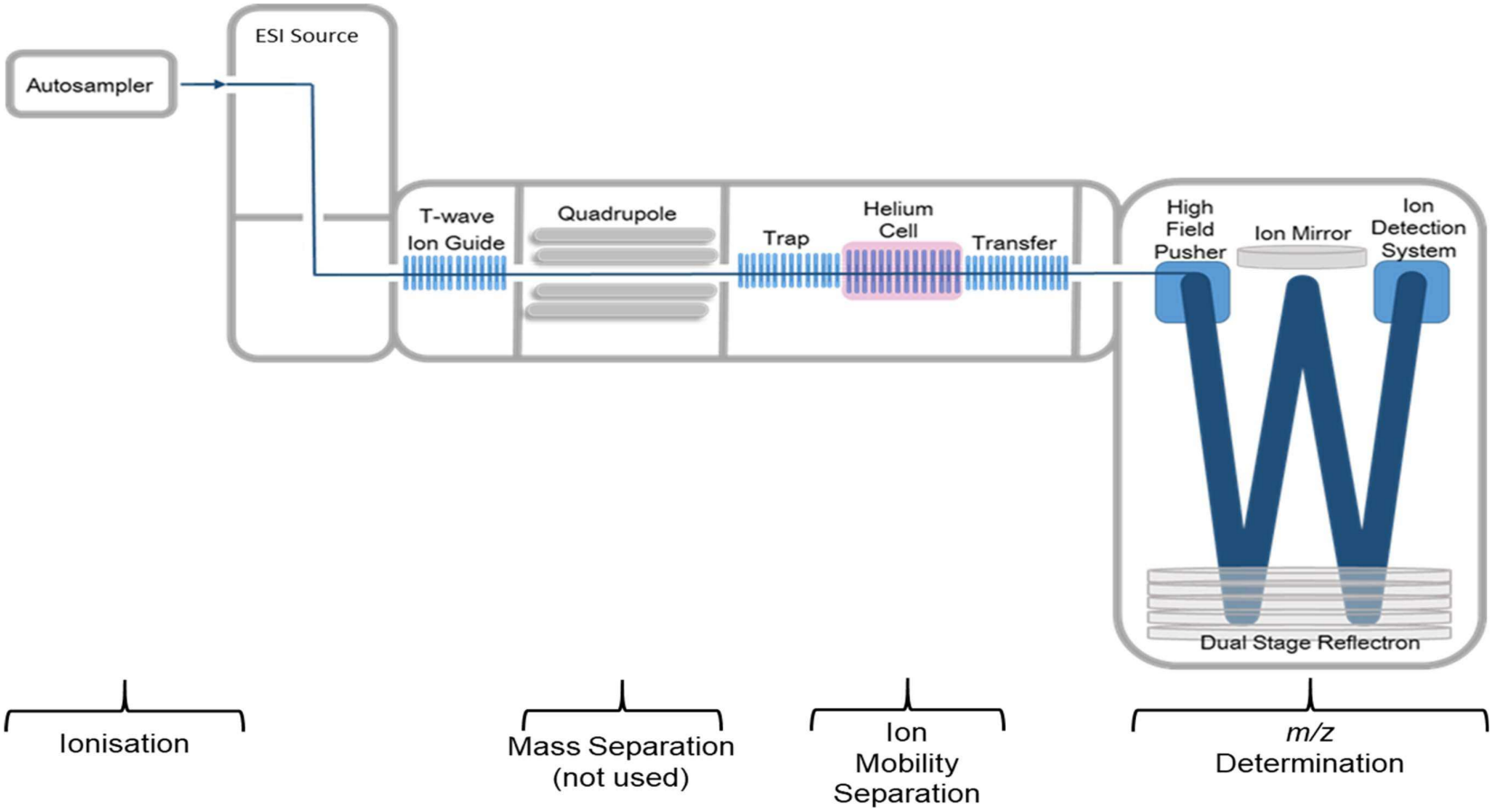

Figure 1.4: Schematic representation of the Synapt G2 IST:MS Mass Spectrometer.

Diagram shows regions of ionisation, mass selection (not used), IMS and m/z determination.

1.7.1.2 Principles of Electrospray Ionisation

At the beginning of an ion mobility experiment, ions are produced when an electrical current is applied to either a gold-coated borosilicate needle or auto-sampler tip, if using an automated source such as a NanoMate, which contains the analyte of interest. This produces a Taylor cone, as shown in figure 1.5. A fine mist of multiply charged solvent droplets containing the analyte are excluded from the Taylor cone, and machine parameters such as cone voltage, cone temperature, and distance from the source must all be optimised to ensure a stable electrospray for optimal analysis (Wilm, 2011). Volatile solvents must be utilised, and with a small sample volume of around 2-10¾l, to ensure production of very small and highly charged droplets.

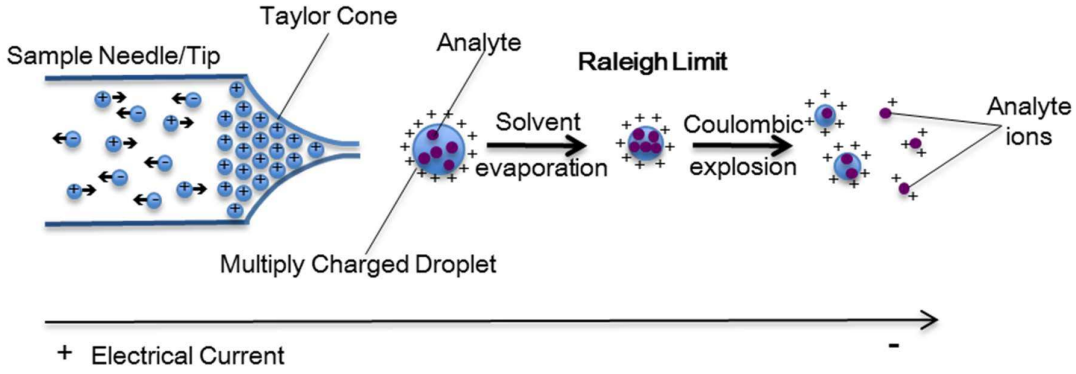

Figure 1.5: Mechanism of Electrospray Ionisation.

Diagram outlining the mechanism of electrospray ionisation, showing the production of a Taylor cone, solvent evaporation, and coulombic explosion, leading to the production of multiply charged analyte ions.

When coulombic repulsion of the charges on the surface of these solvent droplets overcomes the surface tension of the droplet, fission occurs and the droplet forms smaller, progeny droplets, and some of the solvent is removed through evaporation. This point of fission and evaporation is referred to as the Raleigh limit, as highlighted in figure 1.5. These smaller, progeny droplets then undergo further fission and evaporation, until all the solvent is removed and only gaseous, charged ions remain (Ho *et al.*, 2003; Wilm, 2011). The number of charges on the ions depends on the structure of the molecule or protein of interest, and this is determined by the accessible surface area and presence of ionisable functional groups on the molecule, and will be discussed further later.

ESI is referred to as a 'soft-ionisation' technique, which allows for molecules with high molecular weights to be observed easily, and also preserves the conformation and any non-covalent interactions of proteins and protein-complexes (Beveridge *et al.*, 2013). Three models exist to describe the ionisation in an electrospray source; the ion evaporation model, the charge residue model, and the chain ejection model.

The ion evaporation model is usually used to describe ionisation of smaller ions, where shrinkage of the droplets occurs via evaporation, until the field strength on the surface is so large that ions are expelled from the droplet. This type of ionisation is heavily influenced by the chemical properties of the ion, and usually

occurs when the droplet size reaches around 20nm in diameter (Konermann *et al.*, 2013; Wilm, 2011).

The charge residue model is associated with larger ions such as proteins and usually occurs when each droplet only contains one ion. Ions become completely desolvated before gaining charges, which can be positive or negative dependent on the mode of acquisition (Konermann *et al.*, 2013; Wilm, 2011). This model of ionisation preserves non-covalent complexes, as it requires less energy, as the ions are not expelled from within the droplet, but the droplet is removed from around them, and is therefore less damaging. It is generally accepted that compact proteins are ionised via the charge residue model (Donor *et al.*, 2017).

The chain ejection model describes the ionisation method for extended biopolymers such as the extended conformations of ~~T~~syn. The unfolded protein chain is partially ejected from the solvent droplet, leading protons to attach to the exposed portion of the ion. The ion is then further extruded from the droplet, gaining more charges, until it is fully ejected from the solvent (Konermann *et al.*, 2013; Donor *et al.*, 2017).

The number of charges a protein will acquire upon ionisation, also known as its charge state (CS) is dictated by the number of basic amino acid residues available on its surface for ionisation (Coveyr *et al.*, 1988; Loo *et al.*, 1988) which is itself dictated by the electrostatic repulsions between protonated basic residues thus forming its tertiary structure (Schnier *et al.*, 1995). Ionisation may be

performed in either positive or negative mode, supplying the protein with either positive or negative charges, by addition or removal of electrons. When a protein is ionised, it may then be referred to as a charge state ion (CSI), for example a conformation of said protein bound to 14 positive charges may then be referred to as the +14 CSI.

Folded proteins with a compact CCS generally only acquire 2 to 8 bound charges, so have CSIs of +2 to +8 for example, due to the limited number of basic residues on the surface of the protein. Unfolded proteins pick up a higher number of charges on ionisation, as they have a more extended structure, and a higher number of ionisation sites are available. Higher CSIs representing extended protein conformations are present within the lower *m/z* range, whilst smaller, more globular proteins pick up fewer charges and are found within the higher *m/z* range, therefore an increase in charge state often corresponds with an increase in CCS (Vargas *et al.*, 2017).

During acquisition of a protein, particularly with IDPs such as Tsyn, multiple charge states will be observed, due to the conformational flexibility of proteins, as some will have more exposed ionisable sites available than others. The range of these charges is referred to as the charge state distribution (CSD). Folded proteins will display a narrower CSD due to the limited number of basic residues on the surface of the protein, and limited flexibility, and tend to display a small CSD of around 2 to 6 different species within the mass spectra. Unfolded proteins

however display a wider CSD due to their increased flexibility, and increased exposed basic residues, and will display a wider range of peaks on the mass spectra.

A protein's CSD can be significantly altered by solution conditions, therefore care must be taken to ensure sampling is performed in a manner that retains the protein in its native state. This is a particular problem with IDPs such as α-syn. Non-physiological solvent conditions such as low pH or the presence of alcohols can significantly alter the CSD of a protein (Beveridge *et al.*, 2015; Duce *et al.*, 2017) so care must be taken to keep solution conditions as physiologically relevant as possible.

1.7.1.3 Ion Mobility Separation

After ionisation and injection into the sampling cone, ions travel through the stacked ring ion guide and quadrupole mass filter, before being pulsed into a drift tube filled with an inert buffer gas, in the case of the Synapt G2, N_2.

1.7.1.3.1 Drift Time IMS

In drift time ion mobility separation, a weak direct current (DC) electric field is applied to the drift cell, and ions are drawn through via their interaction with the electric field, colliding with the buffer gas as they travel. In this case, a molecule's transit time through the drift cell is determined by both its charge; with a higher

number of charges gained during ionisation resulting in a quicker transition, and its conformation; with the more collisions encountered with the gas causing the molecules speed of transition to slow.

1.7.1.3.2 Travelling Wave IMS

In a travelling wave experiment, the DC current applied over the drift cell is not linear, but in a transient wave form. The drift tube consists of 168 x 0.5mm electrode plates, 1mm apart, in which a radio-frequency (RF) is applied to guide the ions transit. A continuous series of DC voltage pulses are applied to the ion guide, moving the ions through the drift cell.

Following a gated release from the trap ion guide region, a pocket of ions is released into the drift cell and 200 mass spectra are acquired, before another packet of ions are pulsed into the drift tube and a further 200 spectra are acquired. Other settings must be adequately tuned to ensure adequate separation of ions, including wave heights, amplitudes, and wave velocities, as well as the type and pressure of the buffer gas (Thalassinos and Scrivens, 2009; Shvartsburg and Smith, 2008).

An ion's speed through the drift cell again is related to the ion's size, charge, gross morphology and its interaction with the buffer gas. High mobility ions, such as those with a small CCS, travel with the wave and pass through the ion guide

faster. Lower mobility ions with an extended structure and smaller CCS, will roll over the top of the waves and are ejected from the drift cell slower.

Due to the stacked ring ion guides within the Synapt G2, ions may also be fragmented during ion mobility separation, either in the trap or transfer region, or both if required. The high sensitivity of the travelling wave allows isobaric species, stereoisomers and conformational isomers to be resolved with great accuracy.

1.7.1.3.3 Time-Of-Flight Mass Analysis

Finally, mass data is acquired by use of time-of-flight (TOF) mass analysis allowing *m/z* to be determined, by examining the flight time of the ions through the TOF component of the mass spectrometer. TOF mass analysers separate ions according to their velocities, which is dependent on the mass of the ion, with lighter ions having shorter flight times than heavier ions.

An ion is accelerated into the TOF analyser via an electrical field of known strength, this means ions with the same charge will have the same kinetic energy. The velocity of the ion will depend on its mass, with heavier ions of the same charge having a longer flight time. The reflectron TOF component of the Synapt G2, utilised for experiments presented in this thesis, has improved mass resolution than a standard, linear TOF detector, as the detector contains ion mirrors, or reflectrons; a stacked series of ring shaped electrodes that create an

electric field by way of a linear voltage gradient, off of which the ions are 唆ounced表 before detection (Mamyrin *et al.*, 1973; Boesl, 2017).

The principle behind reflectron mode TOF is that ions with higher kinetic energy will penetrate further into the stacked electrodes than those with a lower kinetic energy, allowing ions of the same m/z but different kinetics to arrive at the detector at the same time (Boesl, 2017).

1.7.1.3.4 Calculation of CCS from Ion Mobility Data

Once the drift time of an ion has been obtained the CCS can be calculated, with comparison to proteins of known mass and structure. Due to the non-linear electric field within a travelling wave experiment, wave heights, velocities and gas pressures can all affect the recorded drift time of ions. It is therefore, important to account for these differences when calculating the CCS. Experimentally recorded values can be corrected using the following equations, alongside data from calibrant proteins of known CCS.

CCS can be determined from a linear IMS device using equation 1 below:

だ唸 $\frac{\text{媼}\times\text{倡}\sqrt{\text{趲}}}{\sqrt{}}$ $\frac{\text{l·ð}}{\text{媼}_{\text{妄}}4\ \text{嬿}}$ $\frac{\sqrt{}\sqrt{}\ 4}{0\ \sqrt{}::}$ $\frac{\text{儀侗}}{\text{俠 伽}}$

Equation 1: Calculation of CCS on a Linear IMS Instrument.
Calculation of CCS (┫), where *z* is the number of charges on the ion, *e* is the charge on the electron (1.6022 x 10^{-19}C), *kb* is the Boltzmann constant, *T* is temperature of the buffer gas, ¾is the reduced mass, *P* is the buffer gas pressure, *N* is the density of the buffer gas, *E* is the electric field, and *L* is the length of the drift tube.

Correction factors can now be incorporated into the equation, to compensate for the non-linear effects of the triwave, which result in uneven electric fields and uneven temperatures and pressure within the system. Correction parameters can be incorporated into equation 1, to give equation 2, where *A* is a correction factor for the electric field parameters, and *B* is a compensation factor for the non-linear effects of the triwave instrument:

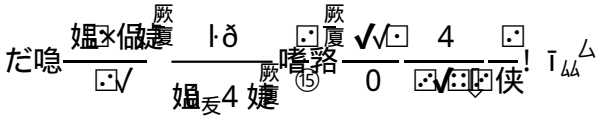

Equation 2: Calculation of CCS(┤) with Incorporation of Correction Factors for Triwave IMS.

Calculation of CCS including correction factors for the non-linear effects of the triwave. A corrects for the electric field, and B corrects for the non-linear effects.

Reduced CCS, or ┤表can then be calculated, which is a charge and mass independent measurement, using equation 3:

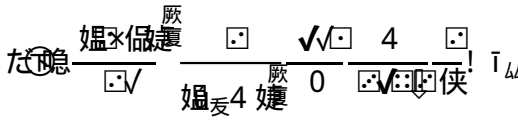

Equation 3: Calculation of reduced CCS (┤表

Drift time data is obtained from standards with known CCS and a calibration curve created, by plotting reduced CCS against drift time, and fitting to determine the A

and B compensation values required for equations 2 and 3, which can then be utilised to determine the CCS of the protein of interest.

1.7.2 ESI-IMS-MS as a Tool for Studying Amyloid Protein Conformation

Ion mobility mass spectrometry has proven unprecedented in its ability to provide information about the structural alterations and misfolding events occurring in a number of amyloid disease related proteins. This has allowed the determination of fundamental, mechanistic details relating to amyloid protein aggregation, including structural changes, kinetics, dynamics, binding interactions, and degrees of heterogeneity in populations from a variety of disease causing proteins, including α-syn (Bernstein *et al.*, 2004; Illes-Toth *et al.*, 2015; Illes-Toth *et al.*, 2013; Mason *et al.,* 2016) and amyloid-β (Alzheimer's disease) (Young *et al.*, 2015)

These proteins have previously been investigated by a range of classical biophysical methods, such as FTIR, CD and NMR spectroscopy, however extracting information pertaining to the aggregation kinetics using these methods is hindered by the transient nature of oligomers species, their low concentrations and the co-population of a range of different oligomeric species of the same mass which cannot be distinguished from each other by any of these methods.

ESI-IMS-MS by contrast has a unique advantage to aid in determining amyloid kinetics and conformational dynamics due to its sensitivity, speed of analysis and

ability to resolve heterogeneous populations (Smith *et al.*, 2009; Young *et al.*, 2015; Beveridge *et al.,* 2013).

1.7.3 Potential Limitations of ESI-IMS-MS

Because of their intrinsic disorder, IDPs display structural heterogeneity within the gas-phase, that is not observed with folded, globular proteins. Initial investigations into IMS suggested that IDPs were retaining memory of their structural flexibility in the absence of solvents, and all solution structures were surviving and being recorded in ESI-IMS-MS experiments (Shelimov and Jarrold, 1997). Other fundamental studies however, indicated that whilst folded proteins retain their native-like states in the gas-phase, and experimentally derived CCSs have been shown to be consistent with theoretical values (Ruotolo *et al.*, 2015; Scarff *et al.*, 2008; Saikusa *et al.*, 2013), those with less secondary structure may undergo unfolding during transfer from the solvent to gas-phase (Bohrer *et al.*, 2008; Zilch *et al.*, 2007), and the unfolding of subunits of globular proteins during ESI-IMS-MS has also been reported (Ruotolo *et al.*, 2005).

More recently however, it has been suggested that these disordered structures may undergo collapse in the absence of solvent. Advances in the understanding of how proteins escape electrospray droplets and form gaseous ions, as described earlier, have also added to concerns of the true relationship between solution and gas-phase conformations of proteins, in particular IDPs (Borysik *et*

al., 2015). Transient elements of secondary structure displayed by IDPs can reduce the hydrodynamic radius of the protein structure, giving rise to conformations of varying compactness during ESI-IMS-MS experiments (Beveridge *et al.*, 2015). It is now understood that IDP domains could remain elongated in the gas-phase, much like the true extended conformations of some proteins, or they may undergo structural collapse in the absence of solvent, leading to more compact, folded structures (Pagel *et al.*, 2013), and therefore care must be taken when interpreting ESI-IMS-MS data.

Combining ESI-IMS-MS experiments with methods such as small-angle X-ray scattering (SAXS), or by comparison of experimentally derived CCSs obtained by ESI-IMS-MS with those determined via molecular dynamics simulations, has allowed gas-phase derived structures and those present in solution to be truly compared, and these have yielded some concerning results. SAXS, in combination with genetic algorithm judging optimisation of ensembles (GAJOE) for validation, confirmed there was an absence of gas-phase determined structures, for a range of IDPs, in solution. IDPs were found to sample a 3- to 5-fold broader conformational space in the gas-phase compared to solution. A unimodal distribution of conformations was observed using SAXS, whereas three subpopulations of extended, intermediate and compact conformations were observed by ESI-IMS-MS (Borysik *et al.*, 2015). This suggests that the ESI process is generating additional subpopulations, and conformations, with the proteins observed to become more compact in the absence of solvent (Borysik

et al., 2015). SAXS also demonstrated compaction of the sw15-sfr1 protein, which has a role in homologous recombination, in the gas-phase, where structures were observed to be 56% more compact upon ESI-IMS-MS (Saikusa *et al.*, 2013). Molecular dynamics simulations conducted alongside ESI-IMS-MS of the p53 protein also determined regions of the protein complex to have 50-60% more compact conformations than those predicted under solution conditions (Pagel *et al.,* 2013).

Authors of these studies therefore suggest that extended IDPs can become trapped in ESI droplets during the electrospray process and become ionised more akin to globular proteins, undergoing structural collapse during solvent evaporation. The subpopulations observed via ESI-IMS-MS therefore may represent an array of ionisation techniques, as opposed to pre-formed states present in solution (Borysik *et al.*, 2015; Saikusa *et al.*, 2013; Pagel *et al.*, 2013). Care must therefore be taken when interpreting ESI-IMS-MS data, as the CCS determined experimentally may not necessarily represent the true CCSs observed in solution.

1.8 ESI-IMS-MS of α-Synuclein

1.8.1 ESI-IMS-MS of WT α-Synuclein

Due to its intrinsic disorder, ESI-IMS-MS acquisitions of WT αsyn yield results with altered CSD表and conformational dynamics dependent on the acquisition

parameters, and the composition of the buffers, therefore there is are a variety of different reports. In positive ion mode, a variety of CSD表have been reported in the literature for the monomeric protein, when acquired in similar, near physiological solution conditions. Several of these reports also note the presence of dimeric species with varying CSDs, and all have been summarised in table 1.2.

The conformational dynamics are slightly different between reports. One study reports four distinct conformations, spanning CSI表+24 to +14, +17 to +10, +13 to +7 and +10 to +5 (Beveridge *et al.*, 2013), whereas another reports detection of three distinct conformations, with average CCS表of 1200ð^2, 1500ð^2 and 2530ð^2 detected (Illes-Toth *et al.*, 2013), and another just two conformational families with average CCS of 1043ð^2 and 2742ð^2 was reported (Beveridge *et al.*, 2015). More recently, as many as eight distinct conformations have been identified by the use of Gaussian fitting to resolve conformational families, and these show a distinct pattern of extended conformations reducing in intensity before disappearing in favour of more compact species (Mason *et al.*, 2016).

The CSD and conformational distribution of WT ŧsyn is altered by solution conditions such as altered pH. A number of studies utilising buffers with a lower pH yielded a range of results, including +12 to +3 at pH 2.5 (Beveridge *et al.*, 2015) and +12 to +3, with dimers of +13 to +7 (Beveridge *et al.*, 2015), showing a narrowed CSD and increased population of more compact conformational species.

Monomer CSD	Dimer CSD	pH	Reference
+24 to +5	-	6.8	Beveridge *et al.*, 2013
+20 to +5	-	6.8	Beveridge *et al.*, 2015
+20 to +5	+23 to +10	6.8	Phillips *et al.*, 2015
+20 to +6	-	7.0	Illes-Toth *et al.*, 2015
+19 to +5	-	6.8	Beveridge *et al.*, 2013
+18 to +6	+21 to +13	6.8	Illes-Toth *et al.*, 2013
+15 to +5	-	6.8	Mason *et al.,* 2016
+13 to +4	+15 to +7	7.4	Kang *et al.*, 2012

Table 1.2: Comparison of WT ΠSyn Charge State Distributions

Comparison of previously reported monomeric and dimeric WT Πsyn CSDs, acquired using positive ion mode ESI-IMS-MS.

Negative ion mode ESI has also been utilised to investigate WT Πsyn. CSD表of -16 to -6, with dimers of -21 to -17 when analysed at pH 7 was reported (Bernstein *et al.*, 2004), with an average 喷of 2530 ð².

Decreased CSD表 favouring more compact conformations at altered pH conditions have also been observed in negative ion mode, with a CSD of -11 to -6, centred at the -8 ion reported at pH 2.5, and the average CCS was also demonstrated to decrease to 1690ð² (Bernstein *et al.*, 2004). It appears therefore that there is a large degree of heterogeneity in the observed data sets and the mode of acquisition is critical in determining the observed CSD. Nevertheless, all

studies observed populations of extended and compact states when analysed by MS.

1.8.2 ESI-IMS-MS of Tsyn Ligand Binding

ESI-IMS-MS is proving a useful tool to analyse the interactions of IDPs such as Tsyn with a variety of ligands such as metal ions, to determine their effects on the conformational dynamics of the proteins.

Investigations utilising ESI-IMS-MS with 10mM ammonium acetate buffer, deduced that the dominant CSI of Tsyn shifted from +14 to +8 upon addition of copper. This also coincided with an increase in the more compact conformations at the majority of CSIs, for example at the -8 CSI, unbound protein was present in 3 conformations, with of the protein present in the most compact of these conformations. Upon binding of copper however, this increased to 30% of the total protein at this CSI (Natalello *et al.*, 2011). More recently another study utilising ESI-IMS-MS to investigate copper binding also demonstrated an increased CSD, from +15 to +5 to +16 to +5, and an increase in the more compact conformations within CSIs, upon the binding of one or more copper ions (Mason *et al.*, 2016).

These observed increases in the compact state correlate with an increase in aggregation rates and demonstrate the importance of the compact state in aggregation

ESI-IMS-MS has proven itself unprecedented in its ability to categorise the conformational dynamics of IDPs such as T-syn, and is an incredibly useful tool for investigating disease-relevant proteins and potential drug candidates or targets.

1.9 Aims and Objectives

The overall hypothesis of the work is that Tsyn aggregation can be modulated by altering the population of the compact aggregation-prone state by post translational modifications and ligand binding. Here ESI-IMS-MS and a range of spectroscopy techniques were used to investigate the conformational changes and aggregation of Tsyn *in vitro*. Cell culture models were used to investigate intracellular aggregation.

To achieve these aims, the following objectives were identified:

- ¿ To determine the effect of post translational modifications in the form of phosphorylation mimics on the metal binding characteristics of Tsyn: the subsequent effects on the conformation of the monomeric state will be determined by ESI-IMS-MS and resulting aggregation properties investigated.
- ¿ To determine if aggregation of Tsyn can be inhibited by the presence of small molecule inhibitors. To this end alterations of the compact state of the protein and the model of ligand interaction will be investigated by ESI-IMS-MS in the presence of curcumin derivatives.
- ¿ To determine how the phosphorylation state of Tsyn in cell culture affects copper-induced intracellular aggregation and determine if copper-induced aggregation can be inhibited using curcumin derivatives.

Chapter 2 - Materials and Methods

2.1 Materials

2.1.1 Buffers and Solutions

Buffer solutions are shown in table 2.1.1.

Buffer	Composition
TBS	50mM Tris (Fisher Scientific #77-86-1), 150mM NaCl (Fisher #10428420) (pH 7.6)
TBS-T	50mM Tris, 150mM NaCl, 0.05% Tween20 (Fisher #9005-64-5) (pH 7.6)
Anion Exchange Buffer A	25mM Tris, 10mM NaCl (pH 8.0)
Anion Exchange Buffer B	25mM Tris, 1M NaCl (pH 8.0)
Blocking Buffer 1	TBS, 5% dried milk (Marvel), 0.05% Tween20
Blocking buffer 2	TBS, 0.5% dried milk (Marvel)
Complete Media	DMEM (Thermo Fisher #42430-025), 50,000 units penicillin/0.1mg/ml streptomycin (Thermo #15140-122), 10% FCS (Thermo #10270-106)
E. coli Cell Lysis Buffer	10mM Tris, 100¾g/ml Lysozyme (Sigma Aldrich #L6876), 20¾g/ml DNase (Sigma #DN25), 20¾g/ml RNase (Sigma #RN6513), Protease Inhibitor Cocktail (Sigma #SRE0055), PMSF (Thermo #36978) (pH 8.0)
Gel Running Buffer	25mM Tris, 192mM glycine (Fisher #56-40-6), 0.1% SDS at pH 8.5
Lysogeny Broth (LyB)	10g Tryptone (Sigma #T7293), 5g Yeast Extract (Oxoid #LP0021), 10g NaCl
Size Exclusion (SE) Buffer	25mM Tris, 10mM NaCl at pH 8.0

Table 2.1: Buffer solutions.

2.2 Methods

2.2.1 Protein Preparation

2.2.1.1 Protein Production

A pET23a plasmid containing the appropriate T-syn insertion (WT or the mutants S87D or S129D) was combined with BL21-Gold DE3 competent *Escherichia coli (E. coli)* cells (Agilent Technologies, #200121) in a culture tube at a ratio of 1:50, v/v, alongside a control tube containing no plasmid. Tubes were kept on ice for 30mins with occasional mixing, followed by heat-shock in a water bath at 42ºC for 45s, followed by a further 2mins on ice. Sterile LyB was added, followed by incubation with shaking at 37ºC for 35mins. The starter cultures were centrifuged at 3,000 rpm for 5mins, in a Thermo Fisher Fresco 21 centrifuge, 80% of the supernatant was discarded, and cells were resuspended in the remaining 20%. Petri dishes were prepared with LyB containing agar and 1% ampicillin (Fisher Scientific, #FL-04-0406). 90% of the resuspension containing the plasmid was added, before incubation overnight at 37ºC. Following incubation, one colony was selected from the plate and added to LB-broth containing 100mg/ml ampicillin, before incubation overnight at 37ºC with shaking at 250rpm on an orbital shaker. Five 2L conical flasks containing 1L auto-induction media without trace metals (Thermo #K6803) were warmed in an incubator at 37ºC overnight.

The following day, 15ml of incubated culture was added to each conical flask, which were then further incubated with at 37ºC with agitation at 250rpm for 24hrs.

Cell pellets were collected by centrifugation at 8,000 rpm, in a Sorval RC6+ centrifuge using a F10x 6x500Y rotor, for 20 minutes, and the supernatant discarded. If purification was not to be performed immediately, pellets were frozen and stored at -20ØC.

2.2.1.2 Protein Purification

2.2.1.2.1 Crude Purification

Cell pellets were thawed at room temperature for 30mins if required, before resuspension in 50ml *E. coli* cell lysis buffer (table 2.1.1) and incubation at room temperature for 30mins. The cell lysate was put on ice before further lysis via sonication at 45% for 1 minute, in pulses of 10s on, followed by 10s off. Insoluble material was removed by centrifugation at 10,000 rpm, in an Eppendorf 5804 R centrifuge, for 40mins before acidification to pH 4.5 by the addition of HCl (Fisher #A508). The lysate was centrifuged at 10,000 rpm for a further 30mins, in the same centrifuge, to remove any remaining insoluble material, before neutralisation to pH 8.0 with addition NaOH (Fisher #1310-73-2).

2.2.1.2.2 Anion Exchange Chromatography

Anion exchange chromatography was performed on an AKTA Prime (GE Healthcare, UK) liquid chromatography machine using a 50ml column loaded with Q-sepharose resin (Sigma-Aldrich, #GE17-0510-01), equilibrated with three

column volumes of buffer A (table 2.1.1) at 4 ØC. The protein was loaded onto the column at 3ml/min in buffer A and eluted using buffer B (table 2.1.1) via a gradient protocol of 20ml 0-20%, 100ml 20-80% and 20ml 80-100%. Fractions containing the highest concentration of protein were selected from the chromatogram, as shown in appendix 2A, and the presence of protein confirmed by SDS-PAGE electrophoresis. Fractions containing the highest concentration of protein were selected for buffer exchange using SnakeSkin dialysis tubing (Thermo Scientific, #68035) floated in ultrapure distilled water (ddH_2O) with stirring at 4ØC. Water was replaced 6 times over 24hrs, before the fractions were removed, snap-frozen in liquid nitrogen, then freeze-dried to remove the water and lyophilise the protein.

2.2.1.2.3 SDS-PAGE

Plates were set up as per manufacturer¶s instructions (BioRad) with a 1.5mm gap between the two, and gels cast as per table 2.1 on the following page, with 15 well combs inserted whilst setting to create sample wells.

Samples were mixed 1:1 with tris-glycine loading buffer before loading into wells, alongside a pre-stained, broad range protein ladder (NEB, #P7706S). Electrophoresis was performed, utilising the previously described gel running buffer (Table 2.1.1) at 150V for 1hr before staining with Instant Blue (Expedeon,

#ISB1L) for 20 minutes. Gels were imaged on a LiCor scanner utilising the Image Studio software with the 700 channel selected.

Reagent	Resolving Gel Volume (mL) (10%)	Stacking Gel Volume (mL) 3%
MilliQ ddH_2O	9	3.6
2M TrisHCl pH 8.8	4.5	-
0.5M TrisHCl pH 6.8	-	0.7
10% (w/w) SDS	0.225	0.050
40% 29:1 acrylamide:bisacrylamide	9	0.6
10% (w/w) APS (Sigma #A3678)	0.1125	0.025
TEMED (Sigma #9281)	0.03	0.01

Table 2.2: SDS-PAGE Gel Components.

Components of an SDS-PAGE gel. Reagents were added in the order shown above.

2.2.1.2.4 Size Exclusion Chromatography

Previously freeze-dried protein was resuspended in size SE buffer (table 2.1) before loading into a 5ml injection loop using a sterile syringe filter. Size

exclusion was performed using a HiLoad 26/600 Superdex 200 pg column (GE Healthcare, UK), on an AKTA prime machine, equilibrated with 900mls SE buffer. Protein was eluted at a flow rate of 1ml/minute at a temperature of 4ØC. Fractions containing the highest protein concentrations were identified from the chromatogram, as shown in appendix 2B, and subjected to SDS-PAGE electrophoresis as described in section 2.2.1.2.1. Fractions containing the highest and purest protein, based on SDS-PAGE results, were selected for dialysis in SnakeSkin dialysis tubing (Sigma #86035), and buffer exchange was performed utilising the same method as following anion exchange. Fractions were snap frozen in liquid nitrogen, freeze dried and stored at -20ØC until required.

2.2.1.2.5 Determination of Protein Concentration

A small amount of protein was dissolved in the appropriate buffer, depending on the experiment performed, and its absorbance acquired at 280nm, on either a UV/Vis spectrophotometer (Jenway) or a NanoDrop spectrophotometer. Absorbance readings and the extinction coefficient of Tsyn, 5960 $M^{-1}cm^{-1}$, were used to determine the molar concentration.

2.2.2 Dot Blotting

WT Tsyn and potentially phosphorylated Tsyn was spotted onto nitrocellulose membrane with a 0.45mm pore size (Sigma #GE10600002) before blocking with

blocking buffer 1 (table 2.1) for 1hr with rocking at room temperature. Membranes were washed with TBS-T (table 2.1) three times for 3mins. The primary polyclonal rabbit antibody, anti phospho-synuclein pSer^{129} (Sigma #SAB4503996), or monoclonal mouse anti-α-syn, syn211 (Sigma #S5566) diluted at 1:2000 in TBS-T with 5% milk, was added to the membranes for 1hr at room temperature with rocking. The membranes were washed with 1xTBS-T an additional three times, before addition of the secondary antibody, IR Dye 680RD goat anti-rabbit immunoglobulin (Ig) (Thermo #31105), at 1:15,000 in TBS-T with 5% milk for 1hr at room temperature with rocking. The membranes were washed a final three times with 1xTBS-T before imaging using a LiCor scanner utilising the Image Studio software with the 700 nm channel.

2.2.3 ESI-IMS-MS

All mass spectra and ion mobility information were acquired using electrospray ionisation travelling wave ion mobility mass spectrometry, performed on a Synapt-G2 tri-wave ESI-IMS-MS (Waters, Manchester, UK) in positive ion mode utilising helium (He) and nitrogen (N_2) gases. Mass spectrometry settings for cone voltage, source temperature, trap and transfer collision energies, trap bias, IMS wave settings, backing pressures and helium cell pressures were optimised for each set of mass spectrometry experiments. These will be specified within the appropriate chapters. The Synapt was attached to an Advion Triversa

NanoMate autosampler, operated with gas pressure at 0.7 psi and tip voltage of 1.7kV.

2.2.3.1 Calculation of Calibrant Protein CCS

The Synapt was calibrated internally to within a 95% confidence window, using sodium iodide (NaI) (Waters #700001593). Proteins with known masses and CCS, ubiquitin from bovine erythrocytes, cytochrome c from equine heart, and myoglobin from equine heart, were dissolved in 50% acetonitrile, 10% trifluoroacetic acid and 40% ddH_2O (v/v/v) to a final protein concentration of 10 ¾M and data acquired under the appropriate mass spectrometry settings, dependent on the experiment being performed. Mass spectra were examined using the MassLynx 4.1 software (Waters, Manchester), and ATDs of the different CSIs of the calibrant proteins were extracted.

The peak arrival time, or drift time, (tD) was determined from the raw data, and converted to corrected drift times (tD') using equation 4 below:

Equation 4: Calculation of Corrected Drift Times at a Single Wave Height.

Calculation of corrected drift times, where t□ is corrected drift time, tD is measured drift time. The C constant is derived from within the mass spectrometry software, as the □nhanced duty cycle delay coefficient□and usually ranges from 1.4-1.6 dependent on the machine used.

Reduced CCSs (噯) of each CSI for the calibrant proteins were also determined using equation 5 below:

だ㊀鴨だ媼ⅵ·□ 脹 ∫線修

Equation 5: Calculation of calibrant reduced CCS, where *z* is the charge state of the ion and *r* is the reduced mass.

Corrected tD' were then plotted against 噯 and a line of best fit determined, as shown in figure 2.1, to determine the A' and B values required to determine the 噯 of the protein conformation as per equation 3 in chapter 1.

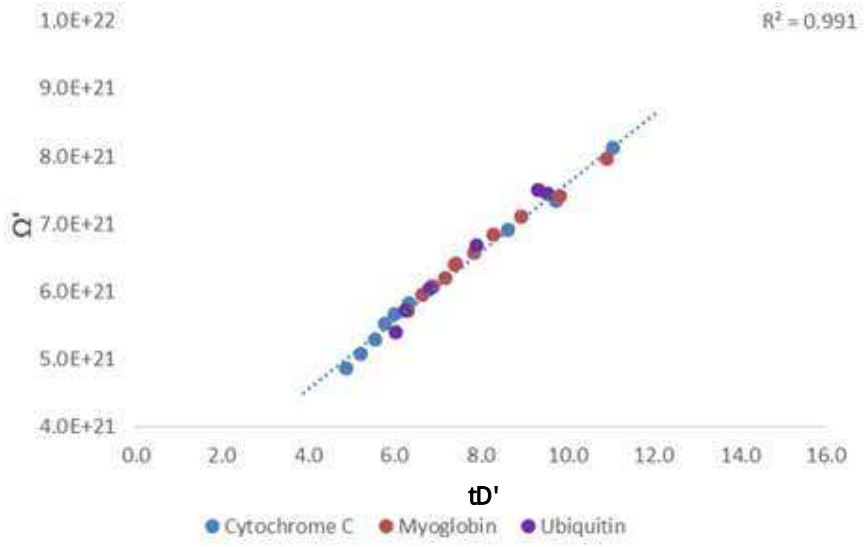

Figure 2.1: Example Calibration Data Set.

Example calibration data set acquired utilising tD' and 噯 for cytochrome c, myoglobin and ubiquitin. R^2 value shows the regression analysis.

2.2.3.2 Gaussian Fitting for Determination of Conformational Equilibrium

Gaussian models of probability were utilised to determine the relative proportions of the different conformations present within each CSI of the protein, using ATD data obtained from the chromatograms. Fitting was achieved using the least square regression method, to fit the minimum number of Gaussian distributions under the chromatogram, via multiples of equation 6:

$$y = \frac{A}{w\sqrt{\pi/2}} e^{\frac{-(x-x_0)^2}{2.w^2}}$$

Equation 6: Gaussian equation utilised to determine conformational distributions at each CSI, where A is the total area under the curve, x_o is the centre of the peak, and w is the width of the peak at half height.

2.2.3.3 ESI-IMS-MS for the Study of Monomeric Proteins Interaction with Metals

Protein was resuspended in 50mM ammonium acetate (AA), and its concentration determined via NanoDrop, before dilution to 10¾M final concentration. Where appropriate, metal ions ($CuCl_2$, $FeCl_2$, $ZnCl_2$, $MgCl_2$, $MgCl_2$, FeS, ZnS, MgS) at 10, 20, 50 and 100¾M diluted in the appropriate buffer were added, and 5¾ of the sample was immediately injected into the mass spectrometer using the NanoMate autosampler, and mass spectra acquired in

the range 800-3000 *m/z*. Instrument parameters utilised for each experiment are outlined in chapter 3 and 4.

2.2.3.4 ESI-IMS-MS for the Study of Monomeric αSyn and Oligomeric Complexes Interaction with Curcumins

70µM WT αsyn was diluted in 50mM AA and, where appropriate, natural curcumin or the derivatives were added, to a final concentration of 10µM or 70µM, in a final DMSO concentration of 1% or ethanol concentration of 1% or 10% v/v. The appropriate concentration of DMSO and ethanol was also added to curcumin free samples as a control. 5µl of each sample was then loaded onto the mass spectrometer using a NanoMate autosampler, with spectra acquired in the range 500-3000 or 500-5000 *m/z*. When appropriate, samples were then incubated at room temperature or 37˚C, with or without agitation at 300rpm, for up to 48 hours for further analysis.

Instrument parameters are specified in chapter 4.

2.2.4 Thioflavin-T Assays for Aggregation Studies

2.2.4.1 Thioflavin-T to Assess Metal Induced αSyn Aggregation

WT, S87D and S129D αsyn were added to 50mM AA, and the concentration determined as described previously. 100mM stocks of $CuCl_2$, $FeCl_2$, ZnS, $MgCl_2$

and $MnCl_2$ were prepared in 50mM AA, and diluted to a final concentration of 1mM in the same buffer. 20mM ThT was prepared in 50mM AA, sterile filtered, and diluted to 100μM in the same buffer. Samples were prepared in a black 96 well plate (Thermo #437111) to the following final concentrations; protein 70μM, thioflavin-T 10μM and metal 70μM, with the addition of glass beads to aid agitation. Plates were analysed using a Clariostar plate reader (BMG Labtech) with readings taken hourly for 6 days, with excitation at wavelength 440nm and emission of 480nm.

2.2.4.2. Thioflavin-T to Assess the Effect of Curcumins on α-Synuclein Aggregation

WT αsyn was dissolved in 50mM ammonium acetate and the concentration determined as described. 100mM stocks of natural Curcumin and one of 13 of its derivatives were prepared in 100% DMSO, and diluted to a final concentration of 7mM and 1% DMSO in the same buffer. 20mM ThT was dissolved 50mM ammonium acetate, sterile filtered and diluted to 100μM in the same buffer. Samples were prepared to the following final concentrations; protein 70μM, ThT 10μM and curcumins 70μM. Samples were shaken continuously at 300rpm at 37°C for 6 days, then transferred to a black 96 well plate with the addition of 10μM ThT and analysed using a Clariostar plate reader with excitation at wavelength 440 and emission of 480nm.

2.2.4.3 Thioflavin-T to Assess the Effect of Curcumins on Lysozyme Aggregation

Lysozyme was prepared at a final concentration of 70¾M in ddH_2O at pH 2.5. 70¾M curcumin and 1% DMSO were added to the required samples, along with control samples containing 1% DMSO only. Samples were shaken at 650C for 6 days before being transferred to a black 96 well plate along with 10¾M ThT diluted in ddH_2O at pH 2.5 and analysed using a Clariostar plate reader with excitation at wavelength 440nm and emission of 480nm.5

2.2.5 Cell Culture

2.2.5.1 Maintenance of cell lines

SHSY5Y neuroblastoma cells of passage numbers 12-30 were maintained in T-75 cell culture flasks (Sigma #CLS3290) incubated at 37¸C with 5% CO_2, grown in DMEM media containing phenol red and glutamax, along with 10% Foetal Calf Serum (FCS) and 1% Pen/Strep (Thermo #15070063), a solution of containing 5000 units/ml of penicillin and 5000 ¾g/ml streptomycin. When confluence of around 80% was reached, cells were washed with 1% phosphate buffered saline (PBS) (Thermo #10010023) and unadhered using trypsin (Thermo #25300054). Following centrifugation at 10,000rpm in a Sorval RT7 centrifuge, and resuspension in 10mls media, cells were either passaged at a 1:3 ratio, when they reached a confluence of 80%, or counted using Trypan Blue dye (Thermo #15250061) and a Countess cell counter ready for experimental use.

2.2.5.2 Immunocytochemistry

Cells were plated in chamber slides at a confluence of 30,000 cells/well and left overnight to adhere before treatment with complete DMEM media. $CuCl_2$ was added at concentrations of 100μM, 200μM, 300μM, 400μM and 500μM. Cells were incubated for 48 hours before being rinsed with PBS then fixed in ice-cold 100% methanol at -20˚C for 10mins. Fixed cells were then treated with Sudan Black (Sigma #380B) for 10 minutes before being washed in PBS plus 0.05% tween20 three times for 3mins with agitation at 200rpm. Cells were blocked in TBS plus 5% powdered milk, and rocked for 1 hour at room temperature, before being washed with PBS as previously described. Primary antibodies, monoclonal mouse anti-αsyn (Sigma #S5566) or polyclonal rabbit anti phospho-synuclein $pSer^{129}$ at 1:2000 were added in TBS-T plus 5% powdered milk and rocked for 1hr at room temperature. Slides were washed further with 1xPBS before addition of the appropriate fluorescent secondary antibody Texas Red, either anti-mouse (Thermo #T862) or anti-rabbit (Thermo #T6391) at 1:1000 in TBS-T plus 5% powdered milk and rocked at room temperature for 1 hour. Slides were further washed with PBS before mounting with Vectashield DAPI mounting medium (Fisher #NC9029229) and cover slipping. Slides were then imaged using a fluorescent microscope, with 40x and 100x objectives, utilising Image Capture Pro software to acquire images.

2.2.5.3 Antibody Validation

To ensure the phos129 antibody was specific to phosphorylated forms of the protein, a simple dot blot control was performed, as described in section 2.2.2. As shown in figure 2.2 below, when the phos129 antibody was exposed to recombinant WT α-syn (A). No binding was observed, suggesting this antibody is unable to bind to the unmodified form of the protein.

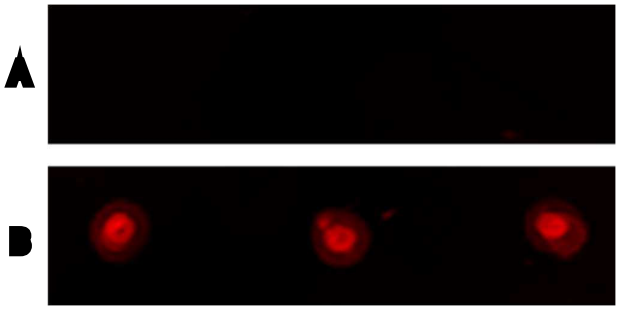

Figure 2.2: Phos129 Antibody Validation Dot Blot.

Dot blots of WT α-syn probed with primary antibodies A) phos129 for α-syn phosphorylated at serine-129, and B) Syn211 specific to unmodified WT α-syn, amino acids 121-125.

To ensure the fluorescent secondary antibodies described previously were specific to the syn211 and phos129 antibodies, control wells were included in immunocytochemistry experiments; one well negative for primary antibody and

positive for secondary antibody, and another well positive for primary antibody and negative for secondary antibody. Example images can be seen in figure 2.3.

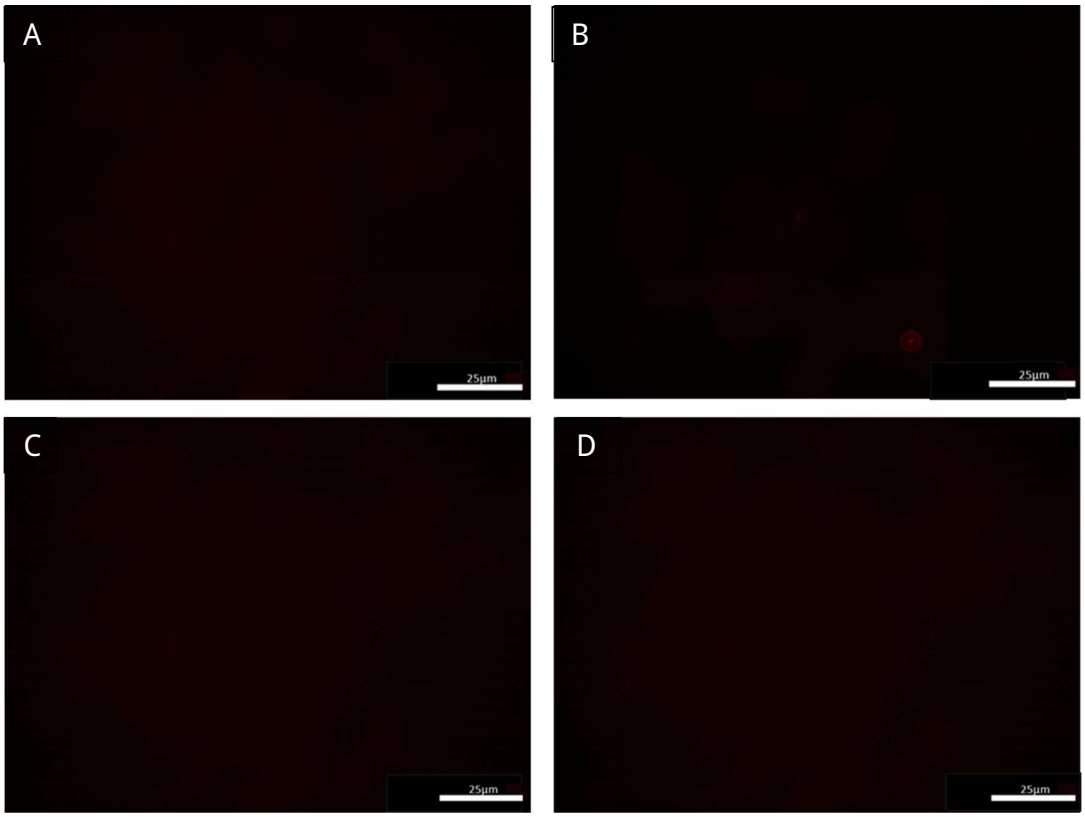

Figure 2.3: Secondary Antibody for Immunocytochemistry Validation.

Immunocytochemistry was performed on SHSY5Y cells as described in section 2.2.5.2. A) Untreated cells +cyt211 and +Texas red, B) Untreated cells -cyt211 and +Texas red, C) Untreated cells +phos129 and +Texas red, D) Untreated cells -phos129 and +Texas red.

2.2.5.4 Trypan Blue Viability Assay

Cells were transferred into T-25 cell culture flasks (Sigma #CLS3815-24EA) at a confluence of 1,000,000 cells/flask and incubated overnight before treatment with complete DMEM media with the addition of CuCl2 at concentrations of 100┼M, 200┼M, 300┼M, 400┼M and 500¾M, and an untreated flask containing complete DMEM only. After 48hrs cells were unadhered with trypsin, centrifuged at 1000rpm for 5mins in a Sorval RT7 centrifuge, to form a pellet before resuspension in complete DMEM. 10¾ of cells were added to an equal amount of Trypan Blue, and total cell viability was determined using a Countess cell counter.

2.2.5.5 Analysis of Cell Images for Aggregates and Apoptosis

Four Images were taken of each experimental condition, utilising the Image Capture Pro software, to ensure at least 200 cells were present within each the data set. Data sets were then blinded by a second party through a random file naming system. 200 cells per data set were then counted for cells containing aggregates inclusions, or one of the signs of apoptosis, highlighted in chapter 5. Three repeat experiments were compared, and positive cell numbers were averaged to synthesise graphs, using the Prizm software (GraphPad, USA).

2.2.5.6 Analysis of Cell Images for Fluorescence Intensity

Fluorescence intensity of cells stained for T-syn was analysed using the ImageJ software. Ten cells per condition were selected using the software, along with a small section of the background image for each cell, extracting data for the area, integrated density, and mean grey value for each cell. The corrected total cell fluorescence (CTCF) of each selected cell was then calculated by multiplying the area of the cell by the mean fluorescence of the background readings (McCloy *et al.*, 2014; Burgess *et al.*, 2010). Values from the 10 cells were then averaged, and three repeat experiments were compared to perform statistical analysis.

2.2.6 Statistical Analysis

All statistical analysis for ThT assays and cell experiments was performed utilising the non-parametric, Kruskall-Wallis ANOVA test, on the Stats Direct software (Stats Direct Ltd, UK). This was then paired with the Conover-Inman test, to compare significance between all conditions. All graphs were created using the Prism software.

Chapter 3 – The Effect of Phosphorylation Mimics and Metal Ions on α-Synuclein Conformation and Aggregation

3.1 Introduction

It has been well documented that αsyn found in the LB of PD patients has undergone a variety of PTMs including phosphorylation, ubiquitination, nitration, acetylation and truncations (Barrett and Greenamyre, 2015; Duce *et al.*, 2017; Oueslati, 2016; Fujiwara *et al.*, 2002; Popova *et al.*, 2015; Schmid *et al.*, 2013). The majority of PTM sites are found within the highly disordered C-terminal region of the protein, including the phosphorylation sites Y125, S129, Y133 and Y136 (Oueslati, 2016). LBs are also known to be highly metal rich, and it has been well established that metal ions such as copper can accelerate the aggregation of αsyn *in vitro* (Uversky *et al.*, 2001). The metal binding domains are primarily located within the C-terminal region of the protein, in close proximity to and encompassing the phosphorylation sites as shown in figure 1.2 in chapter 1.

The relationship between phosphorylation and metal-induced aggregation of αsyn and whether this has clinical relevance, have still to be fully determined, and investigations thus far have yielded conflicting results. Studies utilising C-terminal fragments of αsyn, of residues 119-132 indicated there to be no effect of S129 phosphorylation on the proteins interaction with metal ions (Liu and Franz, 2007). However, a later study utilising the fragment 107-140, encompassing the entire C-terminal region, suggested S129 phosphorylation resulted in increased

binding affinities for the divalent metals Cu^{2+}, Pb^{2+} and Fe^{2+} (Lu *et al.*, 2011). There have however been no studies utilising the full protein, and therefore it is still to be fully determined what the relationship between phosphorylation and metal ion binding is in terms of PD pathology.

3.1.1 Phosphorylation of τsyn

τSyn has five known phosphorylation sites; two at serine residues 87 and 129, and another three located at tyrosines 125, 133 and 136 (Oueslati, 2016; Paleologou *et al.*, 2010). These phosphorylation sites appear to be conserved throughout all synuclein species in humans (Paleologou *et al.*, 2010). Phosphorylation at tyrosine residues appears to be predominantly associated with membrane binding, with phosphorylation at Y125 specifically playing an important role (Schreurs *et al.*, 2014). Data currently suggests that phosphorylation at S87, S129 and Y39 all prevent the binding of τsyn with biological membranes. It has also been suggested that phosphorylation at Y125 has a neuroprotective role and prevents the formation of neurotoxic oligomeric species (Chen *et al.*, 2009).

The role of phosphorylation at the serine residues is currently less clear, though phosphorylation at S129 has been suggested to have a role in autophagy and cellular clearance of τsyn via proteolytic degradation (Chau *et al.*, 2009; Machiya *et al.*, 2010; Tenreiro *et al.*, 2014). Under normal physiological conditions,

approximately 4% of αsyn is phosphorylated at one or more of these sites (Tenreiro *et al.*, 2014). In LBs however, 90% of αsyn has been found to be phosphorylated at serine 129, suggesting a pathological role for this modification (Anderson *et al.*, 2006). The questions of how αsyn phosphorylation modulates αsyn normal function, and what role this phosphorylation has on the aggregation of the protein, whether it be suppressive or enhancing of aggregation, are still yet to be fully determined.

3.1.1.1 Pathological Role of αsyn Phosphorylation

A variety of animal model studies have been conducted to investigate the role of S129 phosphorylation on the pathogenesis of PD, however these studies have produced conflicting results. Studies conducted in *Drosophila melanogaster* and transgenic murine models both suggested a pathogenic role for the modification (Chen and Feany, 2005; Freichel *et al.*, 2007), whereas a study utilising *Caenorhabditis elegans* nematode worms suggested a protective role for S129 phosphorylation, via a reduction in membrane binding (Kuwahara *et al.*, 2012). In *Drosophila*, preventing phosphorylation via amino acid substitution from serine to alanine both increased aggregate formation rates and reduced dopaminergic loss, whilst mimicking phosphorylation with amino acid substitution to aspartic acid enhanced the toxicity of αsyn. This suggests that increased aggregate load may be protective, whilst also suggesting a pathological role for phosphorylation

(Chen and Feany, 2005). Similarly in a transgenic mouse model where A30P αsyn was overexpressed, all pathologically relevant αsyn samples extracted from the mouse models were found to be phosphorylated at S129, suggesting a pathologic role for the modification (Freichel *et al.*, 2007).

A more recent study utilizing budding yeast *Saccharomyces cerevisiae*, found that blocking phosphorylation using an amino acid substitution of serine to alanine, resulted in a slower clearance of αsyn aggregates from an SH-SY5Y cellular model in relation to WT αsyn, which is in agreement with the findings from the *Drosophila* study and suggests it may have a role in autophagy (Tenreiro *et al.*, 2014). The same study concluded that phosphorylation reduced the toxic effects within the SH-SY5Y cell model (Tenreiro *et al.*, 2014). Further studies in a rat models concluded there was no difference between phosphorylated and non-phosphorylated forms of the protein, and suggested modification at this site to be neither protective or pathogenic (da Silveira *et al.*, 2009; McFarland *et al.*, 2009).

Currently it is unclear what role phosphorylation of αsyn has on the pathogenesis of PD. It is difficult to come to a definitive conclusion from the highly contradictory, currently available data, but it is clear that phosphorylation at serine 129 plays an important role in the aggregation of αsyn.

3.1.1.2 Phosphomimetics of Tsyn

Phosphorylation at serine residues can be mimicked by substituting the native amino acid for aspartic acid, whereas glutamic acid can substituted to mimic phosphorylation at a tyrosine or threonine residue (Dephoure *et al.*, 2013). Mimicking phosphorylation of a serine residue in this manner functions due to the carboxyl group on aspartic acid, which provides a similar negative charge (-1) to that of phosphoserine (-1.5), thus the conformational dynamics and any ligand interactions with the protein would be expected to behave in a similar manner. This process has been confirmed using the tau protein, where SDS-PAGE and cellular studies confirmed that substituting serine for aspartic acid at residue 327 resulted in the same conformational changes and microtubule assembly properties observed with phosphorylated tau (Leger *et al.*, 1997). Phosphomimic mutants are now extensively used in research for a variety of applications (Dissmeyer and Schnittger, 2011;Fraser *et al.*, 2014), including conformational studies(Hara *et al.*, 2006), mass spectrometry (Jovcevski *et al.*, 2015) and studies into the effects of phosphorylation on Tsyn aggregation (Chen and Feany, 2005; Chau *et al.*, 2009; Oueslati *et al.*, 2012; Paleologou *et al.*, 2008).

3.1.2 The Role of Metal Ions in Parkinson's Disease

Increasing evidence is emerging for the role of dysfunctional metal homeostasis in the development and progression of a number of neurodegenerative diseases (Chen *et al.*, 2016). Concentrations of several transition metals, including copper and iron, are known to be increased in aging brains (Morita *et al.*, 2001), and the levels of these metals, along with zinc, are also known to be elevated in the brains of patients with PD and AD, and are found in increased concentrations within the LBs of PD patients (Dexter *et al.*, 1989;Riederer *et* al., 1989; Hirsch *et al.*, 1991;J enner and Olanow, 1996;Lovell *et al.*, 1998).

3.1.2.1 Homeostasis and the Physiological Role of Metal Ions

Metal ions play vital roles in a number of physiological processes including, but not limited to, cell structure maintenance, gene expression regulation, neurotransmission and antioxidant response (Chen *et al.*, 2016). Oligodendrocyte development and neurotransmitter production are also processes which have also been shown to be dependent on metal ions (Todorich *et al.*, 2009; Fitzpatrick, 1989), therefore they are extremely important for a variety of normal processes occurring within the human brain.

Transition metals, which include copper, iron, zinc, magnesium and manganese, are essential co-factors for almost half of all proteins (Waldron *et al.*, 2009). For example, tyrosine hydroxylase, which catalyses the conversion of tyrosine to

dopamine, requires ferrous iron to complete its function (Fitzpatrick, 1989; Duce *et al.*, 2017). Correct brain development in infancy is also known to require optimum iron levels (Lozoff and Georgieff, 2006), and physiological iron is also important for the regulation of cellular development, mitochondrial respiration, and the production of myelin (Duce *et al.*, 2017). Iron response elements are also a known factor in post-transcriptional control of gene expression, and these are commonly found in proteins involved in iron homeostasis (Wang and Pantopoulos, 2011). Iron is the most abundant trace element in the human body (Carboni and Lingor, 2015), and in the form of Fe(II) has been demonstrated to caused oxidative damage within cells via promoting the formation of reactive oxygen species (ROS), leading to oxidative stress. This includes the formation of hydroxyl free radicals via a Fenton reaction with hydrogen peroxide (H_2O_2) (Santner and Uversky, 2010).

It has also previously been proposed that T-syn may possess some ferrireductase activity and can reduce Fe^{3+} to Fe^{2+} utilising copper bound to the protein to cycle between oxidized and reduced forms of the metal, and this may explain why the protein has the ability to bind these metals (Davies *et al.*, 2011). Copper is also a known cofactor for several cellular proteins, such as cytochrome c oxidase, which is involved in the mitochondrial production of ATP, and Cu/Zn-superoxide dismutase (SOD1), which plays a role in ROS detoxification.

3.1.2.2 Metals and Parkinson's Disease: Epidemiology and Pathology

Initial investigations into the role of metals in PD pathogenesis began over ninety years ago. Despite this, there has been no progress in utilising metals as a therapeutic target thus far. Elevated levels of iron in the brains of Parkinson's patients was first reported by Lhermitte and colleagues as far back as 1924, when deposits of the metal were observed to be co-localised to Lewy bodies using Pearl's staining (Lhermitte *et al.*, 1924). The link between heavy metals and PD was further solidified in 1989, when two separate studies identified increased levels of iron and zinc in the brains of PD patients, upon post mortem examination (Dexter *et al.*, 1989; Riederer *et al.*, 1989). Some studies have also documented an increase in the Fe^{3+}/Fe^{2+} ratios in the brains of PD patients (Sofic *et al.*, 1988; Riederer *et al.*, 1989). In contrast, copper levels in the *SNPC* were found to be reduced in comparison to control brains (Dexter *et al.*, 1989), however high levels of copper had also been identified in the cerebrospinal fluid of PD patients around that time (Pall *et al.*, 1987).

A number of epidemiological studies also noted that individuals with chronic industrial exposure to heavy metals, including copper, iron, manganese, zinc and aluminium amongst others, had an increased incidence rate of PD when compared with the general population (Gorell *et al.*, 1999; Gorell *et al.*, 2004; Coon *et al.*, 2006). This led to metal ions coming to the forefront of PD research, and metal homeostasis being identified as a potential therapeutic target in this area.

Since these initial observations, increasing evidence has been gathered relating altered metal homeostasis to the progression of neurodegenerative diseases (Chen *et* al., 2016; Montes *et* al., 2014; Barnham *et al.*, 2004; Zecca *et al.*, 2004). In addition to concentrations of metals, such as iron and copper, being increased in normal aging brains (Morita *et al.*, 1994), they are also increased in the brains of patients with neurodegenerative diseases. High levels of copper, zinc, and iron are found in and around amyloid plaques in AD brains (Lovell *et al.*,1998). Increased levels of Fe(III) and reduced levels of the Fe(III)-binding protein ferritin were observed in the brains of PD patients (Dexter *et al.*,1991). Increased iron deposits in the *substantia nigra* are associated with -syn positive Lewy bodies in PD and neurodegeneration with brain iron accumulation (Hirsch *et al.*, 1991; Tofaris *et al.*, 2007).

Similar alterations in metal homeostasis were observed with toxin induced animal models of PD. An accumulation of iron was observed in the *substantia nigra* of 1-methyl-4-phenyl-1,2,3,6-tetrahydropyridine (MPTP)-treated mice, which is likely a result of the observed up-regulation of transferrin receptor expression and iron uptake (Kalivendi *et al.*, 2004; Mandel *et al.*,2004). Although these observations may be consequences of the disease progression, experimental studies using $FeCl_3$ injected directly into the *substantia nigra* of rats resulted in a 95% reduction in striatal dopamine and altered behaviour, supporting the idea that iron initiates dopaminergic neuron degeneration in PD (Youdim *et al.*, 1991).

3.1.2.3 Metals and τ-Synuclein

A large body of research is available to date regarding the interaction of τsyn with polyvalent metal ions such as copper, iron, manganese, lead and zinc, and has been reviewed by Santner and Uversky (2010, and more recently by Carboni and Lingor, (2015). It was concluded in these reviews that although it is known that some metals trigger the aggregation of τsyn and can exert cellular toxicity, not all mechanisms of metal-induced toxicity have been determined, and the interaction of τsyn with metal ions warrants further investigation in order to enable development of more specific and innovative drugs against PD.

2D-NMR spectroscopy is one method which has been utilized to investigate the binding of divalent metal ions to τsyn. Studies suggest these metal ions predominantly bind to the C-terminus of τsyn, at the DPDNEA motif (aa119-124), as shown in figure 1.2 in chapter 1, containing Asp-121, Asn-122 and Glu-123, which are believed to be the anchoring residues for Fe(II), Cu(II), Mn(II), Co(II) and Ni(II) (Binolfi *et al.*, 2006).

Copper is known to enhance the aggregation and fibrillation of τsyn *in vitro*, and an increased population of the more compact, aggregation prone states has been observed in the presence of this metal by NMR, circular dichroism studies, ESI-IMS-MS and calorimetric titrations (Natalello *et al.*, 2011; Binolfi *et al.*, 2008; Binolfi *et al.*, 2010; Mason *et al.*, 2016). Binding of metal ions to the C-terminus of the protein has been suggested to alter the charge of the protein, leading to

structural collapse (Bernstein *et al.*, 2004). Quantum and molecular dynamics simulations also indicated the binding of copper to H50 causes the development of a P-hairpin within the protein, at aa36-56, thus accelerating its aggregation (Yu *et al.*, 2015; Rose *et al.*, 2011). One example of this copper-induced conformational change can be seen in figure 3.1.

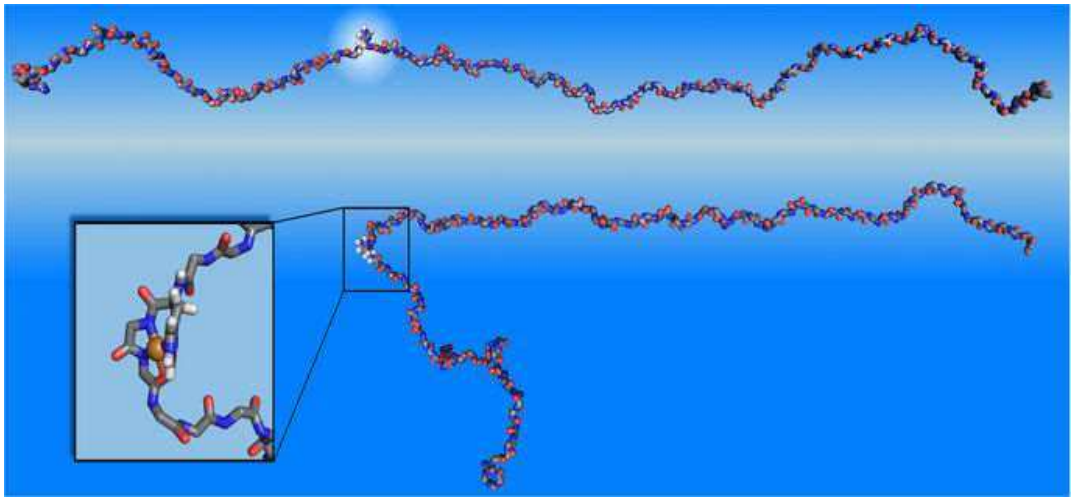

Figure 3.1: Example of a Copper-Induced Conformational Change to ΠSyn

Example of a Copper(II)-Induced Conformational Change to ΠSyn, as determined by molecular dynamics simulation. Top: Unbound Πsyn highlighting the H50 residue. Bottom: Binding of Cu (II) to H50 results in a P-hairpin fold at this residue (Used with permission from Rose *et al.*, 2011).

TSyn has been shown to have a high affinity for copper binding, and has been shown to bind the metal at three specific sites, though up to 16 potential binding sites have been proposed in the literature (Ahmad *et al.*, 2012). A high affinity binding site has been observed at the N-terminus, where the free nitrogen on the amino terminal anchors the metal ion. A second, lower affinity site has been observed at histidine 50, anchored by the imidazole ring of the amino acid, and a third low affinity site at the C-terminus involving the previously mentioned Aspo-121, Asn-122 and Glu-123 residues have also been identified (Binolfi *et al.*, 2012; Mason *et al.*, 2016; Binolfi *et al.*, 2006). The protein has been demonstrated to bind copper ions more readily than any other metal currently investigated (Binolfi *et al.*, 2006).

Iron has also been shown to increase the aggregation rate of Tsyn in vitro, leading to faster accumulation of protein aggregates and amyloid fibrils (Binolfi *et al.*, 2006; Uversky *et al.*, 2001). Divalent iron has also been demonstrated to bind to the C-terminus of Tsyn via 2D-NMR studies, and this metal also appears to be utilizing Asp-121 as an anchoring residue (Binolfi *et al.*, 2006; Peng *et al.*, 2010).

3.2 Aims and Objectives

In this chapter, ESI-IMS-MS along with ThT assays will be utilised to investigate the binding of a variety of metal ions to recombinant WT ŧsyn, and two mutant forms of the protein, where amino acid substitution from serine to aspartic acid has been utilized to mimic phosphorylation at both serine residues individually within the protein. The conformation of the protein upon metal binding was investigated to elucidate further data about the pathological relevance of both phosphorylation and metal binding in the progression of Parkinson's disease and other synucleinopathies.

The main aims of this chapter were to:

- Determine the relationship between phosphorylation of ŧsyn at serine residues and the subsequent alterations to the aggregation and conformational dynamics of the protein *in vitro*
- Determine the relationship between serine phosphorylation and the binding of metal ions, and the subsequent effects on the conformation and aggregation of ŧsyn *in vitro*
- Determine the relative contributions of each conformational state at each CSI for the three protein variants, with and without exposure to metal ions

3.3 Results

All mass spectrometry experiments in this chapter were performed under the following conditions, on a Synapt G2 Q-TOF mass spectrometer in positive ion mode; source temperature 60(0, sampling cone 45V, trap collision energy 2.0V, transfer collision energy 4.0V, Trap DC bias 45, IMS wave velocity 800 m/s, IMS wave height 200V, backing pressure 2.93mbar and helium cell pressure 1.42e3mbar.

ATDs were analysed to determine both the CCS of Tsyn and its phosphomimic variants at each conformation, and the relative proportion of each of these conformations at each CSI, under the different conditions.

3.3.1 Tsyn has an Altered Charge State Distribution and Conformational Equilibrium Between ESI-IMS-MS Acquisitions

As previously discussed, Tsyn is highly heterogeneous due to its intrinsic disorder, and therefore exists in a range of conformations at all times, dependent on its environment. These conformations range from highly compact, aggregation prone globular-like conformations at CSIs +8 to +5, to flexible, more extended worm-like structures at CSIs +18 to +9, and these can be observed using ESI-IMS-MS, as shown in figure 3.2.

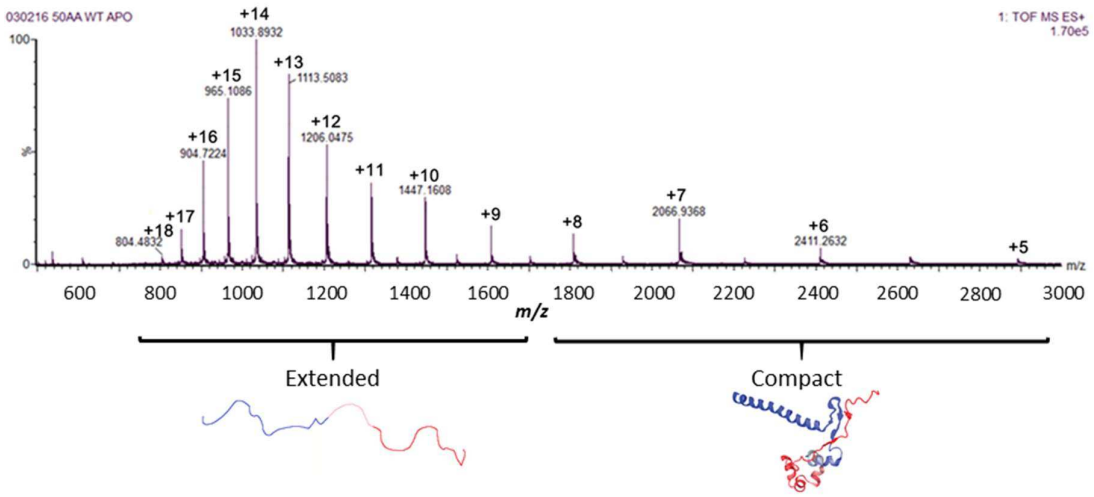

Figure 3.2. Typical ESI-MS Mass Spectra of WT α-Syn.

Typical ESI-IMS-MS mass spectra of WT α-syn, acquired in 50mM ammonium acetate in positive ion mode. Extended conformations are observed in the m/z range 600-1600m/z and compact conformations are observed in the range 1600-3000m/z.

IDPs such as α-syn have a high degree of plasticity and are therefore highly prone to conformational changes depending on their solution conditions, mode of preparation, temperature and several other variables. This can also lead to batch-to-batch and day-to-day variability in the data sets. To demonstrate this, ESI-IMS-MS data was collected during three different months, August 2016, February 2016 and November 2015, using two different batches of recombinant protein, one during November 2015 and February 2016, and another during August 2016. ATDs were extracted from the individual spectra to investigate this batch-to-batch and experiment-to-experiment variability.

As demonstrated in figure 3.3, slight differences in drift times and conformational distributions are observed between experiments, when a different protein batch is compared or between different acquisition periods on the mass spectrometer. These differences result in a change in the relative proportion of populations between conformational states, at each CSI, of up to 8% when acquired at different times. The +14 and +7 CSIs have been displayed here, as the +14 CSI is the most abundant extended ion in the majority of experiments, and the +7 CSI is the most abundant of the compact conformations.

Proteins stored for extended periods, or proteins exposed to higher numbers of freeze-thaw cycles may also result in differences within the mass spectra. For example, in figure 3.4, the same batch of recombinant α-syn was acquired in 50mM ammonium acetate, under the same conditions, several months apart. There are clear differences between the two spectra, including the appearance of a third, intermediate conformational family group in the aged protein, whereas with the fresh protein only two families are seen. Other data (not shown) using an older protein batch also resulted in a narrower CSD of + 16 to +5, with dominant ions of +11 and +7. To limit this variability, it was decided that protein preparations over 6-8 weeks old were no longer suitable for use in ESI-IMS-MS experiments. This discrepancy is something that the ion mobility community must further address, and care must be taken when interpreting data.

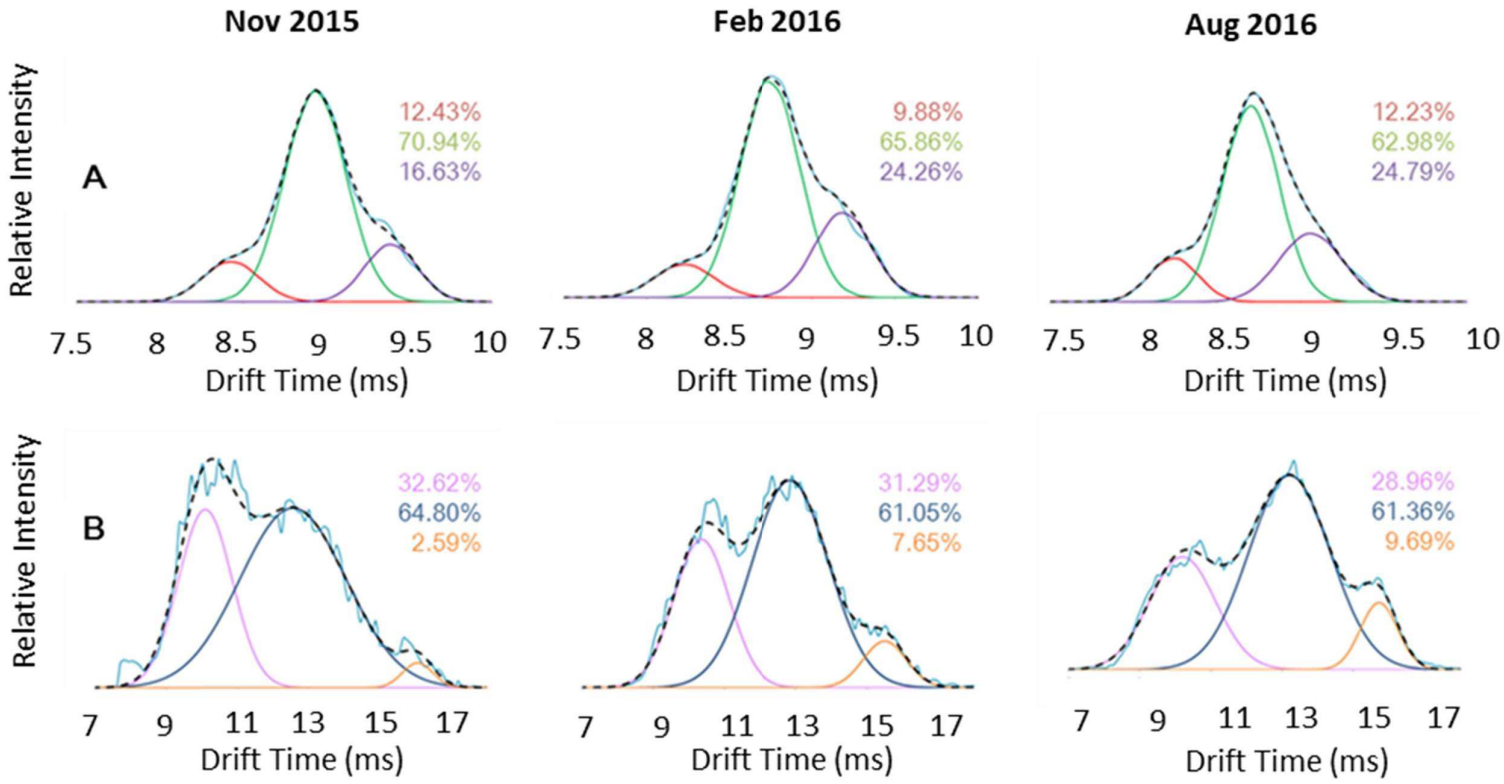

Figure 3.3: Comparison of WT α-Syn ATDs Acquired on Different Dates.

ATDs of the +14 (A) and +7 (B) CSs of 10uM α-syn acquired by ESI-IMS-MS in 50mM ammonium acetate, at three different time points within a one-year time frame, using two batches of protein; one Nov 2015 and Feb 2016 and another in Aug 2016, with Gaussian distributions fitted to determine relative abundances of each population.

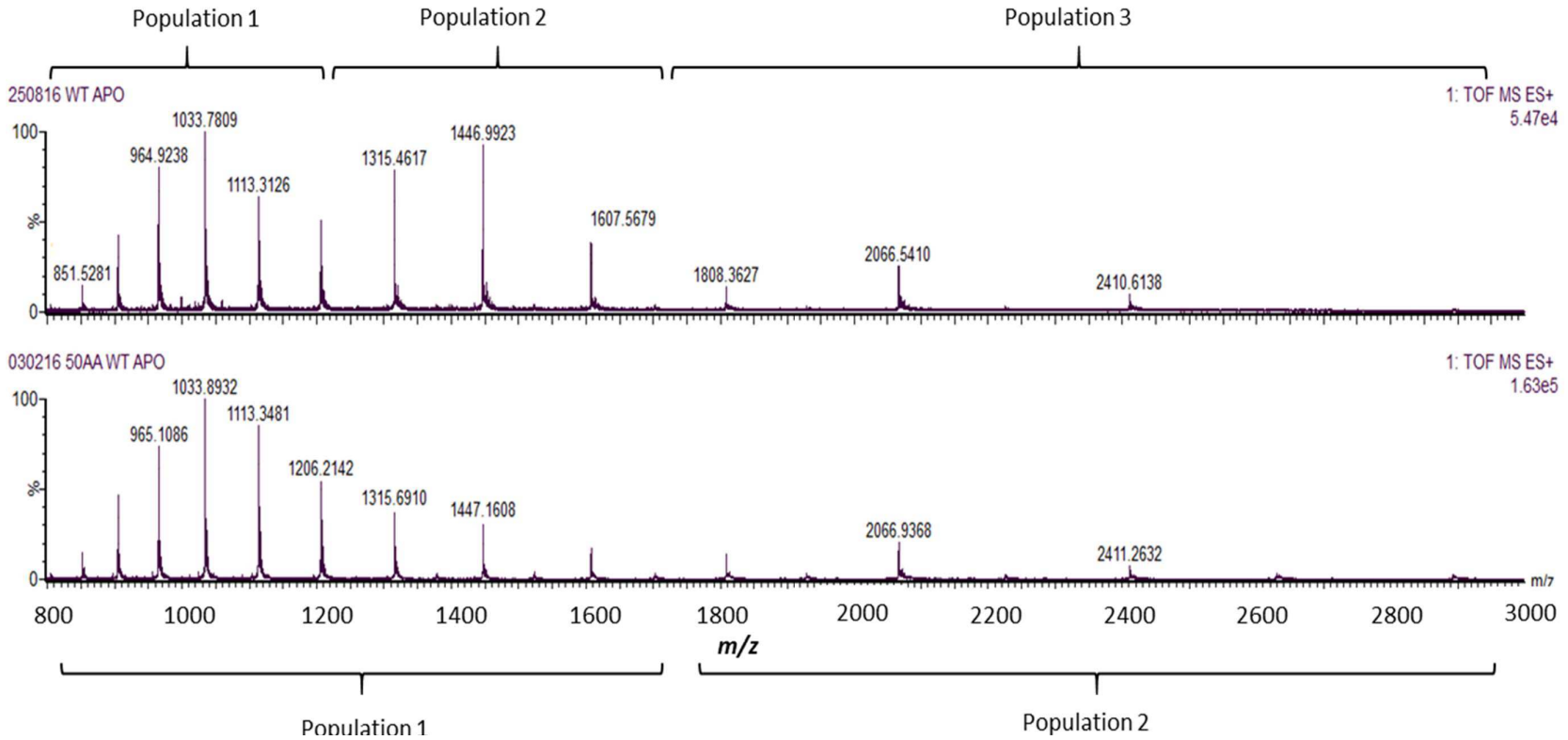

Figure 3.4: Comparison of WT-pyn spectra Acquired on Different Days.

Comparison of two WT-pyn spectra acquired in 50mM ammonium acetate several months apart, by ESI-MS-MS in positive ion mode.

Re-acquisition of samples within the same day however, show less variation. Figure 3.5 displays drift time chromatograms of two samples of 10μM α-syn in 50mM ammonium acetate taken within 4 hours of each other. The percentage differences are much lower than the samples taken on different months, with variations of <5% in the conformational populations.

Due to these discrepancies in the datasets acquired over different periods, it was decided to analyse and compare only data acquired at a single time period, using proteins produced within the same batch. Because of the 8% difference observed between the three data sets presented in figure 3.3, for the remainder of this chapter, data with differences of 10% or less was not interpreted as a significant alteration to the conformational population.

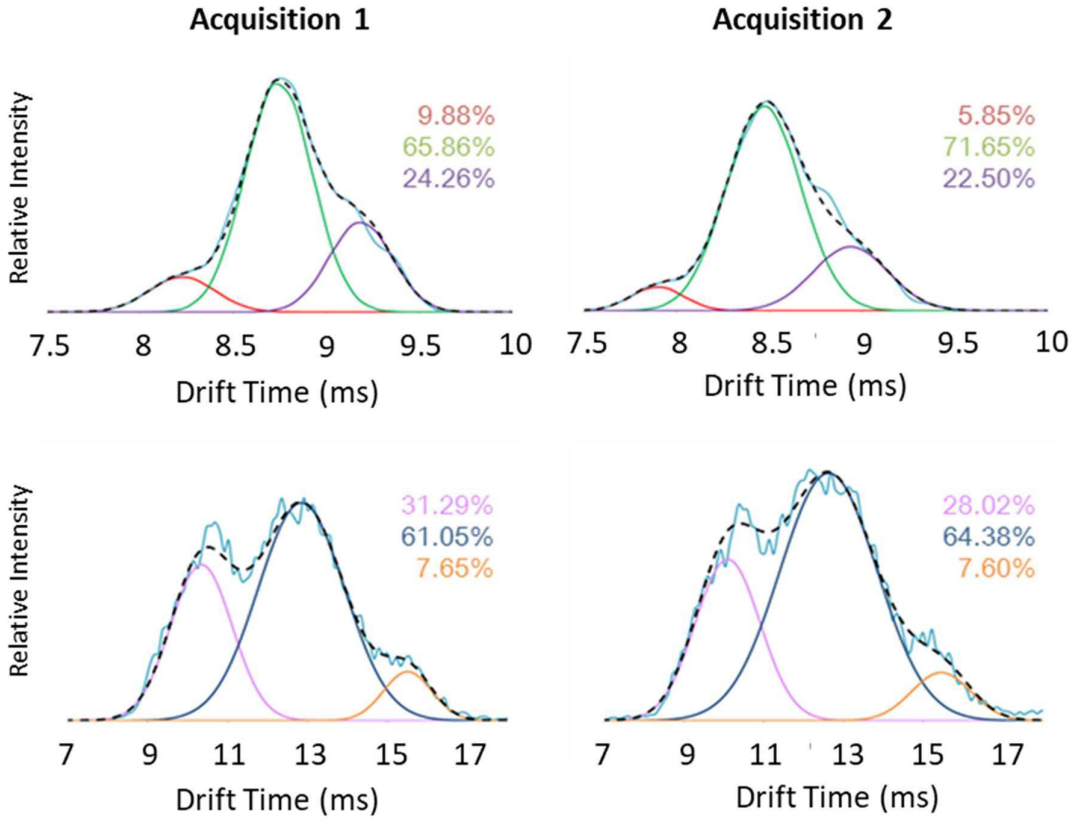

Figure 3.5: Comparison of WT α-Syn ATDs Acquired in a Short Timeframe.

WT α-syn in 50mM ammonium acetate acquired using ESI-IMS-MS in positive ion mode. Two separate experiments conducted within a short timeframe show little difference in arrival time distribution.

3.3.2 S87D and S129D Mutant -syn occupy the same conformational families as WT -syn

ATDs were analysed to determine the CCS of S87D and S129D -syn, which were then plotted against the CSIs to determine the conformational arrangement of the protein.

Figure 3.6 shows the ATD of all CSIs of WT -syn, when acquired using ESI-IMS-MS in positive ion mode, in 50mM ammonium acetate buffer and with a protein concentration of 10¾M. Under these conditions, eight distinct conformations, ranging in size from 1303.7 ð^2 to 3185.5 ð^2, can be observed throughout the different CSIs. Different conformational states are shared by multiple CSIs, and these can be observed to become more compact, as determined by their decreased CCS, at the lower CSIs. The peak centre for each conformation has been plotted in figure 3.7 and the drift scope plot utilised to determine the conformational distribution can be observed in appendix 3.A. For the remainder of the thesis, conformational states will be referred to by the lettering system outlined in table 3.1 on the following page.

The relative population of more extended species can be observed to reduce in favour of an increase in the more compact conformations, as the charge on the ion decreases. For example, within the higher charge states of +18 to +11, the most extended conformer, conformation A, can be seen to disappear as the more compact conformations B and C increase in proportion, before they are too reduced, in favour of the more compact species in CSIs +11 to +5.

Conformational Family	Chromatogram Colour	CSI Range
A	Purple	+18 to +11
B	Green	+18 to +10
C	Red	+18 to +8
D	Light Blue	+11 to +8
E	Orange	+11 to +7
F	Dark Blue	+10 to +5
G	Lilac	+9 to +5
H	Fuscia	+6

Table 3.1: Lettering System for ⊐Syn Conformational Families.

Lettering system for conformational families observed during positive ion mode ESI-IMS-MS of 10¾M ┬syn acquired in 50mM ammonium acetate.

ESI-IMS-MS demonstrated that both S87D and S129D ┬syn mutants occupied the same eight conformational states as WT ┬syn. Drift scope mobilograms utilised to obtain conformational information of WT, S87D and S129D ┬syn can be observed in appendices 3A to 3C and the ATDs for both proteins can be viewed in appendices 3D and 3F, respectively. Graphs plotting CSIs against CCS for the two mutant proteins may be viewed in appendices 3E and 3G.

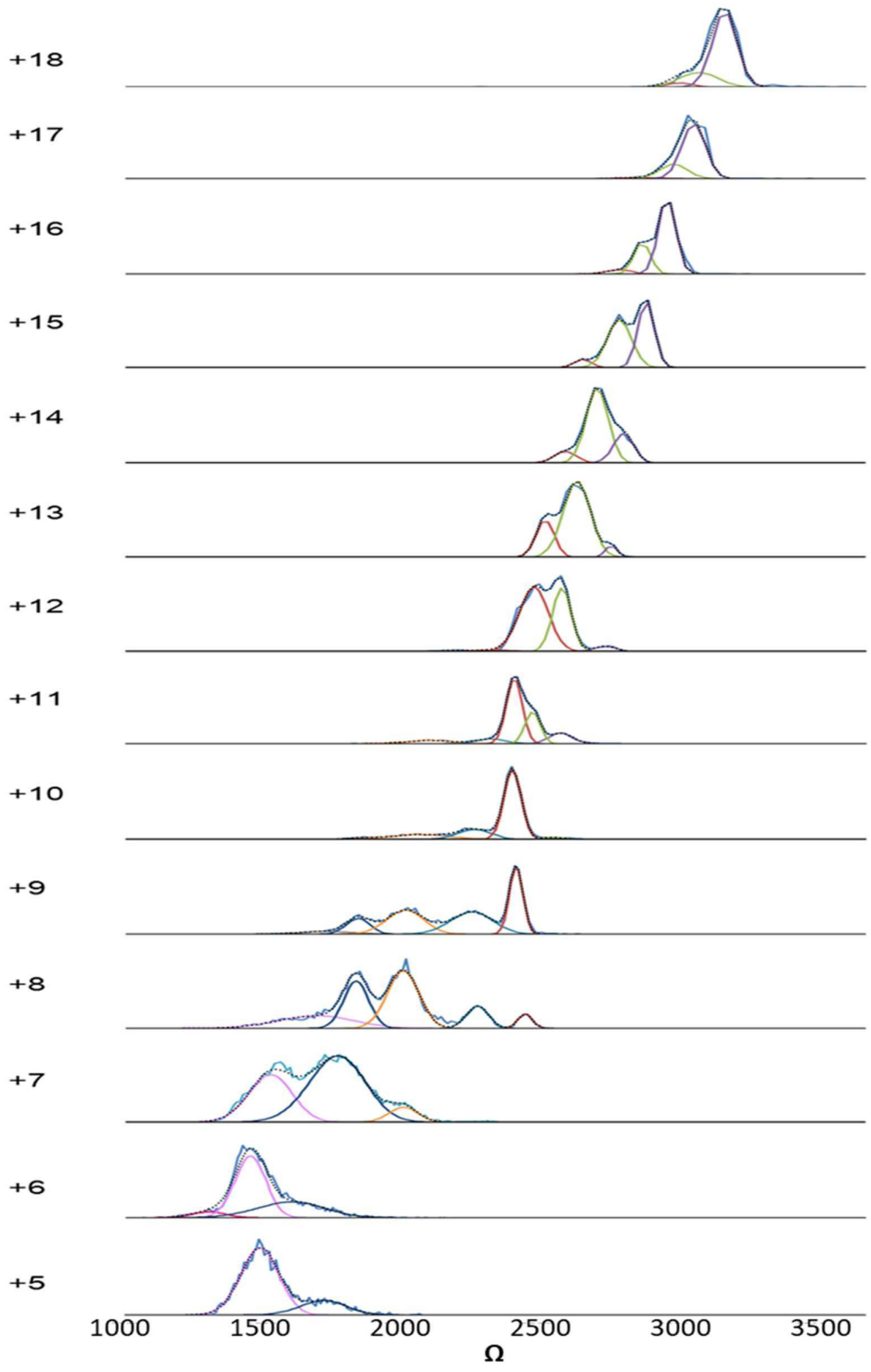

Figure 3.6: WT □Syn ATDs.

ATD of each CSI of WT -syn acquired by ESI-IMS-MS in 50mM ammonium acetate using ESI-IMS-MS in positive ion mode.

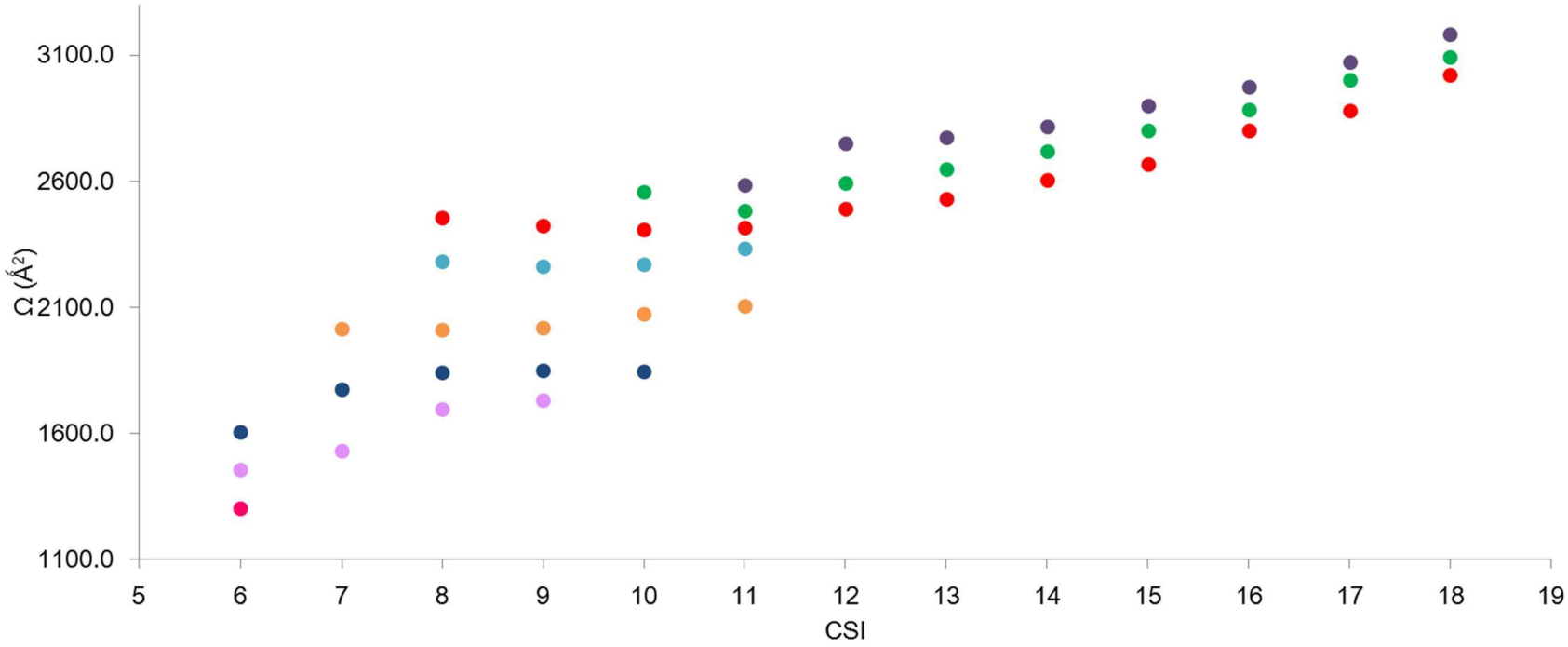

Figure 3.7: WT α-Syn Conformational Distribution.
Conformational arrangement of WT α-syn acquired in 50mM ammonium acetate using ESI-IMS-MS in positive ion mode. WT α-syn occupies 8 distinct conformational families, represented by the different colours.

CCSs of the +7 and +14 CSIs are not altered significantly upon mimicking phosphorylation at these residues, as shown in table 3.2. Data suggests therefore that this modification does not provide enough of an altered charge to the protein to result in significant conformational changes.

CSI	A	B	C
WT + 14	2817.6	2721.2	2605.0
S87D + 14	2807.8	2717.7	2607.8
S129D + 14	2794.2	2720.2	2639.5
CSI	E	F	G
WT + 7	2014.8	1775.3	1530.1
S87D + 7	2021.4	1792.9	1550.7
S129D + 7	2008.2	1774.6	1530.9

Table 3.2: WT, S87D and S129D ⊐Syn +14 and +7 CSS Comparison. Comparison of the CCS, displayed in ð², of the +14 and +7 CSIs of the three protein variants, acquired in 50mM ammonium acetate by ESI-IMS-MS.

The conformational distribution at each CSI was also examined, and overall no large scale alterations to the conformational equilibria were detected. There were slight alterations at some CSIs however, which have been outlined in grey boxes on figures 3.8A-C. Within the extended CSIs, slight alterations could be observed at CSIs +17, +14, +13 and +11. At CSI +17, S129D Πsyn had an increased proportion of conformation B and decrease of conformation A in comparison with

both the WT and S87D variants. At the +13 CSI, S87D was determined to have an increased proportion of conformation C via a reduction in the more extended conformation B, compared to the WT and S129D proteins, and this pattern was also observed with both S87D and S129D Πsyn in comparison to the WT at CSI +14. These alterations suggest the phosphomimic variants to have a slightly more compact structure overall, at these CSIs. However, at the +11 CSI, both S87D and S129D Πsyn demonstrated an increased proportion of the extended conformation B in comparison to the WT, suggesting a more extended structure. Within the more compact CSIs, observed alterations are again mixed. At the +6 CSI, Gaussian fitting determined S129D Πsyn to have a decreased proportion of conformation F, via a slight increase in the more compact conformations, F and G, suggesting a more compact and amyloidogenic structure for this protein variant. However, at the +5 CSI, S87D demonstrated a decrease in compact conformation G via a slight increase in the more extended conformation F, suggesting a less amyloidogenic structure for this protein variant. All changes observed again were small overall, and Gaussian fitting of this data therefore suggests that mimicking phosphorylation at either S87 or S129 has little effect on the overall conformational distribution or CCS of Πsyn, and this would suggest that these three protein variants should have the same aggregation propensity. Some small alterations were observed however that may suggest some conformations of S129D Πsyn to be slightly more amyloidogenic than WT or S87D Πsyn.

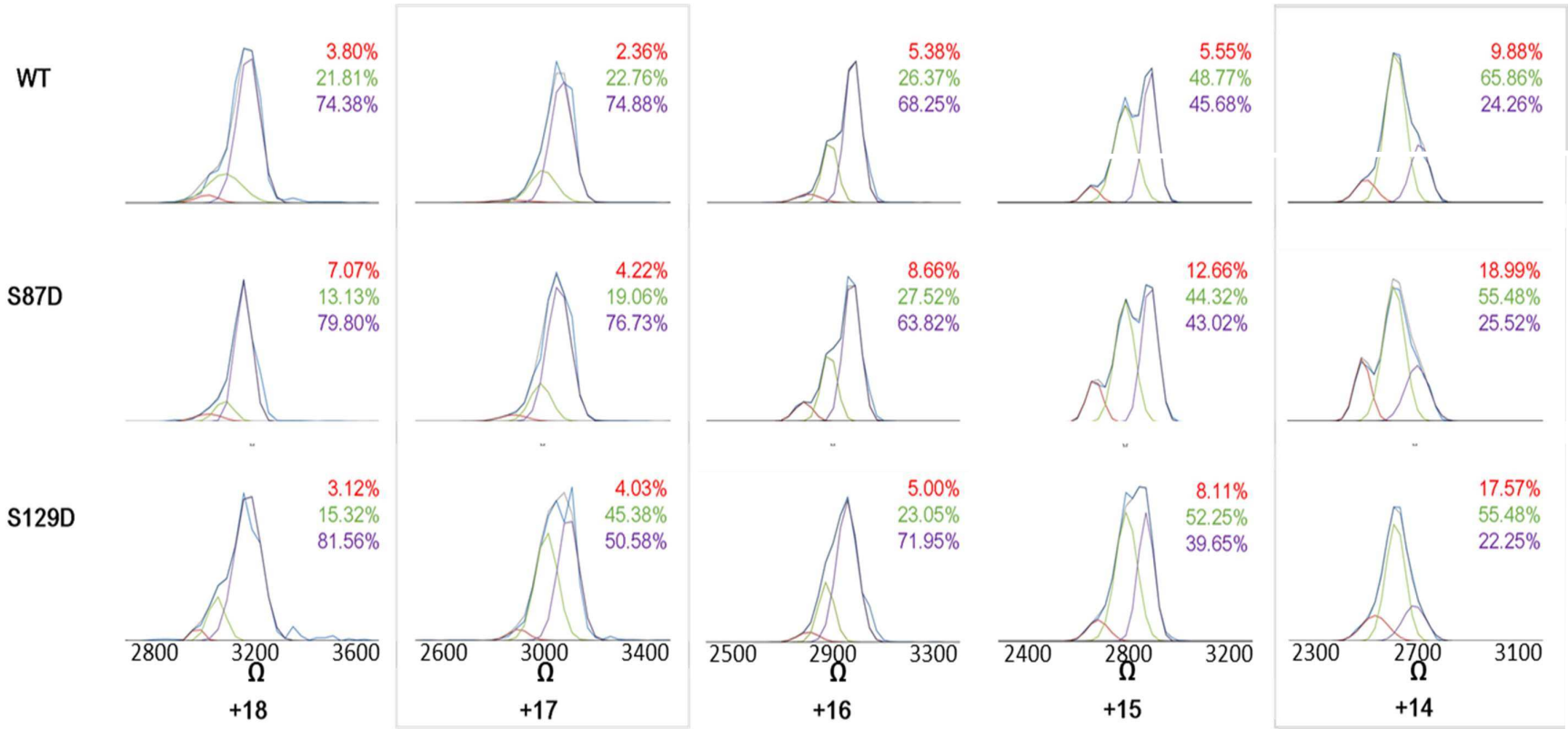

Figure 3.9A: ATDs and CCS of WT, S87D and S129D IBys. CSs +18 to +14.
A) ATDs and CCSs of 100µM WT, S87D and S129D α-syn in 50mM ammonium acetate from IST-IMS-MS experiments conducted in positive ion mode. Percentages of each conformation at each CS were calculated using Gaussian fitting. CSs with conformational distributions displaying differences of over 10% between proteins are highlighted with grey boxes.

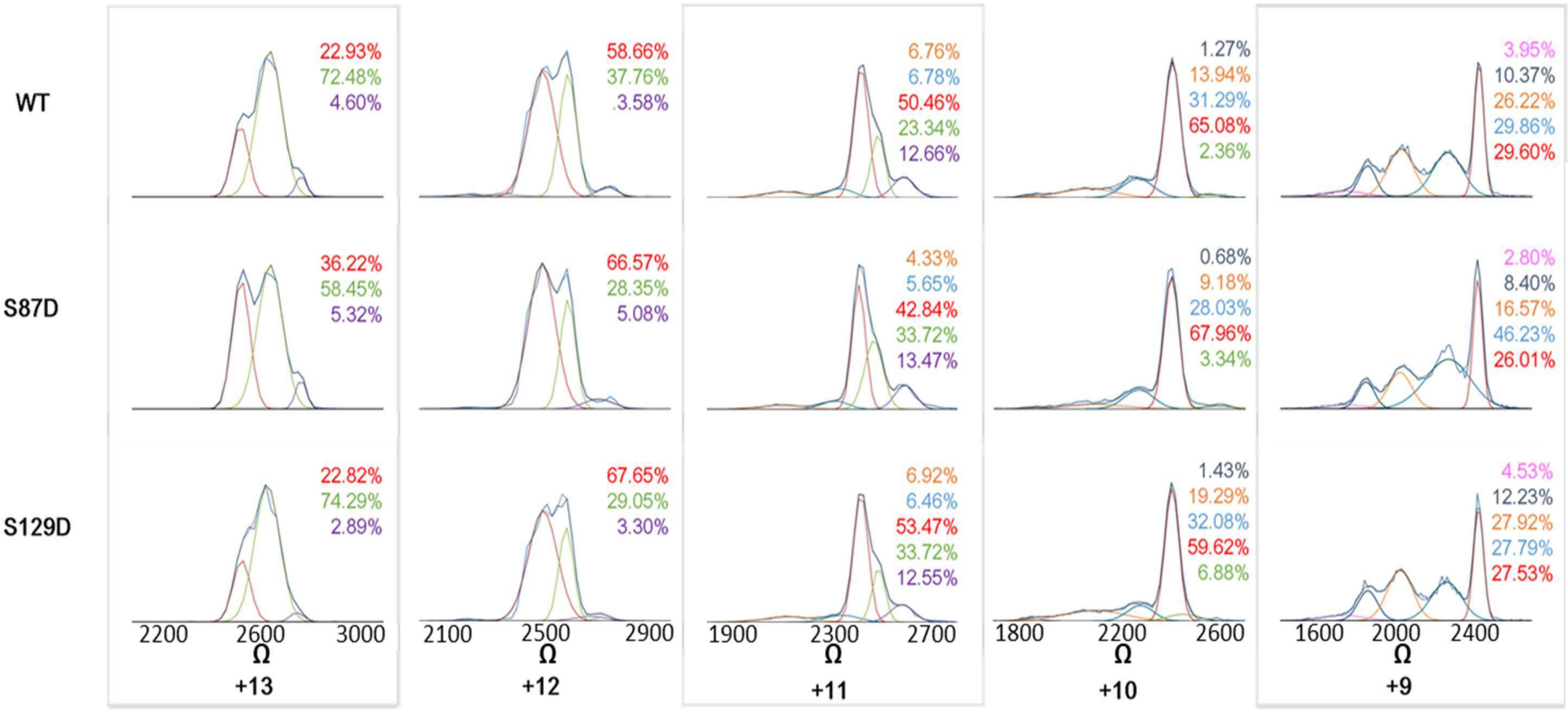

Figure 3.5B: ATDs and CCSs of WT, S87D and S129D IByn. CSIs +13 to +9.
ATDs and CCSs of 100µM WT, S87D and S129D α-syn in 50mM ammonium acetate from IST-IMS-MS experiments conducted in positive ion mode. Percentages of each conformation at each CSI were calculated using Gaussian fitting. CSIs with conformational distributions displaying differences of over 10% between proteins are highlighted with grey boxes.

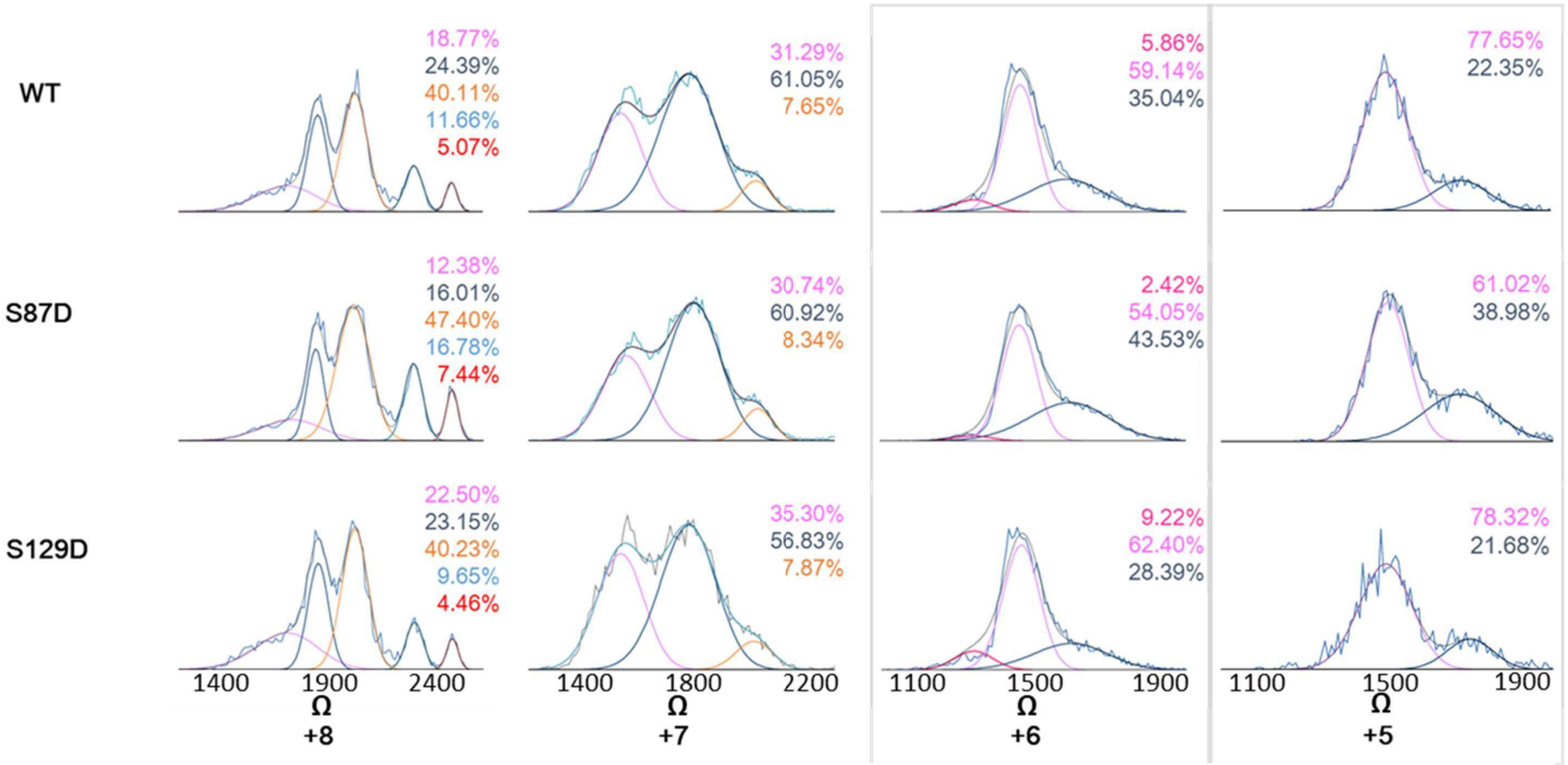

Figure 3.9C: ATDs and CCSs of WT, S87D and S129D IByn. CSIs +8 to +5.
ATDs and CCSs of 100µM WT, S87D and S129D α-syn in 50mM ammonium acetate from IST-IMS-MS experiments conducted in positive ion mode. Percentages of each conformation at each CSI were calculated using Gaussian fitting. CSIs with conformational distributions displaying differences of over 10% between proteins are highlighted in grey boxes.

3.3.3 Mimicking Phosphorylation at Serine 87 or Serine 129 Causes Little Alteration to the CSD of ΠSyn

As demonstrated in figure 3.9, spectra C, WT ΠSyn has a CSD of +18 to +5. Two distinct conformational family groups can be directly observed from the spectra as a whole; extended conformations ranging from CSI +18 to the +9, with the +14 CSI being the most abundant, and more compact conformations at CSIs +8 to +5, with the +7 CSI in highest abundance.

S87D ΠSyn also demonstrated the same CSD as WT ΠSyn, when acquired under the same conditions, with two conformational families observed, ranging from CSIs +18 to +9 and +8 to +5, as shown in spectra B on figure 3.9. This suggests both proteins to be occupying a similar range of conformations, with the same ionisation ability as the WT.

S129D ΠSyn, shown in spectra A, has a slightly narrower CSD of +17 to +5, which may be indicative of a more compact range of conformations overall, as the most highly charged of the CSIs on the WT and S87D spectra, +18, cannot be observed above the signal to noise ratio. The intensity of this CSI is however very low in the WT and S87D spectra, at around just 5% relative intensity in comparison to the highest intensity peak, CSI +14. Again, two conformational families can be clearly seen on the mass spectra; an extended family ranging from charge states +17 to + 9, and the more compact conformations at CSIs +8 to +5.

A reduction in intensity of the extended +17 to +15 CSIs is also observed within the S129D spectra in comparison to the S87D and WT variants, as shown with grey lines on figure 3.9. CSI +17 has a relative intensity of around 15% in the WT spectra, and around 20% in the S87D spectra, whereas this is reduced to around 10% in the S129D spectra. The +16 CSI has a relative intensity of around 45% in the WT spectra, 50% in the S87D spectra, and just 35% in the S129D spectra, and the +15 CSI has a relative intensity of around 75% in the WT spectra, 80% in the S87D spectra, and just 65% in the S129D spectra. This suggests that S87D Πsyn may have a higher proportion of more extended CSIs than WT Πsyn, and S129D may exist in an equilibrium containing proportionally less of these more extended conformations than both the WT and S87D variants. The dominant CSI for WT and S87D τsyn is the +14 CSI, whereas for S129D both the +14 and more compact +13 CSIs appear dominant in the spectra again indicating a shift to lower CSIs. This loss of the +18 CSI and shift of the dominant ion to a slightly lower charge state would indicate a slight alteration in the overall conformation of the protein, towards more compact states, though this difference does not appear to be large overall.

Dimeric species of τsyn can also be observed in all three spectra on figure 3.9. For WT and S87D τsyn, dimers of CSIs +23 to +11 were observed, whereas more extended dimer CSIs of +25 to +11 were seen within the S129D spectra, suggesting additional dimers and of greater conformational variety and increased physical size are being formed within the S129D sample.

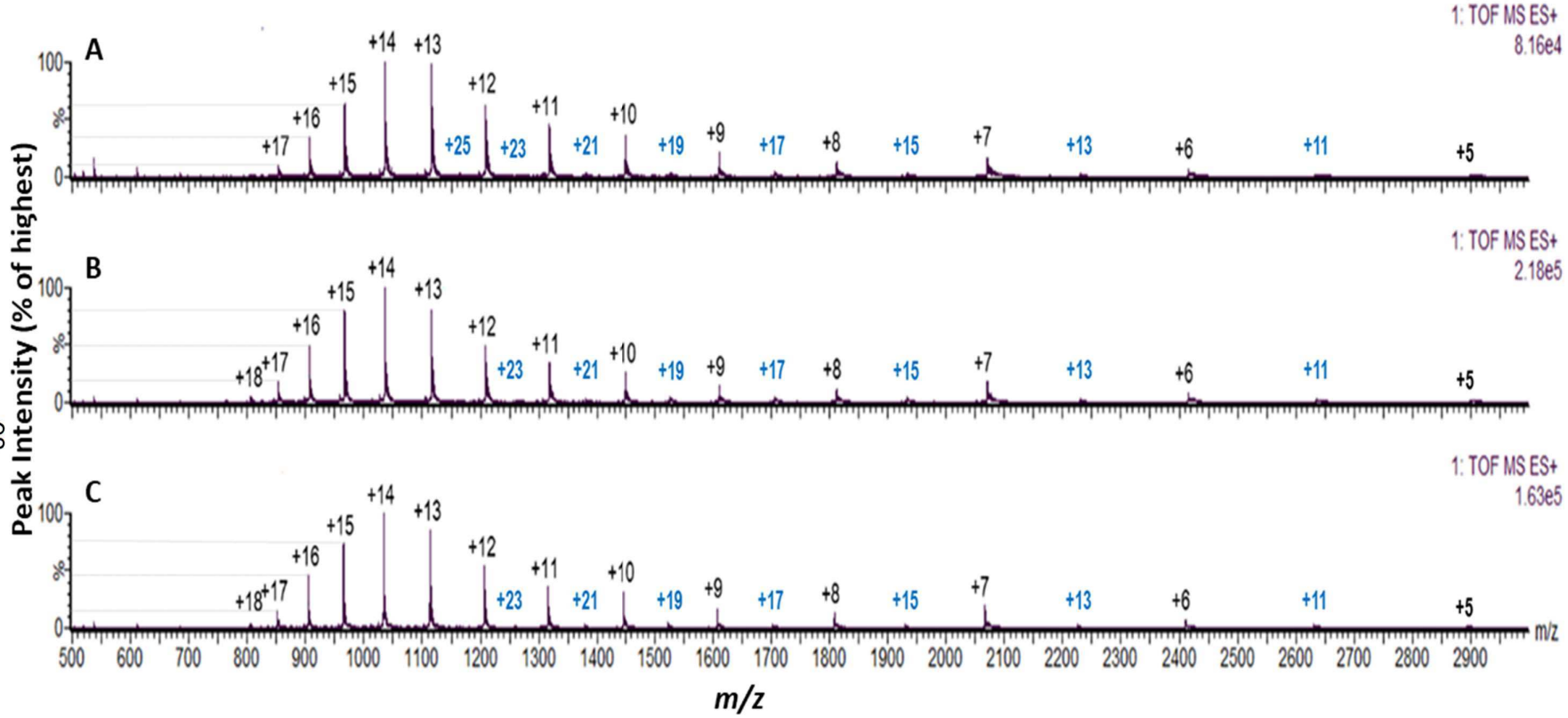

Figure 3.5: CSDs of WT, S87D and S129D α-Syn Acquired by ESI-IMS-MS.

CSDs of A) S129D, B) S87D and C) WT α-syn, acquired in 50mM ammonium acetate using ESI-IMS-MS in positive ion mode (Monomer/Dimer).

3.3.4 Copper (II) Binding to αSyn can be Observed by ESI-IMS-MS

To investigate the conformational changes observed upon metal binding, αsyn was exposed to copper, iron, zinc, manganese and magnesium. As shown in figure 3.10, only the binding of copper is observable by ESI-IMS-MS, despite the other metals being known to both affect the aggregation rate of the protein (Uversky *et al.*, 2001) and having been demonstrated to bind to the protein by other techniques such as NMR spectroscopy, tyrosine fluorescence quenching, and ESI-MS (Golts *et al.*, 2002; Binolfi *et al.*, 2006; Peng *et al.*, 2010; Liu and Franz, 2007). A range of buffers and concentrations were used in an effort to further investigate metal binding, including 5, 10, 25, 50 and 100mM ammonium acetate, 50mM ammonium bicarbonate, 10mM 4-methylmorpholine, water:MeOH and water:ACN:MeOH, however none of these facilitated the observation of metal binding. Metals with different counter ions were also investigated, and a range of mass spectrometry machine parameters were attempted, including increased and decreased cone voltages, increased and decreased trap and transfer settings, and altered backing pressures.

Multiple similar experiments were performed with the S87D and S129D αsyn, without metal binding being observed. This suggests that ESI-IMS-MS may be unsuitable for observations of metal binding. It is also possible that the metal ions are complexing with a component of the buffer solution, such as the acetate in the ammonium acetate buffers making the ion unavailable for binding.

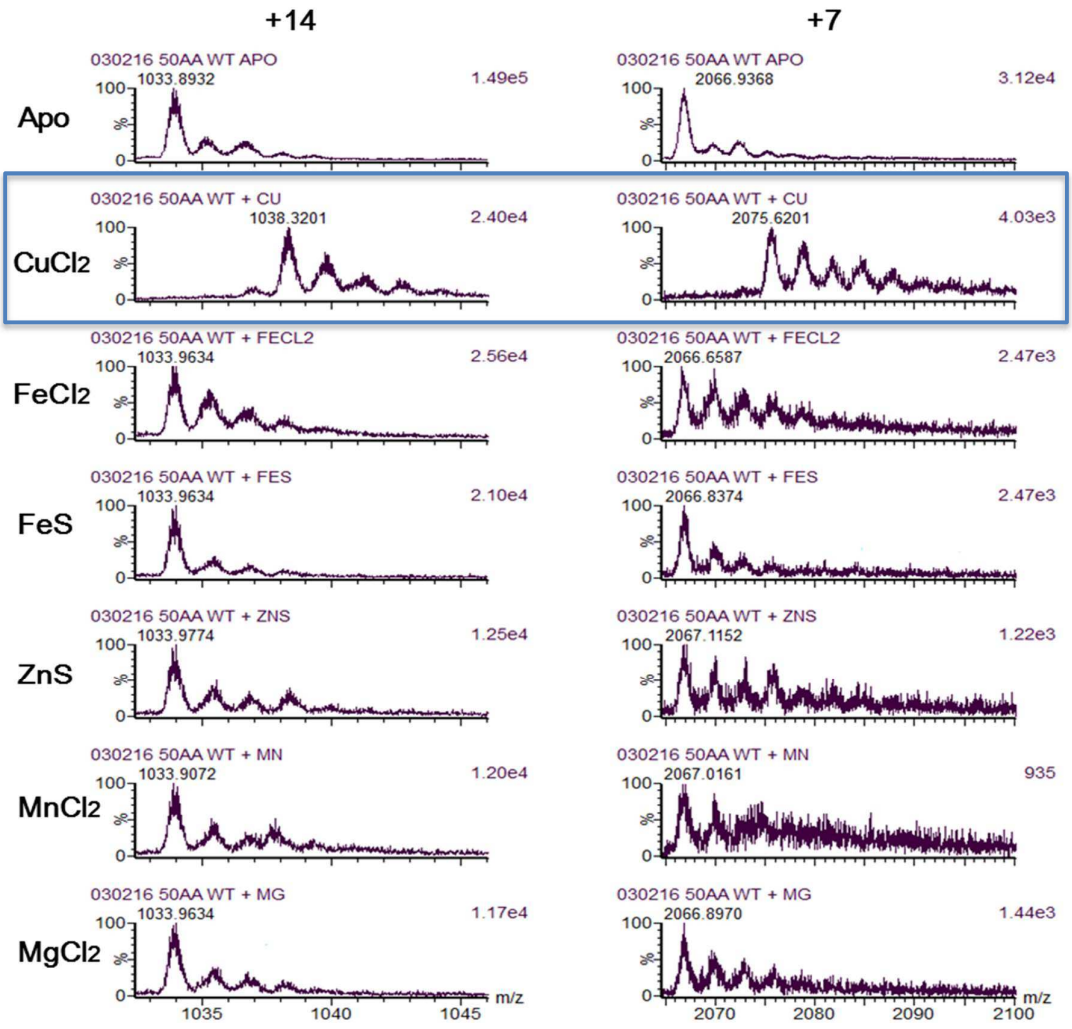

Figure 3.16: Expanded +14 and +7 CSs of WT IBys Demonstrating the Binding of Metal Ions.

Expanded mass spectra peaks of the +14 and +7 CSs of 100M WT -ys in 50mM ammonium acetate buffer, with or without addition of equimolar $CuCl_2$, $FeCl_2$, FeS, ZnS, $MnCl_2$ and $MgCl_2$, acquired by ESI-MS in positive ion mode.

3.3.5 Addition of Equimolar Copper Increases the CSD of all Πsyn Variants and Increases the Intensity of the Extended Charge States

As shown in figure 3.11A and 3.11B, upon immediate addition of equimolar $CuCl_2$ to 50mM ammonium acetate containing 10¾M of either the proteins, another more extended CSI appears for all three variants, widening the CSD for WT and S87D to +19 to +5, and S129 to +18 to +5. The CSD does not however further widen upon increasing the protein-copper ratio above 10¾M.

The dominant CSI within the extended conformational families of the WT protein also shifts towards the lower CSIs with increasing copper concentration, with a shift from +14 within the apo spectra, to +12 at a 100¾M $CuCL_2$ concentration, suggesting a shift in equilibria towards the more compact conformations.

The dominant CSI of S129D Πsyn remains constant, with an almost equal share between the +14 and +13 CSIs under all conditions, suggesting only slight changes in the conformational states of the protein in the presence of increasing copper concentrations. The dominant CSI of S87D Πsyn shifts towards the more extended +15 CSI at a 50¾M $CuCl_2$ concentration, suggesting a shift towards the more extended conformations. The dominant CSI within the compact conformations of all three Πsyn variants remains constant at +7.

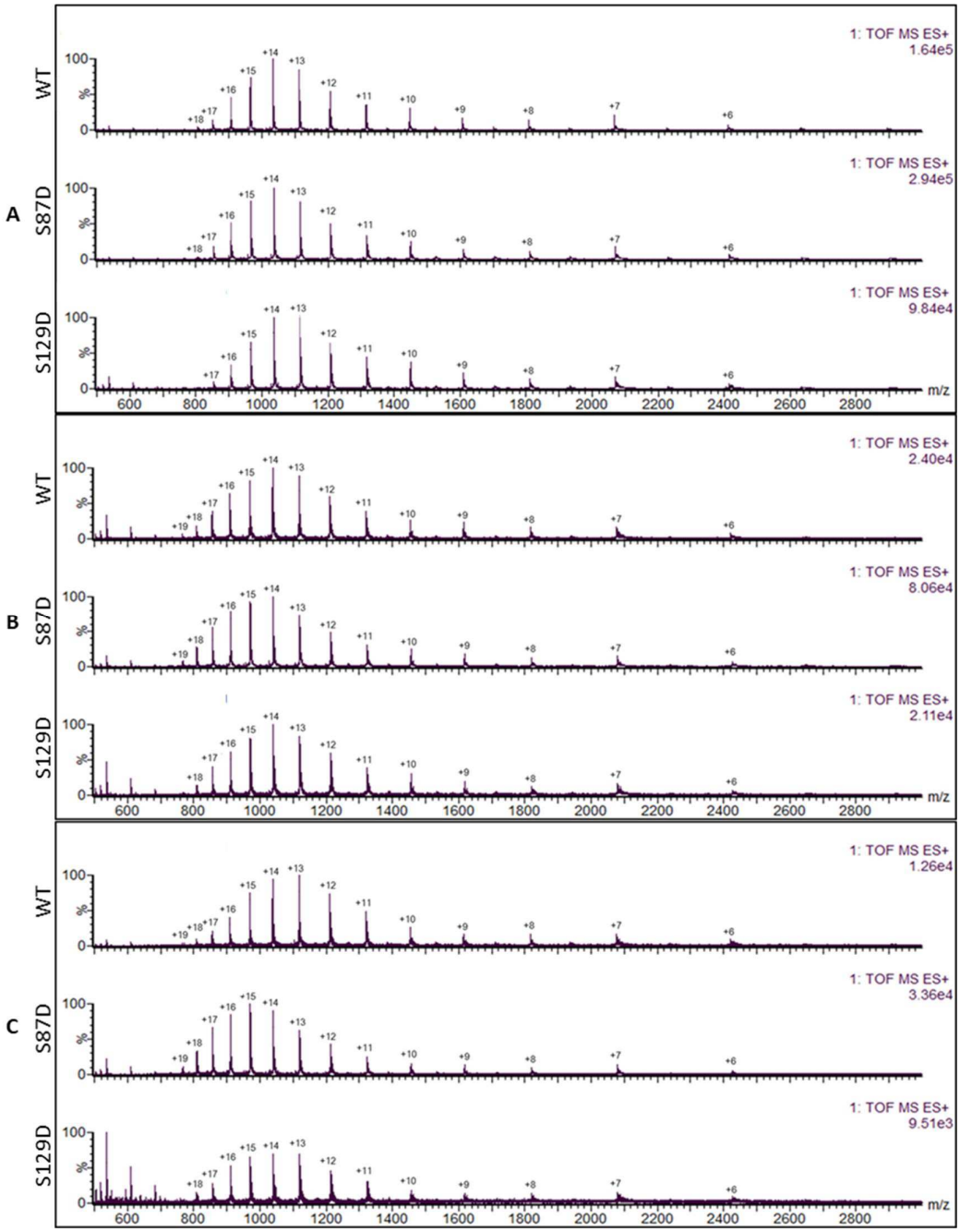

Figure 3.11A: Effect of increasing $CuCl_2$ Concentration on the CSD of WT, S87D and S129D α-syn.

CSDs of WT, S87D and S129D α-syn in the presence of increasing concentrations of $CuCl_2$. A) Untreated, B) 10μM $CuCl_2$, C) 20μM $CuCl_2$.

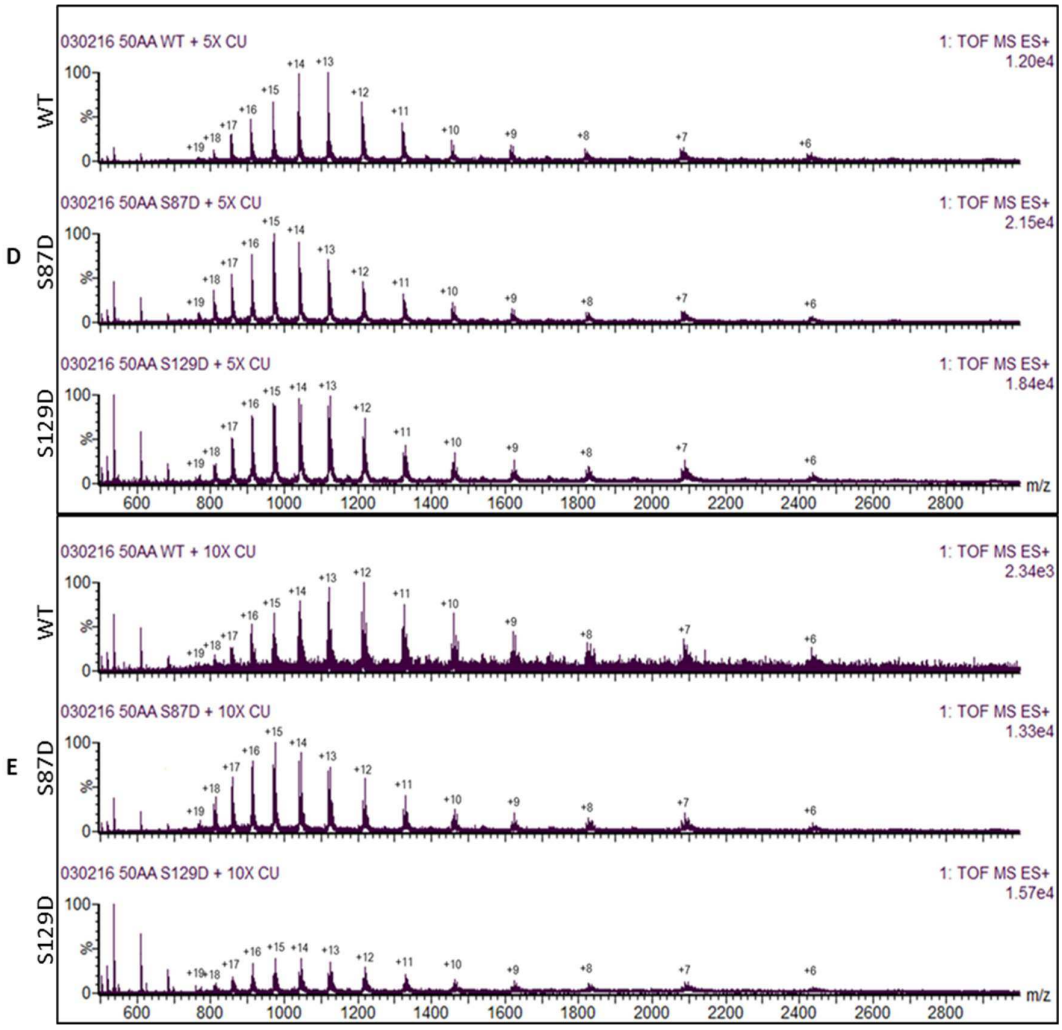

Figure 3.11B: Effect of increasing $CuCl_2$ Concentration on the CSD of WT, S87D and S129D α-syn.

CSDs of WT, S87D and S129D α-syn in the presence of increasing concentrations of $CuCl_2$. D) 50μM $CuCl_2$, E) 100μM $CuCl_2$.

3.3.6 Binding of Copper Causes and Increase in the Proportion of the Most Compact Conformations at Each Charge State Ion, For All Three Protein Variants Investigated

In section 3.3.5, the addition of copper ions to the WT -syn solution shifted the expanded states CSD towards the lower CSIs, suggesting a shift towards the more compact states, despite the initial widening of the CSD observed upon addition of equimolar $CuCl_2$.

As previously described, each CSI of -syn represents multiple conformations of the protein, of slightly altered degrees of compactness but with the same ionisation ability. In this section, the conformational distribution of each CSI of the three protein variants, apo and in the presence of $CuCl_2$, will be investigated via Gaussian fitting of the ATDs.

Figure 3.12 shows the relative shifts in conformational equilibrium for the most dominant extended CSI, +14, of all three proteins, in the presence of increasing copper concentrations. Very little alteration in conformational equilibrium is observed with either protein at this CSI, other than with WT -syn after a $CuCl_2$ concentration of 50¾M with 10¾M -syn is reached, where an increase in the more compact conformation C, is observed, from around 10% in the apo sample to 23 and 32% in the presence of 50 and 100¾M $CuCl_2$, respectively. However, little alteration can be observed overall within the extended states, indicating the conformations are not dramatically affected by the addition of this metal ion.

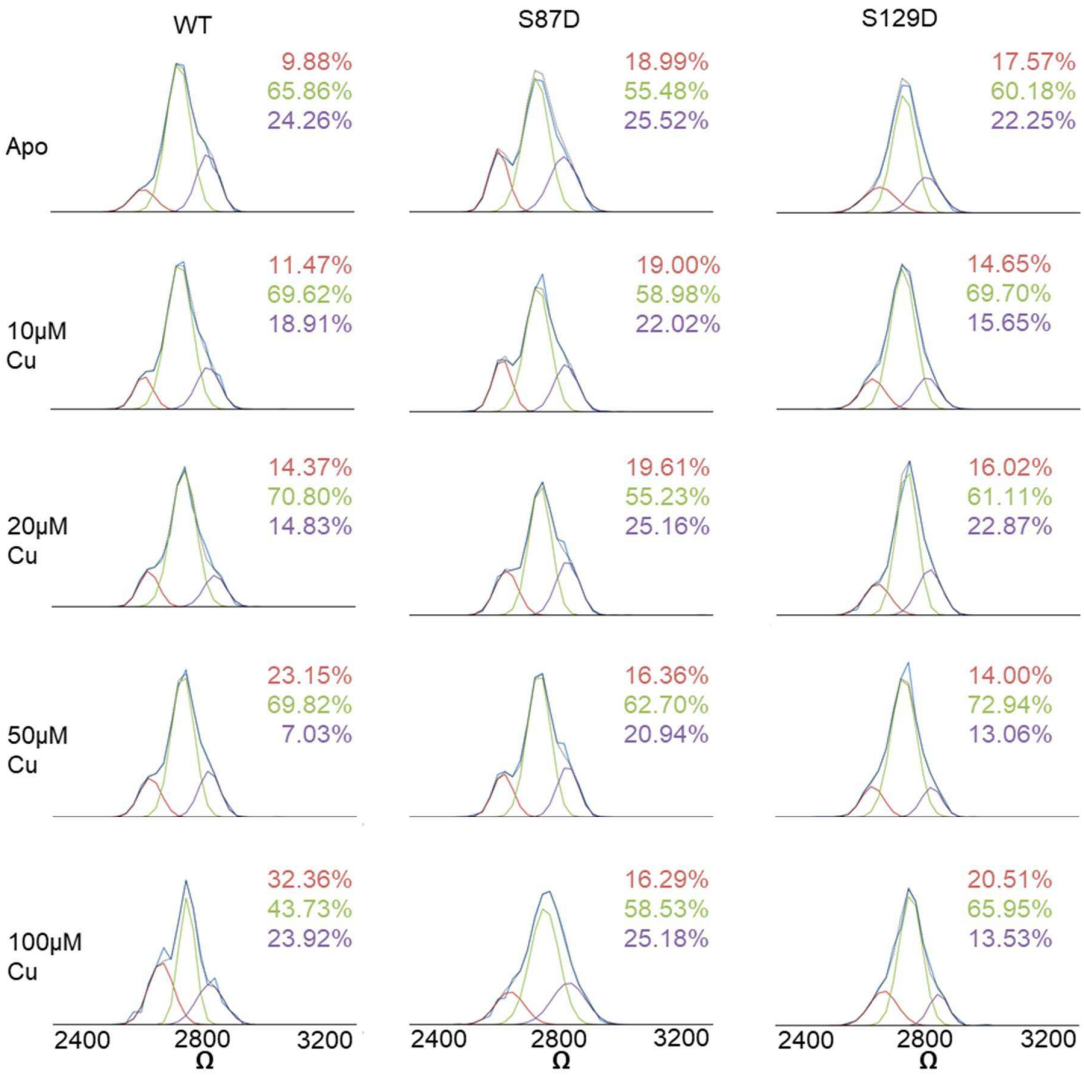

Figure 3.12: Effect of Increasing Copper Concentration on the Conformational Equilibrium of the +14 CSI of WT, S87D and S129D Ilyn.

The +14 CSI, representative of the extended conformations, of WT, S87D and S129D Ilyn, at increasing $CuCl_2$ concentrations. Conformations A, B and C.

Figure 3.13 shows the shows the relative shifts in conformational equilibrium for the +7 CSI, representative of the compact CSIs, of all three proteins. A

substantial increase in the most compact of the three conformations present at this CSI, G, is observed upon addition of equimolar $CuCl_2$ and above. At an equimolar protein and copper concentration, an increase of 22.55%, from 31.29% apo to 53.84% of the total protein at this charge state is observed. This occurs via a reduction in the more extended conformations, F and E. Conformation E is completely absent from the chromatogram of WT -syn after addition of 100¾M $CuCl_2$. Notably this state is completely lost for S129D -syn after addition of 20¾M $CuCl_2$. This data indicates that the compact CSIs and conformations are affected by the addition of copper ions, where a shift in the equilibrium towards the more collapsed conformations is observed.

For the remainder of this section, only the equimolar -syn and $CuCl_2$ results will be discussed, as representative of the action on copper of the different conformational states of -syn and its variants. Gaussian fitting of all CSIs may be viewed in appendices 3L to 3X. As shown in appendices 3L-3P, at CSI +19 to +15, S87D -syn undergoes little alterations to its conformational equilibrium upon the binding of copper. WT and S129D -syn however show more notable changes, with a reduction in the more extended conformation A, in favour of the more compact conformation, B. At the +14 and +13 CSIs, two of the more dominant peaks within the spectra, no significant alterations occur upon copper binding, as shown in appendices 3Q & 3R. At CSI +12 in appendix 3S, a reduction in conformation C is observed with the binding of copper, which was unexpected as it is the most compact conformation at this CSI.

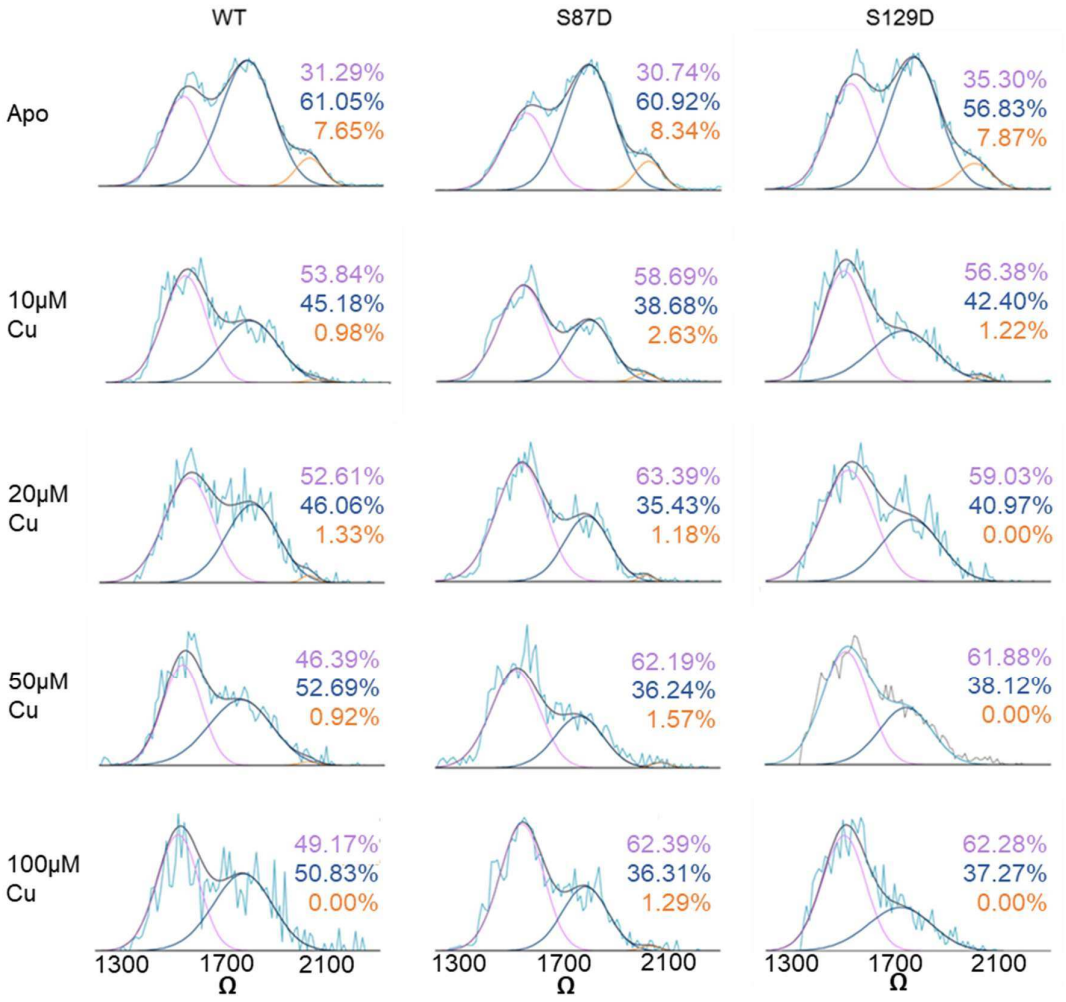

Figure 3.13: Effect of Increasing Copper Concentration on the Conformational Equilibrium at the +7 CSI of WT, S87D and S129D hSyn.

The +7 CSI, representative of the compact conformations, of WT, S87D and S129D hSyn, at increasing $CuCl_2$ concentrations. Conformations A, B & C.

At CSI +11, shown in appendix 3T, and through the lower CSIs, S87D hSyn begins to respond more akin to the other variants, and new, compact conformations appear for all proteins as the equilibrium of extended conformers

further decreases in favour of more compact species. For all three variants at the +11 CSI, a reduction in conformations B and C is observed in favour of, D. Unexpectedly, an increase in the most extended conformation, A, is also seen. At CSI +10 in appendix 3U, an increase in the increasingly compact conformations C, D, E and F is observed, along with a reduction in B. A similar pattern is followed at CSI +9 in appendix 3V, where the extended C and D reduce and an increase in E, F and G is seen, and conformation B is no longer present. At CSI +8 shown in appendix 3W, C, D and E reduce in favour of F and G, and at CSI +7 in appendix 3X, C and D are gone, and an increase in G via reduction in F and E is observed.

Interestingly, no notable changes were observed at CSIs +6 and +5, as shown in appendices 3Y & 3Z, despite being the most compact, and CSI +6 containing the only instance of the most compact conformation, conformation H. This was true for all concentrations of $CuCl_2$ investigated.

This data together suggests that mimicking phosphorylation at serine residues does not result in large increases in the more compact, aggregation prone states of the protein overall, in comparison to the WT. Copper ions however do have the ability to alter the conformational equilibrium of all three proteins investigated, and increase the population of the more aggregation prone conformations populated at CSIs +8 to +5.

3.3.7 Mimicking Phosphorylation at Serine129 but not Serine 87 Increases the Copper Binding Affinity of -syn

To determine their binding affinities for copper, the three protein variants were each dissolved in 50mM ammonium acetate at a protein concentration of 10¾M, followed by addition of increasing concentrations of $CuCl_2$, indicated on the figures as 1x, 2x, 5x, 10x, representing 10, 20, 50 and 100 ¾M $CuCl_2$, respectively.

As demonstrated in figure 3.14, extended states of the three protein variants, represented by the +14 CSI, readily bind just two copper ions at an equimolar (1x) and 20¾M $CuCl_2$ (2x) concentration. Upon addition of 50¾M $CuCl_2$ (5x), the S129D variant begins to bind three copper ions. Also at this concentration, the majority of S129D is bound to two copper ions, whereas WT and S87D are mostly bound to one. When the copper concentration is increased to 100¾M (10x), all three proteins bind three copper ions, and a fourth copper peak appears. At this concentration the dominant peak for both WT and S87D is almost equally shared between -syn bound to one or two coppers, whereas the majority of S129D is bound to two ions.

The compact conformations populated at CSIs +8 to +5, of all three protein variants, have a higher copper binding affinity than the extended CSIs. As shown in figure 3.15, with the +7 CSI, all three proteins bind three copper ions when

exposed to 50¾M (5x) $CuCl_2$, as opposed to 100¾M (10x) $CuCl_2$ for the extended states.

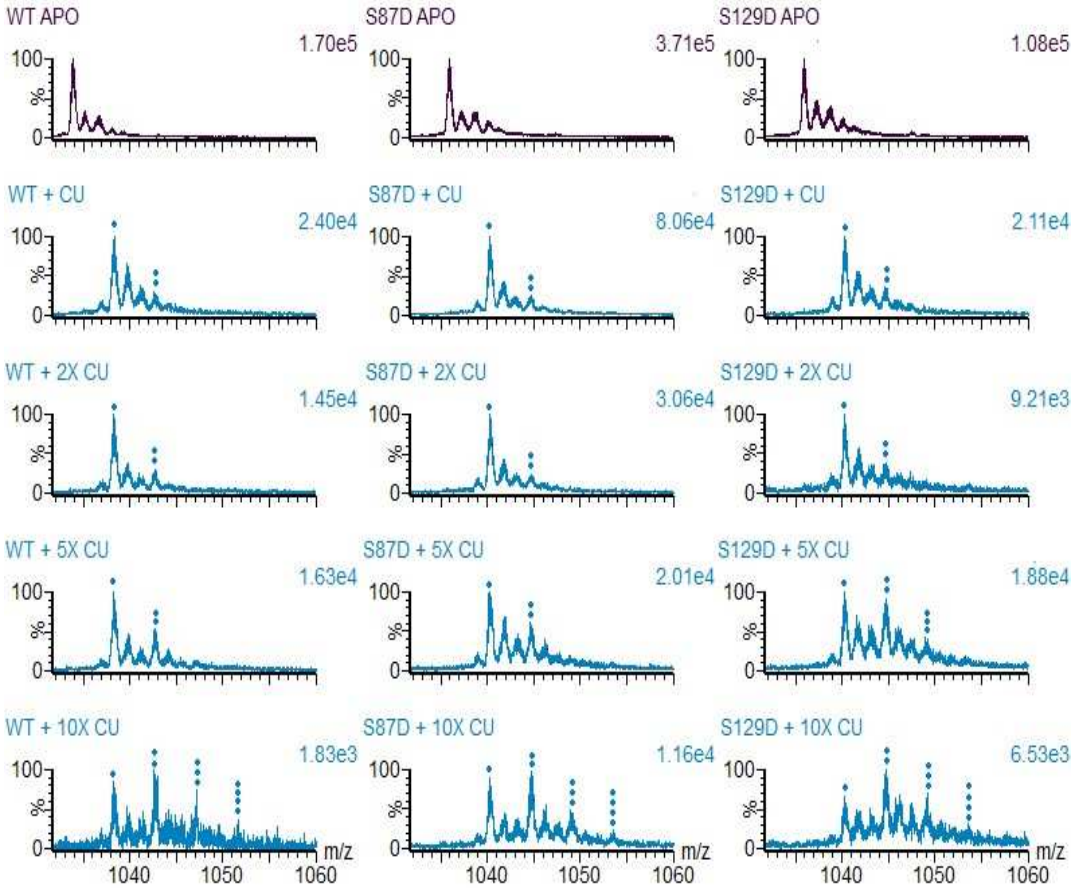

Figure 3.14: Copper Binding Affinities of the +14 CSI of WT, S87D and S129D Π Syn.

Copper binding affinities at the +14 CSI of 10¾M WT, S87D and S129D Τsyn in 50mM ammonium acetate buffer, at increasing $CuCl_2$ concentrations, as determined by ESI-IMS-MS in positive ion mode. (1x=10¾M $CuCl_2$, 2x=20¾M $CuCl_2$, 5x=50¾M $CuCl_2$, 10x=100¾M $CuCl_2$).

The same binding pattern is observed as with the extended CSIs, with WT and S129D being almost equally bound to one or two copper ions, and S129D being mostly bound to two ions, and a much smaller proportion being bound to three coppers. At a 100¾M (10x) $CuCl_2$ concentration all three proteins bind four copper ions, with the majority of WT and S87D binding two ions, whereas the dominant peak for S129D is almost equally shared between protein bound to two or three copper ions. Data presented here demonstrates that S129D -syn has a higher binding affinity for copper than WT or S87D.

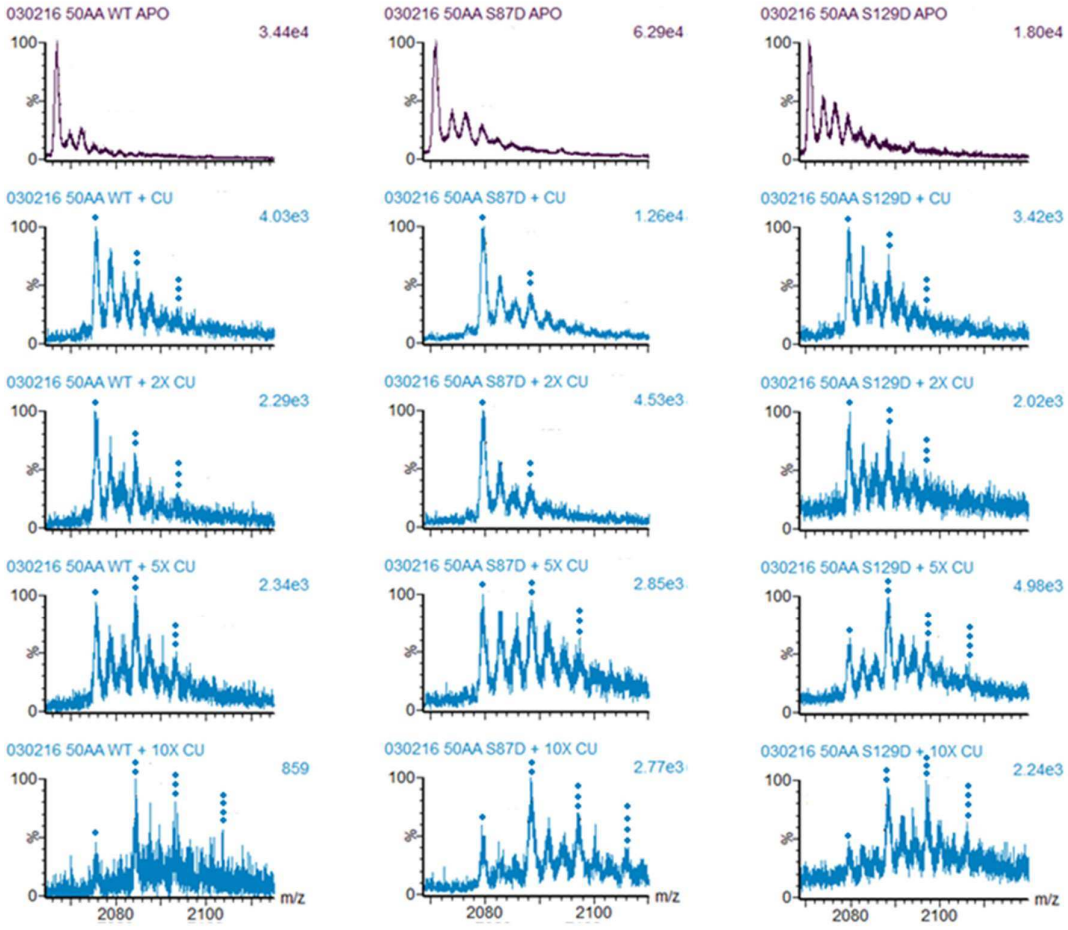

Figure 3.15: Copper Binding Affinities of the +7 CSI of WT, S87D and S129D ll Syn.

Copper binding affinities at the +7 CSI of 100M WT, S87D and S129D -syn in 50mM ammonium acetate buffer, at increasing $CuCl_2$ concentrations, as determined by ESI-IMS-MS in positive ion mode. (1x=100M $CuCl_2$, 2x=200M $CuCl_2$, 5x=500M $CuCl_2$, 10x=1000M $CuCl_2$).

3.3.8 Mimicking Phosphorylation at Serine 87 Slows the Aggregation Rate of T-syn *in vitro*

ThT assays were conducted in 50mM ammonium acetate buffer, with 70¾M T-syn plus 70¾M metal ions and 10¾M ThT. High protein concentrations were utilised to aid in the initiation of aggregation, which was monitored for 116 hours. Data was normalized to the highest fluorescence reading to produce sigmoidal traces, as shown below.

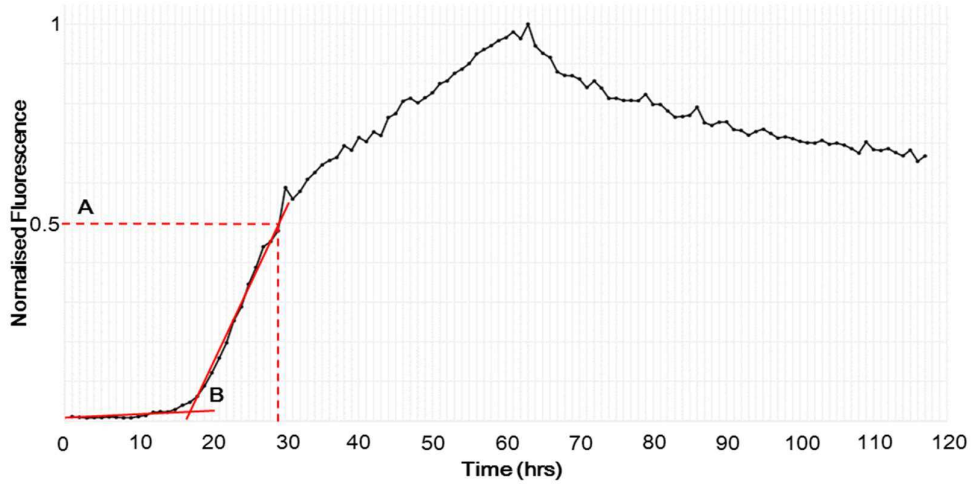

Figure 3.16: Example $t_{1/2}$ and L_e Calculation from Thioflavin-T Data.

ThT data was normalised to the highest fluorescence value. The time taken for each protein to reach half maximum fluorescence ($t_{1/2}$) was determined using the method labelled A. The lag end (L_e) was determined via method B.

As shown in figure 3.16, the data was fitted to determine the time taken for the protein to aggregate to half its highest value ($t_{1/2}$) labelled in figure 3.16 as method A, and the end of the lag phase (L_e) was determined by plotting a line of best fit

for the lag phase and the exponential growth phase, and calculating the intercept of the two, labelled method B in the figure (Mason *et al.*, 2016).

As shown in figure 3.17, the S87D τsyn variant has a slower aggregation rate than WT or S129D overall, whereas S129D has an increased rate over WT. The WT protein has an average $t_{1/2}$ of 42.3¹ 14.8hrs, whereas the $t_{1/2}$ of S87D was increased to 54¹ 5.3hrs, and S129D had the shortest $t_{1/2}$ overall at 27.3¹ 2.1hrs. Significance was only determined between the S87D and S129D sample however, with S129D showing a significantly increased rate of aggregation ($p<0.05$).

The lag phase of WT τsyn aggregation lasts on average 25.7¹ 7.7hrs, whereas lag times for the phosphomimic mutants S87D and S129D are both reduced in comparison, to 23.6¹ 4.1 and 19.2¹ 1.2, respectively. The lag end of S87D was significantly slower than WT τsyn ($p<0.05$) and the end of the lag phase was significantly faster for S129D than S87D ($p<0.05$). Again, no significance was determined between WT and S129D τsyn, likely due to the variability in aggregation rates, particularly with the WT sample. Hence the S129D τsyn variant aggregates more rapidly than the WT or the S87D proteins.

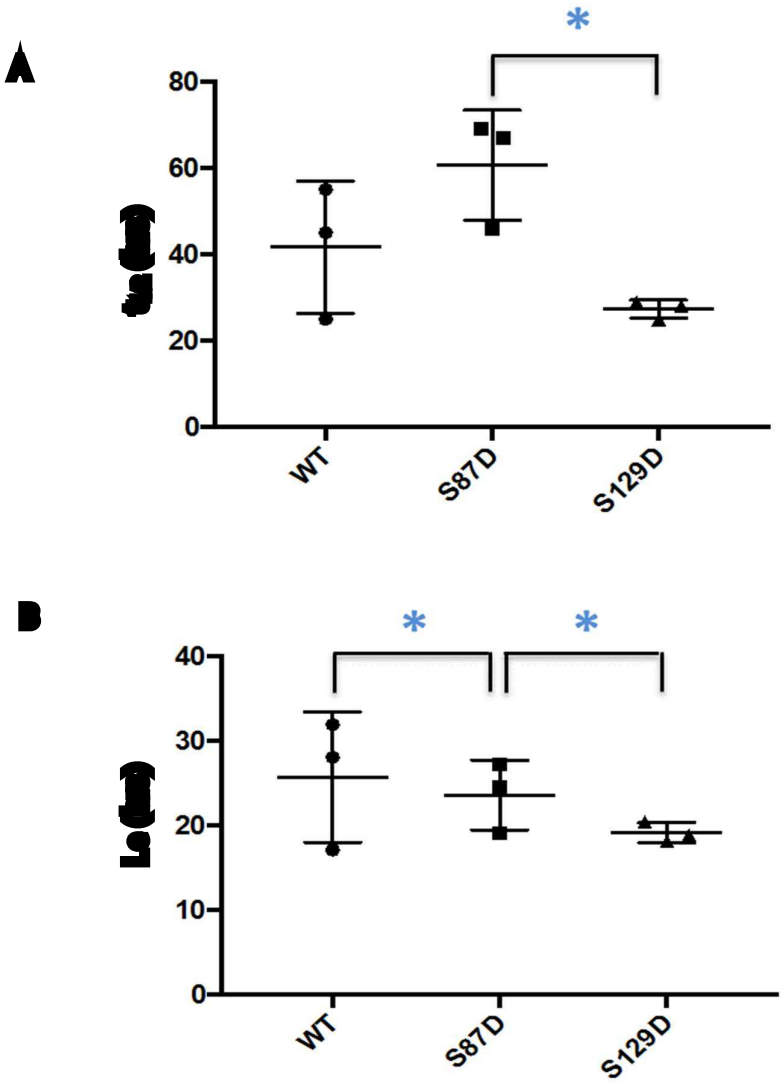

Figure 3.17: ThT Assay Comparing Aggregation Rates of WT, S87D and S129D hSyn.

A) Average $t_{1/2}$ values of WT, S87D and S129D α-syn observed from three separate ThT experiments. B) Average lag time end values of WT, S87D and S129D α-syn from three separate ThT experiments. (* $p<0.05$).

3.3.9 S129D αSyn Aggregates Fastest of All Variants in the Presence of Metals

As shown in figure 3.18, WT αsyn aggregation rates are increased in the presence of equimolar copper. A significant reduction ($p<0.05$) in both $t_{1/2}$, from an average 42.3¹ 14.8hrs to 18.3¹ 6.7hrs, and lag time ($p<0.05$) from an average 25.7¹ 7.7 to 12.3¹ 5.6hrs can be observed, demonstrating copper can increase the aggregation rate of WT αsyn. This data is in keeping with previously published findings (Mason *et al.*, 2016; Uversky *et al.*, 2001; Binolfi *et al.*, 2006), and suggests the presence of copper ions aid in the pathogenesis of PD, by increasing the rate at which amyloid fibrils are formed through the increased population of the collapsed monomeric conformations.

In the presence of equimolar iron however in ammonium acetate buffers, as shown in figure 3.18, the average lag time of the WT protein does not change in the presence of iron, at 24.6¹ 2.4hrs, compared with 25.7¹ 7.7 for the untreated sample, however the $t_{1/2}$ value is decreased to just 34.3¹ 3.2hrs from 42.3¹ 14.8 hrs, which suggests the elongation rate is faster than that of apo WT.

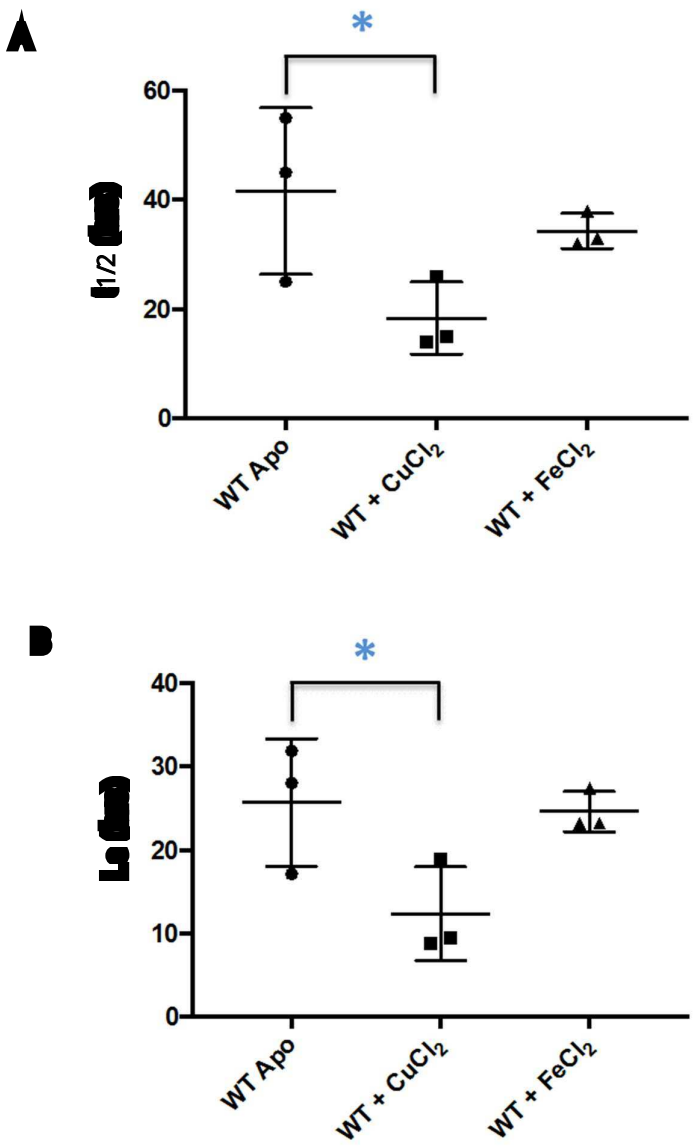

Figure 3.13: ThT Assay of WT hDyn With or Without $CuCl_2$ or $FeCl_2$.

A) Averaged $t_{1/2}$ values for WT hDyn apo, and in the presence of equimolar $CuCl_2$, from three independent ThT experiments. B) Averaged lag time and values for WT hDyn apo, and in the presence of equimolar $CuCl_2$, from three independent ThT experiments. (* $p<0.05$).

As shown in figure 3.19, S87D reacts in a similar manner to WT in the presence of metals, but has a longer aggregation rate. In the presence of equimolar copper, $t_{1/2}$ is significantly reduced ($p<0.05$) from an average 54.0¹ 5.3hrs to 32.0¹ 2.0hrs, and the lag phase is significantly reduced ($p<0.05$) from 23.58¹ 4.1hrs to 20.3¹ 0.8hrs in comparison to the untreated protein. As the aggregation rates overall are slowed in comparison to the WT protein, this would suggest that the protein is less amyloidogenic and potentially less pathogenic. However, like the WT protein this propensity to aggregate can be increased via the addition of copper.

The S87D mutant also acts in a similar manner to WT in the presence of equimolar iron. With the S87D T-syn variant however, an increase ($p<0.01$) in $t_{1/2}$ is observed of 54hrs to 78.8hrs, and the lag phase is also extended ($p<0.01$) to 40hrs from 22hrs in buffer alone. This was found to have greater statistical significance than the increase demonstrated upon incubation with copper, demonstrating the presence of iron slows the aggregation rate of this variant.

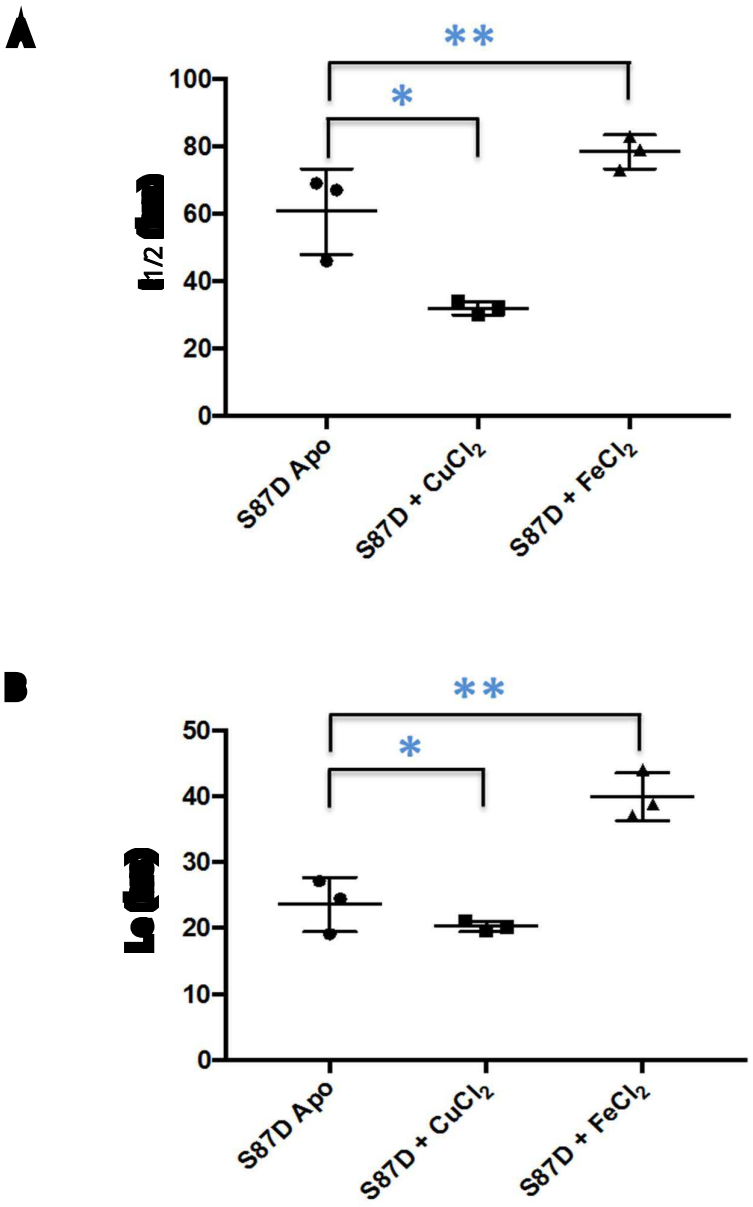

Figure 3.13: ThT Assay of S87D IDyn With or Without $CuCl_2$ or $FeCl_2$.

A) Averaged $t_{1/2}$ values for S87D IDyn apo, and in the presence of equimolar $CuCl_2$, from three independent thioflavin-t experiments. B) Averaged lag time and values for S87D IDyn apo, and in the presence of equimolar $CuCl_2$, from three independent ThT experiments. (* $p<0.05$, ** $p<0.01$).

The S129D mutant has the fastest aggregation rate overall in comparison to WT and S87D, as shown in figure 3.20. It also acts in a similar manner to WT in the presence of metals, with an increased aggregation rate in the presence of copper, and decreased rate in the presence of iron.

As shown in figure 3.20, when diluted with equimolar copper, the protein has a significantly decreased ($p<0.01$) lag time from 13.7hrs to 7.8hrs, which is the most pronounced reduction observed for all proteins. The $t_{1/2}$ value is also significantly reduced ($p<0.05$) from 27.3hrs to 14.3hrs.

In the presence of equimolar iron, lag time is statistically significantly increased ($p<0.01$) from 13.7hrs to 49.8hrs, and $t_{1/2}$ was also significantly increased ($p<0.01$) from 27.3hrs to 60hrs. Once again this was a more significant alteration than the increase in aggregation observed with copper.

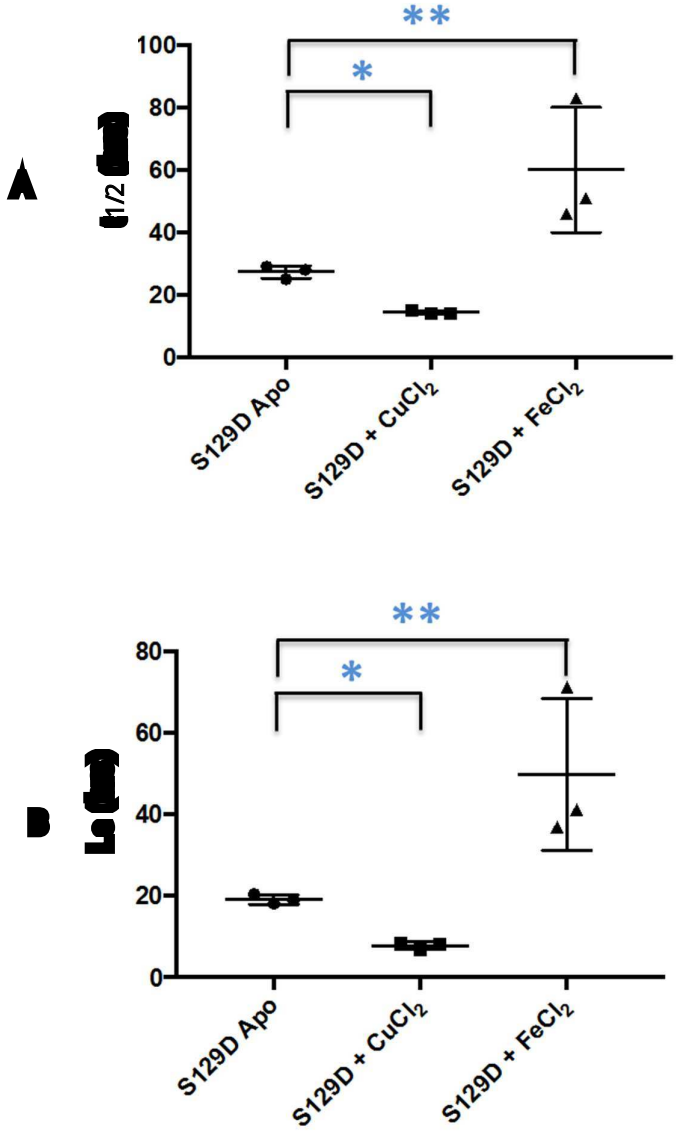

Figure 3.28: ThT Assay of S129D hSyn With or Without $CuCl_2$ or $FeCl_2$.

A) Averaged $t_{1/2}$ values for S129D α-syn apo, and in the presence of equimolar $CuCl_2$ or $FeCl_2$, from three independent ThT experiments. B) Averaged lag time values for S129D α-syn apo, and in the presence of equimolar $CuCl_2$ or $FeCl_2$, from three independent ThT experiments. (* $p<0.05$, ** $p<0.01$).

3.4 Discussion

Results presented in this chapter support the hypothesis that αsyn phosphorylation at S129 has pathological significance for the development of PD, whereas S87 phosphorylation appears to have a protective effect.

When CSDs of the three protein variants were examined from ESI-IMS-MS experiments, S129D αsyn appeared to have a narrower CSD of +17 to +5 compared with +18 to +5 for the WT and S87D variants. If this is a true result, it suggests that S129D αsyn has a narrower conformational distribution overall. However, as discussed in chapter 1, questions are arising around the true reflection ESI-IMS-MS and gas-phase conformations have on the conformations present within the solution. Both unfolding and compaction of protein species and protein subunits of IDPs in the gas-phase have been previously reported (Ruotolo *et al.*, 2005; Zilch *et al.*, 2007; Bohrer *et al.*, 2008; Pagel *et al.*, 2013; Borysik *et al.*, 2015), and it appears that, rather than reflecting true solution conditions, ESI-IMS-MS creates a broader conformational equilibrium containing both species present in solution, and those which are artefacts of the electrospray process. Multiple repeats of the experiment were performed, with the same CSD observed each time. We can be confident therefore, that the S129D variant displays a CSD consistent with a more compact conformation. However, it cannot be confirmed exactly which of these species observed, for all three proteins, are a true reflection of those present within the solution.

When the ATDs of each protein were compared, no significant alterations to the conformational distribution of the two phosphomimic proteins were noted in comparison to the WT.

ESI-IMS-MS data shows that the addition of $CuCl_2$ to the Πsyn solution resulted in an increase in the proportion of the most compact conformations present within the compact CSIs +8 and +7 for all three protein variants. S129D Πsyn was determined to have a higher binding affinity for copper ions, and S87D a lower affinity, relative to the WT protein. S129D was also shown via ThT assay to have an increased aggregation rate in comparison to WT, and S87D had a slower aggregation rate than both other variants. The aggregation rate of all three proteins was increased upon incubation with $CuCl_2$, and decreased upon incubation with $FeCl_2$. Overall these results indicate that S129 phosphorylation results in a protein that is more amyloidogenic than the WT protein, and has a higher affinity for copper ions.

Changes in the spectral properties of what should be identical Πsyn samples are seen within this chapter, and have been well documented previously. These differences may be accounted for by several factors. Variation between protein batches may be partially accounted for by the protein production method, by recombinant expression in *E. coli*. Slight alterations within the preparation can arise during sample handling, for example; the buffer composition, time spent in dialysis, time spent on the freeze drier, or whether the protein has been frozen

between growth in *E. coli* and its initial anion exchange chromatography purification step. Despite care being taken to be consistent between preparations, the process has many manual steps, so there are opportunities for small variations to occur. Residual salts in the purification buffers can also alter the solution conditions and therefore the protein conformation and this could be an issue if there is variation in the dialysis or purification steps.

Differences in conformational distribution between machine acquisitions months apart, particularly differences in drift times, can be also accounted for by several factors, including settings on the mass spectrometer, for example increased pressure in the ion mobility cell, atmospheric pressure changes around the ESI source and changes in the position of the ESI source, which is a particular issue if using a detachable auto-sampler such as the NanoMate. The mass spectrometer used in these experiments was also subject to mode changeover every few weeks between ESI and MALDI, which may cause other slight internal differences, for example with the Q-TOF pressure. Calibration of the mass spectrometer should eliminate a number of issues with the internal settings, but atmospheric changes external to the machine are difficult to account for experimentally.

There is a general issue within the ion mobility research community around differences in CCSs observed between research groups and their publications. This may be due to a lack of standardisation in machine settings, buffer

composition and molarity, and protein production methods between groups, as some research groups purchase pre-made proteins, whereas others produce them by recombinant expression. Differences between identically made samples run using the same buffer and same machine settings have previously been reported in the literature, for example two experiments conducted on the same day with Πsyn by the Bowers research group showed a CSD of +21 to + 5 for the initial sample, with the second sample from the same source run later in the day producing a CSD of +19 to + 5 (Beveridge *et al.*, 2015). These discrepancies between data sets observed within ESI-IMS-MS experiments may also be a consequence of the production of artefact species during electrospray.

Ex vivo material from different patient and animal sources has also been found to give conflicting results in ESI-MS experiments. For example, when endogenous Τsyn was isolated directly from mouse brain tissue, and subjected to mass spectrometric analysis for the first time, it was identified as an unstructured monomer containing significant post-translational modifications, including acetylation of the N-terminus, with a determined mass of 16,408 ± 894 Da, rather than the predicted 14,485 Da (Burrŭ *et al.*, 2013), however the error observed within these experiments is extremely large at ± 894 Da, which does not lend much support to the findings. Fauvet *et al* also demonstrated that Τsyn isolated from human erythrocytes was predominantly an intrinsically disordered monomer, also using ESI-MS to confirm the mass and demonstrated the existence of two protein species each with a different post-translational

modification; the main species with a mass of 14,504 Da, corresponding with a single acetylation on the protein, and a second at 14,519 Da, consistent with a single methionine addition. CSD data of the purified protein are not shown, however they did determine the CSD of recombinant -syn as +19 to +12 CSIs, following both native and denaturing purification protocols (Fauvet *et al.*, 2012). Kang *et al*, also report that both N-terminal acetylated recombinant -syn and non-acetylated recombinant -syn, under mild physiological conditions, present primarily as a disordered monomer by ESI-IMS-MS, with CSDs of +14 to +7 and +13 to + 7 respectively (Kang *et al.*, 2012) and this is in keeping with more recently reported data on WT vs acetylated forms (Mason *et al.*, 2016). The data presented in the literature on the conformational state of -syn demonstrates that it is clearly influenced by the modes of preparation and the initial source of the material being analysed.

Given these variations between both *ex-vivo* and recombinant proteins, results obtained in this chapter for WT -syn are largely in keeping with those previously recorded. Recently published data from this research group also showed there to be eight distinct conformations of WT -syn when acquired in 50mM ammonium acetate at a concentration of 10¾M using positive ion mode EDI-IMS-MS, using the same fitting methods as those reported here (Mason *et al.*, 2016). Relative proportions of the conformations at each charge state were very similar to results presented here, and the same pattern of extended conformer reduction in favour of more compact species can be seen. However, there was a slight difference in

CCS calculation at CSI +7 of ~60 ð², though this small change is in keeping with differences in CCS recorded in the literature (Phillips *et al.*, 2015; Beveridge *et al.*, 2015). The wider CSD of WT αsyn observed in experiments presented in section 3.3.3 has also previously been reported by this research group, where acquiring WT αsyn in 50mM ammonium acetate showed a CSD of +18 to +6. This data was however, acquired using borosilicate glass capillaries rather than a NanoMate ion source (Illes-Toth *et al.*, 2013). A similar distribution of dimers was also noted in this study, with CSIs between +21 and +13 being observed (Illes-Toth *et al.*, 2013).

Other previously reported studies have observed fewer conformational species, despite observing a wider CSD. For example, in positive ion mode WT αsyn was observed to populate four different conformations, again differentially characterised by their varying degrees of compactness (Beveridge *et al.*, 2013). The most compact conformation spanned CSIs +5 to +10, the compact intermediate conformer spanned the +7 to +13 CSIs, the more disordered intermediate spanned the +10 to +17 CSIs, and the most expanded conformer spanned CSIs +14 to +24 (Beveridge *et al.*, 2013). This again can be put down to differences in mass spectrometry settings and the protein表intrinsic disorder. Given the inherent variability observed with WT αsyn MS data presented in the literature, the data presented in this chapter are consistent with our own and other research groups.

ESI-IMS-MS spectra or conformational distributions for the S87D and S129D Tsyn variants have not previously been reported. The S129D mutation has been investigated utilising C-terminal fragments of the protein, but no spectra for the whole proteins exist (Lu *et al.*, 2011). Data presented in this chapter suggests the S129D mutant Tsyn has a higher propensity to aggregate, and therefore may be the more pathogenic of the variants investigated, due to its slightly more compact conformational distribution, as demonstrated by its narrower CSD, and the increased CSD of the dimeric species.

Metal binding studies showed that only copper binding to Πsyn was observable under MS compatible conditions. The binding of magnesium and iron to WT Tsyn has previously been demonstrated by NMR spectroscopy, tyrosine fluorescence quenching, and ESI-MS (Golts *et al.*, 2002; Binolfi *et al.*, 2006; Peng *et al.*, 2010). The iron binding observed within ESI-MS experiments however was achieved via addition of iron in the complex $Fe(NH_4)_2(SO_4)_2$, and performed on a linear ion trap mass spectrometer, and was also conducted in 50% methanol, which is not physiologically relevant and would be unsuitable for conformational studies conducted in this chapter. Binding of metal ions such as Cu(II) and Fe(II) to Tsyn peptides has previously been observed using ESI-MS using 50/50 v/v MeOH and H_2O and by chemiluminescence (Liu and Franz, 2007; Lu *et al.*, 2011). Again, these buffers are not physiologically relevant, and attempts to reproduce this data here using the whole protein were unsuccessful. A range of different buffers and concentrations were investigated in this chapter, in an attempt to observe binding

of iron, zinc, magnesium and manganese, including 5, 10, 25, 50 and 100mM ammonium acetate, 50mM ammonium bicarbonate, 10mM 4-methylmorpholine, and water:ACN:MeOH. Metals with other counter ions such as FeS, ZnS and MnS were also investigated, and a range of mass spectrometry machine parameters were applied. One possible reason that metal binding is not observed is that the metal ions are complexing with a component of the buffer, such as the acetate in the ammonium acetate buffers. ESI-IMS-MS may also be unsuitable for observations of metal binding due to the addition of the drift tube and the low affinity of the interaction, and collisions with the buffer gas may dissociate ligand binding. It is possible this is what has occurred in experiments presented in this chapter, as the other metal ions investigated are known to have a much lower binding affinity for Tsyn, and therefore may only be weakly associated and readily dissociated. Despite the lack of binding observed in ESI-IMS-MS experiments, Fe(II) was still found to slow the aggregation rate of WT, S87D and S129D Πsyn *in vitro*. It is likely that the binding was dissociated during the IMS stages of the mass spectrometry experiments, due to its low binding affinity.

The appearance of further CSIs and an increase in the intensity of extended conformations upon copper binding has however been reported in the literature, with a widening of CSD from +15 to +5 increased to +17 to +5 observed upon addition of equimolar $CuCl_2$ (Mason *et al.*, 2016). The majority of other research investigating copper binding by ESI-IMS-MS report the protein binding two copper ions, though some studies in the literature suggest the protein may be

able to bind as many as 16 copper ions (Ahmad *et al.*, 2012). A study using ESI-IMS-MS in negative ion mode, and utilising glycine to prevent the low affinity, non-specific binding of copper to Tsyn, found the protein bound up to 2 copper ions at a 6:6.66 protein to copper ratio (12┼M Tsyn plus 80┼M copper), however without glycine the protein bound 3 copper ions at this concentration, which is in keeping with the results presented here (Natalello *et al.*, 2011).This study also demonstrated an increase in the number of copper ions binding with increasing copper concentration, with one copper ion binding at concentrations lower than the protein level, and increasing to two after the copper level was above that of the protein (Natalello *et al.*, 2011). Increased copper concentration and therefore increased copper binding is also known to increase the T-helical content of Tsyn, as investigated by far-UV CD investigation (Ahmad *et al.*, 2012). Some studies, as previously mentioned, suggest there may be up to 16 binding sites in total for metal ions to WT Tsyn, suggesting there could be 14 non-specific binding motifs this binding is most likely brought about by non-specific electrostatic attraction (Ahmad *et al.*, 2012).

Currently three copper binding sites have been well established; one at the N-terminus, one at H50, and a third in the C-terminal region (Binolfi *et al.*, 2012). Initial studies suggested H50 to be the high affinity, initial binding site, and this is the case for copper binding to a large number of amyloid proteins (Ahmad *et al.*, 2012), though more recent studies suggest this is not the case, and the N-terminal to be the highest affinity binding site with H50 and the C-terminal region

as lower affinity sites, as copper does not bind to histidine residues at pH levels below 6.0, but still readily binds copper ions at pH 2.5. T and T-synuclein however have the same EPR spectra when bound to copper, but the single histidine residue is in a different position; amino acid 65 instead of 50, therefore this also suggests this is not the high affinity or specific binding site otherwise the EPR spectra would be notably different (Ahmad *et al.*, 2012). A more recent study suggests H50 may be required for N-terminal copper binding to physiologically relevant N-terminal acetylated Tsyn, as H50Q mutant Tsyn missing the histidine residue, has a greatly impaired copper binding ability compared with N-terminally acetylated unmodified Tsyn (Mason *et al.*, 2016), though no differences were observed between unmodified H50Q and WT Tsyn

Previously published data analysing the CSD of Tsyn in the presence of Cu^{2+} also reveals a decrease in disordered conformers and a shift towards the more highly compact conformations. The binding of copper ions to Tsyn is known to cause a stable turn like structure in the protein at the H50 binding site, and this folding offers favourable conditions for T-sheet nucleation as the protein is pulled round to become adjacent with itself. Hydrogen bonds form between proximal amino acid side chains, anchoring and stabilizing the structure, and a T-sheet is formed. This serves as a template for further T-sheet formation and stacking of the protein (Rose *et al.*, 2011). It is still unclear where the primary copper-anchoring site is located on the protein, however data presented here would lend support to the primary site being H50, as the introduction of a stable turn into the Πsyn sequence

upon Cu (II) binding (Rose *et al.*, 2011), would cause a suitable compaction of the protein to produce the conformational changes observed in these experiments. As no further compaction was observed upon the binding of multiple copper species within experiments presented here, it is likely that the binding of the first copper ion occurs at H50, introducing this turn into the protein and causing compaction, and the binding of further ions to the N or C-terminus has little effect on the conformation of the protein thereon.

As no novel conformations appear to be produced upon copper binding, rather a shift between previously existing conformations, this suggests Tsyn must readily sample this copper induced shape within its normal equilibrium, it is possible copper acts as the anchor for securing the entry to the amyloid aggregation pathway, rather than inducing the amyloid-forming conformations itself. The ability of metal ions, particularly Cu^{2+} to promote oligomerisation and amyloid fibril formation of Tsyn has been previously well established (Ahmad *et al.*, 2012; Uversky *et al.*, 2001), though very little data to date exists on the aggregation kinetics of the S87D or S129D phosphomimic mutants, or how metal ions affects this aggregation. Studies into the aggregation kinetics of S129D vs WT Tsyn have suggested there is no difference in the aggregation rate between the two proteins. It must be considered that ThT experiments conducted here were performed in 50mM ammonium acetate rather than the commonly used tris buffer, in keeping with the mass spectrometry analysis performed here. These changes in conditions will have affected the aggregation rates.

3.5 Conclusions

All experiments outlined in this chapter support the hypothesis that phosphorylation at serine129 promotes the pathogenesis of PD. Data presented here shows faster aggregation times and increased interaction with metal ions as a result of mimicking phosphorylation.

The S129D protein aggregates faster than WT or S87D αsyn, and this effect is increased in the presence of $CuCl_2$. Copper binding to all three protein variants investigated, induces a shift to more compact states but does not cause the formation of novel conformations. It appears then that binding pushes the equilibrium towards the more amyloidogenic conformations which are already sampled by the protein within the equilibrium and may be acting to stabiles these compact states resulting in an increase in aggregation.

A summary figure outlining the role of copper (II) binding and phosphorylation at S129 in increasing the aggregation of αsyn can be observed in figure 3.21. It appears copper binding causes a stable, turn-like structure on the αsyn protein, which causes a shift towards the more compact species within the protein equilibrium. These compact species then further aggregate into oligomers, protofibrils and eventually the mature fibrils observed within LBs. Phosphorylation at S129 also causes an increase in the aggregation rate of the protein, however the modification does not cause dramatic conformational changes to the protein, so it is still as yet unclear how this modification is causing

an increase in the formation of oligomeric species. It could be that the charge on the protein causes it to more readily self-associate, or bind trace metals, but further investigation will be required to confirm this. Given the increased affinity of S129D to bind copper, this stabilisation of the aggregation prone compact states may be further enhanced by the presence of the phosphomimic, and interaction with the H50 binding site.

The S87D protein variant had the opposite effect, supporting previous suggestions that this modification could be protective. The presence of Fe (II) in the samples, despite binding being unobservable during ESI-IMS-MS analysis, also caused a delay in aggregation rates. It is still unclear however how these pathways are functioning, but the site of phosphorylation does appear to be important in controlling the aggregation of the protein.

Care must be taken in interpreting data from this chapter, due to the discrepancies with ESI-IMS-MS and the use of phosphomimics, therefore data should now be acquired using the fully phosphorylated protein and using alternative methodologies in conjunction with ESI-IMS-MS, to fully elucidate the method of S129 phosphorylation on the increased aggregation of the protein.

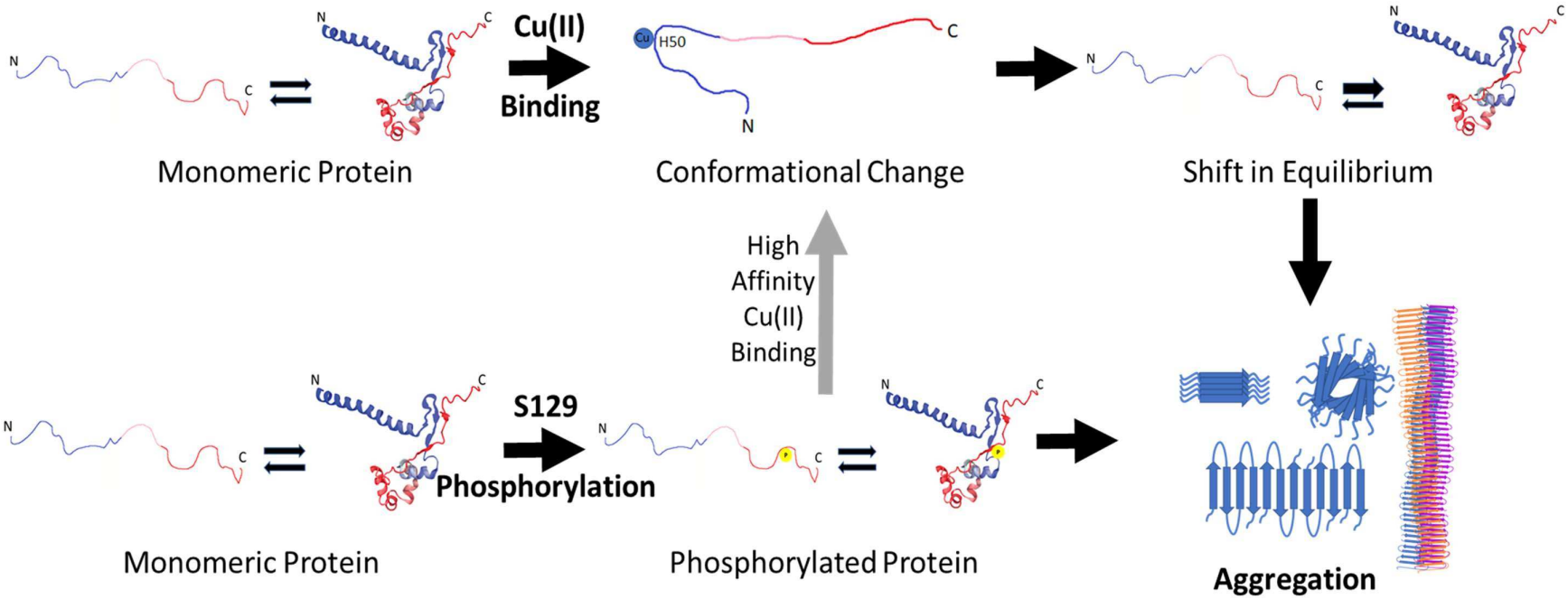

Figure 3.21: Proposed Mechanisms of Cu(II) and S129D-Induced Increase in Aggregation

The two proposed mechanisms by which Cu(II) and S129 phosphorylation increase the aggregation rate of Hyn *in vitro*. Top: The binding of Cu(II) causes a conformational change, shifting the equilibrium towards the more compact states, inducing increased aggregation. Bottom: S129 phosphorylation does not alter the conformation of the protein, or cause a shift towards the compact states, however aggregation is again accelerated, suggesting an alternative mechanism or pathway to that induced by the binding of Cu(II). The two pathways are potentially linked, as indicated with the grey arrow, via the high affinity Cu(II) binding site at H50, as S129D Hyn has a higher affinity for Cu(II) binding.

Chapter 4 哑The Effects of Curcumin and its Derivatives on ┳-Synuclein Aggregation

4.1 Introduction

Curcumin is a polyphenolic compound found in the rhizomes, or underground stems, of the *Curcuma longa* plant and a variety of other *Curcuma* plant species. The yellowy-orange crystalline compound is most commonly encountered in the spice turmeric, and in its natural form it has been used for medicinal and culinary purposes in Chinese and Indian culture for thousands of years. Due to its extensive use for a wide variety of ailments and in the preparation of numerous culinary dishes, curcumin has been dubbed 裔ndian gold哟 Its historic medicinal uses include the treatment of inflammation, dyspepsia, stress and mood disorders (Witkin and Li, 2013).

Recently curcumin has been proving its potential as a therapeutic for a range of diseases, including multiple types of cancers (Davatgaran-Taghipour *et al.,* 2017; Allegra *et al.,* 2017) and neurological disorders. Publications citing curcumin on PubMed have risen steadily since 2003 (Ji and Shen, 2014), with a search for 裔urcumin哟ielding 9970 results at the time of writing compared to just 1014 in 2003. Curcumin has shown numerous pharmacological properties, including antioxidant, anti-inflammatory, anti-bacterial, anti-cancer, anti-spasmodic and anti-viral functions (Ji and Shen, 2014; Modasiya and Patel, 2012; Jha *et al.*, 2016). Curcumin has progressed into clinical trials for a number of diseases and

disorders, including colorectal neoplasia (Carroll *et al.*, 2011), depression (Lopresti *et al.*, 2015; Sanmukhani *et al.*, 2014) and AD (Ringman *et al.*, 2005; Baum *et al.*, 2008).

Curcumin has been gaining interest as a potential treatment for Parkinson's disease, due to its ability to reduce the aggregation of α-syn, along with several other amyloidogenic proteins, *in vitro*. These include Aβ (Yang *et al.*, 2005), TTR (Ferreira *et al.*, 2011) and PrP (Hafner-Bratkovič *et al.*, 2008). This suggests a possible common mode of action and it could therefore potentially be utilized as a therapeutic for a number of related amyloid diseases.

4.1.1 Curcumin Chemistry

The structure of curcumin was elucidated in 1910 and identified as 1,7-bis(4-hydroxy-3-methoxyphenyl)-1,6-heptadiene-3,5-dione, also known as diferuloylmethane. The molecular formula of curcumin is $C_{21}H_{20}O_6$, and it has a molecular weight of 368.38 Da. Natural curcumin, when purified from plant sources, contains around 77% of the compound we term curcumin, plus two related compounds; demethoxycurcumin (18%) and bis-demethoxycurcumin (5%), the structures of which are shown in figure 4.1, and all three belong to a group of compounds known as diarylheptanoids. Any future reference to curcumin in this chapter is referring to the first structure displayed in figure 4.1. Curcumin itself is insoluble in water at acidic and neutral pH, but soluble in polar

and non-polar organic solvents, and in alkali or organic solvents such as glacial acetic acid, DMSO or ethanol (Modasiya and Patel, 2012).

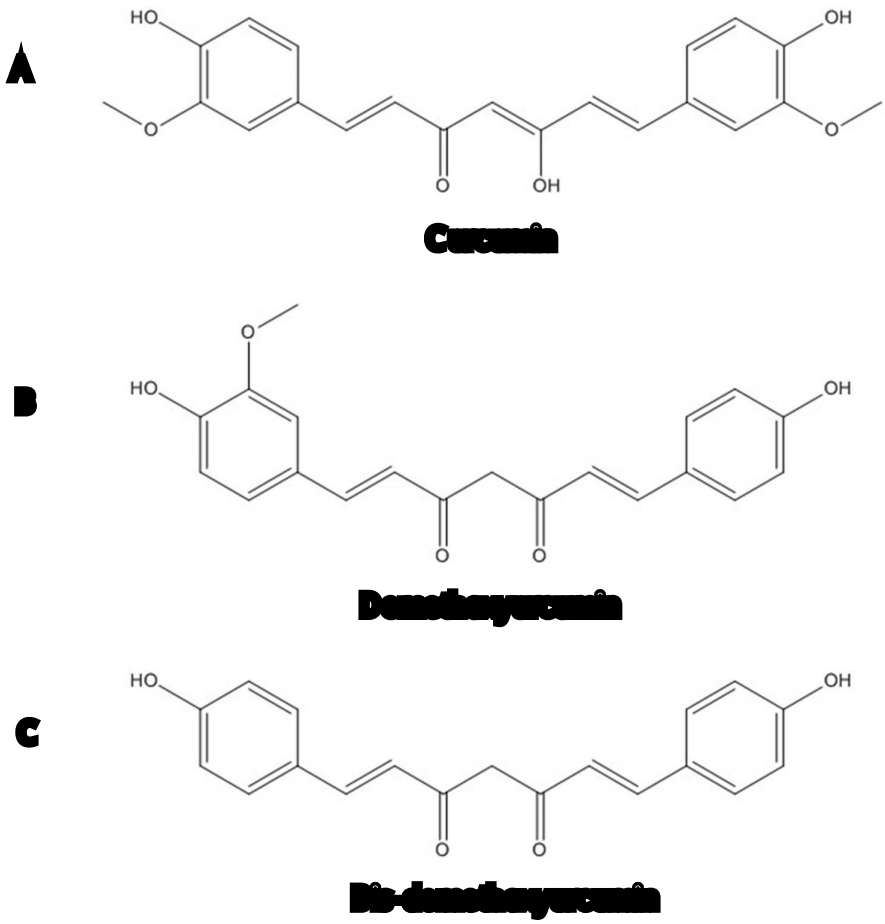

Figure 4.1: Natural Curcumin Structures.

The structures of A) curcumin, B) demethoxycurcumin and C) bis-demethoxycurcumin. Adapted from Sandur *et al*, 2007.

4.1.2 Curcumin Bioavailability

Despite curcumin's promise as a therapeutic for a wide range of diseases, its clinical use has been hindered by the molecule's poor bioavailability. Curcumin is almost completely insoluble in water, is rapidly metabolised in the gastrointestinal tract and undergoes glucoronidation in the liver and because of this, it has demonstrated inadequate tissue absorption (Ringman *et al.*, 2005; Kundu *et al.*, 2016). It has however been demonstrated to cross the blood brain barrier (BBB) in several mouse models of Alzheimer's disease (Yang *et al.*, 2005; Kundu *et al.*, 2016; Ringman *et al.*, 2005; Garcia-Alloza *et al.*, 2007; Mishra and Palanivelu, 2008). Several research groups have also used piperine as an adjuvant to improve curcumin's oral bioavailability, with promising results in animal models (Singh *et al.*, 2015; Panahi *et al.*, 2014; Ucisik *et al.*, 2013; Shoba *et al.*, 1998). More recently, a study utilising piperine in combination with lipid nanoparticles greatly improved oral bioavailability in an *in vivo* mouse model, and demonstrated that the combination could still effectively cross the BBB (Kundu *et al.*, 2016). Piperine is known to inhibit hepatic glucoronidation, aiding the evasion of metabolism (Ringman *et al.*, 2005). Piperine alone has also been demonstrated to have neuroprotective effects, with anti-inflammatory, anti-apoptotic and anti-oxidative stress functions being reported, making its pairing with curcumin even more exciting as a possible treatment for PD (Shrivastava *et al.*, 2013; Al-Baghdadi *et al.*, 2012).

4.1.3 Curcumin as an Inhibitor of Amyloid Aggregation

The first reported success of curcumin as a potential anti-amyloid therapeutic was in 1998, when it was demonstrated that curcumin could block the activity of NFkB, a protein complex involved in DNA transcription, and prevent A-induced apoptosis in human SK-N-MC cells, a neuroblastoma cell line (Kuner *et al.*, 1998). A further study in 2001 also confirmed that curcumin, demethoxycurcumin and bis-demethoxycurcumin were all effective at protecting both rat pheochromacytoma PC12 cells and human umbilical vein endothelial cells from A(1-42) induced oxidative damage (Kim *et al.*, 2001).

Since then, several *in vitro* and *in vivo* studies have proven curcumin's effectiveness in reducing the amyloid formation of several different proteins. The research was entirely focussed on A and Alzheimer's disease until 2008, when curcumin was shown by both western blot and in an SH-SY5Y cell model, to inhibit the aggregation of -syn (Pandey *et al.*, 2008). Curcumin has also been demonstrated to reduce the aggregation of the PrP protein *in vitro*, using ThT assays, where an increased lag time and 6-fold reduction in aggregate formation was observed. In the same study it was also demonstrated that low doses of curcumin could effectively rescue cells from apoptosis induced by exposure to amyloid fibrils of PrP (Lin *et al.*, 2013).

Curcumin is also known to have antioxidant properties, which may be how it exerts its effects on amyloid aggregation. It has been discussed in the literature that increased oxidative stress caused by overexpression of -syn or relating to

increased levels of metals, such as iron, in the *SNPC* plays a key role in PD development and progression. This is believed to occur through the production of ROS (Jenner and Olanow, 1996; Dexter *et al.*, 1989). It has also been shown that -syn oxidised at methionine residues, aggregates more slowly than the unmodified protein via ThT studies. This is suggested to be due to the production of stable, non-toxic oligomeric forms, which halt aggregation at this point, preventing the formation of mature amyloid fibrils (Glaser *et al.*, 2005; Uversky *et al.*, 2002; Zhou *et al.*, 2010). Oxidation at these residues has also been observed to alter the protein membrane binding properties, potentially shielding membranes from oxidative damage (Schildknecht *et al.*, 2013). It has however been demonstrated that certain metals may induce fibrillation of the protein, despite methionine oxidation (Yamin *et al.*, 2003). This suggests there may be both beneficial and pathogenic roles for oxidised -syn, and these roles may vary in different diseases (Schildknecht *et al.*, 2013). It may be the effect of oxidative stress on the dopaminergic cells, as opposed to oxidation of -syn, itself which is driving the protein aggregation and cell-death in PD.

Phenolic antioxidants such as curcumin act as hydrogen donors, which inhibit the propagation of free radical chain reactions (Venkateswarlu *et al.*, 2005), reducing the damaging effect. Inhibition of free-radical species may therefore be a possible mechanism for curcumin prevention of -syn aggregation. It has also been suggested that curcumin exerts antioxidant effects through its inhibition of cyclooxygenase-2 (COX-2), lipoxygenase (LOX) and inducible nitric oxide

synthase (iNOS), enzymes which are all important mediators of the inflammatory response (Menon and Sudheer, 2007).

Curcumin has promise in the treatment of a variety of diseases and by modifying the molecule, it should be possible to create a variety of bioavailable versions to solve several medical problems, from neurological diseases such as PD and AD, to a variety of cancers. This chapter with focus on the use of ESI-IMS-MS and ThT aggregation assays to investigate the effect of curcumin, and thirteen derivatives of the natural molecule, on the aggregation and conformation of T syn, providing evidence for its potential use as an anti-amyloid drug for use in Parkinson disease.

4.1.4 Potential Problems with Curcumin Experiments

It should be noted that experimentally, curcumin is known to interfere with ThT readings, due to the yellow colour and intrinsic fluorescence of the molecule (Hudson *et al.*, 2009), but despite this the technique is still commonly used, as long as appropriate control measures are taken (Yanagisawa *et al.*, 2015; Lin *et al.*, 2013; Jiang *et al.*, 2012; Pal *et al.*, 2016; Mirhashemi, 2012). Fluorescence of curcumin is also known to increase slightly upon protein binding, causing a red shift in max. Care must be taken therefore to account for this intrinsic fluorescence, when studying the anti-amyloid properties of this molecule and its derivatives, when using ThT assays.

To control for the intrinsic fluorescence of the curcumin molecules, an initial baseline fluorescence reading was taken a few minutes after preparation, and these were subtracted from the end-point reading. The initial fluorescence values of each derivative screened can be seen in appendix 4A.

4.2 Aims and Objectives

In this chapter, ESI-IMS-MS along with ThT assays will be utilised to investigate the anti-amyloid properties of natural curcumin and thirteen of its derivatives to screen for potential anti-amyloid drugs of the future.

The main aims of the chapter were to:

- Investigate the anti-amyloid properties of natural curcumin and thirteen in-house synthesised curcumin derivatives to determine whether the anti-amyloid propensity of the molecule could be improved via modification
- Investigate the mechanism of anti-amyloid action via ESI-IMS-MS to determine which protein species, monomeric or oligomeric, are being bound and acted on by the curcumins

4.3 Results

4.3.1 Instrument Settings and Considerations

In order to observe the interaction of curcumin with αsyn, mass spectrometry conditions were optimised. Early experiments presented in section 4.3.2, used the following conditions; cone voltage 45V, source temperature 60°C, Trap DC Bias 45, backing pressure 4.34mbar, trap 15V and transfer 20V. Later experiments from section 4.3.3 onwards, were conducted using a lower trap and transfer settings of 10V and 15V respectively, and backing pressure of 3.47mbar. Higher trap and transfer energies can cause fragmentation of some proteins and dissociation of ligands during ESI-IMS-MS experiments, and can also supress or dissociate oligomeric species within a sample (Schenauer and Leary, 2009; Young *et al.*, 2014). Later experiments with lower trap, transfer and backing pressure values allowed for curcumin binding to be observed, which was not visible in the earlier experiments, suggesting that for mass spectrometry experiments involving αsyn and curcumin, these settings should be reduced to avoid the apparent dissociation of the curcumin molecule from the protein.

4.3.2 Curcumin and its Derivatives Inhibit the Aggregation of αSyn *in vitro*

Natural curcumin was purchased from Sigma Aldrich (#C1386). A library of thirteen curcumin derivatives was kindly provided by Dr Akram Khan from the Biomolecular Sciences Research Centre at Sheffield Hallam University, the structures and predicted molecular weights of which can be seen in table 4.1.

Curcumin	Predicted Molecular Weight	Structure
Natural Curcumin	368.38	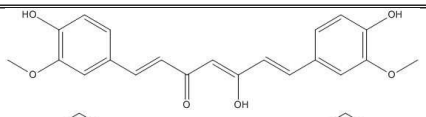
Derivative 1	336	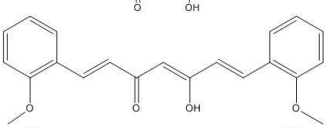
Derivative 2	364	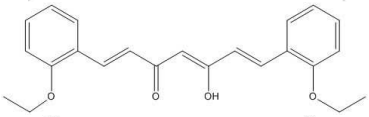
Derivative 3	392	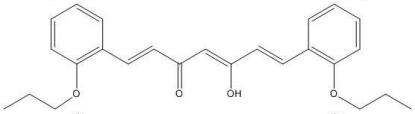
Derivative 4	420	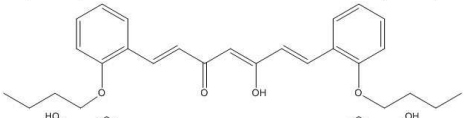
Derivative 5	408	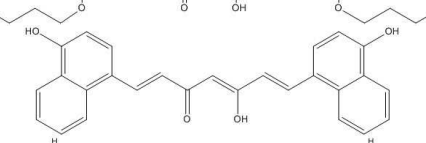
Derivative 6	390	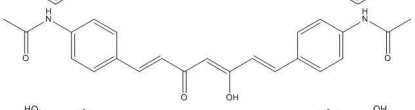
Derivative 7	398	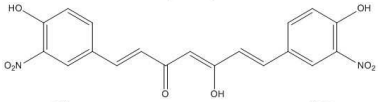
Derivative 8	396	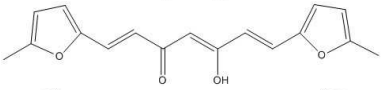
Derivative 9	284	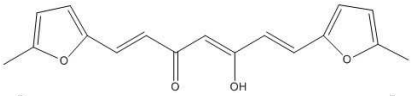
Derivative 10	312	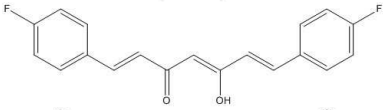
Derivative 11	376	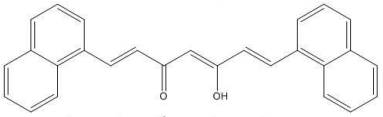
Derivative 12	432	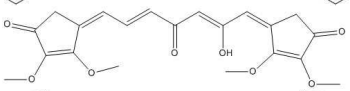
Derivative 13	316	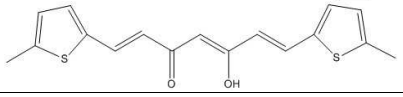

Table 4.1: Structures of Natural Curcumin and Curcumin Derivatives.

Structures and predicted molecular weight values of natural curcumin and thirteen in-house prepared derivatives, kindly provided by Dr Akram Khan of Sheffield Hallam University.

To determine the effects of each of these derivatives on amyloid formation, ThT assays were conducted in 50mM ammonium acetate buffer, to mimic conditions utilised during mass spectrometry experiments, with WT -syn at a high concentration of 70¾M to induce aggregation. Curcumin and derivatives were diluted appropriately so the final concentration of curcumin was equal to that of the protein, and the final DMSO volume was 1%. As a control, the same concentration of DMSO was also added to the WT -syn samples. Samples were incubated for 4 days at 37ØC with continuous shaking, as described in section 2.2.4.2, to induce the formation of amyloid fibrils, before an end-point fluorescence reading was obtained. Experiments were conducted in triplicate, and error bars generated from the standard deviation of the mean. Results are presented as a percentage value of the aggregation of the WT -syn only sample fluorescence.

Results shown in figure 4.2 clearly show decreased fluorescence signals, indicative of a lack of amyloid formation, in the presence of natural curcumin, and several derivatives screened. Natural curcumin reduced the amount of -sheet containing aggregates to around 23¹ 0.05% of the total found in the WT -syn alone sample, with a reduction in fluorescence signal of 76.9¹ 0.05% being observed, with significance of $p<0.0001$ as calculated by non-parametric Kruskal-Wallis and post-hoc Conover-Inman test. Significance of all derivatives screened in comparison to the WT Πsyn sample and the natural curcumin sample can be seen in table 4.2.

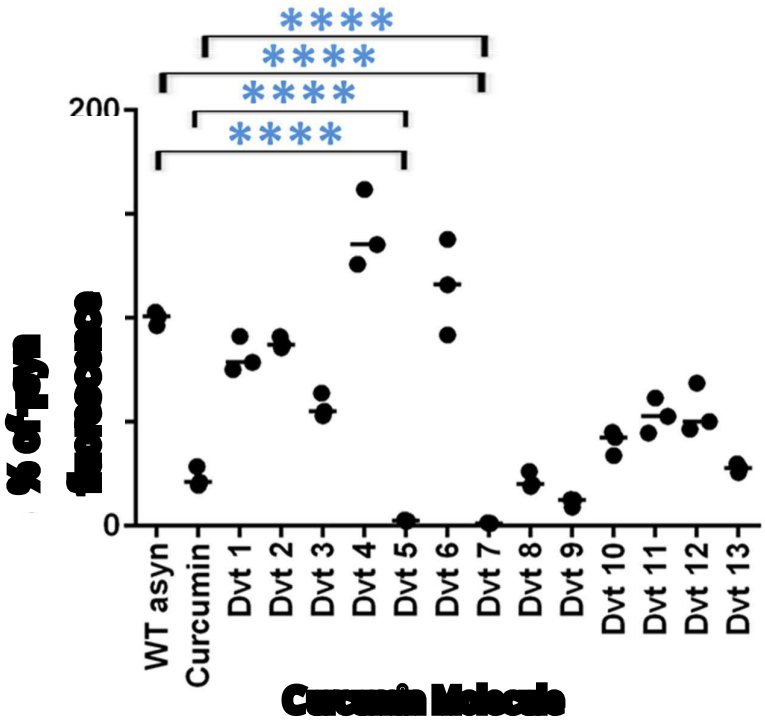

Figure 4.2: Curcumin Derivative Screen for α-Syn Aggregation Inhibition.

End point fluorescence readings from a ThT assay investigating the effects of 70μM natural curcumin or curcumin derivatives (Dv) on the aggregation of equimolar WT α-syn, after subtraction of the initial t=0 fluorescent reading. Results are shown as a percentage of the α-syn only sample (** = p<0.0001). Only the significance of derivatives 5 and 7 are shown on the graph.**

Derivatives 1, 2, 3, 5, 7, 8, 9, 10, 11, 12 and 13 all also significantly reduced the fluorescence signal of the samples compared to the protein alone ($p<0.05$ 唖 $p<0.0001$), whereas derivative 4 caused a significant increase in fluorescence signal ($p<0.05$) with an increase of 41.1¹ 0.19% being observed. Derivative 6 caused no significant alterations to fluorescence either way. This demonstrates that not all derivatives of curcumin would be suitable in either preventing or treating amyloid aggregation, and there is structural specificity to the prevention of aggregation. Hence, specific functional groups on the molecule are key to this interaction, and will be discussed in greater detail later in the chapter.

Three of the derivatives screened, numbers 5, 7 and 9, were significantly more effective at reducing protein aggregation than natural curcumin, with a reduction in fluorescence signal of 97.4¹ 0.005% ($p<0.0001$), 98.7¹ 0.003% ($p<0.0001$) and 88.5¹ 0.02% ($p<0.0001$) respectively being observed. In contrast, derivatives 1, 2, 3, 4, 6, 10, 11 and 12 were all significantly less effective than the natural molecule, with an increase in fluorescence observed in comparison. Derivatives 8 and 13 showed no significant change, suggesting they are equally as effective as natural curcumin.

Curcumin	Significance Over αSyn Only	Significance Over Natural Curcumin
Natural Curcumin	P<0.0001	(Increased) P<0.0001
Derivative 1	P=0.003	(Increased) P<0.0001
Derivative 2	P=0.0115	(Increased) P<0.0001
Derivative 3	P<0.0001	(Increased) P<0.0001
Derivative 4	(Increased) P=0.0266	(Increased) P<0.0001
Derivative 5	P<0.0001	P<0.0001
Derivative 6	-	(Increased) P<0.0001
Derivative 7	P<0.0001	P<0.0001
Derivative 8	P<0.0001	-
Derivative 9	P<0.0001	P=0.0048
Derivative 10	P<0.0001	(Increased) P=0.0012
Derivative 11	P<0.0001	(Increased) P<0.0001
Derivative 12	P<0.0001	(Increased) P<0.0001
Derivative 13	P<0.0001	-

Table 4.2: Significance of Curcumin Derivatives Anti-Amyloid Aggregation Propensity Over αSyn Alone or Natural Curcumin.

P values were determined using Kruskall-Wallis and post-hoc Conover-Inman statistical analysis. Table cells without stated P values (-) were not significant.

To assess whether the enhanced effect of the derivatives was exclusive to αsyn, a second amyloidogenic protein was also investigated. Lysozyme was chosen as it assembles at pH 2.0 and 65°C (Cao *et al.*, 2004) and hence the ability of the

derivatives to bind to amyloid proteins could be investigated under alternative assembly conditions. Aggregation studies were conducted as described in section 2.2.4.3, and an initial fluorescence reading was again taken and subtracted from the end-point results to account for the intrinsic fluorescence of the curcumins.

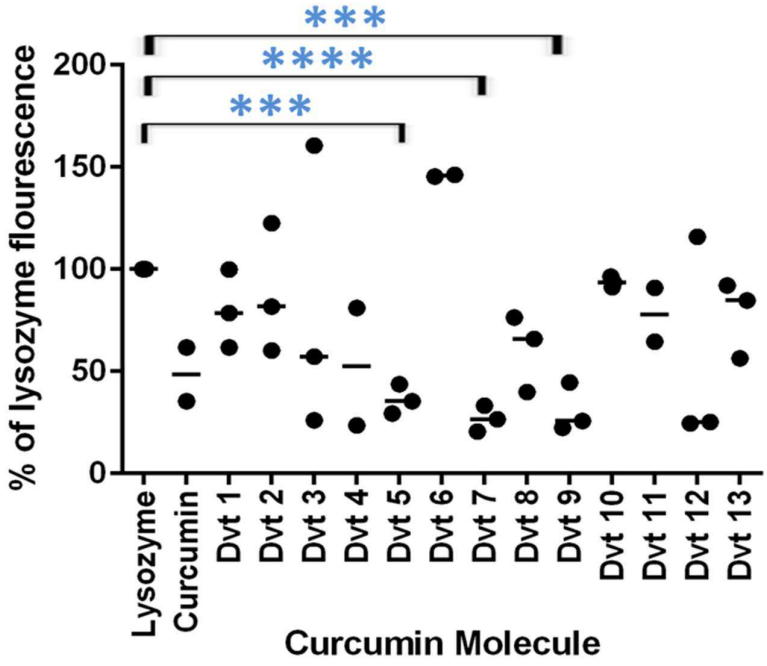

Figure 4.8: Curcumin Derivative Screen for Lysozyme Aggregation Inhibition ⇩ End-point fluorescence readings from a ThT assay investigating the effects of 70µM natural curcumin or derivatives (Dvt)on the aggregation of equimolar lysozyme, after subtraction of the initial t=0 fluorescent reading. Results are shown as a percentage of the lysozyme only sample (* = p<0.001, **** = p<0.0001).**

As shown in figure 4.3, the action of curcumin and its derivatives on lysozyme aggregation followed a slightly different pattern to that seen with WT Tsyn in figure 4.2. Natural curcumin was again highly effective at reducing the total aggregates, in comparison to lysozyme alone, with a reduction in fluorescence signal of 67.6 ¹ 0.29% being observed in comparison to the lysozyme alone sample. Only two successful repeats of the natural curcumin samples were obtained for this experiment, so statistics could not be performed to compare the natural molecule with the untreated, or derivative containing samples. Derivatives 5, 7 and 9 were again highly effective at reducing the aggregation observed in the untreated sample, with a reduction in fluorescence of 63.8¹ 0.08% ($p<0.001$), 73.2¹ 0.06% ($p<0.0001$) and 69.1¹ 0.14% ($p<0.001$) observed respectively. Derivatives 8 and 12 were also determined to cause a significant decrease in lysozyme aggregation ($p<0.05$ and $p<0.05$, respectively) and interestingly derivative 4, which significantly increased the aggregation of Πsyn ($p<0.05$), had the opposite effect on lysozyme, causing a significant ($p<0.05$) decrease in the aggregation of this amyloid protein. The significance of all curcumin衰 effectiveness at inhibiting lysozyme aggregation can be seen comparatively in table 4.3.

Given that both Tsyn and lysozyme aggregation can be inhibited by curcumin, but there are differences in the anti-amyloid properties of the derivatives between the proteins, this would suggest that different curcumin derivatives will have differing efficacies dependent on the protein of interest, and these would need to be carefully designed and optimised for each individual amyloidogenic protein.

Curcumin	Significance Over Lysozyme Only	Significance Over Natural Curcumin
Natural Curcumin	Not available (N/A)	N/A
Derivative 1	-	N/A
Derivative 2	-	N/A
Derivative 3	-	N/A
Derivative 4	P=0.0202	N/A
Derivative 5	P=0.0049	N/A
Derivative 6	-	N/A
Derivative 7	P=0.0008	N/A
Derivative 8	P=0.0492	N/A
Derivative 9	P=0.0013	N/A
Derivative 10	-	N/A
Derivative 11	-	N/A
Derivative 12	P=0.0155	N/A
Derivative 13	-	N/A

Table 4.3: Significance of Curcumin Derivatives Anti-Amyloid Aggregation Propensity Over Lysozyme Alone or Natural Curcumin.

P values were determined using Kruskall-Wallis and post-hoc Conover-Inman statistical analysis. Table cells without stated P values (-) were not significant. N/A is stated where statistical analysis could not be performed due to low n numbers.

4.3.3 Curcumin Slows the Time-Induced Autoproteolytic Fragmentation of Monomeric αSyn

To investigate the mode of action of curcumin and its derivatives in reducing αsyn aggregation, a range of mass spectrometry experiments were performed. WT αsyn was dissolved in 50mM ammonium acetate with equimolar natural curcumin or one of the 13 derivatives, dissolved in DMSO with a final concentration of 1%, and subjected to positive ion mode ESI-IMS-MS. Mass spectrometry in this section was performed with a cone voltage of 45V, source temperature 60(0)C, Trap DC Bias 45, backing pressure 4.34e0, trap 15.0 and transfer 20.0.

As shown in figure 4.4, after immediate addition of curcumin or derivatives 5 or 7, no immediate mass shift was observed and no new ions corresponding to the protein bound to one or more curcumin molecules were detected. The same lack of binding was observed for all 13 derivatives tested, as shown in appendix 4B. This would indicate that these curcumin molecules do not readily bind to either the extended or compact monomeric αsyn conformations within these samples.

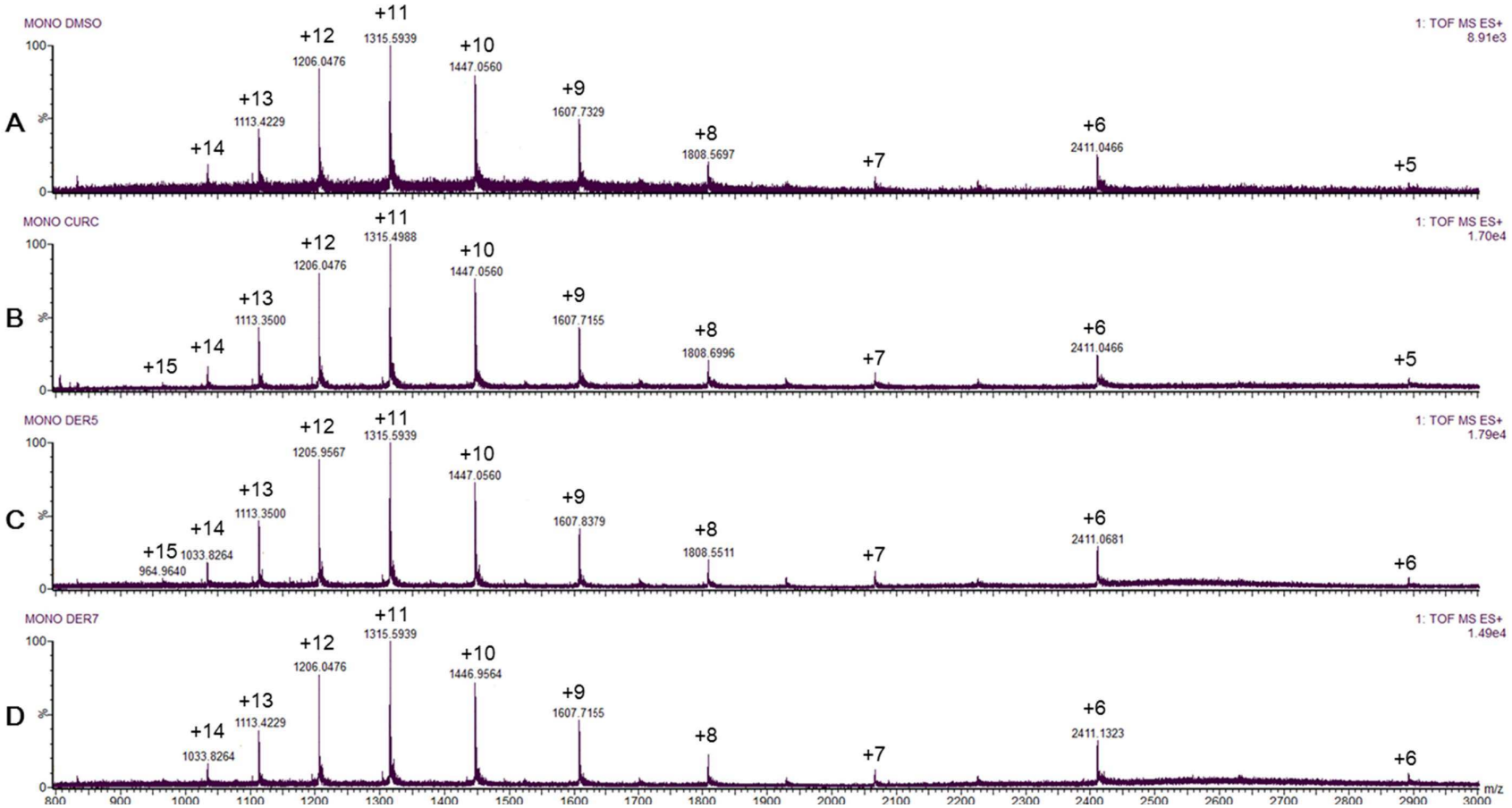

Figure 4.4. ESI-MS-MS Spectra of WT-pyn with Natural Curcumin, Derivative 5 and Derivative 7.

Positive ion mode ESI-MS-MS of 700M WT-pyn in 50mM ammonium acetate with 1% DMSO, with or without the presence of equimolar curcumins. A) WT-pyn, B) WT-pyn + natural curcumin, C) WT-pyn + derivative 5, D) WT-pyn + derivative 7.

Ion mobility data was examined to investigate if any conformational changes had occurred to the protein, despite the apparent lack of binding. Individual peaks were selected from the drift scope plot and exported to mass lynx separately to avoid any overlapping drift times from other CSIs. No alterations to the extended conformations of the protein, within the higher CSIs, were observed, determined by alterations to the protein走ATDs upon immediate addition of either natural curcumin or derivatives 5 and 7, as shown in appendix 4C. However, when the compact states were examined, a decrease in the most compact states present within these CSIs was observed, as shown in figure 4.5, via Gaussian fitting to the +6 CSI.

This decrease in the compact state suggests curcumin, despite not extensively binding to the monomeric protein, may be influencing the equilibrium of the conformations observed within the more compact CSIs. The observed reduction in percentage of the most compact species from 16.88% of the total protein at CSI +6, in the presence of DMSO alone, is most pronounced with derivative number 5, where a reduction to just 2.78% is observed, in comparison to 13.90% with natural curcumin.

To investigate any potential delayed changes to binding or the oxidation state of the protein, repeat spectra were acquired over time. Samples were left at room temperature for 48h, for further investigation by ESI-IMS-MS. Ion mobility data was again examined, and no notable differences in conformational equilibrium were observed for the extended CSIs +14 to +10 (appendix 4D), equivalent to

that observed at time zero. There were also little differences observed at the compact CSIs in comparison to the time zero findings. As shown in figure 4.6, and table 4.4, at the +6 CSI, the proportion of the most compact conformation, H, had increased in the apo sample, and again samples containing curcumin or derivatives had a decreased proportion of the protein present in this conformation.

At this time point, derivative 7 appeared to be the most efficient at reducing the compact states. An increase in the most compact conformation, H, is observed in the curcumin free samples with a percentage of 48.83% of the total protein, in comparison to just 16.88 at t=0, whereas in the presence of natural curcumin this conformation is reduced to just 17.49%, and with derivatives 5 and 7 to 17.16% and 10.28% respectively. This suggests that, despite a lack of binding to the protein, the altered solution conditions brought about by the curcumin is reducing the proportion of the more amyloidogenic conformations within the sample, and shifting the equilibrium in favour of the more extended, less amyloidogenic states. No additional adduct peaks were observed at any time point and, as shown in figure 4.7, after 48hrs of incubation peaks corresponding to bound protein were still absent from the spectra. No other mass shifts were identified on any CSIs.

The conformational alterations to the +6 CSI, at both time points, have been tabulated for comparison in table 4.4 after the figures.

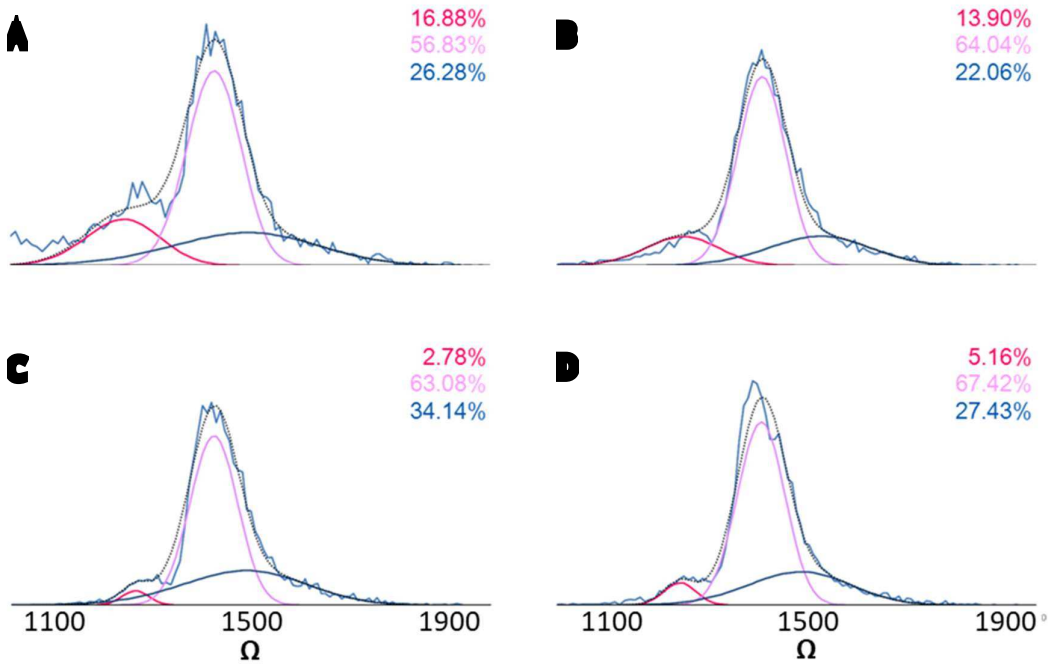

Figure 4.5: ATDs of the +6 CSI of TBYN upon Immediate Addition of Curcumin. Gaussian fitting was performed on the +6 charge state ion of WT TBYN after immediate addition of A) 1% DMSO, B) 1% DMSO + equimolar natural curcumin, C) 1% DMSO + equimolar derivative 5, and D) 1% DMSO + equimolar derivative 7. Conformations F, G, H.

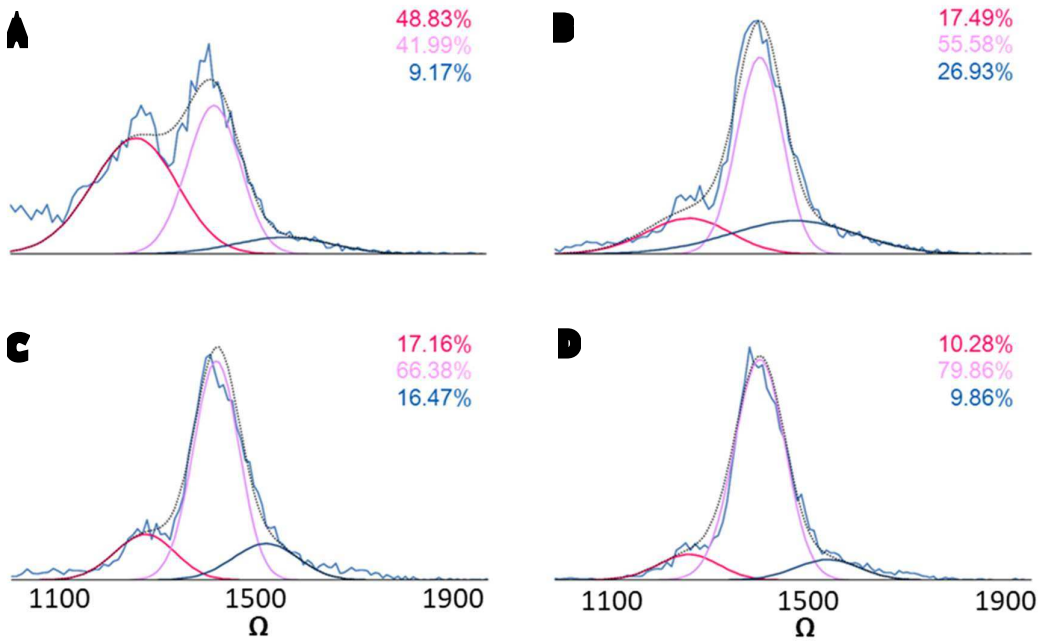

Figure 4.6: ATDs of the +6 CSI of IBys after 48hrs Incubation with Curcumins. Gaussian fitting was performed on the +6 charge state ion of WT-pys after 48hrs incubation with A) 1% DMSO, B) 1% DMSO + equimolar natural curcumin, C) 1% DMSO + equimolar derivative 5, and D) 1% DMSO + equimolar derivative 7. Conformations F, G, H.

	t=0hrs			t=48hrs		
	F	G	H	F	G	H
Untreated	26.28%	56.83%	16.88%	9.17%	41.99%	48.83%
Curcumin	22.06%	64.04%	13.90%	26.93%	55.58%	17.49%
Derivative 5	34.14%	63.08%	2.78%	16.47%	66.38%	17.16%
Derivative 7	27.43%	67.42%	5.16%	9.86%	79.86%	10.28%

Table 4.4: ATD alterations to +6 CSI of WT ΠSyn in the Presence of Curcumins. ATDs are shown as a percentage of each conformation present within the +6 CSI of WT Πsyn, after immediate addition and following 48hrs incubation with curcumin, or derivatives 5 or 7. Conformations F, G & H.

It was also observed during these experiments that the addition of curcumin and its derivatives appear to prevent the autoproteolytic fragmentation of the protein observed after 48hrs in the absence of curcumin, also shown in figure 4.7.

In the sample containing 1% DMSO, fragment ions can be observed between the usual monomeric and dimeric protein CSIs observed, at *m/z* 1011.35 and 1348.13. These two fragment ions are of a higher intensity than any of the monomeric peaks in the protein only spectra at this time point, and these have been highlighted in grey boxes on figure 4.7, on the following page.

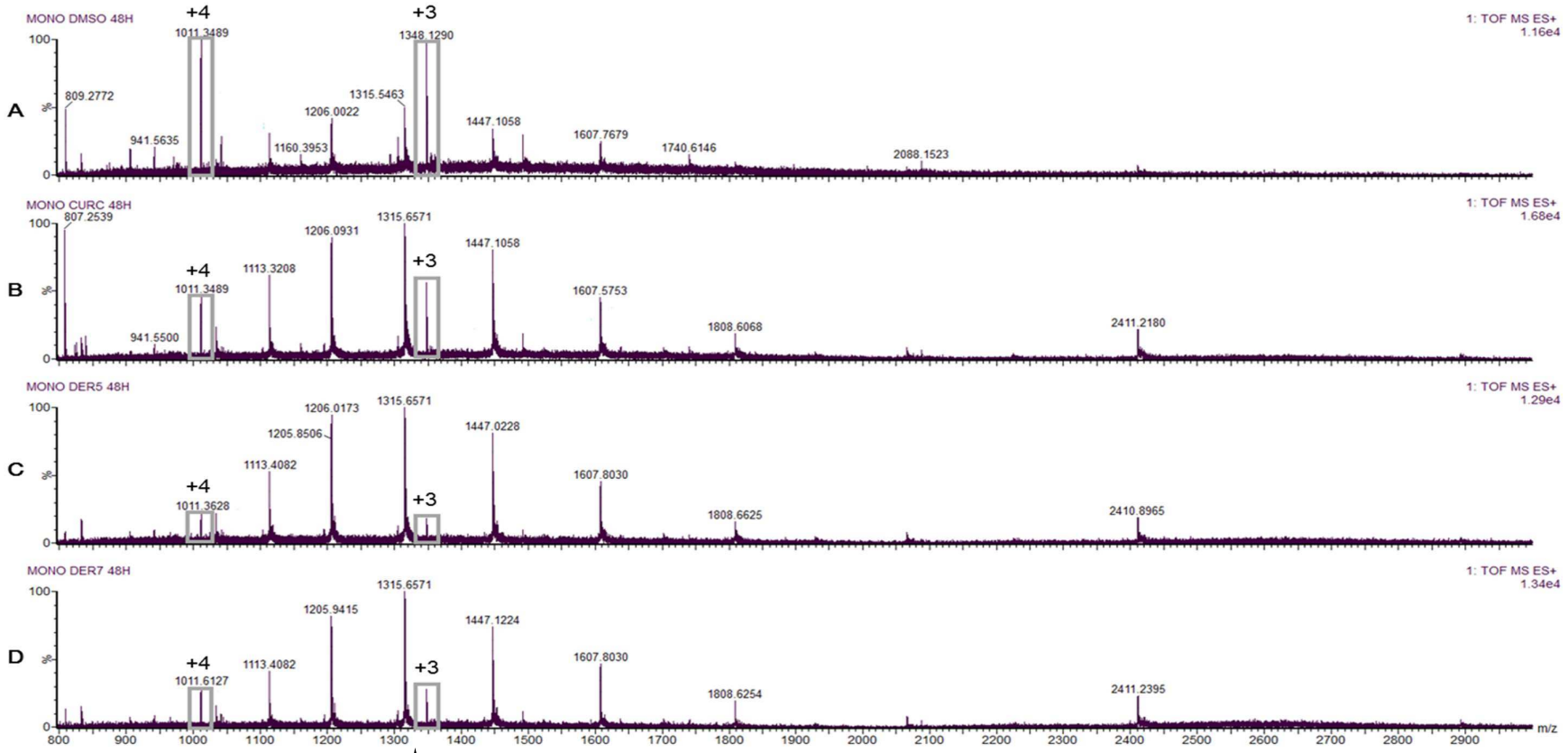

Figure 4.7: ESI-MS Spectra of WT-pSyn after 48hr Incubation with Curcumin.

ESI-MS of 70µM WT-pSyn in 50mM ammonium acetate with 1% DMSO, with or without the presence of equimolar curcumin after 48hrs incubation at room temperature. A) WT-pSyn, B) WT-pSyn + natural curcumin, C) WT-pSyn + derivative 5, D) WT-pSyn + derivative 7. Novel fragmentions, highlighted in grey boxes, can be observed.

The most intense of the fragment peaks, with a predicted *m/z* of 1011.39 represents the +4 CSI of a fragment comprised of amino acid residues 1-39, and the second, with a predicted *m/z* of 1348.19 represents the +3 CSI of the same protein fragment. This region of the protein includes the N-terminus, its acetylation site, and one of the protein's copper binding sites.

In the sample containing natural curcumin, the intensity of this peak relative to the +11 CSI of T-syn is greatly reduced. The intensity of the fragment ion peaks is then further reduced in the samples containing derivatives 5 and 7, relative to the +11 CSI, with derivative 5 appearing to reduce the intensity of the fragment ions more than derivative 7. This suggests that the curcumin molecules may be protecting the T-syn monomer from autoproteolytic fragmentation.

Other alternative fragment ions are also observed within the spectra and are of lower intensity than any of the intact protein peaks, these are listed in table 4.5. Despite a peptide fragment of aa1-18 being observed, no corresponding fragment of aa19-140 was detected. This may be due to further proteolysis of the 19-140 fragment into smaller sections, which are below the limit of detection, or further aggregation of this fragment.

Lower intensity fragment ions, are still reduced relative to the full-length protein in the presence of natural curcumin, or derivative numbers 5 and 7, akin to the 1-39 fragment ions, with derivative 5 appearing to show a greater reduction. No binding of any of the curcumin derivatives was observed to any of the fragment ions detected.

Observed Mass Range *(m/z)*	Predicted Mass *(m/z)*	Charge State Ion	Amino Acid Residues
941.55-941.56	941.56	+2	1-18
1011.35-1011.61	1011.39	+4	1-39
1305.46-1305.59	1305.54	+8	40-140
1348.13-1348.15	1348.19	+3	1-39
1491.94-1492.11	1491.9	+7	40-139
1740.45-1740.83	1740.38	+6	40-139
2088.11-2088.37	2088.26	+5	40-139

Table 4.5: Fragment ions of WT αsyn observed by ESI-IMS-MS after 48hrs Incubation with Curcumins.

Fragment ions of 70µM WT αsyn observed by ESI-IMS-MS after 48hrs incubation with or without natural curcumin or derivative 5 or 7, at room temperature.

4.3.4 Curcumin Selectively Binds to Oligomeric Species of αsyn

Increasing evidence from *in vitro* and *in vivo* studies, suggest that it is in fact the oligomeric species causing neurotoxicity in PD rather than the mature amyloid fibrils themselves (Glabe and Kayed, 2006; Karpinar *et al.*, 2009; Winner *et al.*, 2011; Martin *et al.*, 2012; Danzer *et al.*, 2009; Danzer *et al.*, 2007), therefore curcumin and the derivatives acting upon these species, rather than the monomeric protein, could be advantageous for its potential role as a curative or

preventative treatment. As curcumin and its derivatives cannot be observed to bind to the monomeric protein under mass spectrometry conditions, it was hypothesised that it may be exerting its effect on the oligomeric species, as has been suggested in previous studies (Singh *et al.*, 2013).

WT α-syn was dissolved in 50mM ammonium acetate to a final concentration of 70¾M, and curcumin was added in ethanol to a final concentration of 70¾M with 10% EtOH. As shown in appendix 4E, there is no visible difference between drift scope mobilograms or mass spectra of WT α-syn alone or WT α-syn with the addition of EtOH, indicating there are no gross effects on CSD or conformation brought about by the solvent, and no alterations to CSD were observed.

At this relatively high protein concentration, and under ESI-IMS-MS conditions described earlier in the chapter, WT α-syn monomers display a CSD of +18 to +4 CSIs. Low order oligomeric species including dimers, with a CSD of +7 to +23, trimers with a distribution of +10 to +17 and a single tetramer of CSI +15 can also be observed in the higher *m/z* ranges. The appearance of lower order oligomeric species is likely due to the higher protein concentrations utilised in these experiments, which were chosen because they can induce aggregation and the formation of oligomers. The *m/z* range of the drift scope mobilogram containing the most distinguishable oligomeric species, *m/z* 1800-5000, has been expanded in figure 4.8, where monomeric and oligomeric species have been labelled with numbers corresponding to the number of monomers in the protein complex.

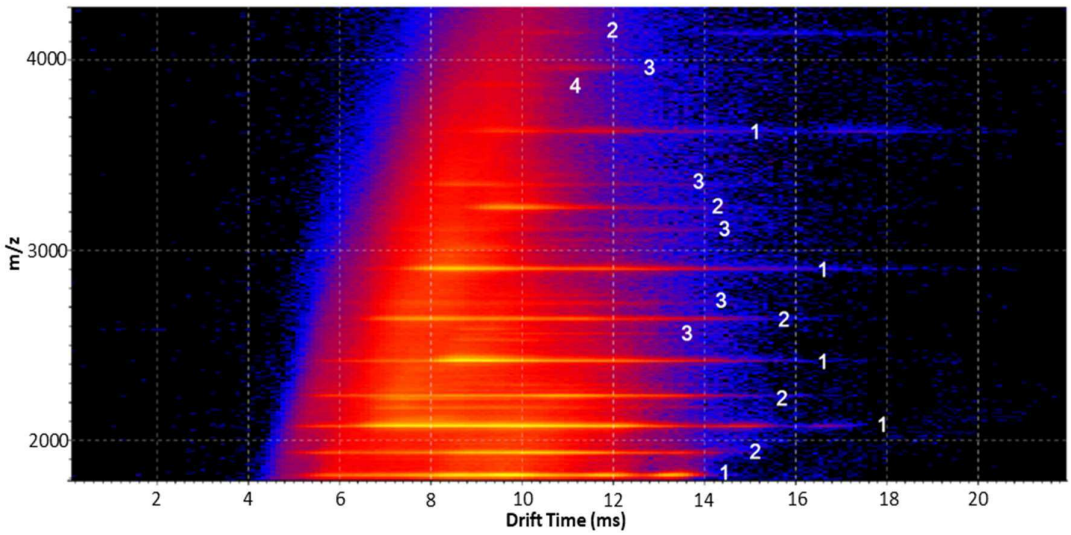

Figure 4.8: DriftScope Plot of 70µM ΠSyn Showing Oligomeric Species Present. IMS-MS of 70µM α-Syn in 50mM ammonium acetate shows species ranging from monomers to tetramers within the drift scope mobilogram, labelled by the number corresponding to the number of monomers within the protein complex.

Upon immediate addition of equimolar curcumin, novel peaks could be detected within the drift scope plot, next to the dimer peaks represented by CSIs +9 to +12, as shown in figure 4.9, where they have been highlighted in white boxes. These peaks also include the monomer peaks corresponding to the +5 and +6 CSIs, as they co-populate both monomers and dimers. Dimers, trimers and tetramers were also reduced in intensity within the drift scope mobilogram in the presence of equimolar curcumin, as shown in figure 4.10, which suggests that those present in the sample prior to addition of curcumin may have been dissociated.

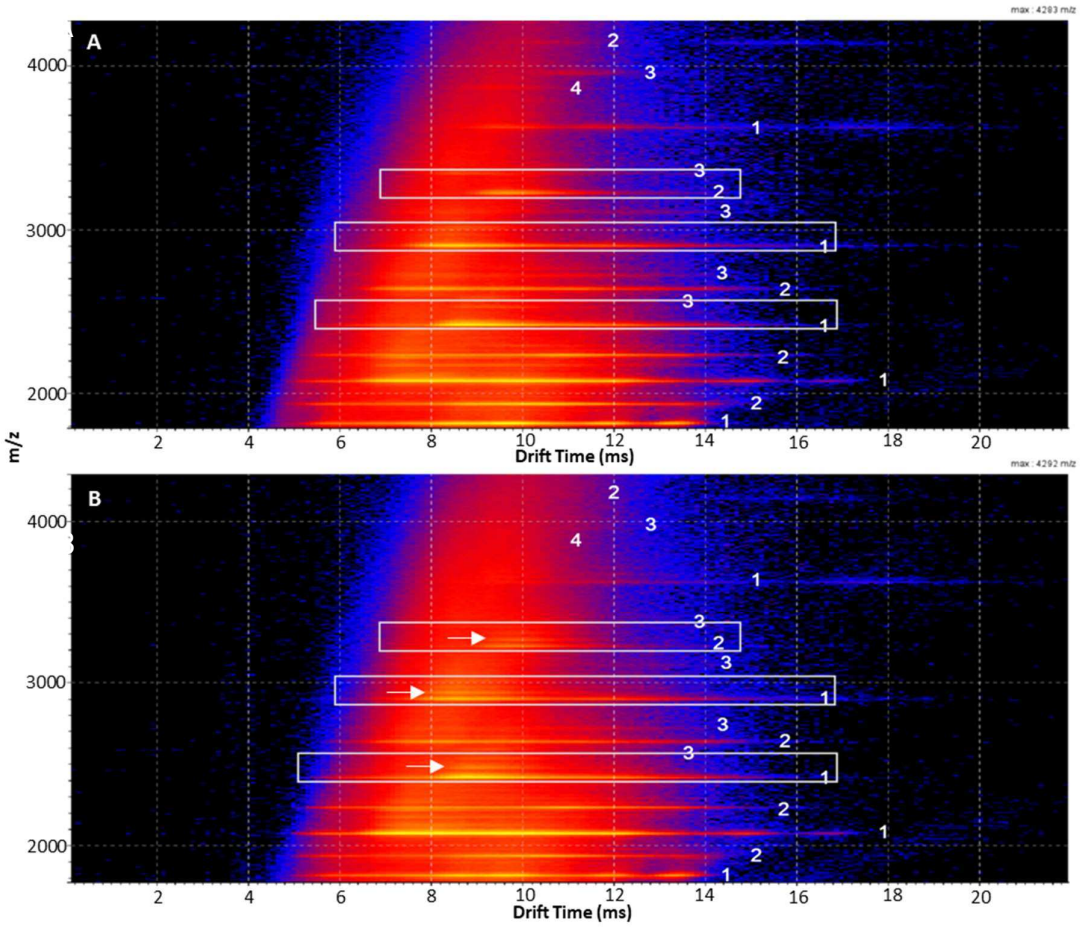

Figure 4.8: Driftscope of 700µM WT-pSyn and 10% ETOH, With and Without Curcumin.

A) 700µM WT-pSyn + 10% ETOH, B) 700µM WT-pSyn + 10% ETOH + 700µM natural curcumin. Upon addition of equimolar curcumin, novel peaks (indicated by white arrows) can be detected next to the monomer/dimer peaks of CSIs +5/+10 and +6/+12, and the dimer peaks of CSIs +8, which have been highlighted in white rectangles, and a reduction in intensity of oligomeric species was observed.

Mass spectra were extracted from the drift scope mobilogram, and peaks corresponding to bound curcumin were visible at the dimer CSIs of +9 and +11, and the monomer/dimer peaks of +5/+10 and +6/+12, as shown in figure 4.11.

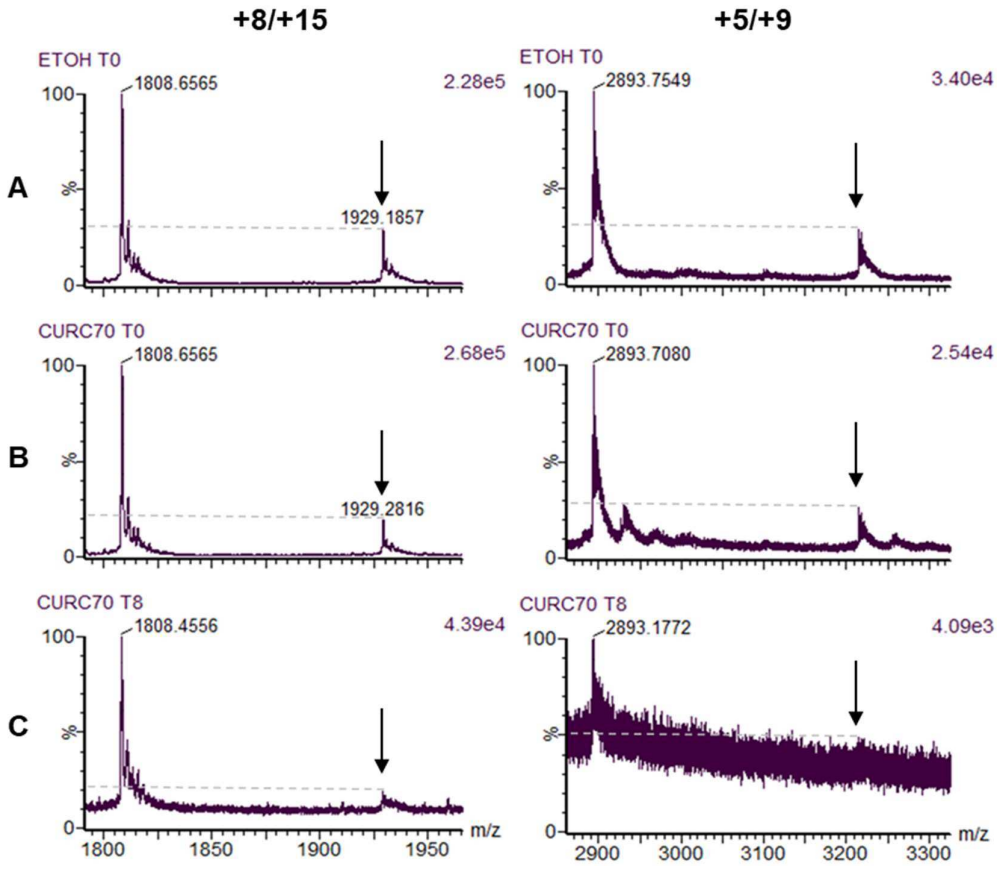

Figure 4.10: Extracted monomer and dimer spectra peaks of 70µM WT IBys in 50mM Ammonium Acetate, with and without Curcumin.

Extracted spectra peaks of the +8 monomer/+15 dimer CSI and the +5 monomer/+9 dimer CSI, demonstrating a reduction in peak intensity of the dimeric species, highlighted with arrows, over the extracted protein (A), after B) immediate addition of equimolar curcumin and C) after 8hrs incubation with equimolar curcumin. Dotted lines highlight dimer peak intensity.

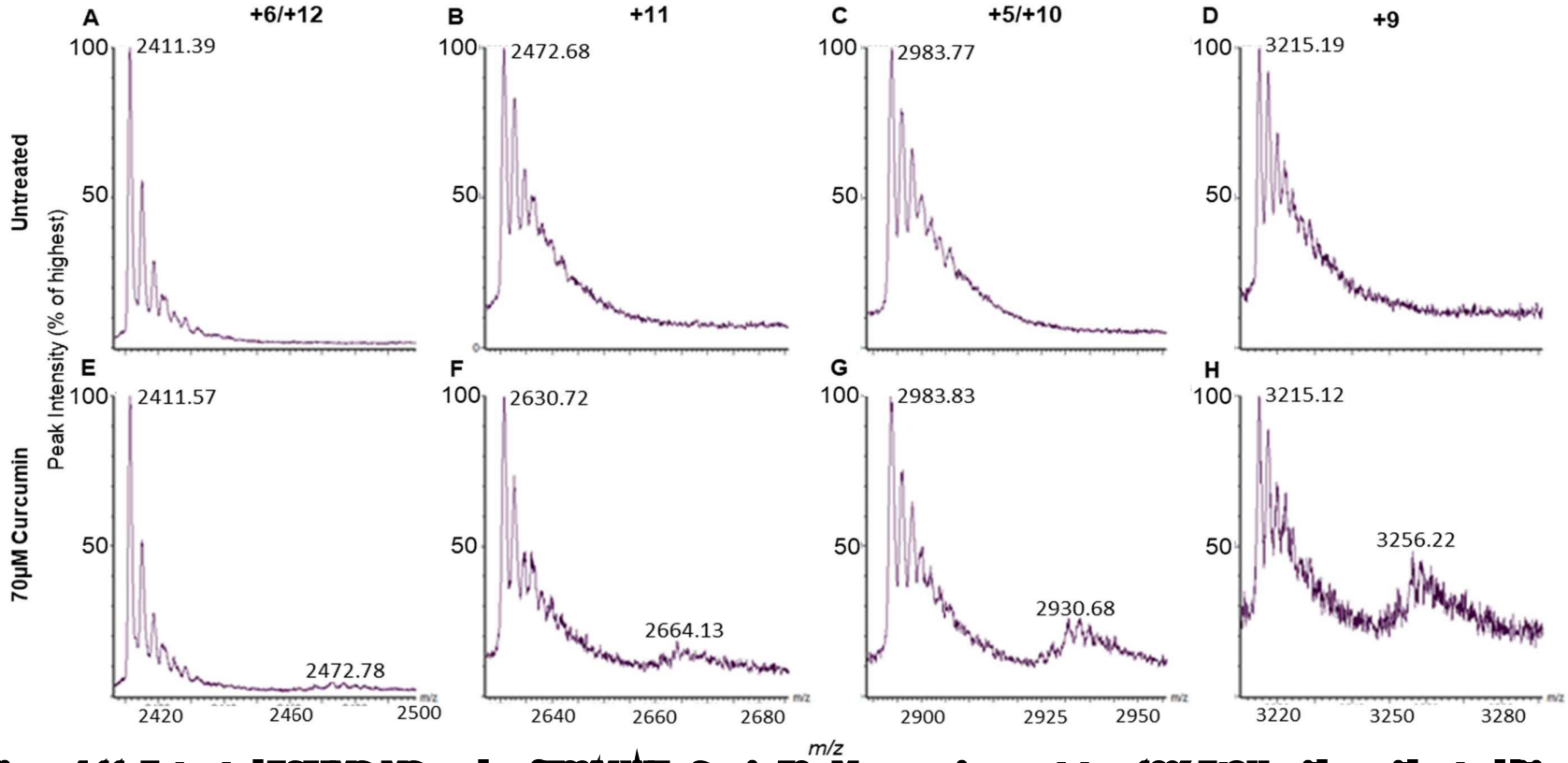

Figure 4.11: Extracted IST-MS-MS peaks of 70μM WT α-Syn in 50mM ammonium acetate + 10% EtOH, with or without addition of 70μM curcumin.

Extracted IST-MS-MS spectra peaks demonstrating the binding of curcumin to dimeric species of WT α-Syn, at CSE: A) +6/+12 monomer/dimer; B) +11 dimer; C) +5/+10 monomer/dimer; D) +9 dimer; E) +6/+12 + curcumin, F) +11 + curcumin, G) +5/+10 + curcumin, H) +9 + curcumin.

The isotopic distribution of the bound protein in close proximity to the monomer/dimer peaks containing the +5/+10 and +6/+12 CSIs were calculated, with a spacing of 0.1 Da and 0.08 Da respectively. These were determined to correspond to +10 and +12 CSIs, confirming that curcumin was bound exclusively to the dimeric species within the sample as opposed to the monomers at these CSIs.

Monomer/Dimer Peak *(m/z)*	Predicted Mass Mono + 1 Curcumin	Predicted Mass Mono + 2 Curcumin	Predicted Mass Dimer + 1 Curcumin	Predicted Mass Dimer + 2 Curcumin	Observed Mass
2411.57	2472.40	2533.79	2441.70	2472.40	2472.78
2630.72			2663.58	2697.69	2664.13
2983.83	2966.68	2965.88	2929.84	2966.68	2930.68
3215.12			3255.26	3296.20	3256.22

Table 4.6: Predicted and Observed Masses of ΠSyn Monomers and Dimers. **Predicted and observed masses of monomers and dimers at CSIs +6/+12, +11, +5/+10 and +9, in the *m/z* range 2400-3400 bound to one or two molecules of natural curcumin. Predicted masses which have been identified within the spectra are highlighted in green.**

As highlighted in table 4.6, the majority of the dimers bound one curcumin molecule, whereas the dimer under the +6/+12 monomer/dimer peak appeared to bind two molecules of curcumin. The predicted mass of the dimeric +12 CSI bound to one curcumin is 2441.70 and two curcumins is 2472.40, and this compares to 2472.78 in the observed data, indicating this dimeric species had bound two curcumin molecules, and this oligomeric species may have a higher binding affinity for curcumin. The predicted mass for the +10 dimeric species bound to one curcumin is 2929.84 and to two curcumins is 2966.68, and this compares to an observed mass of 2930.68, suggesting this dimeric species has only bound the one molecule. This data indicates that the dimeric species are able to bind curcumin, and that the different dimers may have different binding affinities.

Ion mobility data was also examined for conformational changes occurring to the dimers in the presence of bound curcumin, but no notable alterations to conformational equilibria or CCS were detected in these experiments.

To investigate whether any further reduction in oligomer peak intensities, or increase in curcumin binding to the oligomers could be observed over time, samples were incubated at 37(10 for 8 hours, before further examination by ESI-IMS-MS, and the drift scope plot is shown in figure 4.12. The extended incubation resulted in further reduction in the peaks associated with the oligomeric species observed between *m/z* 2000 and 4300. This demonstrates a time dependent effect of the curcumin on the oligomers.

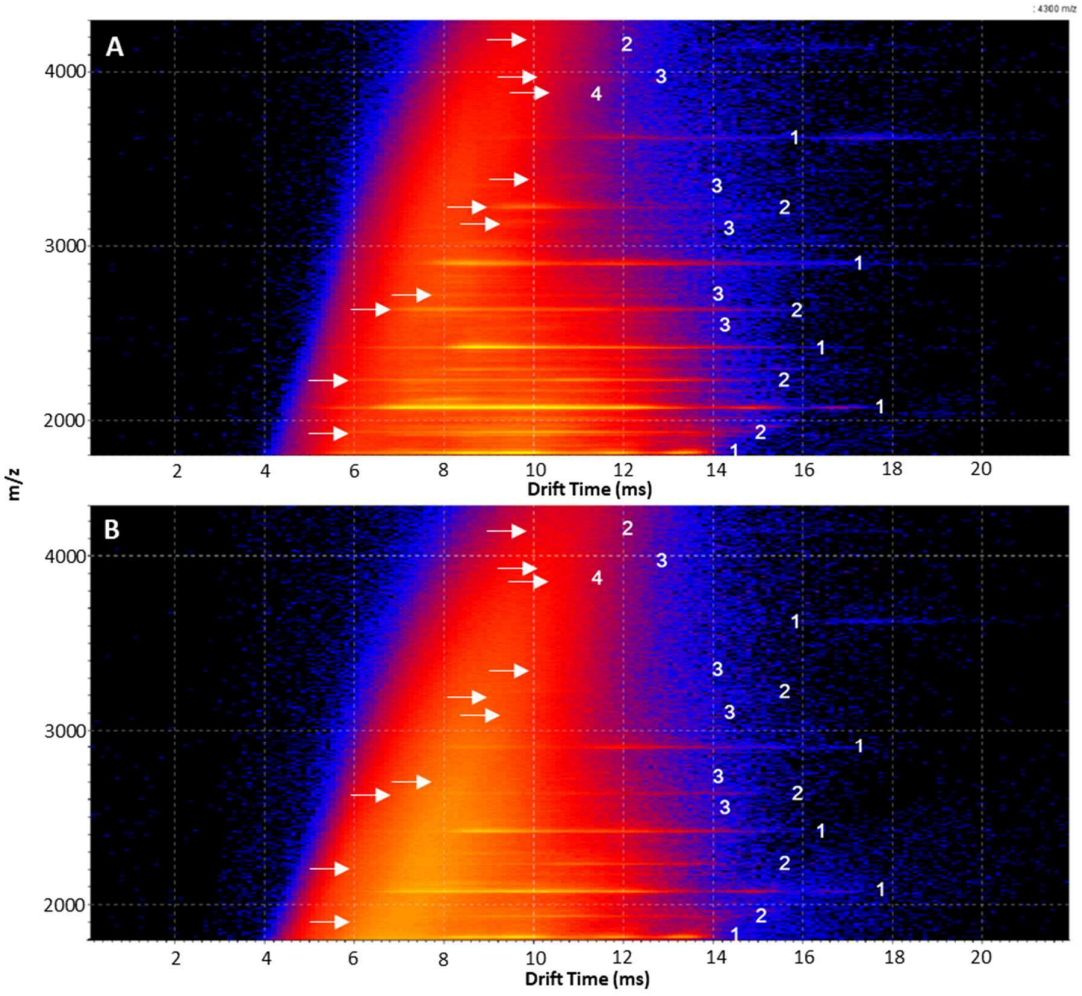

Figure 4.12: Drift Scope of 70μM ᵀʸʳ in 50mM Ammonium Acetate with Equimolar Curcumin, Demonstrating a Reduction in Oligomeric Species.

After 5hrs incubation of 70μM ᵀʸʳ with equimolar natural curcumin, ESI-IMS-MS revealed a further reduction in oligomeric species, indicated by white arrows, as observed from the drift scope multiplexes. A) 70μM WT ᵀʸʳ + 10% ITCH, B) 70μM WT ᵀʸʳ + 10% ITCH + 70μM natural curcumin.

Ion mobility data was examined to investigate the conformational changes to the oligomers upon curcumin binding after 8h. The peaks corresponding to the +11 and +9 dimers were selected individually from the drift scope plots, as they contain only bound dimeric species and there is no co population with monomers, along with those of their curcumin bound counterparts. As with the t=0 samples, no altered peak shapes were detected in these experiments at t=8hours, suggesting no alterations to the dimer conformations had occurred after 8hrs.

In order to determine if there is dose dependence to the action of curcumin, the experiment was repeated using a lower curcumin concentration of 10¾M, with 70¾M T-syn. As shown in appendix 4F, the same reductions in oligomer intensities within the drift scope were observed after immediate addition of curcumin, and in appendix 4G after 8hrs incubation, demonstrating curcumin is effective even when the molarity is 7-fold lower than that of the protein, and there were no alterations to the binding pattern of curcumin observed.

4.3.5 Curcumin Derivatives Displaying Anti-Amyloid Aggregation Properties Also Demonstrate Dissociation of Oligomers

Curcumin in the previous sections has been shown to disaggregate preformed oligomers. To investigate if this mechanism of action was exclusive to natural curcumin, a similar experiment was conducted using the two most successful hits from the derivative screen, derivatives 5 and 7. As a control, derivative 11 was

also examined to ensure that this loss of signal was not due to changes in ionisation brought about by the presence of a small molecule within the sample. This compound displayed moderate anti-amyloid activity *in vitro*, as demonstrated by ThT, but it was significantly less effective than natural curcumin For the successful derivatives, similar results were obtained as with the native curcumin molecule, as shown in figures 4.13 and 4.14. Upon immediate addition of equimolar concentrations of derivative number 5 and 7, shown in figures 4.13 and 4.14 respectively, dimeric species within the original α-syn sample reduced in intensity or disappeared entirely from the drift scope plot, indicating these derivatives also have the ability to dissociate pre-formed α-syn oligomeric species. When the less successful derivative, number 11, was examined, as shown in figure 4.15, upon immediate addition to the α-syn sample, very little difference in the signal of the monomeric or dimeric species in the sample was observed. This data would indicate that the loss of the oligomers with natural curcumin and derivatives 5 and 7 is due to binding or interaction with the dimers as opposed to any ion suppression brought about by the presence of a small molecule in the solution.

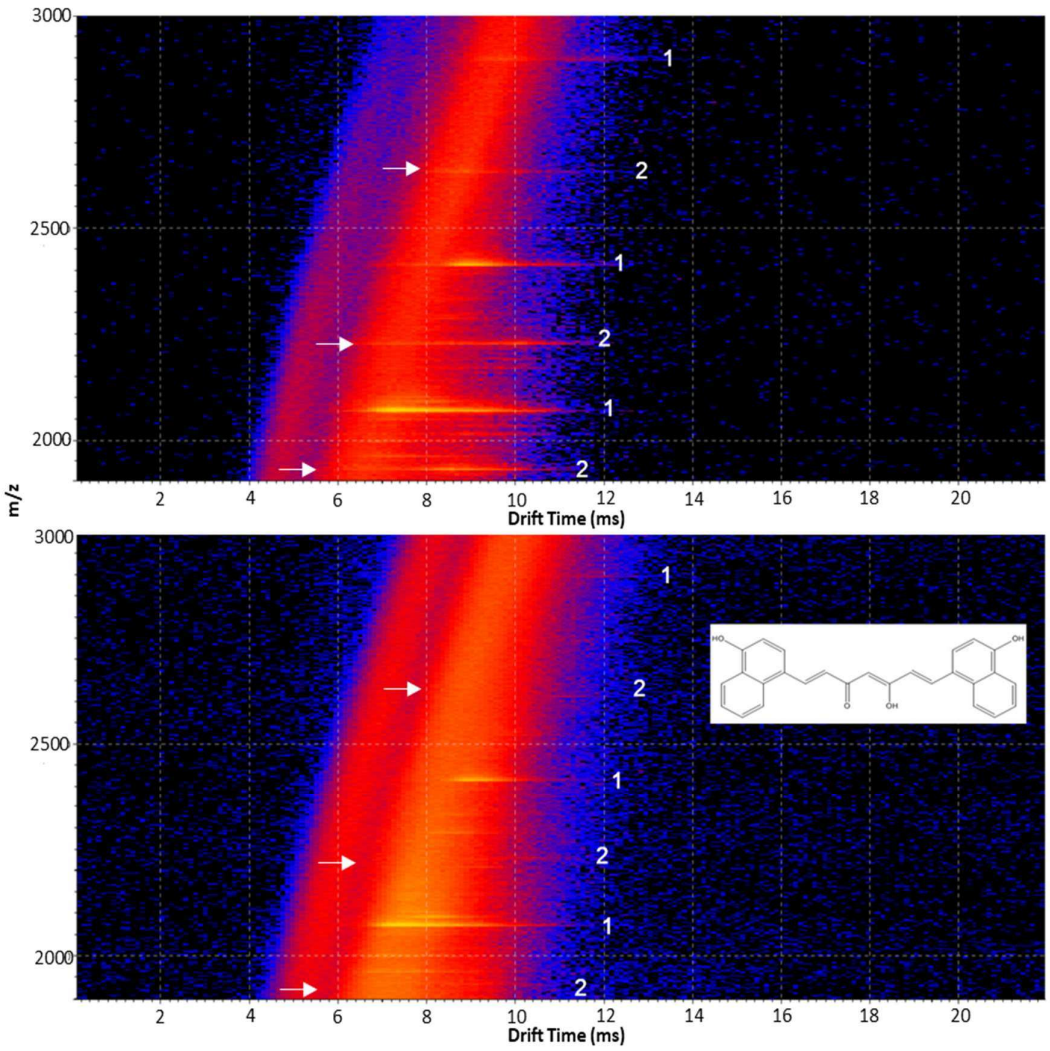

Figure 4.13: Driftscope plots of WT -syn and WT -syn + Derivative 5. Driftscope plots of A) WT -syn + 10% NCH and B) WT -syn + 10% NCH + derivative 5, showing a reduction in dimeric species, indicated by white arrows, after immediate addition of the derivative.

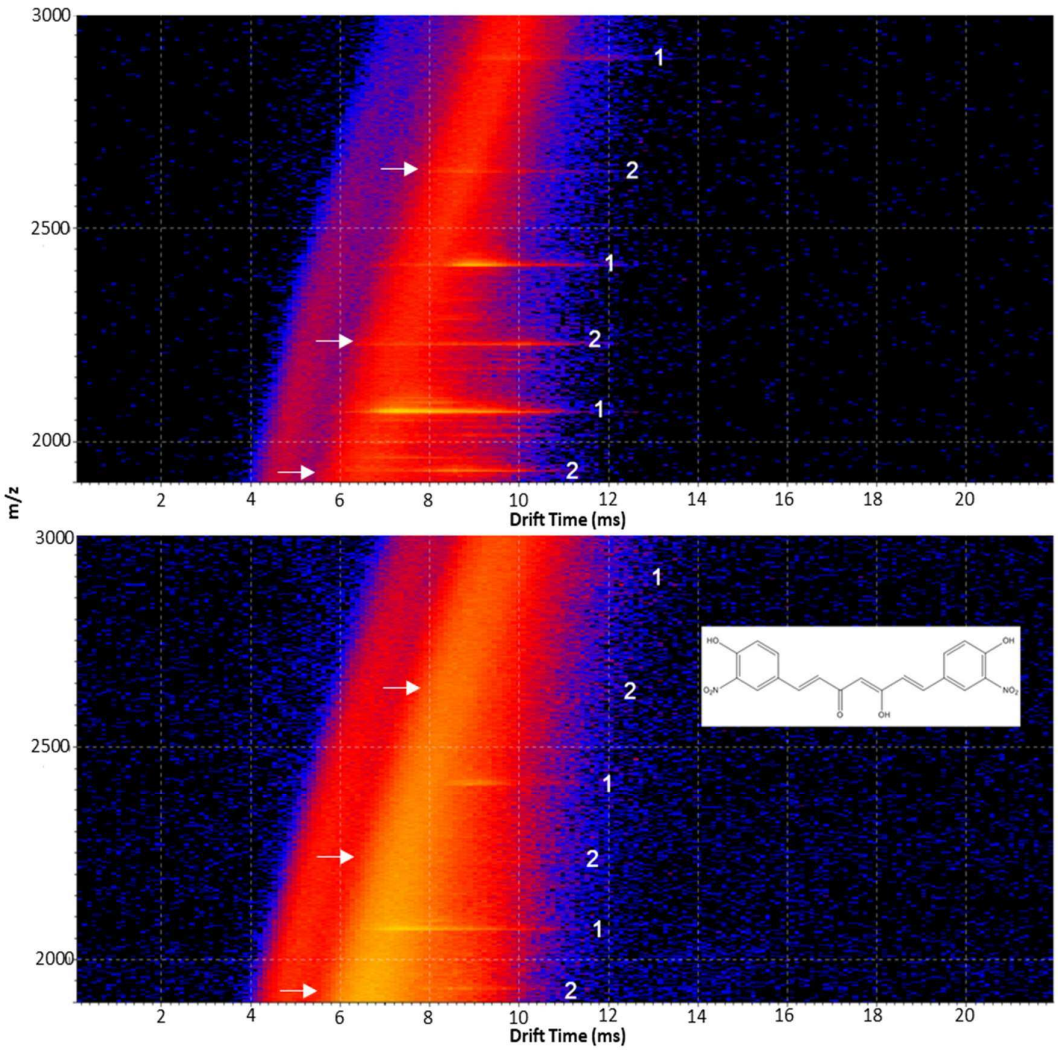

Figure 4.14: Driftscope plots of WT α-syn and WT α-syn + Derivative 7. Driftscope plots of A) WT α-syn + 10% EtOH and B) WT α-syn + 10% EtOH + derivative 7, showing a reduction in dimeric species, indicated by white arrows, after immediate addition of the derivative.

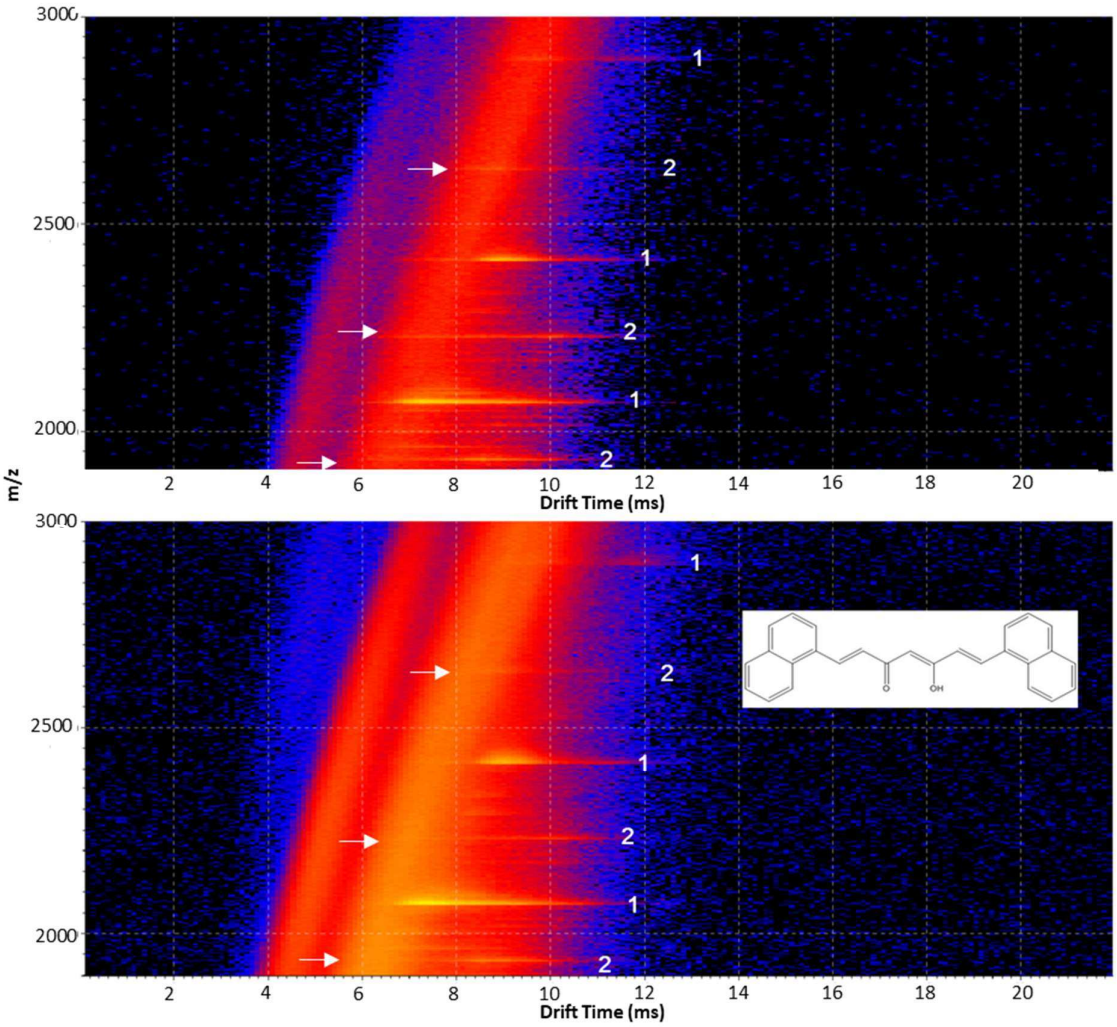

Figure 4.15: Driftscope plots of WT α-syn and WT α-syn + Derivative 11. Driftscope plots of A) WT α-syn + 10% EtOH and B) WT α-syn + 10% EtOH + derivative 11, showing no reduction in dimeric species, indicated by white arrows, after immediate addition of the derivative.

4.3.6 Curcumin binds to the NAC Region of αSyn

As an accompanying experiment, an αsyn mutant with the NAC region of aa61 to 95 removed, was also analysed by ESI-IMS-MS with and without the presence of natural curcumin and derivatives, numbers 5, 7 and 11. Previous studies have suggested that curcumin initially binds to the aliphatic residues found within the hydrophobic NAC region of the protein (Ahmad and Lapidus, 2012; Spinelli *et al.*, 2015; Gautam *et al.*, 2017). After the initial interaction, it has been suggested that the aromatic ring structures within the curcumin molecule further bind to nearby hydrophobic residues (Ahmad and Lapidus, 2012; Gautam *et al.*, 2017). This may lead to a decreased hydrophobic surface area on the protein, which has previously been suggested as a mechanism for curcumin表anti-amyloid action on oligomeric structures in a previous study into αsyn toxicity (Singh *et al.*, 2013). 70¾M curcumin or derivative 5 and 7 were added to 70¾M αsyn with the NAC region deleted. No binding was observed to any of the peaks in the spectrum, as shown in figure 4.16, where the most abundant peak and a more compact peak from higher in the spectra, and shown in appendix 4H, where the spectra as a whole can be seen.

This lends further support to previous reports that curcumin specifically binds to αsyn within the NAC region. This region is known to be essential for the aggregation of the protein. It also demonstrates that there is no non-specific interaction between αsyn and the curcumin molecules, as they are not readily binding to the monomer or protein with a region essential for aggregation

removed. This suggests that the NAC region is required for curcumin binding, and this interaction only occurs with the dimeric species.

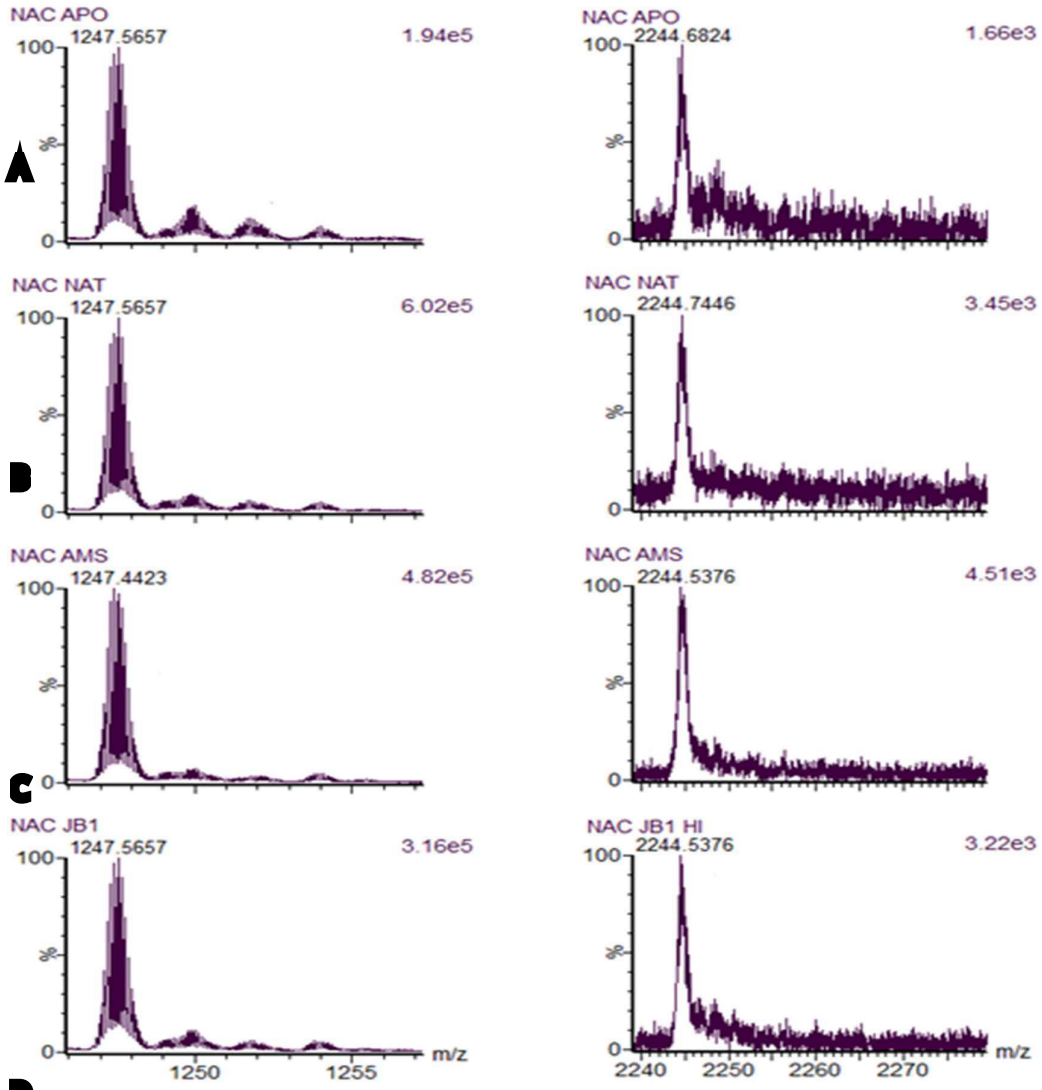

Figure 4.16: Compact and Extended CSIs of NAC 1Syn With or Without Curcumin.

Expanded view of the most abundant and a more compact CSI of NAC deleted 1syn in the presence of curcumin, A) 1syn only, B) + equimolar natural curcumin, C) + equimolar derivative 5 and D) + equimolar derivative 7, showing no mass shift and no novel peaks.

4.4 Discussion

Results presented in this chapter demonstrate that curcumin and several curcumin derivatives can prevent the aggregation of WT Tsyn *in vitro*, seemingly through prevention of autoproteolytic fragmentation and oligomer formation. This appears to occur via dissociation of preformed, low-order, early oligomeric species such as dimers, and prevention of further aggregation, as described in sections 4.2.4 and 4.2.5.

ThT assays were performed to determine the anti-amyloid propensity of natural curcumin and 13 derivatives, on both WT Πsyn and a second amyloidogenic protein, lysozyme. The proposed mechanism of action of ThT is to bind to the T-sheet structures in amyloid aggregates, resulting in a red shift in ┼max, and an increase in fluorescence signal intensity. Curcumin and its derivatives are known to exhibit intrinsic fluorescence, therefore their use in ThT assays has been questioned (Hudson *et al.*, 2009), however the technique is still commonly used and reliable, provided appropriate control measures have been taken (Yanagisawa *et al.*, 2015; Lin *et al.*, 2013; Jiang *et al.*, 2012; Pall *et al.*, 2016; Mirhashemi, 2012). Due to the nature of the experiments reported here, any increase in signal resulting from the curcumin or its derivatives binding to amyloid fibrils would result in aberrantly high signals. This would mean a false negative, as opposed to false low readings or false positives. High fluorescence readings would still indicate that amyloid material had been formed and the curcumin derivative was non-functional in its ability to prevent aggregation. So, while some

potential hits may have been missed via this method, due to their intrinsic fluorescence, those which are producing lower readings can still be considered successful inhibitors of aggregation. Initial fluorescence readings were also taken at t=0 and subtracted from the end point readings, to control for the curcumin表intrinsic fluorescence.

These aggregation studies, initially suggested that natural curcumin and several derivatives of the natural molecule, can inhibit the aggregation of both WT Tsyn and, lysozyme, *in vitro*, with varying degrees of success, dependent on their structure. Not all curcumin derivatives were successful inhibitors however, and derivative 4 in particular caused a significant increase in signal when compared to WT Tsyn alone. The derivatives had different patterns of inhibition for the two proteins investigated, suggesting that different curcumin derivatives will have different efficacies depending on the amyloidogenic protein of interest. In the case of Tsyn, most derivatives significantly reduced the aggregate formation as detected by fluorescence readings in comparison to the protein alone sample, whereas derivative 4 significantly increased the formation of aggregates, and derivative 6 caused no significant alterations either way. Derivatives 5, 7 and 9 significantly reduced aggregate formation in comparison to natural curcumin ($p<0.0001$, $p<0.0001$, and $p<0.005$ respectively), indicating these may be more effective anti-aggregation drugs for Πsyn than the natural molecule.

Structurally it has been suggested that two aromatic groups separated by a planar backbone are essential for inhibition of aggregation of AT (J ha *et al.*, 2016), and

hydrogenation at conjugated double bonds of the central 7 carbon atoms in the backbone has been demonstrated to be important for curcumin's antioxidant properties. The natural molecule contains a phenolic group (-OH) at position-4 on the aromatic ring structures, and a methoxyl group (-OCH3) at position-5. Both derivatives 5 and 7 also contain the phenolic group at position-3 on the aromatic rings, whereas the less successful modulators of aggregation do not, indicating that this must be a key feature for more successful aggregation inhibition. Derivative number 5 also contains an extra aromatic group in the form of a benzene ring at position-4 and position-5 of the natively occurring aromatic group, whereas derivative 7 contains a nitro group ($-NO_2$) at position-4, both these modifications also appear to increase the molecule's anti-aggregation propensity. Derivative number 9 however does not contain the usual benzene ring group, but instead contains a furan ring, or pentene ring containing an oxygen atom at position-4, with a methyl group at position-3.

Interestingly, derivatives 1, 2 and 3 all also significantly reduced the aggregation of T-syn in comparison to the protein alone sample. These derivatives all have an oxygen atom bound to position-5 of the aromatic group, attached to a hydrocarbon chain of 1 to 3 carbon atoms, increasing with derivative number. Derivatives 1 and 2 have a similar effect, whereas derivative 3 demonstrated the largest reduction in aggregation. Derivative 4 however, which showed a significant increase in aggregation, has the same general structure as derivatives 1-3, but the oxygen is on a hydrocarbon chain of 4 carbon atoms, suggesting that

the length of this chain may also be important for anti-amyloid propensity, and when the length is increased over 3 carbon atoms the chain may be too long for the interactions with the protein to take place. It is possible the molecule no longer fits into the space between the T-sheets formed during aggregation. This does not appear to be the case with lysozyme however, as derivative 4 caused a decrease in aggregation of this protein.

In terms of lysozyme, no derivatives appeared more successful at inhibiting aggregation than natural curcumin, and significance could not be determined due to low experimental repeats, however derivatives 5, 7 and 9 again were the most effective inhibitors, significantly reducing the fluorescence signal in comparison to the protein alone sample ($p<0.001$, $p<0.005$ and $p<0.001$, respectively), which again indicates that some modifications of the natural molecule are more successful at inhibiting amyloid aggregation than others. The different actions of the derivatives presented here suggests that careful redesign of curcumin derivatives should allow for more successful inhibition of aggregation of several different amyloid proteins, and different derivatives will have varied degrees of success dependent on the protein of interest.

Natural curcumin has previously been demonstrated to slow the aggregation of Tsyn *in vitro* using the ThT assay in a number of studies, at varying concentrations including 2:1 curcumin to protein ratio (Wang *et al.*, 2010), 1.5:1 curcumin to protein ratio (Ahmad and Lapidus, 2012) and equimolar concentrations (Herva *et al.*, 2014; Ahsan *et al.*, 2015), where a curcumin

derivative, N-(3-nitrophenylpyrazole), was also found to have a similar effect on aggregation (Ahsan *et al.*, 2015). N-(3-nitrophenylpyrazole) has two nitrogen atoms in place of the oxygens on the planar backbone, one of which is also bonded to a benzene ring with a nitro group at position-4. A range of curcumin analogues have also been investigated by another group, however this study determined the rate of aggregation to increase in the presence of curcumins (J ha *et al.*, 2016). This was concluded by the authors to be due to differing buffer conditions used between different research groups, as T syn aggregation is highly affected by its solution conditions as previously noted, and all studies have been completed under different assay conditions, though all at physiologically relevant pH. ThT was also absent from the samples containing curcumin in the J ha *et al.* study, so this may have had some effect on the results, as they were relying on the fluorescence of the curcumin molecule alone as an indicator of aggregation, as opposed to the T-sheet detection of ThT. Similar findings from another group have also suggested curcumin does not inhibit the aggregation of the AT protein, but increases the formation of 奄ff-pathway唔oluble, non-toxic oligomeric species (Yang *et al.*, 2005), and this has also been demonstrated with IAPP (Nedumpully-Govindan *et al.*, 2016). The mechanism of the effect of curcumins on the conformation of IAPP may again have been affected by solution conditions, which is an ongoing problem in research into intrinsically disordered proteins as they are highly sensitive to solution conditions, as previously discussed. Results presented in this chapter however, lend support to findings from the previously

mentioned work (Wang *et al.*, 2010; Ahmad and Lapidus, 2012; Ahsan *et al.*, 2015; Herva *et al.*, 2014) determining that curcumin slows the aggregation of αsyn *in vitro*.

Aggregation of lysozyme has also previously been observed to slow in the presence of natural curcumin using the ThT assay, where curcumin to protein ratios ranging from 0.5:1 to 5:1 demonstrated increasing effectiveness with an increase in curcumin concentration (Borana *et al.*, 2014). Natural curcumin has also been demonstrated to reduce the aggregation of the prion protein PrP *in vitro* using ThT assays, where in the presence of curcumin, a 6-fold reduction in fluorescence was observed (Hafner-BratkoviΦ *et al.*, 2008). Curcumin has also been observed to slow the aggregation of the Aβ protein *in vitro* in a number of studies (Yang *et al.*, 2005; Ono *et al.*, 2004), suggesting that curcumin has anti-aggregation properties against a variety of amyloid forming proteins. As there are conflicting results from research groups however, care must be taken in interpreting results, and careful experimental design should be applied to keep solution conditions as close to physiologically relevant conditions as possible when investigating novel drug candidates.

Results presented in this chapter demonstrate that curcumin and derivatives 5 and 7 appear to slow the autoproteolytic fragmentation of WT αsyn observed by ESI-IMS-MS after 48hours, which may be one mechanism by which it is exerting its anti-amyloidogenic properties. The most prolific fragments observed in the sample without curcumin were N-terminal truncations consisting of the first 39

amino acids. This fragment does not form part of the NAC region, and is therefore unlikely to be able to aggregate itself. It is also conserved in T-synuclein, which is known not to aggregate (Tsigelny *et al.*, 2007).

The counterpart fragment of aa40-140 however does contain the NAC region, along with the highly disordered C-terminal region containing the phosphorylation and some metal binding sites, and is susceptible to aggregation. The cleavage of this region of the protein may be essential for further aggregation, suggested by the much lower intensity of this fragment within the sample, which indicates that this region may have aggregated into higher order species. The prominent aa1-39 fragments observed within these experiments would also not be expected to aggregate, as they also do not contain the NAC region. The cleavage of this N-terminal region may however be essential for the remaining region containing the important NAC component to begin the nucleation step necessary for aggregation to progress.

Autoproteolysis of Tsyn has been suggested to be a key part of the oligomerisation process, and several fragments formed during the aggregation process have previously been identified using techniques such as gel electrophoresis, ESI-IMS-MS and MALDI-MS (Vlad *et al.*, 2011). Fragment aa40-140 has previously been observed using ESI-IMS-MS (Vlad *et al.*, 2011), though it was not determined to be of importance to aggregation in this study and was not examined further than identification via electrophoresis. The same investigations did however deem fragment aa72-140 to be of particular

importance, demonstrating increased aggregation when examined via IMS-MS (Vlad *et al.*, 2011). Fragments of Πsyn have also been demonstrated previously to be intrinsically amyloidogenic. Data presented here indicates that curcumin and its derivatives have the ability to prevent autolytic cleavage of Πsyn and appears to correlate with their ability to prevent amyloid formation, as both derivatives 5 and 7 were also demonstrated to prevent fragmentation, reduce the formation of amyloid material as demonstrated by ThT assay data, and dissociate oligomers as shown by ESI-IMS-MS.

These initial ESI-IMS-MS experiments, presented in section 4.3.3, and the ThT assay data presented in section 4.3.2, were performed with curcumin dissolved in DMSO. DMSO is generally considered an unsuitable solvent for proteins, as it can affect the protein□ conformational distribution, and increased concentrations have been shown to denature and unfold proteins, such as lysozyme and myoglobin, though this has been documented to occur in higher DMSO concentrations than used here (Arakawa *et al.*, 2007; Jackson and Mantsch, 1991). It was observed that the presence of DMSO in the ESI-IMS-MS samples was supressing the most extended CSIs of the protein, as shown in figure 4.17. Specifically, CSIs +15 to +17 are absent from the spectra entirely, and CSIs +14 and +13 are at a much lower intensity than in the DMSO free sample, with a shift of the dominant extended CSI from +13 to +11, and a shift of the dominant compact CSI from +7 to +6 in the presence of a final concentration of 1% DMSO.

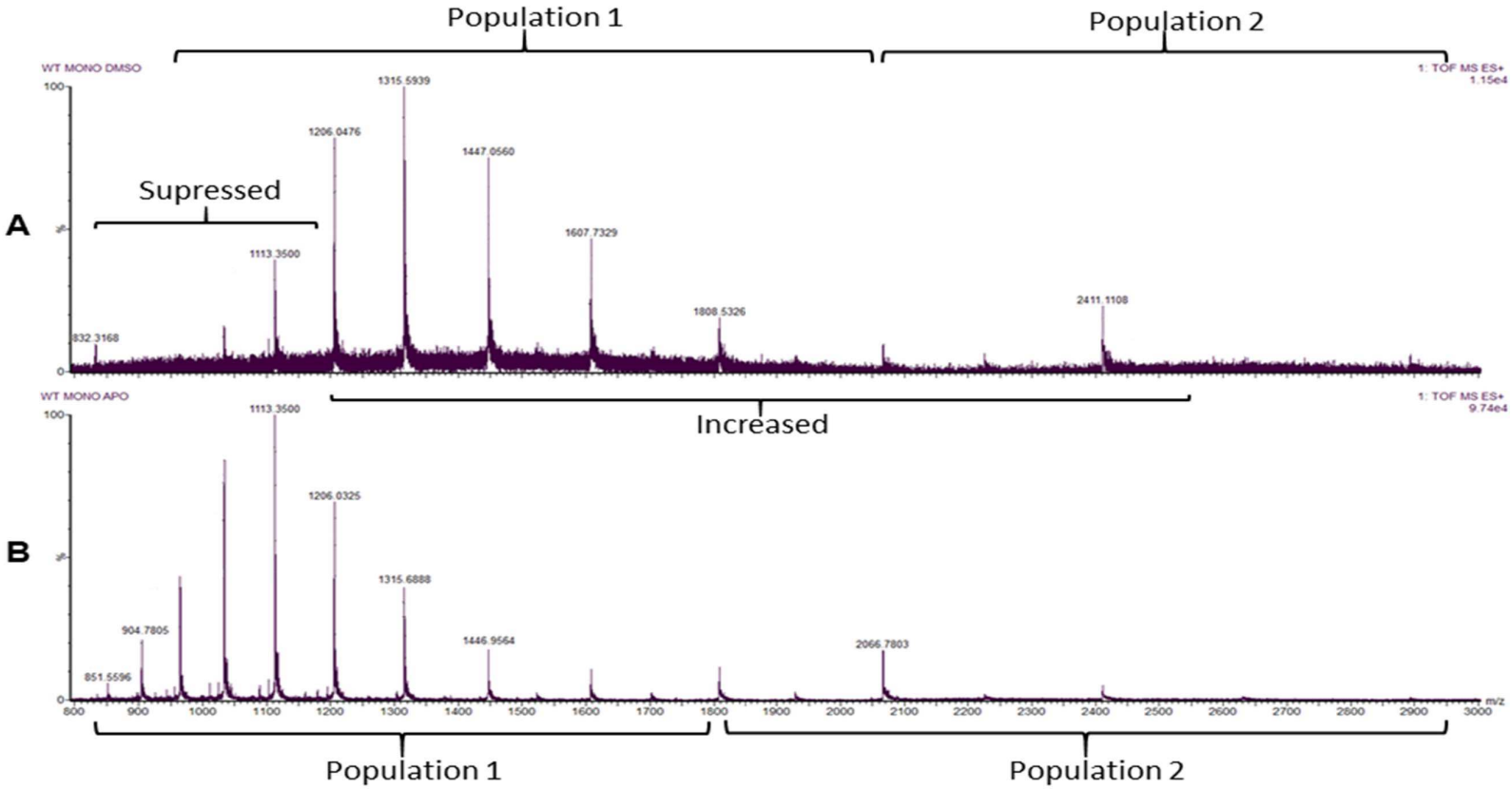

Figure 4.17: Spectra showing suppression of extended CSIs by DMSO.

ESI-IMS-MS spectra of A) 70µM apo in 50mM ammonium acetate + 1%

Due to this suppression, all future ESI-IMS-MS spectra were acquired using curcumin dissolved in a final concentration of 10% EtOH. The presence of 20% EtOH is known to increase the rate of amyloid formation, and is utilised in protocols when synthesising pathogenic oligomers from monomeric α-syn (Illes-Toth *et al.*, 2015; Danzer *et al.*, 2007; Roberts and Brown, 2015). Therefore, any interference from EtOH would be expected to enhance oligomeric species as opposed to repress them.

These later ESI-IMS-MS experiments concluded that curcumin and the derivatives were not binding to the monomeric protein, rather they were exerting their effect on the oligomeric species present within the sample.

Binding of one or more curcumins could be observed to dimeric species within the sample, and this led to a decrease in dimer and trimer intensities as observed within the drift scope mobilograms.

There is a possibility that the oligomeric species disappear in the presence of curcumin as they are aggregating into higher order oligomers and fibrils as a protective mechanism, which has been previously suggested as a mechanism for dealing with the presence of misfolded amyloid proteins, however this does not correlate with the results obtained by ThT assay, where a decrease in signal, indicative of a lack of higher order amyloid material, was observed. It has been previously reported that curcumins may cause aggregation into soluble, less toxic, off-pathway oligomeric species as protective mechanism (Yang *et al.* 2005; Nedumpully-Govindan *et al.*, 2016; Jha *et al.*, 2016). However, no higher order

oligomeric species were observed by ESI-IMS-MS in these experiments, suggesting the most likely mechanism of action observed here to be dissociation of oligomers and prevention of further assembly, through processes such as halting autoproteolytic fragmentation.

It must also be considered that both the generation and disappearance of these oligomeric species could be a product of the electrospray process and transition into the gas phase. As previously discussed in chapters 1 and 3, the conformation of IDPs such as Πsyn can be affected in the gas phase, causing the generation of protein species not present in solution conditions (Borysik *et al.*, 2015; Pagel *et al.*, 2013; Saikusa *et al.*, 2013). However, the more folded and globular a protein, the more stable it is in the gas-phase (Scarff *et al.*, 2008; Saikusa *et al.*, 2013), therefore these structures would be less likely to be affected than monomeric species. Experiments were also repeated a number of times with the same result observed, lending support to the data presented here. It is possible however that the binding of monomeric Πsyn and curcumin did not survive transition into the gas-phase, and this could be why binding to the monomeric form was not observed in these experiments.

Previous studies from other research groups have also suggested that curcumin only binds to oligomeric forms of Τsyn, in keeping with results presented in this chapter. Singh *et al.* used hydrogen-deuterium exchange to demonstrate a weak association of LMW (50-100kDa) Τsyn oligomers with curcumin, where no association with monomeric 14kDa protein was observed. The authors did not

observe any binding to the monomer by AFM, SEC Chromatography or SDS-PAGE analysis, but did again observe binding to oligomers and mature fibrils (Singh *et al.*, 2013). This study did not however report any dissociation of the preformed species into monomeric protein. Data recently presented by Ahmad and Lapidus however, reported that curcumin strongly bound to the monomeric protein, detected by a variety of optical absorbance and fluorescence methods (Ahmad and Lapidus, 2012). The altered morphology of the oligomeric species observed within these studies, corresponds with results from ESI-IMS-MS experiments reported in section 4.3.3, where a decrease in the more aggregation prone compact CSIs was observed. Curcumin has also previously been observed to bind to oligomeric and fibrillar species of the Aβ protein (Yanagisawa *et al.*, 2011). Due to the nature of these previously explored techniques, and the high specificity of mass spectrometry in comparison, data presented in this chapter indicates that curcumin has a disaggregating mechanism of action towards lower order oligomeric species.

Finally, it was also deduced that curcumin cannot bind to βsyn when the NAC region is deleted, indicating this is the binding region for the molecule. This was unsurprising as the molecules do not appear to bind to the monomeric protein, but lends support to previous reports suggesting that this region is important for the binding of curcumin, and essential for the aggregation of the protein (Giasson *et al.*, 2001; Ahmad and Lapidus, 2012).

4.5 Conclusions

Collective evidence presented in this chapter demonstrates that the anti-fibrillary properties of curcumins can operate with multiple amyloid proteins, and suggests the polyphenolic compound could therefore hold potential as a therapeutic for a number of different but related amyloid diseases. Data presented in this section demonstrates that some curcumin derivatives, in particular numbers 5 and 7, have increased anti-fibrillary effects in comparison to the native compound, as observed by the ThT assay screen. These derivatives have also been demonstrated to influence amyloid formation by both Tsyn and lysozyme. They follow a similar but not identical pattern in their inhibition, indicating that different curcumin derivatives have similar effects on aggregate formation, but differ in their effectiveness between different proteins. Activity of the derivatives is related to their structures and, within these experiments, the most successful candidates against Tsyn all contain an OH group attached to the benzene ring at position-3, suggesting this to be important for its anti-fibrillary properties against Tsyn at least. The development of curcumin derivatives as viable drug candidates is also greatly hindered by their poor bioavailability. Synthesising novel curcumin compounds with increased activity and increased bioavailability is therefore a potential viable method for future amyloid targeting therapeutics.

The proposed mechanisms of interaction between curcumins and Πsyn, and how this affects the amyloid aggregation of the protein can be seen in figure 4.17. Overall data presented here demonstrates curcumin and its derivatives slow and

prevent the aggregation of Tsyn *in vitro*, and it appears this mechanism is related to both reducing the fragmentation of the protein, and binding to pre-formed oligomeric species such as dimers, dissociating the protein complexes and thus preventing their further aggregation into amyloid material.

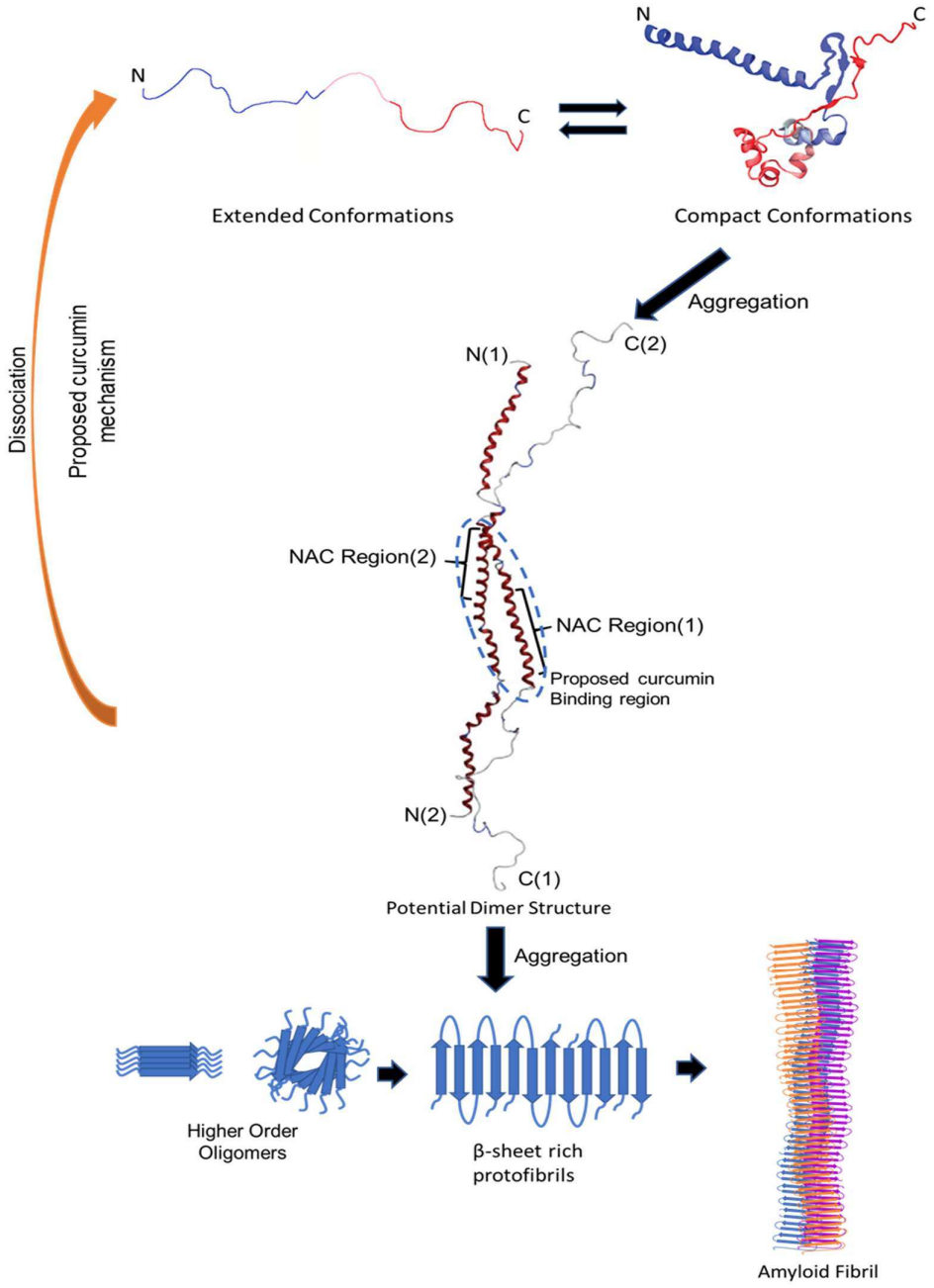

Figure 4.17: Proposed Mechanism of Curcumin Action.
Proposed mechanism of curcumin interaction with the amyloid aggregation pathway of WT Hsp. Compact conformations aggregate into lower order oligomeric species including dimers. Curcumin is proposed to bind to dimeric species within the region highlighted in a dashed blue oval, leading to the dissociation of these dimeric species back into monomeric protein, thus preventing the usual further aggregation into higher order oligomers, protofibrils, then mature amyloid fibrils.

Chapter 5 - Cellular Responses to Cu(II) and Curcumin Treatment

5.1 Introduction

Understanding how αsyn interacts with ligands, such as metal ions and curcumin in solution, provides a wealth of useful information on both the structure of the complexes and alterations to the protein's aggregation propensity. However, to understand these interactions fully, and how they may impact on the pathology of diseases such as PD, it is essential to investigate these interactions at the cellular level.

It has been established that the addition of metal ions, such as copper, to the media of growing SHSY5Y cells results in the formation of intracellular aggregates of αsyn (Wang *et al.*, 2010). It has however yet to be established whether these aggregates are phosphorylated at the potentially pathogenic residue of S129, as is the case for αsyn found in mature LBs of PD patients.

5.1.1 Metal Homeostasis

Transition metals such as copper, iron, zinc, manganese and cobalt are essential for a multitude of regulatory and catalytic roles in the growth of all organisms from the micro to the macro scale. However, excesses of these metals can be toxic,

therefore it is essential for organisms to regulate the intracellular levels of these metals (Jaishankar *et al.*, 2014).

Metal ions play a vital role in a number of cellular processes, including cell structure maintenance, regulation of gene expression, and neurotransmitter release (Chen *et al.*, 2016), and transition metals such as copper and iron have been shown to be essential co-factors for almost half of known proteins (Waldron *et al.*, 2009). Copper and iron are both intrinsically expressed throughout the brain in varied concentrations dependent on the brain region, with high levels being observed within the *SNPC* (Wright *et al.*, 2009).

Copper is a known cofactor for several cellular proteins, such as cytochrome c oxidase, which is involved in the mitochondrial production of ATP, and Cu/Zn-superoxide dismutase (SOD1), which is an antioxidant, with a role in free-radical scavenging (Sathasiviam and Shaw, 2005). The immune system is known to utilise copper as an antimicrobial, with activated macrophages showing a high level of copper within the phagosomes used to capture and disable invading microbes (Festa and Thiele, 2011). Cellular levels of copper are mainly regulated by copper pumps, the failure of which leads to intracellular accumulation of the metal and eventually toxicity and cell death (Arciello *et al.*, 2005).

Almost all cells require iron for activities such as oxygen transport, energy metabolism and DNA synthesis. Iron is essential biochemically due to its redox activity however this activity can be prone to the production of oxidative radicals.

During Fenton reactions iron cycles between its Fe^{2+} and Fe^{3+} states generating ROS such as hydroxyl radicals (Wang and Pantopoulos, 2011). Elevated levels of ROS lead to oxidative stress within the cells, which disrupts cellular processes and results in toxicity, therefore cellular iron must also be tightly regulated. Ferritin and haem transporters are predominantly used to regulate cellular iron levels, and in particular iron bound to ferritin can be transported throughout the body for use in a variety of cellular processes (Keel *et al.*, 2008; Wang and Pantopoulos, 2011).

5.1.2 Tau Phosphorylation

Tau has five known phosphorylation sites, S87, Y125, S129, Y133 and Y136, with these modifications suggested to play roles in processes such as membrane binding (Y125), autophagy (S129) and proteolytic degradation (S129) (Tenreiro *et al.* 2014; Machiya *et al.* 2010; Chau *et al.* 2009). Around 90% of tau found within the LBs of PD patients is found to be phosphorylated at S129, whereas in healthy individuals, only around 4% of the protein has undergone this modification at any possible residue, strongly suggesting a pathological role for this particular modification (Anderson *et al.*, 2006; Fujiwara *et al.*, 2002). Studies aimed at determining this pathological role have so far yielded conflicting results, with both protective and pathogenic roles for S129 phosphorylation reported, and it is therefore unclear what the role of this modification is, in PD pathogenesis.

Four of the five phosphorylation sites are found within the highly disordered C-terminal region of the protein (Oueslati, 2016), which is also the location of the majority of metal binding sites, as shown in figure 1.2 in chapter 1. It is yet to be determined what the effect of phosphorylation, in particular at S129, and the binding of metals to αsyn is on cell viability and protein aggregation in the cellular environment, and whether the two events have a synergistic influence on the pathogenesis of PD.

5.1.3 SHSY-5Y Neuroblastoma Cells as a Model for Neurodegeneration

The cell line SHSY-5Y has been used extensively in PD research due to its dopaminergic properties. This neuroblastoma cell line is a subclone of the cell line SK-N-SH, which was isolated in the 1970s from a bone marrow biopsy of a four year old female with metastatic neuroblastoma, and has undergone three rounds of clonal selection to achieve its phenotype (Biedler *et al.*, 1978; Xicoy *et al.*, 2017). The cells are known to have dopamine-β-hydroxylase and tyrosine hydroxylase activity, and have been demonstrated to convert dopamine to norepinephrine *in vitro*, (Biedler *et al.*, 1978; Ross and Biedler, 1985; Xicoy *et al.*, 2017; Schlachetzki *et al.*, 2013). Because of their phenotype, these cells have been utilised for many years in studies of PD, for example in investigations into αsyn aggregation and candidate drug screens, and studies of the role of αsyn in DA toxicity (Hasegawa *et al.*, 2004; Colapinto *et al.*, 2006; Wang *et al.*, 2010; Xicoy *et al.*, 2017).

5.2 Aims and Objectives

Experiments conducted in this chapter were designed to investigate the links between phosphorylation and copper-induced aggregation of Tsyn within a cellular model. The main objectives were as follows:

- To monitor the induced aggregation and cytotoxicity of Tsyn following metal treatment.
- To determine if Tsyn is phosphorylated within the SH-SY5Y cellular model following treatment with copper.
- To investigate the possible inhibitory effects of natural curcumin on the formation of metal induced aggregates.

5.3 Results

SHSY5Y neuroblastoma cells were exposed to a range of copper concentrations, 100, 300 and 500µM, for 48 hours. Immunocytochemistry utilising the antibody specific to αsyn residues 121-125 (Syn211), and the antibody specific to αsyn phosphorylated at S129 (phos129) was performed, to determine the effect of copper on the intracellular aggregation of αsyn, and the phosphorylation state of the protein in these conditions. Apoptosis and viability of the cells was also assessed using DAPI staining and trypan blue dye.

5.3.1 Incubation of SHSY5Y cells with $CuCl_2$ Causes an Increase in the Formation of Intracellular Aggregates

The number of cells containing aggregates was determined by blinding the images and counting 200 cells per experimental condition. Three repeat experiments were compared for statistical analysis as described in chapter 2. Aggregate numbers were averaged and are presented as a percentage of the total cell count in figure 5.5.

Examples of positively and negatively assigned cells can be observed in figure 5.1, and an example of a scored dataset can be seen in figure 5.2, both of which have been included without the DAPI staining overlay for clarity.

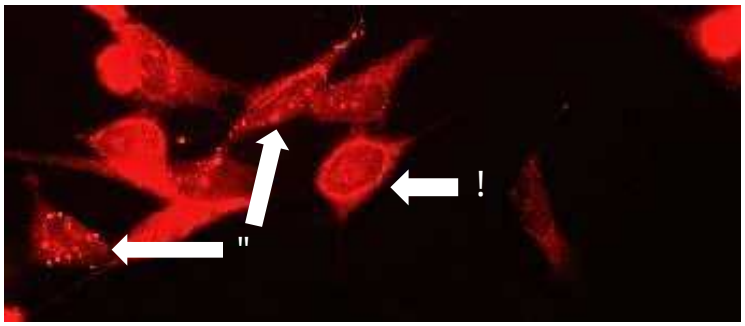

Figure 5.1: Example of Positively and Negatively Assigned Aggregate Staining in SHSYSY Cells.

SHSYSY cells stained with the syn211 antibody to WT α-syn, observed with a 100x objective. A) Negative cell showing only cytoplasmic staining and B) Positive cell showing the presence of intracellular inclusions. 1000x magnification.

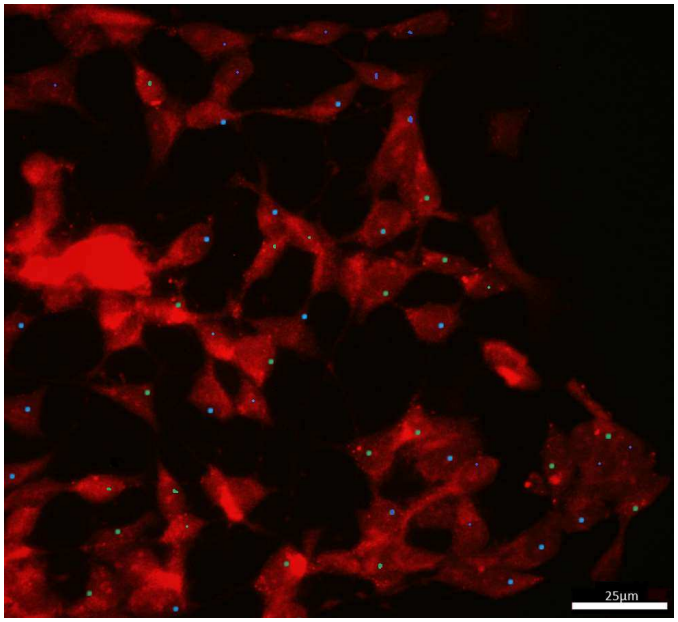

Figure 5.2: Example of a Scored SH-SYSY Dataset.

Blue dots represent cells marked as negative for aggregates. Green dots represent cells marked as positive for aggregates. Over-exposed cells or those not in focus were not scored, as shown, and removed from the dataset.

As shown in figure 5.3, when cells were exposed to increasing levels of $CuCl_2$, aggregated forms of α-syn, as highlighted on each image with white arrows, can be observed within the cells. These can be seen more clearly in the 100x objective example image in figure 5.4.

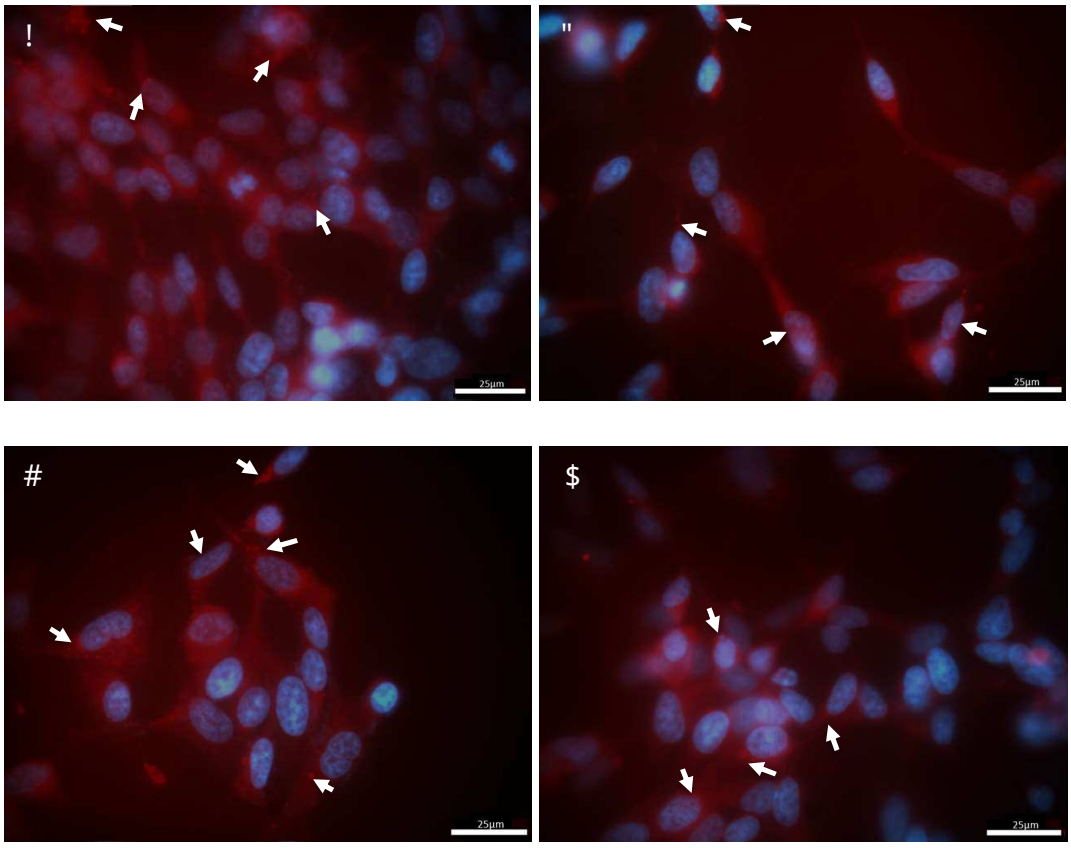

Figure 5.3: Effect of Increasing $CuCl_2$ Concentration on Aggregate Counts in SH-SY5Y Cells Stained with the Syn211 Antibody.

SH-SY5Y cells incubated with increasing levels of $CuCl_2$ for 48hrs and stained with the syn211 antibody specific to α-syn aa121-125. A) Untreated, B) 100µM $CuCl_2$, C) 200µM $CuCl_2$, D) 500µM $CuCl_2$. White arrows point directly to aggregates within select cells in each image.

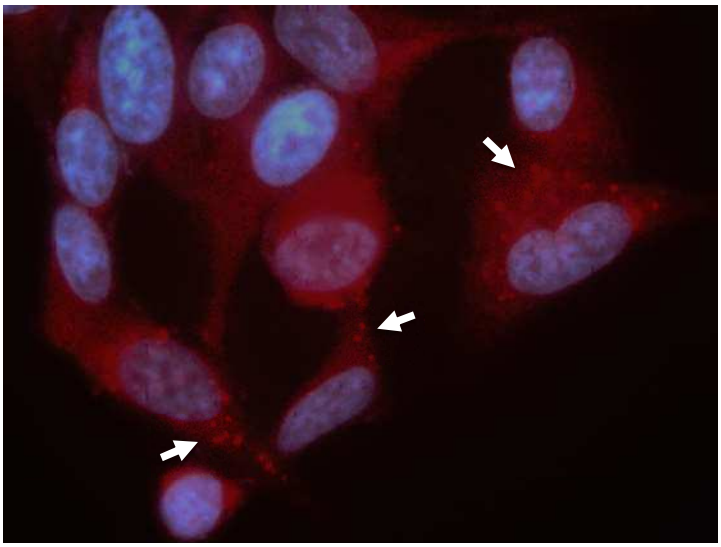

Figure 5.4: Example of Aggregate Formation using 100x Objective.

SH-SY5Y Cells treated with 300μM $CuCl_2$ for 48hrs show formation of punctate Hsyn aggregates. White arrows point directly to aggregates within the cells. 1000x magnification.

Positive staining for Tsyn within the cytoplasm was observed in all cells, due to its intrinsic expression, with the highest intensity being observed ringed around the nucleus, as shown in figure 5.1A, in the untreated samples.

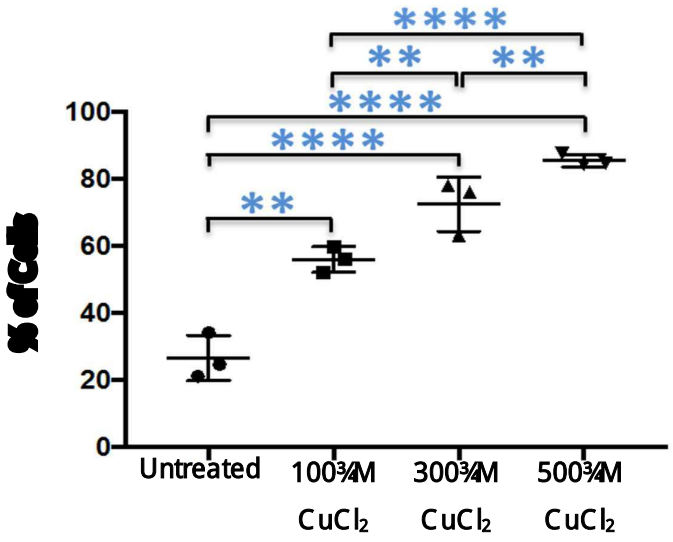

Figure 5.5: Percentage of SH-SY5Y Cells Containing ┬Syn Aggregates Stained for Syn211, upon Increasing $CuCl_2$ Concentration.

Percentage of cells containing distinct intracellular aggregates of ┬syn after exposure to different concentrations of $CuCl_2$ (**= p<0.01, *** = p<0.0001), n=3.**

As shown in figure 5.5, an average 26.5¹ 6.7% of cells in the untreated sample contained distinct punctate aggregates of ┬syn. Upon incubation with 100¾M $CuCl_2$ for 48hrs, a significant ($p<0.01$) increase in cells containing identifiable aggregates to 55.8¹ 3.8% was observed. Upon incubation with 300¾M $CuCl_2$ a significant ($p>0.0001$) increase in aggregates to 72.3¹ 8.1% of cells is observed, and upon incubation with 500¾M $CuCl_2$, a further increase to 86.6 ¹ 3.1% ($p<0.0001$) was seen. This suggests that increasing $CuCl_2$ levels in the media, increases the aggregate load within the cells.

When examining the statistical significance between the different $CuCl_2$ concentrations, also shown in figure 5.5, a significant increase in the percentage of cells containing distinct aggregates is observed between cells incubated with 100¾M $CuCl_2$ and cells incubated with 300¾M $CuCl_2$ ($p<0.01$). Aggregate numbers also significantly increase ($p<0.01$) in between cells incubated with 300¾M $CuCl_2$ and 500¾M $CuCl_2$. This data would also indicate that the extent of the aggregation is dose dependent on the amount of copper used to treat the cells.

The intensity of the Tsyn fluorescence was quantified using ImageJ image analysis software, as described in section 2.2.5.6, as a means of monitoring the expression levels. As displayed in figure 5.6, a significant increase in corrected total cell fluorescence (CTCF) was observed between the untreated cells and those incubated with 300¾M $CuCl_2$ ($p<0.05$), and untreated and cells incubated with 500¾M $CuCl_2$ ($p<0.05$). No significance increase in fluorescence was determined between untreated cells and those treated with 100¾M $CuCl_2$. This suggests that incubation with 300¾M or 500¾M $CuCl_2$ causes an increase in the expression of Tsyn, as determined by increases in the level of fluorescence. Image analysis also indicates that at concentrations greater than 300¾M $CuCl_2$ there is no further increase in Tsyn expression levels, yet the number of identifiable aggregates does increase. Further examples of stained cells utilised to determine these aggregation counts and fluorescence intensities can be observed in appendix 5A-5D.

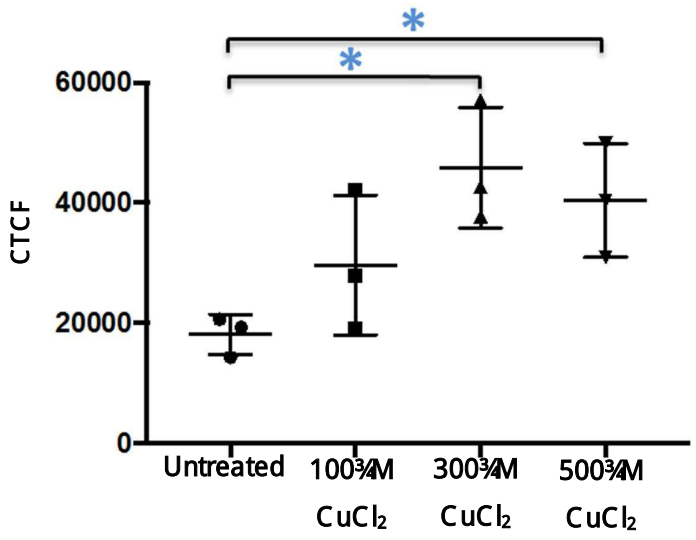

Figure 5.6: ImageJ Analysis of the Fluorescence Intensity of SH-SY5Y Cells Stained with the Syn211 Antibody, at Increasing $CuCl_2$ Concentration.

Fluorescence intensity of SH-SY5Y cells incubated with different concentrations of $CuCl_2$, stained with the Syn211 T-syn antibody, as determined by quantification on ImageJ image analysis software (*p<0.05). n=3.

Data presented here suggests that incubation of SH-SY5Y neuroblastoma cells with increasing concentrations of $CuCl_2$ results in the formation of intracellular aggregates of T-syn, and the percentage of cells containing aggregates increases with increased copper concentration. Data also suggests that the total T-syn level expressed within the cells increases after incubation with 300 and 500¾M $CuCl_2$,

determined by an increase in overall fluorescence, indicating that increased aggregate formation is, in part, due to an increase in expression of T-syn.

5.3.2 Incubation of SHSY5Y cells with $CuCl_2$ Causes an Increase in Apoptosis

To determine whether incubation with copper causes cytotoxicity, cells were also examined for signs of apoptosis upon incubation with $CuCl_2$. Counting measures utilised in section 5.3.1 were followed, counting 200 cells per condition and examining for signs of apoptosis. Apoptotic cells were identified, as shown in figure 5.7, by expression of one or more of three predetermined signals of apoptosis, visible via DAPI staining; chromatin condensation, nuclear elongation and nuclear fragmentation. Cells containing one or more of these signs were marked as positive. Apoptotic cell counts are presented in figure 5.8 as a percentage of the total cell count.

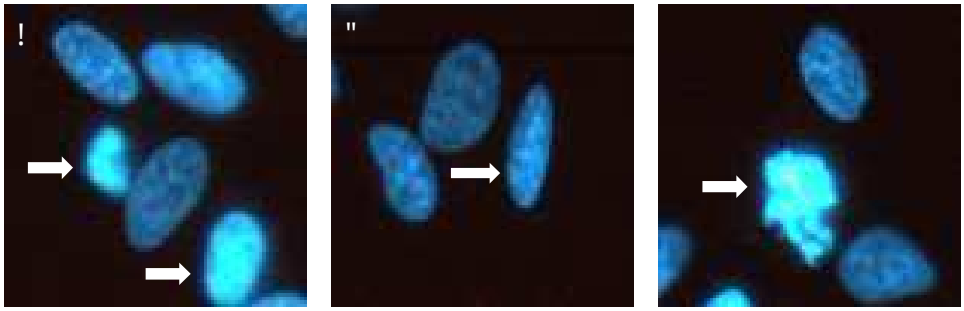

Figure 5.7: Signs of apoptosis in SHSY5Y Cells, Visible With DAPI Staining. A) Nuclear condensation, B) Nuclear elongation and C) Nuclear fragmentation. Taken using a 100x objective. 1000x times magnification.

As shown in figure 5.8, an average 17.7¹ 2.8% of untreated cells showed signs of apoptosis. The percentage of apoptotic cells increased significantly ($p<0.05$) to 58¹ 2.7% upon 48hrs incubation with 100¾M $CuCl_2$. Upon incubation with 300¾M $CuCl_2$, a significant ($p<0.001$) increase to 78.5¹ 4.3% was observed. No further increase in apoptotic cell numbers was observed when cells were incubated with 500¾M $CuCl_2$, with 75.7¹ 4.0 cells showing one or more signs of apoptosis.

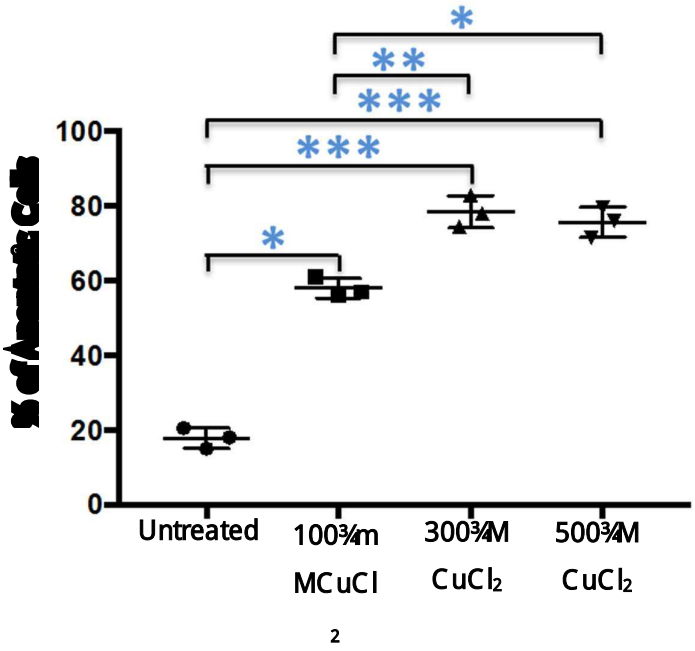

Figure 5.8: Percentage of Cells Showing Signs of Apoptosis after Treatment with $CuCl_2$.

Percentage of cells showing at least one distinct sign of apoptosis after exposure to increasing concentrations of $CuCl_2$ (* = p<0.05, ** = p<0.01, *** = p<0.001). n=3.

As shown in figure 5.8, there is a significant ($p<0.01$) increase in number of apoptotic cells between cells incubated with 100¾M $CuCl_2$ and 300¾M $CuCl_2$, whereas no significant alterations were observed between cells treated with 300¾M $CuCl_2$ and 500¾M $CuCl_2$.

Results here demonstrate that exposure to $CuCl_2$ induces apoptosis in SHSY5Y cells after 48hrs incubation, alongside the formation of intracellular aggregates. Not all apoptotic cells showed signs of aggregate formation, and not all aggregate containing cells showed signs of apoptosis, which may suggest the two mechanisms are independent responses to the presence of the metal ions.

5.3.3 Incubation of SH-SY5Y cells with $CuCl_2$ Causes a Reduction in Cell Viability

Trypan blue dye was used to quantify the level of cell viability following copper treatment for 48 hours. Untreated cells had an average viability of 86.1¹ 3.9%, which was reduced to 57.1¹ 3.9% ($p<0.01$) upon incubation with 100¾M $CuCl_2$, as shown in figure 5.9. Incubation with 300¾M $CuCl_2$ also resulted in a statistically significant ($p<0.0001$) reduction in viability to 48.5¹ 3.4%, and incubation with 500¾M $CuCl_2$ resulted in a further decrease to just 40.9¹ 2.3% ($p<0.0001$).

When statistical analysis was performed between each different $CuCl_2$ concentration, as shown in figure 5.9, a significant ($p<0.01$) decrease in viability was observed between both cells incubated with 100 and 300¾M $CuCl_2$, and between 300 and 500¾M $CuCl_2$, suggesting cell viability decreases with exposure

to increased $CuCl_2$ concentrations. This data correlates well with the image analysis data and indicates that increasing concentrations of copper result in cell death through an apoptotic pathway.

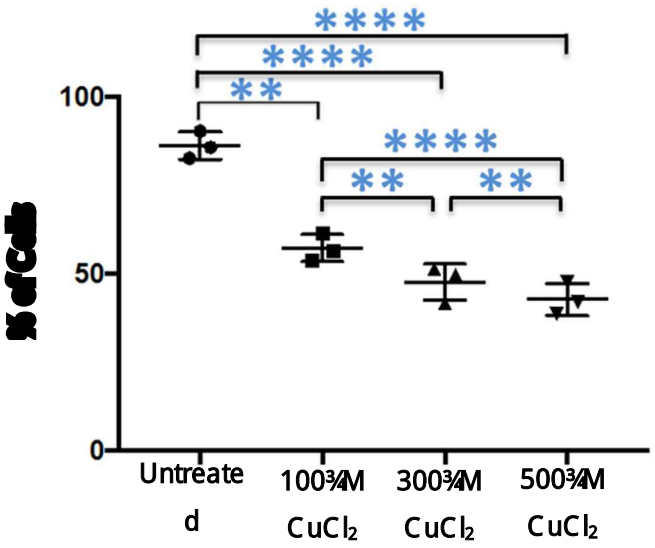

Figure 5.5: Cell Viability of SH-SY5Y Cells After Incubation with $CuCl_2$.

Cell viability of SH-SY5Y cells incubated with increasing concentrations of $CuCl_2$ for 48hrs, shown as percentage of total cells within the sample (= p<0.01, **** = p<0.0001). n=3.**

5.3.4 Incubation of SHSY5Y cells with $CuCl_2$ Induces Aggregates of αsyn Phosphorylated at Serine-129

To investigate the phosphorylation state of both the intrinsic αsyn, alongside the aggregates formed in the presence of $CuCl_2$, SHSY5Y cells were treated with copper and stained utilising antibody specific to αsyn phosphorylated at S129. As shown in figure 5.10, there is positive staining for phosphorylated αsyn in all experimental conditions, including the cells incubated without copper. Figure 5.10A, showing untreated cells, demonstrates a similar pattern of cytoplasmic staining to that observed with the cells stained for syn211 in section 5.3.2. It has been reported previously that around 4% of cytosolic αsyn is phosphorylated at S129 in the healthy human brain (Kim *et al.*, 2014), so a small percentage of phosphorylated cells would be expected. However, the untreated cells analysed here showed a considerable increase over what was expected.

Following treatment with copper, mean numbers were again calculated via the same counting system employed in section 5.3.1, as shown in figure 5.11 and representative images are given in appendices 5E to 5H.

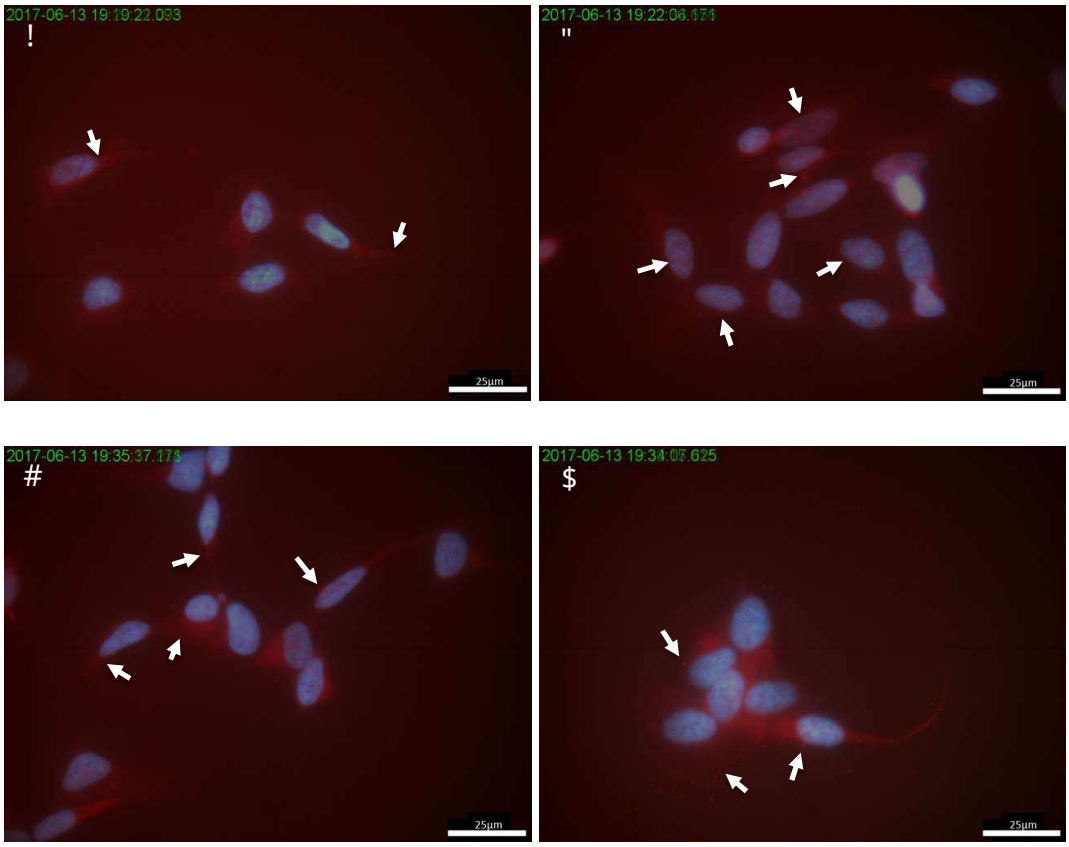

Figure 5.16: Effect of Increasing $CuCl_2$ Concentration on Aggregate Counts in SH-SY5Y Cells Stained with the Ples129 Antibody.

SH-SY5Y cells incubated with different concentrations of $CuCl_2$ for 48hrs and stained with the ples129 antibody specific to α-syn phosphorylated at serine 129. A) Untreated, B) 100µM $CuCl_2$, C) 300µM $CuCl_2$, D) 500µM $CuCl_2$. White arrows point directly to aggregates within select cells in each image.

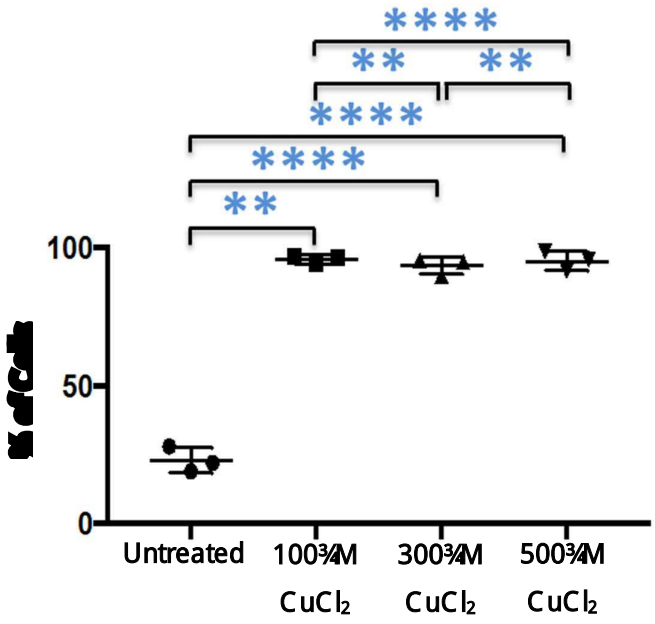

Figure 5.11: Percentage of SH-SY5Y Cells Containing IBSyn Aggregates Stained for Phos129, upon Increasing $CuCl_2$ Concentration.

Percentage of cells containing distinct intracellular aggregates of phosphorylated T-syn after exposure to different concentrations of $CuCl_2$ (* = p<0.05, ** = p<0.01). n=3.

As shown in figure 5.11, an average 23¹ 4.6% of untreated cells contained distinct aggregates stained with the phos129 antibody. Upon incubation with 100¾M $CuCl_2$, a statistically significant increase ($p<0.01$) to an average 95.8¹ 1.6% of cells displayed phosphorylated aggregates of T-syn. Addition of 300¾M or 500¾M $CuCl_2$ resulted in mean cell counts of 93.5¹ 3.1% ($p<0.01$) and 95.2¹ 3.5%

($p<0.0001$) respectively. A significant increase in cells containing aggregates upon increased copper concentration was also noted ($p<0.01$).

When the average fluorescence intensities of the cells were calculated using Image J image analysis software, as shown in figure 5.12, a statistically significant ($p<0.05$) increase in fluorescence was observed with all three $CuCl_2$ concentrations, but no significance was observed between the three concentrations. This again suggests that there is an increase in T-syn expression within the cells, measured via an increase in fluorescence intensity, alongside the increase in aggregate formation.

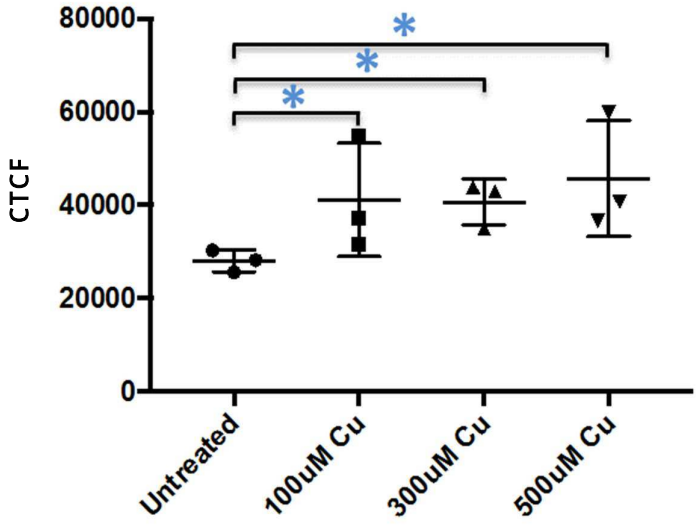

Figure 5.12: ImageJ Analysis of the Fluorescence Intensity of SH-SY5Y Cells Stained with the Phos129 Antibody, at Increasing $CuCl_2$ Concentrations.

Fluorescence intensity of SH-SY5Y cells incubated with different concentrations of $CuCl_2$, stained with the phos129 T-syn antibody, as determined by quantification on ImageJ software (* = $p<0.05$), n=3.

When the aggregate counts between the syn211 and Phos129 immunocytochemistry experiments are directly compared, as shown in figure 5.13, there is a significant increase in the percentage of cells containing phosphorylated inclusions compared with those stained for unmodified Πsyn.

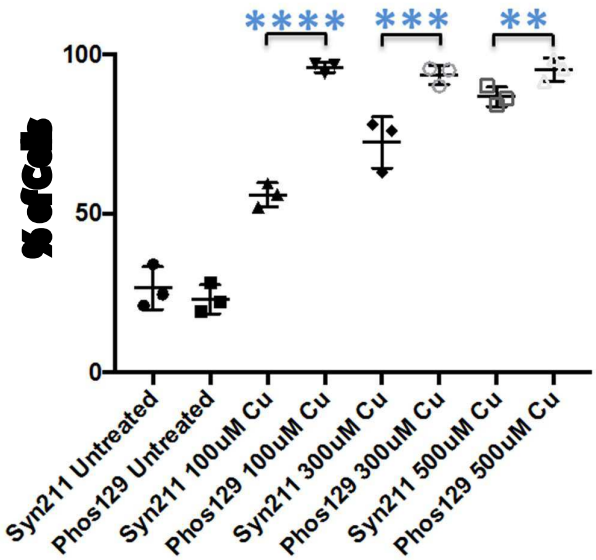

Figure 5.13: Comparison of Cell Percentage Containing Inclusions of Syn211 and Phos129 Stained Aggregates.

Direct comparison of the number of SH-SY5Y cells containing inclusions following incubation with different concentrations of $CuCl_2$. Staining was performed with the anti-syn211 or anti-phos129-πsyn antibodies. Percentage of cells containing distinct aggregates of πsyn (=p<0.01, ***=p<0.001, ****=p<0.0001), n=3.**

Following incubation with 100¾M $CuCl_2$, 55.8¹ % of 3.6cells stained positive for aggregates with the syn211 antibody, however with the phos129 antibody this was significantly ($p<0.0001$) increased to 95.8¹ 1.6%. After incubation with 300¾M $CuCl_2$, 72.3% of cells stained positive for aggregates with syn211, and a significantly ($p<0.001$) higher percentage of 93.5¹ 3.1% stained positive with phos129. After incubation with 500¾M $CuCl_2$, the percentage of cells staining positive for aggregates with the phos129 antibody was again significantly ($p<0.01$) higher than those stained with the syn211 antibody, with counts of 95.2¹ 3.5% and 86.6¹ 3.1%, respectively.

.

5.3.5 Incubation of SHSY5Y with Curcumin Appears to have No Effect on Formation of $CuCl_2$ Induced Aggregates of Tsyn

To determine if the copper-induced aggregation of Tsyn could be prevented, 300¾M $CuCl_2$ was added to the cell media, to induce aggregation, along with three different concentrations of natural curcumin, 4, 7 and 10 ¾M. As shown in figure 5.14, distinct aggregates can still be observed under all experimental conditions.

Cells containing aggregates were counted, employing the system utilised in previous sections. Representative images used to obtain cell counts are shown in appendices 5I to 5L.

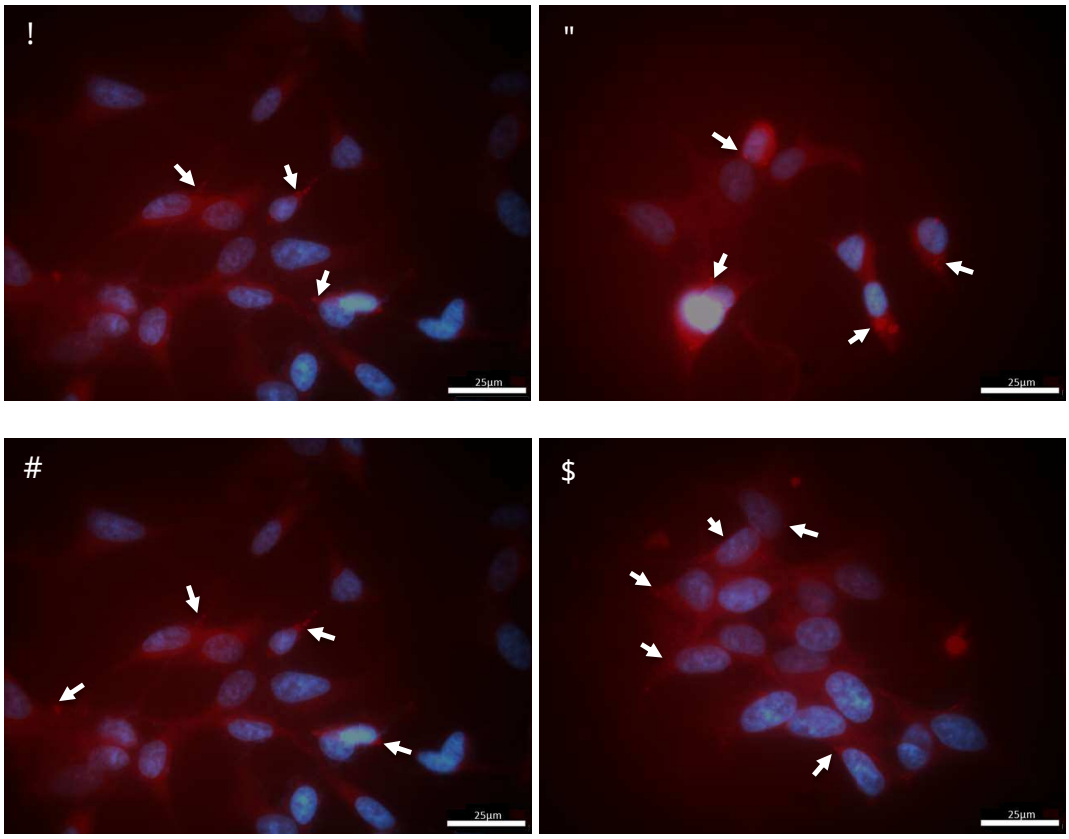

Figure 5.14: Effect of Increasing Curcumin Concentration on Aggregate Counts in SH-SY5Y Cells Treated with 300µM $CuCl_2$ and Stained with the Syn211 Antibody.

SH-SY5Y cells co-incubated with to 300 µM $CuCl_2$ for 48hrs and stained with the syn211 antibody specific to α-syn aa121-125. A) 300 µM $CuCl_2$ only, B) 300 µM $CuCl_2$ + 4µM Curcumin, C) 300µM $CuCl_2$ + 7µM Curcumin, D) 300 µM $CuCl_2$ + 10µM Curcumin. White arrows point directly to aggregates within select cells in each image.

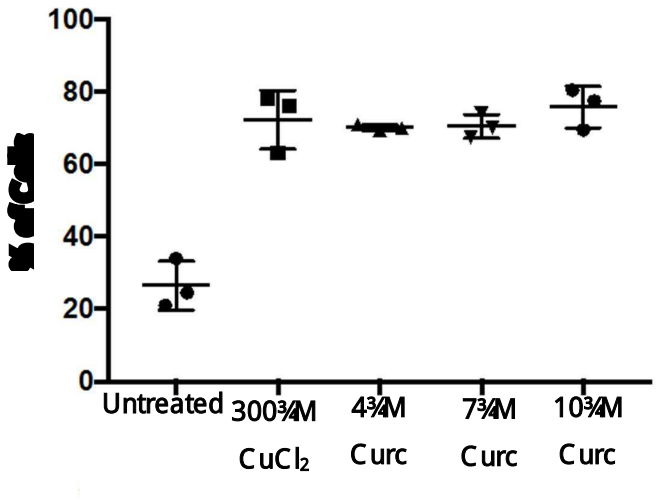

Figure 5.15: Percentage of SH-SY5Y Cells Containing Distinct ¬Syn Aggregates Stained with Syn211, after Co-Incubation with Copper and Curcumin.

Percentage of cells containing distinct intracellular aggregates of ¬-syn after incubation with 300¾M $CuCl_2$ and different concentrations of natural curcumin. No significant alterations were noted between those treated with copper alone or copper and curcumin.

As shown in figure 5.15, and akin to results presented in section 5.4.1, the presence of 300¾M $CuCl_2$ caused a significant increase ($p<0.0001$) in the number of cells containing distinct aggregates of ¬-syn after 48hrs incubation. Untreated cells demonstrated an average 26.5 ± 6.7% of cells containing aggregates, whereas cells treated with 300¾M $CuCl_2$ contained aggregates in an average 72.3 ± 8.1% of cells.

Upon addition of 4¾M natural curcumin alongside 300¾M $CuCl_2$, an average 70.2 ¹ 0.8% of cells were still found to contain aggregates, suggesting the addition of curcumin at this concentration had no effect on the formation of Tsyn aggregates induced by addition of $CuCl_2$ and no statistically significance was seen. The same was true for co-incubation with 300¾M $CuCl_2$ and either 7¾M or 10¾M curcumin, with positive cell counts of 70.5¹ 3.3% and 75.8¹ 5.7%, respectively. This data demonstrates that, in this cell model of PD, addition of natural curcumin alongside incubation with $CuCl_2$ for 48hrs did not prevent the formation of $CuCl_2$ induced aggregates of Tsyn.

5.4 Discussion

Results presented in this chapter demonstrate that the incubation of SH-SY5Y cells in the presence of copper for 48hrs results in the formation of intracellular aggregates of T-syn. These aggregates were identifiable via immunocytochemical staining with the syn211 antibody with the addition of 100, 300 or 500¾M $CuCl_2$ to the media resulting in a significant increase ($p<0.01$, $p<0.0001$ and $p<0.0001$, respectively) in the percentage of cells containing these aggregates. Significant increases ($p<0.01$) in aggregate positive cells were also noted with increased copper concentration, indicating a dose dependence to the response. This increase in aggregate formation also resulted in an increase in the average fluorescence intensity of the cells, as quantified with the use of Image J. Incubation with 300 or 500¾M $CuCl_2$ both resulted in a significant ($p<0.05$) increase in fluorescence intensity. This suggests that the presence of copper may also be inducing an increase in T-syn expression within the cells, alongside an increase in the formation of intracellular inclusions.

Incubation with $CuCl_2$ also resulted in a concurrent increase in apoptosis, as determined via DAPI staining and trypan blue. Incubation with 100¾M $CuCl_2$ caused a significant ($p<0.05$) increase in the percentage of cells demonstrating one or more signs of apoptosis compared with the untreated cells, and a significant increase ($p<0.01$) was again observed in comparison to 100 ¾M $CuCl_2$, when cells were incubated with 300¾M $CuCl_2$. No significant increase was seen when $CuCl_2$ concentration was increased further. Interestingly not all cells

containing aggregates showed signs of apoptosis, which would suggest that it is not the aggregate load itself inducing an apoptotic response in the cells, but another action of the copper ions. Possible causes include an increase in the presence of ROS (Cardaci *et al.*, 2008; Davies *et al.*, 2011). As previously discussed in chapter 3, Tsyn is known to possess ferrireductase activity, utilising copper bound to the protein in the process (Davies *et al.*, 2011). This iron cycling results in the production of ROS species, which are known to induce oxidative stress and apoptotic responses in SHSY5Y cells (Cardaci *et al.*, 2008), therefore this is a plausible theory as to how copper ions induce apoptosis in this model. It has also been previously established that ROS and oxidative stress are key factors in iron-induced Tsyn aggregation in SH-SY5Y cells, so this may be the case for copper. ROS have also been linked with the S129 phosphorylation of Tsyn in an SH-SY5Y model, suggesting the addition of copper may induce an increase in Tsyn phosphorylation (Perfeito *et al.*, 2014). This increase in S129 phosphorylation was also demonstrated by results in this chapter, and it is also plausible that this phosphorylation could be the cause of the apoptotic effects.

This increase in apoptosis was also coupled with a decrease in cell viability, as determined via trypan blue staining. Mean cell viability was significantly ($p<0.01$) reduced upon incubation with 100 ¾M $CuCl_2$ and was significantly ($p<0.01$) decreased further upon increased copper concentrations of 300¾M $CuCl_2$ or 500¾M $CuCl_2$, indicating there is a dose response. Copper has also been previously demonstrated to reduce cell viability to just 50% after treatment with

150¾M for 24 hours (Arciello *et al*,. 2005) and in another study reduction to 50% viability was seen with 200¾M after 48h (Wang *et al*., 2010). Experiments in this chapter were performed with 100, 300 and 500¾M $CuCl_2$, in order to include experiments with both lower and higher copper concentrations than those previously reported, and a similar reduction in viability, to 57.1¹ 3.9%, 48.5¹ 3.4% and 40.9¹ 2.3% respectively was observed.

Previously published data suggests that the extracellular toxicity of Tsyn requires the interaction of copper ions, which results in the formation of a unique type of oligomer, suggested to potentially be the toxic, disease causing state (Wright *et al*., 2009). Due to the increased cell toxicity observed in these experiments, it is also plausible that these are the aggregates observed within experiments, and these aggregates themselves are causative of the increased apoptosis and decreased cell viability observed.

It has previously been reported that copper ions may be essential for aggregate formation, as decreasing intrinsic copper levels via the use of a chelex compound caused a reduction in the percentage of cells containing Tsyn aggregates, from 12.7% of untreated cells, to just 3.8% in the presence of the compound. Incubation with the chelex and 10¾M copper was able to restore the aggregate counts to those of the untreated cells, and addition of 100¾M copper resulted in an increase in cells containing aggregates to 37.7% (Wang *et al*., 2010). Within the Wang study, Tsyn within the untreated and cells treated only with the chelex

compound was predominantly found ringed around the nucleus, comparable to the results presented in this chapter. The study also investigated truncated versions of -syn and H50A mutants, to demonstrate that the N-terminal region of the protein is essential for its aggregation in the presence of copper (Wang *et al.*, 2010). A separate study also determined copper to be essential for the formation of toxic -syn aggregates in an SH-SY5Y model, producing a unique, toxic form of protein complex, and deduced that iron did not induce the formation of toxic oligomers. Copper was also shown to increase the load and toxicity of aggregated forms of the protein (Wright *et al.*, 2009), similar to the results presented here.

Results in this chapter also demonstrate that both copper induced and intrinsic aggregates formed within SH-SY5Y cells, are phosphorylated at the potentially pathogenic amino acid residue S129, with 23¹ 4.6% of untreated cells staining positive. This intrinsic phosphorylation has been reported before, where 10% of cells positively stained for WT -syn also stained positive for the S129 modification (Perfeito *et al.*, 2014). This modification is known to be involved in the clearance of the protein from the cytosol and may mark these aggregates for degradation. When cells were incubated for 48h with the addition of 100, 300 or 500¾M $CuCl_2$ to the media, a significant increase to over 90% ($p<0.01$, $p<0.0001$ and $p<0.0001$, respectively) in the number of cells staining positive for phosphorylated cytoplasmic inclusions of -syn was observed for all treatments, though no difference was noted between the concentrations. When these values were

compared to those obtained with the syn211 antibody for unmodified αsyn, a significantly higher percentage of cells stained positive for phosphorylated inclusions. No difference in inclusion formation was observed between the untreated samples. This suggests that treatment with $CuCl_2$ results in a significantly higher number of cells containing phosphorylated aggregates.

In these experiments, it could not be determined whether all aggregates stained for syn211 were also phosphorylated, however if that was the case then there should be little difference in counts between the experimental data sets, using the different antibodies. It was demonstrated in chapter 2 that the phos129 antibody utilised in these experiments does not have the capacity to bind to WT αsyn. It would generally be expected that the syn211 antibody would bind all αsyn aggregates, despite post-translational modification, but these results suggest that is not the case. It is possible that the phosphorylation at S129 is causing a conformational change which no longer allows the syn211 antibody to bind to the aggregate. This may result as the binding epitope for the syn211 is within the C-terminal very close to this phosphorylation position, at residues 121-125 and could become masked on phosphorylation and subsequent aggregation. The environment of the C-terminal domain of αsyn is also known to change as fibril assembly takes place with the access to this region by nanobodies decreasing on fibril maturation, so it is possible as the protein is phosphorylated it aggregates further, shielding the syn211 binding epitope (Guilliams *et al.*, 2013; El-Turk *et al.*,

2016). What is clear however is that treatment with copper induces the formation of phosphorylated intracellular inclusions.

It is unknown from these results if the copper ions are causing the phosphorylation of the protein, which in turn is driving its aggregation or if aggregation of the protein occurred due to binding of pre-existing phosphorylated protein. It has been shown that overexpression of αsyn within SH-SY5Y cells is sufficient to induce aggregation of the protein, and these aggregates were not found to be phosphorylated at S129 (Kondo *et al.*, 2011). Hence phosphorylation is not a prerequisite for intracellular aggregation.

Given that αsyn is intrinsically phosphorylated in the cytoplasm as seen in the control cells, the presence of copper could induce this version of protein to readily aggregate into the observed inclusions. It is also that the increased copper binding affinity of S129 phosphorylated αsyn has an influence on intracellular aggregation. If the S129 phosphorylated αsyn is binding the copper more readily than WT within the cells, this could be why a higher number of phosphorylated aggregates are observed. If the copper binds more readily, triggering aggregation into phosphorylated aggregates, lower levels of copper may be available for the unmodified αsyn to bind, therefore it would form less aggregates.

Further investigation will however be required to fully determine the role of phosphorylation in metal-induced aggregation, and whether the two are dependent on one another. Such experiments could include the prevention of

phosphorylation by knockdown of key kinases or removal of the phosphorylation site by CRISPR. Results presented here however do suggest that phosphorylated -syn is more likely to be associated with aggregates upon exposure to copper ions, and aggregated -syn appears more likely to be phosphorylated than the non-aggregated forms.

In order to investigate whether the copper induced aggregation of -syn could be prevented in this cellular model, cells were co-incubated with 300¾M $CuCl_2$, which was demonstrated to induce a significantly high number of aggregates, along with a selection of increasing curcumin concentrations. No difference however in the percentage of cells containing distinct aggregates in the presence or absence of curcumin was observed, suggesting that, in this cellular model, curcumin is unable to prevent the copper-induced aggregation of the protein.

Previous studies utilizing SH-SY5Y models demonstrated the ability of curcumin to reduce the toxicity of pre-formed oligomers which were added to the cells, in line with the MS data in chapter 4. Treatment with oligomers alone resulted in a reduction in cell viability to just 60%, whereas co-incubation with oligomers and curcumin increased the viability to 80% (Singh *et al.*, 2013). Another study showed incubation with curcumin reduced the toxic effects of ROS damage, induced by addition of extracellular -syn and increased cell viability (Wang *et al.*, 2010), and a third similar study showed novel curcumin analogues could increase cell viability compared to cells treated with -syn alone (J ha *et al.*, 2016).

It is possible that the aggregation enhancing effects of copper are overriding the inhibitory effect of curcumin on the oligomers by causing a shift to the aggregation prone compact state and increasing the rate of assembly. If the aggregates produced are the unique copper induced oligomers previously described (Wright *et al.*, 2009), this suggests they are too intrinsically stable to be dissociated. Copper is also known to have at least three binding sites on the T syn protein, and it is possible that this binding of copper masks the binding site for curcumin on these oligomers, either through conformational change, or by covering the binding epitope. Data in this thesis suggests dissociation of the lower order species is possible, but this may not be the case for the larger oligomers formed in the presence of copper. It is also plausible that the cell is breaking down the curcumin molecules, or they are not entering the cell in the first place. It is also feasible that the concentrations utilised in this study are not sufficient to influence aggregates formed within cells. Overall, data presented here indicates that curcumin cannot prevent the copper-induced aggregation of T syn.

5.5 Conclusions

As summarised in figure 5.16, results presented in this chapter demonstrate that exposure of SHSY5Y cells naturally expressing Tsyn to increasing concentrations of $CuCl_2$ induces intracellular aggregates of Tsyn, akin to the increase in *in vitro* aggregation observed in earlier ThT assays. The percentage of cells containing Tsyn aggregates is increased significantly upon exposure to increased copper concentrations, indicating there is a dose response to copper-induced aggregation.

Tsyn phosphorylated at S129 has been shown to aggregate faster *in vitro*, and results presented here indicate that the aggregates formed within SHSY5Y cells upon exposure to Cu(II) are also phosphorylated at this residue, and an increased number of phosphorylated aggregates were detected in comparison to phosphorylated. It is likely that these aggregates formed in the presence of copper are the copper-specific oligomers which have been suggested to be the toxic, disease-causing conformations (Wright *et al.*, 2009). Cell viability is also found to be decreased, and apoptosis increased with increasing concentrations of $CuCl_2$, indicating these higher concentrations have an increased apoptotic effect.

Despite being effective at preventing Tsyn aggregation in an *in vitro* assay, co-incubation of SHSY5Y cells with natural curcumin and 300¾M $CuCl_2$ does not appear to have any protective effect on either cell viability, or against the

formation of Cu(II)-induced aggregates, indicating that, in this model, curcumin is unable to prevent the copper-induced aggregation of αsyn.

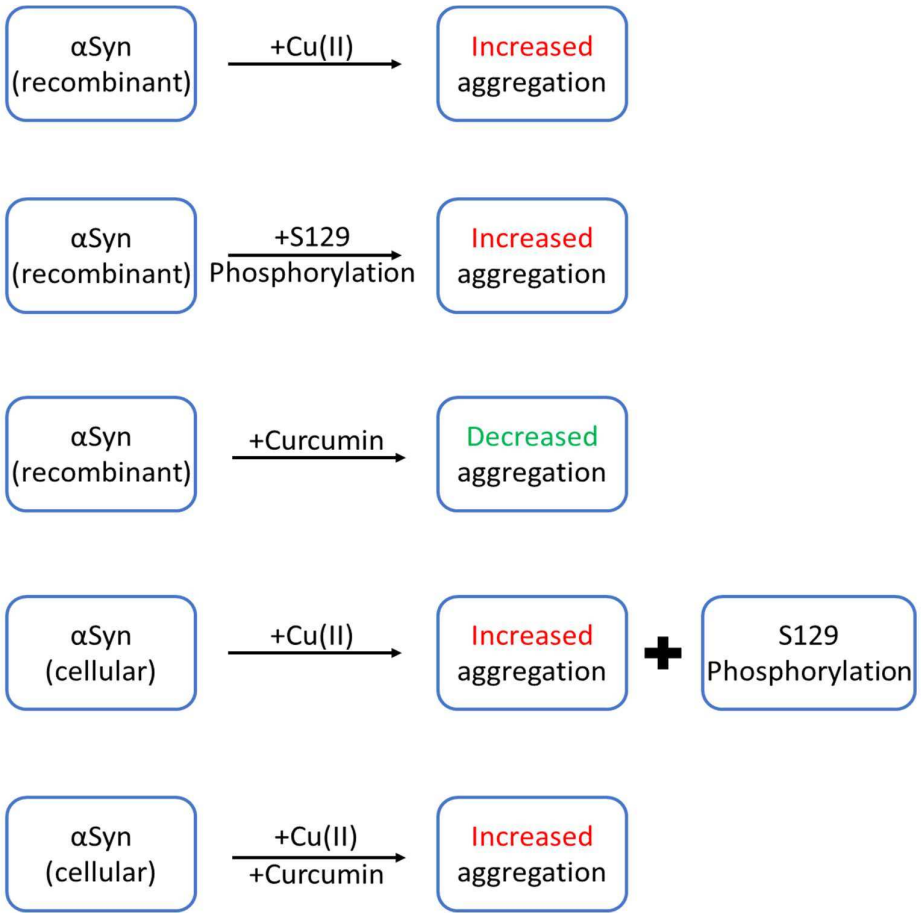

Figure 5.16: Summary of Chapter 5 Findings on the Interaction of Copper, Serine Phosphorylation and Curcumin in an SHSY5Y PD Model.

Both copper and S129 phosphorylation increase the aggregation rate of αsyn *in vitro*. Upon addition of copper to SHSY5Y cell media, an increase in αsyn aggregation and phosphorylation was observed. Curcumin has the ability to prevent the aggregation of αsyn *in vitro*. However, in this cell model, the addition of curcumin to SHSY5Y cells was unable to prevent the aggregation induced by the addition of Cu(II).

Chapter 6 – Final Discussion and Conclusions

The overall hypothesis of this thesis was that α-syn aggregation can be modulated by altering the population of the compact, aggregation prone conformational states present within its normal equilibrium, via processes such as post-translational modification or ligand binding. The aims were to determine the effects of post-translational modification on the metal binding characteristics of α-syn, to determine if aggregation could be inhibited via the use of small molecule inhibitors, specifically curcumin and its derivatives, and to examine the relationship between metal ions and the proteins phosphorylation state in a cellular model of PD.

ESI-IMS-MS was employed to investigate the changes in conformational distribution of α-syn. Chapter 3 presents data acquired relating to the alterations in conformation brought about by mutations mimicking serine phosphorylation, namely S87D and S129D α-syn, and changes in conformation of the three proteins in the presence of copper. In this case, the binding of copper increased the relative proportions of the compact state, and was correlated with an increase in aggregation as monitored by ThT assays. The key findings from this chapter can be viewed in figure 6.1, and will be discussed in sections 6.1 and 6.2. Chapter 4 presents data showing that curcumin derivatives bind to dimeric oligomers of α-syn, but not the monomeric protein. ThT assays were again utilised to demonstrate a reduction in aggregation propensity in the presence of curcumin

and a range of curcumin derivatives. The main findings of this chapter can be viewed in figure 6.3, and will be discussed in sections 6.4. Finally, chapter 5 demonstrated that exposure of a neuronal cell line to copper results in punctate aggregates of both unmodified and phosphorylated αsyn, but the formation of these aggregates could not be prevented by the presence of curcumin. The main findings will be discussed in sections 6.3 and 6.5, and a summary schematic can be viewed in figure 6.2.

IDPs such as αsyn are highly heterogeneous, and can have altered CSDs and conformational distributions between mass spectrometry acquisitions, which has been discussed in the literature (Beveridge *et al.*, 2015), and is evident from the wide range of CSDs and conformational distributions reported (Beveridge *et al.*, 2015; Mason *et al.*, 2016; Illes-Toth *et al.*, 2013; Kang *et al.* 2012). This variation in the data was addressed here by acquiring data sets within as short a time frame as possible to limit the environmental effects on the electrospray process, and utilising freshly made recombinant proteins. For the majority of experiments presented in this document, WT αsyn had a CSD of +18 to +5, well within the range of previously published data (Beveridge *et al.*, 2015; Mason *et al.*, 2016; Illes-Toth *et al.*, 2013; Kang *et al.* 2012), and had two distinct conformational groups evident from the spectra as a whole. The first an extended family spanning conformations +18 to +9 dominated by the +14 CSI, and a second, more compact family spanning conformations +8 to +5, dominated by the +7 CSI. This latter, more compact family is linked with aggregation, in keeping with other

published data (Beveridge *et* al., 2015; Kang *et* al., 2012; Illes-Toth *et al.*, 2013; Mason *et al.*, 2016).

6.1 Insights into the Effect of Phosphorylation on the Conformational Distribution and Aggregation of Tsyn

Results presented in chapter 3 demonstrated that WT Tsyn occupies eight distinct sub-conformations present within the expanded and collapsed conformations, ranging in size from 1303.7 ð² to 3185.5 ð², and these conformations are present in varying proportions throughout multiple CSIs. The Gaussian fitting technique was used, in keeping with recently reported publication (Mason *et al.*, 2016), to investigate the conformational changes brought about by mimicking serine phosphorylation. Substitution of serine residues for aspartic acid, creating protein variants, S87D and S129D, and the subsequent analysis reveals these variants occupy the same eight conformational families as the WT protein, in a similar conformational equilibrium. S129D Tsyn appeared to have a wider CSD overall, though this is possibly an artefact of acquisition. ESI-IMS-MS has recently been discovered to over-exaggerate the conformational dynamics of true solution proteins, causing compaction of IDPs or their subunits (Borysik *et al.*, 2015; Pagel *et al.*, 2013), and altered CSDs have been observed between protein solutions acquired at different times on the same day (Beveridge *et al.*, 2015), therefore care must be taken to not over interpret this data. No significant

alterations to the CCS of the eight conformations are observed between protein variants however, suggesting they have the same conformational distribution overall, and mimicking phosphorylation did not alter the protein significantly.

This data suggests the three proteins should have the same aggregation propensity, as they contained almost identical proportions of the most compact and amyloidogenic states. This was however, not the case. ThT studies determined that S87D τsyn has a slower aggregation rate overall than WT τsyn with an increase in $t_{1/2}$ of aggregation, and an increase in lag time was observed. In contrast, S129D τsyn had a decreased $t_{1/2}$ in comparison to WT τsyn, and a reduction in lag phase was observed. This is in keeping with previously reported findings utilising C-terminal fragments of τsyn phosphorylated at S129, and a phosphomimic S129E, which also showed an increased aggregation propensity (Lu *et al.*, 2011; NΔbling *et al.*, 2014). It is important to note however, that phosphomimics may behave differently to truly phosphorylated τsyn (Oueslati, 2016), and there is a large body of contradictory data already available utilising both phosphomimics and phosphorylated τsyn (Oueslati *et al.*, 2012; Paleologou *et al.*, 2008), therefore it is recommended these experiments are repeated with phosphorylated protein before any definitive conclusions are drawn on the implications of serine phosphorylation on τsyn aggregation in PD.

Data presented in this thesis however suggests that S129D τsyn is more amyloidogenic than WT τsyn, and its S87D counterpart. This lends support to

the hypothesis that αsyn phosphorylated at S129 is pathologically relevant in PD, whereas S87 phosphorylation is not, and could possibly be protective (Oueslati *et al.*, 2012). As the conformational distribution and CCS表 of the two phosphomimic proteins were relatively unchanged in comparison to WT αsyn, this indicates there is another reason mimicking phosphorylation is increasing aggregation rates, other than by increasing the population of the more compact conformational species. This limited change in the relative proportion of the compact state could indicate that this increase in aggregation is determined by the assembly of higher order oligomers, rather than the conformational state of the monomer.

6.2 Insights into the Effect of Phosphorylation on the Interaction of αSyn with Metal Ions

Metals are known to be involved in PD, and have been shown to increase the rate of αsyn aggregation *in vitro.* In chapter 3, ESI-IMS-MS was used to determine the effect of metal binding on the conformation of αsyn. Only the binding of copper to WT αsyn and its phosphomimic variants could be observed with ESI-IMS-MS and the binding of other metals investigated was not seen under the experimental conditions attempted. This is potentially due to dissociation of the metal ligands, due to their low binding affinity, either during the electrospray process or in the interior of the mass spectrometer. It is also possible that

interference from buffer components has prevented binding of the other metals being observed.

Nevertheless, the effect of copper binding on αsyn was determined. Upon addition of equimolar copper to the samples of all three αsyn variants, peaks corresponding to the bound proteins were easily observable. This accompanied the appearance of a novel, more extended CSI within the mass spectra for all three proteins, widening the CSD of WT and S87D αsyn from +18 to +5, to +19 to +5, and the CSD of S129D αsyn from +17 to +5 to +18 to +5.

This widening of the CSD is also accompanied by alterations to the proteins conformational distribution. At CSIs +11 to +5, for all three αsyn variants investigated, an increase in the more compact conformations at each CSI is observed upon the binding of one or two copper ions, with increases in conformations D, E, F, G and H observed. This is in agreement with previously published findings for the WT protein (Mason *et al.*, 2016), and demonstrates that the binding of copper ions to the lower CSIs representing more compact protein structures, causes an increase in the more compact, amyloidogenic conformations. As these conformations are more compact, they would be expected to have a higher propensity for aggregation, increasing the risk of PD (Bernstein *et al.*, 2004; Illes-Toth *et al.*, 2015; Mason *et al.*, 2016). As this is true for all protein variants, and there is little notable difference between the conformational distributions of the three, it suggests that mimicking

phosphorylation at S87 or S129 has little effect on the individual conformational states observed upon copper binding, and suggests copper binding to the variants occurs in the same manner as for the WT protein.

Aggregation rates of the three -Tsyn variants in the presence of copper and iron were investigated using ThT assays, which demonstrated that the incubation of equimolar $CuCl_2$ with all three protein variants, resulted in a statistically significant ($p<0.05$) increase in the rate of aggregation, determined via $t_{1/2}$ and L_e values. This indicates that the conformational changes in favour of more compact species observed upon copper binding, is causing an increase in the aggregation rates of all three proteins.

All three variants display a shift towards the more compact states upon copper binding, resulting in increased aggregation rates over the apo values. The variants did however show differences in their affinities for copper binding. S87D -Tsyn had the lowest binding affinity overall, binding just two copper ions to the compact CSIs at a 10 and 20¾M copper concentration whereas WT and S129D readily bound three. At higher concentrations of 50¾M $CuCl_2$, S129D was able to bind up to 4 copper ions, with the majority of the protein within the sample now being bound to two copper ions. WT and S87D bound three copper ions at this concentration, with most of the proteins bound to one. At a 100¾M concentration, all four proteins bound four copper ions, but the majority of S129D within the sample was now bound to three ions. S87D and WT predominantly bound to two

ions at this concentration. This indicates that mimicking phosphorylation at S129 results in a higher binding affinity over WT and S87D. Some studies have concluded that phosphorylation overall resulted in a lower binding affinity for copper (Oueslati *et al.*, 2012), whilst others indicated an increased binding affinity (Lu *et al.*, 2011), though these studies utilised C-terminal fragments rather than the whole protein. The data demonstrates that S129D α-syn has a higher affinity for copper ions than the WT version of the protein. This may help to explain why in intracellular inclusions and *ex vivo* LB material, the protein is both phosphorylated and rich in metal ions.

It was also noted in these investigations that only the binding of the first copper ion, to either protein variant, caused a significant alteration to the proteins conformation, as assessed by Gaussian fitting. It has been previously suggested that the H50 copper binding site is the initial, high affinity site, and it has also been demonstrated that Cu(II) binding to this domain causes a significant alteration to the conformation, via the introduction of a P-hairpin turn at this residue (Rose *et al.*, 2011).

Due to the significant alteration observed upon the binding of the first copper ion, but not subsequent ions, this supports the hypothesis that this is the residue is where the copper ions are initially binding, and it is this modification that results in the conformational changes required to alter the equilibrium and trigger increased aggregation, rather than the binding to other residues.

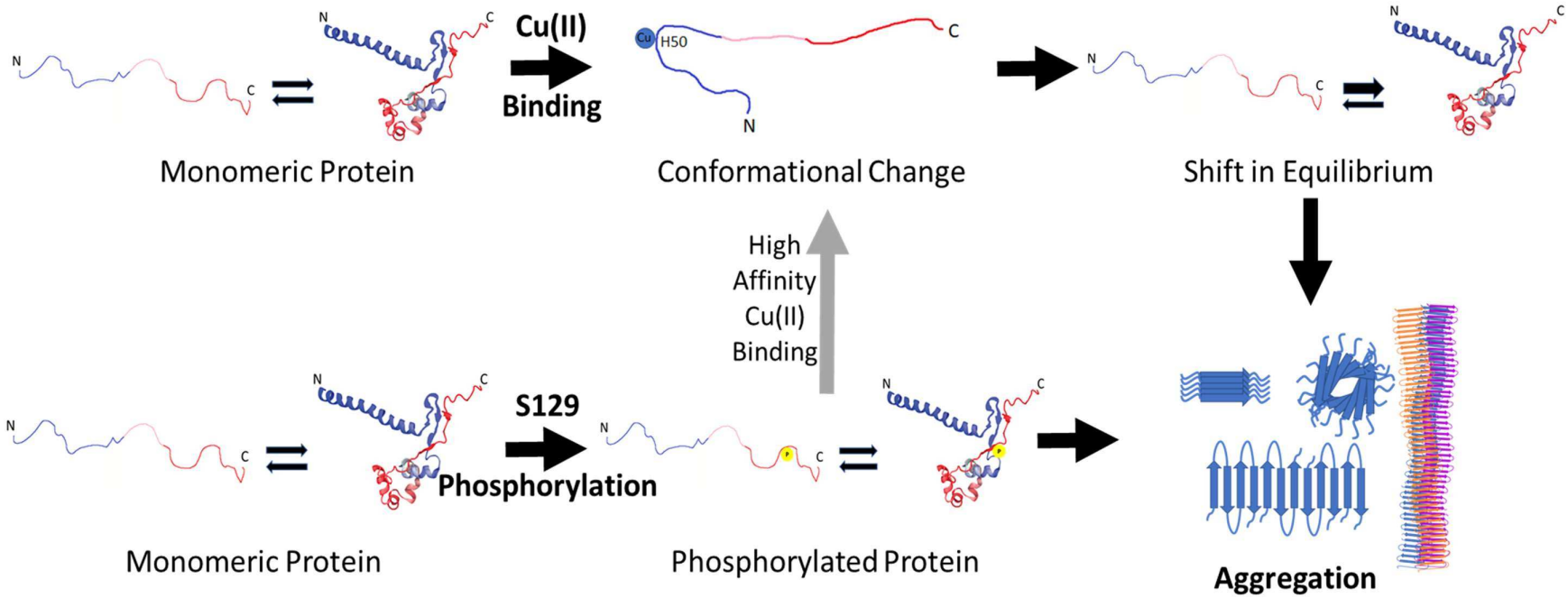

Figure 6.1: Effect of Cu(II)-binding and Phosphorylation on fDyn Aggregation.
The two proposed mechanisms by which Cu(II) and S129 phosphorylation increase the aggregation rate of fDyn *in vitro*. Top: The binding of Cu(II) causes a conformational change, shifting the equilibrium towards the more compact states, inducing increased aggregation. Bottom: S129 phosphorylation does not alter the conformation of the protein, or cause a shift towards the compact states, however aggregation is again accelerated, suggesting an alternative mechanism or pathway to that induced by the binding of Cu(II). The two pathways are potentially linked, as indicated with the grey arrow, via the high affinity Cu(II) binding site at H50, as S129D fDyn has a higher affinity for Cu(II) binding.

6.3 Insights into the Effect of Metal Ions on Intracellular Aggregation and Phosphorylation of αSyn

Data presented within chapter 5 demonstrates that incubation of SH-SY5Y cells with copper for 48 hours causes a significant ($p<0.01$-0.0001) increase in the number of cells containing intracellular aggregates of WT αsyn. This number also further increases ($p<0.01$) with increasing copper concentration, indicating a dose response to treatment with this metal. This increase in aggregates also coincided with an increase in fluorescence intensity within the cells ($p<0.05$), suggesting an increase in overall αsyn expression levels, upon incubation with either 300 or 500μM $CuCl_2$. It has previously been suggested that copper is a requirement for intracellular aggregation. When intrinsic levels of the metal are reduced via use of a chelex compound, intracellular aggregation was greatly reduced. This loss of aggregation propensity could be both recovered, and increased in untreated cells via further copper addition (Wang *et al.*, 2010).

Incubation with copper also resulted in an increase ($p<0.01$) in the percentage of cells containing one or more signs of apoptosis, as determined by DAPI staining, and a decrease in cell viability as determined by trypan blue staining, which again increased significantly with increased copper concentration ($p<0.01$). This is in keeping with previously published reports that incubation with copper reduces viability to 50% (Arciello *et al.*, 2005; Wang *et al.,* 2010).

Interestingly, not all cells containing high numbers of aggregates were apoptotic, which suggests it is not the aggregate load causing an increase in toxicity within these cells, but potentially another action of copper. One possibility could be increased oxidative pressure, or increased production of ROS, and -syn is known to hold some ferrireductase activity, utilising copper bound to the protein in the process, which would lead to an increased formation of ROS such as hydroxyl free radicals, and is a potential mechanism of action here.

Data presented in chapter 5 also demonstrated that the majority cells in the presence of copper contain aggregates which are phosphorylated at S129. This suggests addition of copper appears to promote the formation of phosphorylated aggregates, and this may well be linked to the higher affinity for copper of phosphorylated -syn. A low level of S129 phosphorylated -syn is present within the cells intrinsically, and this pool of protein may preferentially bind the copper due to its higher binding affinity, resulted in the observed aggregates, and it is known once bound to copper the protein has a higher propensity for aggregation. It is still unclear as to whether the addition of copper is causing an increase phosphorylated -syn within the cells, and whether this aids in driving the increased formation of aggregates observed.

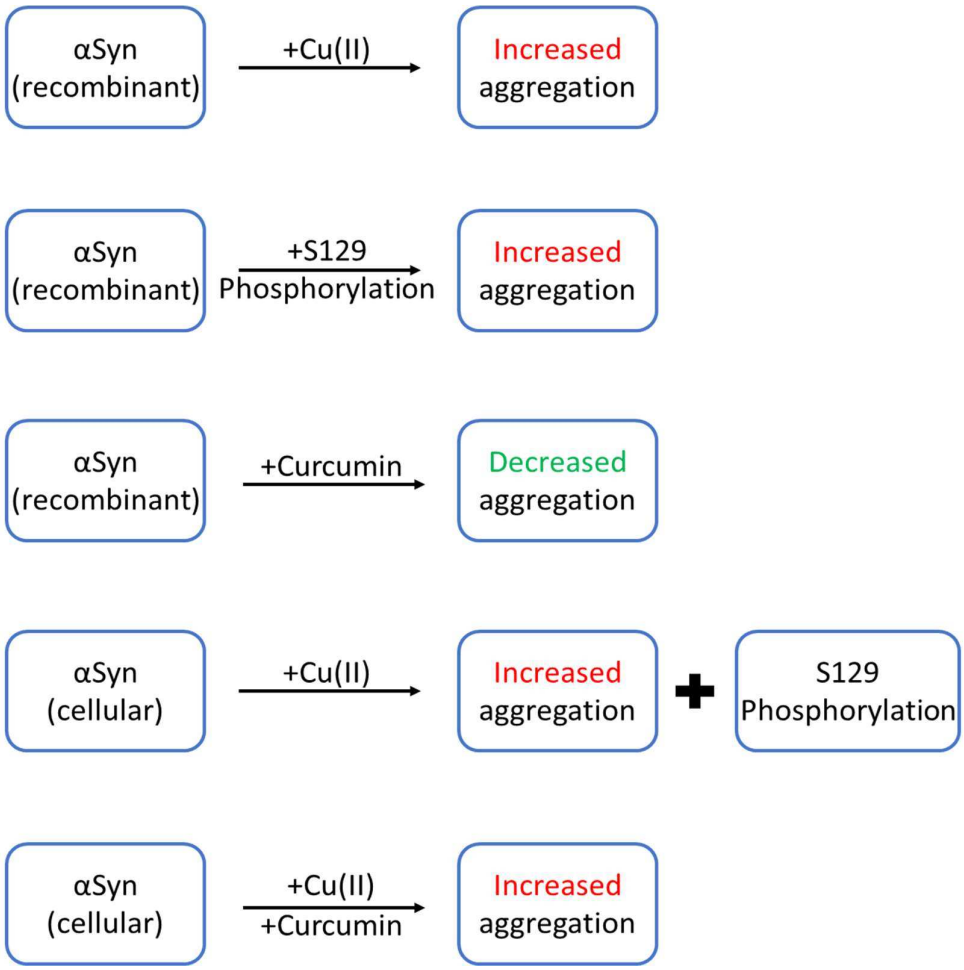

Figure 6.2: Summary of the Interaction Between Cu(II), Serine Phosphorylation and Curcumin in an SHSY5Y Model of PD.

Chapter 4 demonstrates that both copper and S129 phosphorylation increase the aggregation rate of αsyn *in vitro*. In chapter 5, upon addition of copper to SHSY5Y cell media, an increase in both αsyn aggregation and phosphorylation was observed. Curcumin was shown in chapter 4 to prevent the aggregation of αsyn *in vitro*. However, in chapter 5, in this SHSY5Y cell model, the addition of curcumin to SHSY5Y cells was unable to prevent the aggregation induced by the addition of Cu(II).

6.4 Insights into the Interaction of WT αSyn Monomers and Oligomers with the Polyphenolic Compound Curcumin and a Variety of Curcumin Analogues

One potential therapeutic strategy for the treatment of PD is the prevention of aggregation of αsyn via the use of small molecule inhibitors. The polyphenolic compound, curcumin, has previously been demonstrated to reduce the aggregation of WT αsyn *in vitro* (Pandey *et al.*, 2008; Singh *et al.*, 2013; Yanagisawa *et al.*, 2015). To determine whether the compound, which has poor bioavailability in its natural form, could be improved upon in terms of its anti-amyloid propensity, ESI-IMS-MS experiments and ThT assays were performed, utilising a selection of curcumin derivatives.

ThT assays demonstrated that natural curcumin significantly ($p<0.0001$) reduced the formation of amyloid aggregates to around 23% of the total found in the WT αsyn alone sample, in keeping with previous studies (Wang *et al.*, 2010; Jha *et al.*, 2016; Ahsan *et al.*, 2015; Pandey *et al.*, 2008; Singh *et al.*, 2013; Yanagisawa *et al.*, 2015). The majority of derivatives significantly reduced the fluorescence signal of the samples compared to the protein alone ($p<0.05$ 唖$p<0.0001$), with derivatives 5 and 7 almost inhibiting aggregation entirely, whereas derivative 4 caused a significant increase in fluorescence signal ($p<0.05$), and derivative 6 caused no significant alterations to fluorescence either way. Derivatives 5 and 7 were both found to be significantly ($p<0.0001$) more effective than natural

curcumin. Both these derivatives share a phenolic group at position-3 on the native aromatic ring, that appears to be of importance, indicating that modifications of the molecule could provide a good candidate for novel therapies for PD.

The derivatives were also investigated for their anti-amyloid properties against another amyloidogenic protein, lysozyme, whose aggregation can also be reduced by the presence of natural curcumin. The derivatives followed a similar but not identical pattern of inhibition to with T-syn, however derivatives 5 and 7 were again the most effective ($p<0.001$ and $p<0.0001$, respectively). This indicates that not all derivatives of curcumin will be suitable in either preventing or treating amyloid aggregation, so specific functional groups on the molecule must be key to this interaction with the different amyloid proteins, therefore careful design of the molecules is needed to create successful potential drugs for different amyloidosis.

To investigate the anti-amyloid mechanism of curcumin and derivatives 5 and 7, a number of ESI-IMS-MS experiments were performed. Neither the natural molecule nor the two derivatives were observed to bind the monomeric protein, even after extended incubation times. After this extended incubation however, it was observed that the presence of natural curcumin or derivative 5 or 7 prevented the autoproteolytic fragmentation observed in the untreated sample after 48hours. Fragmentation of T-syn has previously been identified as an important

step in aggregation (Vlad *et al.*, 2011), therefore the prevention of this auto fragmentation could be one of the mechanisms by which curcumins exert their anti-aggregation properties on αsyn.

Currently published literature is contradictory, and reports have been published claiming both curcumin binds to the monomeric species of αsyn (Ahmad and Lapidus, 2012), and stating it only binds to oligomeric forms of the protein (Singh *et al.*, 2013). ESI-IMS-MS data presented here strongly suggests that curcumins could not bind the monomer, whereas binding was observed only to low order oligomeric forms, such as dimeric species, supporting the work of Singh and colleagues.

ESI-IMS-MS also indicated that curcumin and derivatives 5 and 7 could not only bind to these dimers, but dissociate dimers pre-formed within the sample, as observed via a reduction in intensity within drift scope mobilograms. This dissociation was not observed with another curcumin derivative, number 11, which had a lower anti-aggregation propensity. The control demonstrates that the loss in signal intensity is not a result of the presence of the small molecule effecting the ionisation process, and is specific to the interactions between αsyn and the curcumin molecules.

It was also demonstrated via ESI-IMS-MS that curcumin could not bind to αsyn with the NAC region deleted, however this is most likely due to the inability of this αsyn variant to dimerise. It also supports previous reports of this region encoding

being curcumins binding motif (Ahmad and Lapidus, 2012). It has been suggested that curcumin binds to the NAC region and increases the reconfiguration rate of Tsyn as a mechanism. It is possible the NAC region becomes more exposed upon oligomer formation, allowing the binding of curcumin, where this region may be more shielded in monomeric forms of the protein (Wong and Krainc, 2017). It is therefore possible that oligomer formation exposes the NAC region, allowing the curcumins to bind to the protein, leading to dissociation of the oligomers into monomeric species, which have a reduced fragmentation rate and therefore a reduced rate of aggregation.

6.5 Insights into the Effect of Curcumin on Metal Ion-Induced Intracellular Aggregation of TSyn

When SH-SY5Y cells were co-incubated with $CuCl_2$ and natural curcumin, no reduction in aggregate formation in comparison to cells incubated with $CuCl_2$ alone was observed, suggesting curcumin had no effect on copper-induced aggregate formation. Previous studies have demonstrated an increase in cellular viability upon incubation with curcumins (Singh *et al.*, 2013; Jha *et al.*, 2016), but there is no previous data available on the incubation of cells with metals and curcumins. It is likely that the effect of copper binding is too stable to be overridden by curcumin, especially as it has a much weaker binding affinity for Tsyn than copper ions, as previously demonstrated here. It is also possible that

the oligomeric species formed within the cells upon copper exposure are too highly ordered for the curcumin to interact with and dissociate, as the proposed binding site within the NAC region may be shielded. It appears that the intracellular aggregation brought about by the presence of copper cannot be inhibited by curcumin or its derivatives.

6.6 Final Conclusions

In summary, this thesis has demonstrated that the conformational state of α-syn can be modulated by small molecule interactions. Molecules that increase the population of the compact states, such as copper ions, increase the rate of aggregation, and molecules such as curcumin which disrupt oligomeric assembly, prevent this aggregation. Modification of the protein by phosphorylation, mimicked here with the exchange of serine for aspartic acid, resulted in increased rates of aggregation in vitro, an effect which was further enhanced by the presence of copper. In cell culture, copper induces the formation of phosphorylated, intracellular aggregates, but this could not be prevented by curcumin. These observations support the idea that phosphorylation of α-syn at S129 has a direct role to play in PD, and that this role can be modulated by exposure to copper. An overall summary figure of the thesis findings can be seen in figure 6.3.

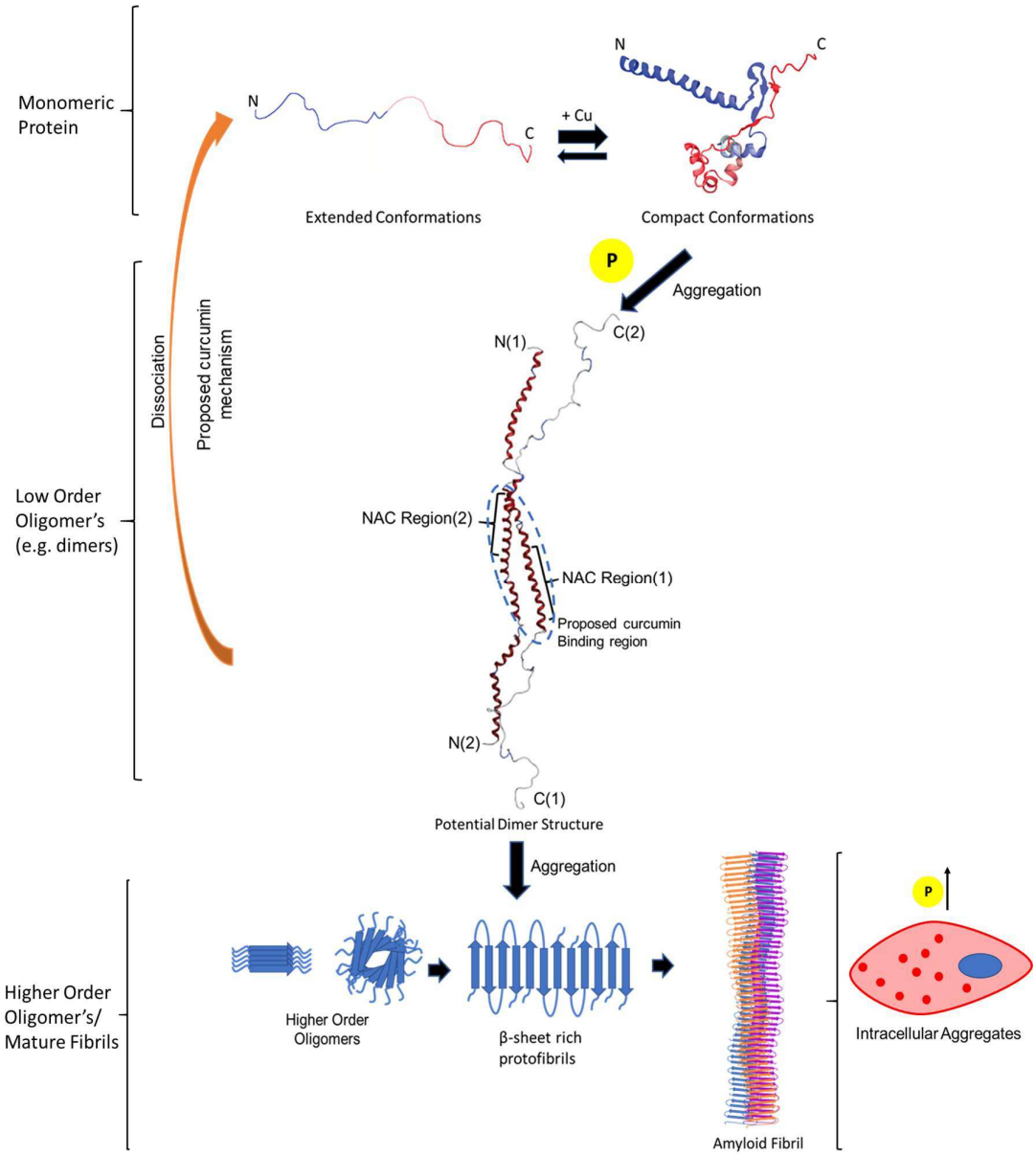

Figure 6.2: Overall Summary of Main Thesis Findings.
Copper binding, particularly at the HSD binding domain, pushes the conformational equilibrium of Tau towards the compact conformations, increasing its aggregation. Phosphorylation at S129 also increases Tau aggregation, through an unknown pathway. Copper induces formation of Tau aggregates within an SHSY5Y PD cell model, which are also phosphorylated at S129. Curcumin is proposed to bind to disordered Tau, within the NAC region, and prevent this aggregation. However, curcumin is unsuccessful at preventing copper-induced aggregate formation within the SHSY5Y cell model.

Chapter 7 – Future Work

7.1 Phosphorylation and Metal Interactions

7.1.1 Phosphorylation of α-Syn

As phosphorylation of WT α-syn was not successfully completed within this project, it is now important to conduct the same experiments utilising protein which has been successfully phosphorylated, to both determine differences between actual phosphorylated protein and the phosphomimics, which are still regularly utilised in research due to their ease of production in comparison.

7.1.2 Phosphorylation and Metal Interactions of *Ex Vivo* α-Syn

It would be also very interesting to examine *ex vivo* α-syn from PD patients via ESI-IMS-MS and investigate both the phosphorylation state of the protein and its conformational distribution. For example, α-syn from the cerebrospinal fluid of PD patients could be purified via affinity precipitation, and LC-MS before investigation via ESI-IMS-MS to determine any metal binding, conformational changes upon metal binding, or in comparison to recombinant proteins, or to investigate whether *ex vivo* material has any further propensity to bind metals or aggregate *in vitro.*

7.2 Interactions of αSyn and Curcumin

7.2.1 Confirmation of Anti-Aggregation Propensity

As the ThT assay is susceptible to interference from other fluorescent sources, such as the curcumin molecules investigated, it is important to investigate their effect on aggregation of αsyn via another, non-fluorescent technique before this data is ready for publication. Incubation with the curcumin derivatives followed by imaging via electron microscopy to visualise the aggregates formed is a viable alternative to investigate their effects, without the potential for bias caused by their intrinsic fluorescence.

7.2.2 Increased Bioavailability of Curcumin Molecules

Though curcumin appears to be a viable candidate for PD therapy, due to results presented in this investigation and elsewhere, the problem with its bioavailability must be overcome before curcumin can progress to clinical trials in humans.

Synthesising alternative curcumin derivatives based on insights from this study and others will provide a good basis to begin designing novel curcumin molecules with increased bioavailability and increase anti-aggregation propensities, for PD and other amyloid diseases.

7.2.3 Further Investigations into the Prevention of Copper-Induced Aggregation by Curcumins

The relationship between copper-induced aggregation and whether curcumin could be utilised to prevent this aggregation also warrants further investigation. A ThT assay containing both copper and curcumins would give further insight into whether copper-induced aggregation could be prevented by this molecule or one of its derivatives. ESI-IMS-MS was attempted utilising both copper and curcumin, and early experiments indicated that curcumin did not prevent the copper-induced conformational changes observed with the compact conformations of the protein. This was not repeated enough or with a large enough variety of copper and curcumin concentrations to draw definitive conclusions, therefore should be further examined.

7.3 Cellular Responses to Metal Ions and Curcumin

7.3.1 Confirmation of Phosphorylation State

Due to the unexpected results obtained when using the antibody specific to T-syn which has undergone phosphorylation at serine-129, an alternative method of investigation should be employed. It is possible the antibody was binding to another protein within the cells, which could be why there was an increase in

inclusions, for example stress bodies look extremely similar, as do aggregates of the transcription protein EIF2$_T$, so this exclusivity cannot be fully confirmed.

7.3.2 Further Investigation into Curcumins Effect on Metal Induced Aggregates

In vitro ESI-IMS-MS results and aggregation studies suggested curcumin should be protective against the formation of intracellular aggregates. This however was not the case in cellular investigations conducted here. It is possible the curcumin was not taken up by the cells in the first place, so this requires further optimisation and investigation before definitive conclusions can be drawn. It would also be interesting to examine the effects of copper and curcumin on cells stained with the phos129 antibody, to determine if there are any effects on the phosphorylated aggregates.

References

Ahmad, A. *et al.* (2012) 'Peculiarities of copper binding to alpha-synuclein.', *Journal of biomolecular structure & dynamics*, 29(4), pp. 825–42.

Ahmad, B. and Lapidus, L. J. (2012) 'Curcumin prevents aggregation in α-synuclein by increasing reconfiguration rate', *Journal of Biological Chemistry*, 287(12), pp. 9193–199.

Ahsan, N. *et al.* (2015) 'Curcumin Pyrazole and its derivative (N-(3-Nitrophenylpyrazole) Curcumin inhibit aggregation, disrupt fibrils and modulate toxicity of Wild type and Mutant γ-Synuclein', *Scientific Reports*, 5(1), p. 9862.

Al-Baghdadi, O. B. *et al.* (2012) 'Inhibition of monoamine oxidase by derivatives of piperine, an alkaloid from the pepper plant Piper nigrum, for possible use in Parkinson's disease', *Bioorganic and Medicinal Chemistry Letters*, 22(23), pp. 7183–188.

Al-Chalabi, A. *et al.* (2009) 'Genetic variants of the alpha-synuclein gene SNCA are associated with multiple system atrophy.', *PloS one*, 4(9), p. e7114.

Allegra A, Innao V, Russo S, Gerace D, Alonci A, M. C. (2017) 'Anticancer Activity of Curcumin and Its Analogues: Preclinical and Clinical Studies', *Cancer Investigation*, 35(1), pp. 1–2.

Anderson, J. P. *et al.* (2006) 'Phosphorylation of Ser-129 is the dominant pathological modification of γ-synuclein in familial and sporadic lewy body disease', *Journal of Biological Chemistry*, 281(40), pp. 29739–9752.

Arakawa, T., Kita, Y. and Timasheff, S. N. (2007) 'Protein precipitation and

denaturation by dimethyl sulfoxide〔*Biophysical Chemistry*, 131(1–3), pp. 62–70.

Arciello, M., Rotilio, G. and Rossi, L. (2005) 'Copper-dependent toxicity in SH-SY5Y neuroblastoma cells involves mitochondrial damage〔*Biochemical and Biophysical Research Communications*, 327(2), pp. 454–459.

Babu, M. M. *et al.* (2011) 'Intrinsically disordered proteins: Regulation and disease〔*Current Opinion in Structural Biology*, pp. 432–440.

Baksi, S., Tripathi, A. K. and Singh, N. (2016) 'Alpha-synuclein modulates retinal iron homeostasis by facilitating the uptake of transferrin-bound iron: Implications for visual manifestations of Parkinson〔s disease〔*Free Radical Biology and Medicine*, 97, pp. 292–306.

Barrett, P. J. and Timothy Greenamyre, J. (2015) 'Post-translational modification of〔-synuclein in Parkinson〔disease〔*Brain Research*, 1628, pp. 247–253.

Baum, L *et al.* (2008) 'Six-month randomized, placebo-controlled, double-blind, pilot clinical trial of curcumin in patients with Alzheimer disease〔*Journal of Clinical Psychopharmacology*, 28(1), pp. 110–113.

Bernstein, S. L. *et al.* (2004) 'Synuclein: Stable compact and extended monomeric structures and pH dependence of dimer formation〔*Journal of the American Society for Mass Spectrometry*, pp. 1435–1443.

Beveridge, R. *et al.* (2013) 'Mass spectrometry methods for intrinsically disordered proteins〔*The Analyst*, 138(1), pp. 32–42.

Beveridge, R. *et al.* (2015) 'Relating gas phase to solution conformations: Lessons from disordered proteins〔*Proteomics*, 15(16), pp. 2872–2883.

Biedler, J. L. *et al.* (1978) 嗖ultiple neurotransmitter synthesis by human neuroblastoma cell lines and clones.悲*Cancer research*, 38(11 Pt 1), pp. 3751唖.

Binolfi, A. *et al.* (2006) 嗖teraction of ┳-synuclein with divalent metal ions reveals key differences: A link between structure, binding specificity and fibrillation enhancement悲*Journal of the American Chemical Society*, 128(30), pp. 9893唖9901.

Binolfi, A. *et al.* (2008) 嗖ite-specific interactions of Cu(Ⅱ) with沓and沓synuclein: Bridging the molecular gap between metal binding and aggregation悲*Journal of the American Chemical Society*, 130(35), pp. 11801唖1812.

Binolfi, A. *et al.* (2010) 嗖ioinorganic chemistry of Parkinson悲disease: Structural determinants for the copper-mediated amyloid formation of alpha-synuclein悲*Inorganic Chemistry*, 49(22), pp. 10668唖0679.

Binolfi, A. *et al.* (2012) 嗖ioinorganic chemistry of copper coordination to alpha-synuclein: Relevance to Parkinson悲disease悲*Coordination Chemistry Reviews*, pp. 2188唖201.

Boesl, U. (2017) 嗖ime-of-flight mass spectrometry: Introduction to the basics悲*Mass Spectrometry Reviews*, pp. 86唖09.

Bohrer *et al*. (2008) 'Biomolecule analysis by ion mobility spectrometry'. *Annu Rev Anal Chem*, 1, pp293-327.

Borana, M. S. *et al.* (2014) 嗖urcumin and kaempferol prevent lysozyme fibril formation by modulating aggregation kinetic parameters悲*Biochimica et Biophysica Acta - Proteins and Proteomics*, 1844(3), pp. 670唖80.

Borysik *et al.* (2015) 'Ensemble methods enable a new definition for the solution to gas-phase transfer of intrinsically disordered proteins'. *EMBO J,* 137(43), pp. 13807-17.

Brown, D. R. (2007) 'Interactions between metals and alpha-synuclein--function or artefact?' *The FEBS journal*, 274(15), pp. 3766-74.

Brown, D. R. (2009) 'Metal binding to alpha-synuclein peptides and its contribution to toxicity' *Biochemical and Biophysical Research Communications*, 380(2), pp. 377-81.

Burgess, A. *et al.* (2010) 'Loss of human Greatwall results in G2 arrest and multiple mitotic defects due to deregulation of the cyclin B-Cdc2/PP2A balance.' *Proceedings of the National Academy of Sciences of the United States of America*, 107(28), pp. 12564-.

Burrů, J. *et al.* (2010) 'Alpha-synuclein promotes SNARE-complex assembly in vivo and in vitro.' *Science (New York, N.Y.)*, 329(5999), pp. 1663-.

Burrů, J. *et al.* (2013) 'Properties of native brain α-synuclein' *Nature*, 498(7453), pp. E4-E6.

Cao, A., Hu, D. and Lai, L. (2004) 'Formation of amyloid fibrils from fully reduced hen egg white lysozyme.' *Protein science : a publication of the Protein Society*, 13(2), pp. 319-24.

Carboni, E. and Lingor, P. (2015) 'Insights on the interaction of alpha-synuclein and metals in the pathophysiology of Parkinson' disease.' *Metallomics : integrated biometal science*, 7(3), pp. 395-404.

Cardaci, S. *et al.* (2008) 嗖eactive oxygen species mediate p53 activation and apoptosis induced by sodium nitroprusside in SH-SY5Y cells.悪 *Molecular pharmacology*, pp. 1234嗤5.

Carroll, R. E. *et al.* (2011) 嗖hase IIa clinical trial of curcumin for the prevention of colorectal neoplasia悪*Cancer Prev Res.(Phila)*, 4(1940嗤215 (Electronic)), pp. 354嗤64.

Chandra, S. *et al.* (2004) 嗖ouble-knockout mice for alpha- and beta-synucleins: effect on synaptic functions.悪*Proceedings of the National Academy of Sciences of the United States of America*, 101(41), pp. 14966嗤1.

Chau, K. Y. *et al.* (2009) 嗖elationship between alpha synuclein phosphorylation, proteasomal inhibition and cell death: Relevance to Parkinson悪 disease pathogenesis悪*Journal of Neurochemistry*, 110(3), pp. 1005嗤013.

Chaudhuri, T. K. and Paul, S. (2006) 嗖rotein-misfolding diseases and chaperone-based therapeutic approaches悪*FEBS Journal*, pp. 1331嗤349.

Chen, L. *et al.* (2009) 嗖yrosine and serine phosphorylation of alpha-synuclein have opposing effects on neurotoxicity and soluble oligomer formation悪*Journal of Clinical Investigation*, 119(11), pp. 3257嗤265.

Chen, L. and Feany, M. B. (2005) 嗖lpha-synuclein phosphorylation controls neurotoxicity and inclusion formation in a Drosophila model of Parkinson disease.悪*Nature neuroscience*, 8(5), pp. 657嗤3.

Chen, P., Miah, M. R. and Aschner, M. (2016) 嗖etals and Neurodegeneration悪 *F1000Research*, 5 (no pagi(7431.1), pp. 1嗤2.

Colapinto, M. *et al.* (2006) 'α-Synuclein protects SH-SY5Y cells from dopamine toxicity', *Biochemical and Biophysical Research Communications*, 349(4), pp. 1294–300.

Coon, S. *et al.* (2006) 'Whole-body lifetime occupational lead exposure and risk of Parkinson's disease', *Environmental Health Perspectives*, 114(12), pp. 1872–1876.

Danzer, K. M. *et al.* (2007) 'Different species of α-synuclein oligomers induce calcium influx and seeding', *Journal of Neuroscience*, 27(34), pp. 9220–9232.

Danzer, K. M. *et al.* (2009) 'Seeding induced by α-synuclein oligomers provides evidence for spreading of α-synuclein pathology', *Journal of Neurochemistry*, 111(1), pp. 192–203.

Davies, P., Moualla, D. and Brown, D. R. (2011) 'Alpha-synuclein is a cellular ferrireductase', *PLoS ONE*, 6(1).

Dephoure, N. *et al.* (2013) 'Mapping and analysis of phosphorylation sites: a quick guide for cell biologists.', *Molecular biology of the cell*, 24(5), pp. 535–42.

Dexter, D. T. *et al.* (1989) 'Increased nigral iron content and alterations in other metal ions occurring in brain in Parkinson's disease.', *Journal of neurochemistry*, 52(6), pp. 1830–836.

Dissmeyer, N. and Schnittger, A. (2011) 'Use of phospho-site substitutions to analyze the biological relevance of phosphorylation events in regulatory networks', *Methods in Molecular Biology*, 779, pp. 93–38.

Donor, M. T. *et al.* (2017) 'Extended Protein Ions Are Formed by the Chain

Ejection Model in Chemical Supercharging Electrospray Ionization䀝*Analytical Chemistry*, 89(9), pp. 5107唀114.

Drew, S. C. *et al.* (2008) 唆u2+ binding modes of recombinant alpha-synuclein--insights from EPR spectroscopy.䀝*Journal of the American Chemical Society*, 130(24), pp. 7766唀3.

Duce, J. A. *et al.* (2017) 唆ost translational changes to ┳-synuclein control iron and dopamine trafficking; a concept for neuron vulnerability in Parkinson䀝 disease䀝*Molecular Neurodegeneration*. Molecular Neurodegeneration, 12(1), p. 45.

Ecroyd, H. and Carver, J. A. (2008) 唆nraveling the mysteries of protein folding and misfolding䀝*IUBMB Life*, pp. 769唀74.

Eichner, T. and Radford, S. E. (2011) 唆 Diversity of Assembly Mechanisms of a Generic Amyloid Fold䀝*Molecular Cell*, pp. 8唀8.

Eisenberg, D. and Jucker, M. (2012) 唆he amyloid state of proteins in human diseases䀝*Cell*, pp. 1188唀203.

El-Agnaf, O. M. A. *et al.* (1998) 唆ggregates from mutant and wild-type䁡-synuclein proteins and NAC peptide induce apoptotic cell death in human neuroblastoma cells by formation of䁢sheet and amyloid-like filaments䀝*FEBS Letters*, 440(1唀), pp. 71唀5.

El-Turk, F. *et al.* (2016) 唆tructural Effects of Two Camelid Nanobodies Directed to Distinct C-Terminal Epitopes on ┳-Synuclein䀝*Biochemistry*, 55(22), pp. 3116唀3122.

Elahi, F. M. and Miller, B. L. (2017) 唉 clinicopathological approach to the diagnosis of dementia悥*Nat Rev Neurol.*, 13(8), pp. 457-476.

Eriksen, J. L., Przedborski, S. and Petrucelli, L. (2005) 唉ene dosage and pathogenesis of Parkinson悥disease悥*Trends in Molecular Medicine*, pp. 91唖6.

Fauvet, B. *et al.* (2012) 唉-Synuclein in central nervous system and from erythrocytes, mammalian cells, and Escherichia coli exists predominantly as disordered monomer悥*Journal of Biological Chemistry*, 287(19), pp. 15345唖15364.

Ferreira, N., Saraiva, M. J. and Almeida, M. R. (2011) 唉atural polyphenols inhibit different steps of the process of transthyretin (TTR) amyloid fibril formation悥*FEBS Letters*, 585(15), pp. 2424唖430.

Festa, R. A. and Thiele, D. J. (2011) 唉opper: An essential metal in biology悥*Current Biology.*, 21(21), pp. 877-883.

Fitzpatrick, P. F. (1989) 唉he metal requirement of rat tyrosine hydroxylase悥*Biochemical and Biophysical Research Communications*, 161(1), pp. 211唖15.

Forman-Kay, J. D. and Mittag, T. (2013) 唉rom sequence and forces to structure, function, and evolution of intrinsically disordered proteins悥*Structure*, pp. 1492唖1499.

Fowler, D. M. *et al.* (2007) 唉unctional amyloid - from bacteria to humans悥*Trends in Biochemical Sciences*, pp. 217唖24.

Fraser, J. A. *et al.* (2014) 唉hosphomimetic mutation of the N-terminal lid of MDM2 enhances the polyubiquitination of p53 through stimulation of E2-ubiquitin

thioester hydrolysis㸧*Journal of Molecular Biology*., 427(8), pp. 1728㹼747.

Freichel, C. *et al.* (2007) 㹻ge-dependent cognitive decline and amygdala pathology in ㄱ-synuclein transgenic mice㸧*Neurobiology of Aging*, 28(9), pp. 1421㹼435.

Fujiwara, H. *et al.* (2002) 㹻-Synuclein is phosphorylated in synucleinopathy lesions㸧*Nature Cell Biology*, 4(2), pp. 160㹼64.

Garcia-Alloza, M. *et al.* (2007) 㹻urcumin labels amyloid pathology in vivo, disrupts existing plaques, and partially restores distorted neurites in an Alzheimer mouse model㸧*Journal of Neurochemistry*, 102(4), pp. 1095㹼104.

Gautam, S. *et al.* (2017) 㹻olyphenols in combination with ㄱ-cyclodextrin can inhibit and disaggregate ㄱ-synuclein amyloids under cell mimicking conditions: A promising therapeutic alternative㸧 *Biochimica et Biophysica Acta (BBA) - Proteins and Proteomics*., 1865(5), pp. 589-603.

Giasson, B. I. *et al.* (2001) 㹻 Hydrophobic Stretch of 12 Amino Acid Residues in the Middle of㸧-Synuclein Is Essential for Filament Assembly㸧*Journal of Biological Chemistry*, 276(4), pp. 2380㹼386.

Glabe, C. G. and Kayed, R. (2006) 㹻ommon structure and toxic function of amyloid oligomers implies a common mechanism of pathogenesis.㸧*Neurology*, 66(2 Suppl 1), pp. S74㹼78.

Glaser, C. B. *et al.* (2005) 㹼ethionine oxidation, ㄱ-synuclein and Parkinson㸧 disease㸧*Biochimica et Biophysica Acta - Proteins and Proteomics*, pp. 157㹼69.

Golts, N. *et al.* (2002) 㹼agnesium inhibits spontaneous and iron-induced

aggregation of ┳-synuclein㸹*Journal of Biological Chemistry*, 277(18), pp. 16116㹼16123.

Gorell, J. M. *et al.* (1999) 㸼ccupational metal exposures and the risk of Parkinson㸹disease㸹*Neuroepidemiology*, pp. 303㹼08.

Gorell, J. M. *et al.* (2004) 㸽ultiple risk factors for Parkinson㸹disease㸹*Journal of the Neurological Sciences*, 217(2), pp. 169㹼74.

Grabenauer, M. *et al.* (2008) 㸼permine binding to Parkinson㸹 protein ┳-synuclein and its disease-related A30P and A53T mutants㸹*Journal of Physical Chemistry B*, 112(35), pp. 11147㹼1154.

Gregersen, N. *et al.* (2006) 㸼rotein misfolding and human disease㸹*Annu Rev Genomics Hum Genet*, 7, pp. 103㹼24.

Guilliams, T. *et al.* (2013) 㸽anobodies raised against monomeric ┳-synuclein distinguish between fibrils at different maturation stages㸹*Journal of Molecular Biology*, 425(14), pp. 2397㹼411.

Hafner-Bratkovi3, I. *et al.* (2008) 㸼urcumin binds to the㧠-helical intermediate and to the amyloid form of prion protein - A new mechanism for the inhibition of PrPSc accumulation㸹*Journal of Neurochemistry*, 104(6), pp. 1553㹼564.

Hammer, N. D. *et al.* (2008) 㸼myloids: Friend or Foe?㸹*Journal of Alzheimer㸹 disease*㸻*JAD*, 13(4), pp. 407㹼19.

Hara, T. *et al.* (2006) 㸼ytokinesis regulator ECT2 changes its conformation through phosphorylation at Thr-341 in G2/M phase.㸹*Oncogene*, 25(4), pp. 566㹼578.

Hasegawa, T. *et al.* (2004) 嗖ccelerated alpha-synuclein aggregation after differentiation of SH-SY5Y neuroblastoma cells.悲*Brain research*, 1013(1), pp. 51唾.

Herva, M. E. *et al.* (2014) 嗖nti-amyloid Compounds Inhibit酗 -Synuclein Aggregation Induced by Protein Misfolding Cyclic Amplification (PMCA)悲*Journal of Biological Chemistry*, 289(17), pp. 11897唾1905.

Hirsch, E. C. *et al.* (1991) 嗖on and Aluminum Increase in the Substantia Nigra of Patients with Parkinson悲 Disease: An X-Ray Microanalysis悲 *Journal of Neurochemistry*, 56(2), pp. 446唾51.

Ho, C. S. *et al.* (2003) 嗖lectrospray Ionisation Mass Spectrometry: Principles and Clinical Applications悲*Clinical Biochemistry Reviews*, 24(March 2016), pp. 3唾2.

Hudson, S. A. *et al.* (2009) 嗖he thioflavin T fluorescence assay for amyloid fibril detection can be biased by the presence of exogenous compounds悲*FEBS Journal*, 276(20), pp. 5960唾972.

Illes-Toth, E. *et al.* (2015) 嗖istinct higher-order **T**-synuclein oligomers induce intracellular aggregation悲*Biochemical Journal*, 468(3), pp. 485唾93.

Illes-Toth, E., Dalton, C. F. and Smith, D. P. (2013) 嗖inding of dopamine to alpha-synuclein is mediated by specific conformational states悲*Journal of the American Society for Mass Spectrometry*, 24(9), pp. 1346唾354.

Jackson, M. and Mantsch, H. H. (1991) 嗖eware of proteins in DMSO悲*Biochimica et Biophysica Acta (BBA)/Protein Structure and Molecular*, 1078(2), pp. 231唾35.

Jahn, T. R. and Radford, S. E. (2008) 嗖olding versus aggregation: Polypeptide

conformations on competing pathways. *Archives of Biochemistry and Biophysics*, pp. 100–17.

Jaishankar *et al.* (2014) 'Toxicity, mechanism and health effects of some heavy metals'. *Interdisciplinary Toxicology,* 7(2), pp. 60-70.

Jankovic, J. (2008) "Parkinson's disease: clinical features and diagnosis." *JNNP*, 79(4), pp. 368–76.

Jenner, P. and Olanow, C. W. (1996) "Oxidative stress and the pathogenesis of Parkinson's disease." *Neurology*, 47(6 Suppl 3), pp. S161–70.

Jensen, P. H. *et al.* (1999) "α-synuclein binds to tau and stimulates the protein kinase A-catalyzed tau phosphorylation of serine residues 262 and 356." *Journal of Biological Chemistry*, 274(36), pp. 25481–5489.

Jha, N. N. *et al.* (2016) "Effect of curcumin analogs on α-synuclein aggregation and cytotoxicity." *Scientific Reports*, 6, p. 28511.

Ji, H.-F. and Shen, L. (2014) "The multiple pharmaceutical potential of curcumin in Parkinson's disease." *CNS & neurological disorders drug targets*, 13(2), pp. 369–73.

Jiang, T. *et al.* (2012) "Inhibitory effect of curcumin on the Al(III)-induced Aβ42 aggregation and neurotoxicity in vitro." *Biochimica et Biophysica Acta - Molecular Basis of Disease.*, 1822(8), pp. 1207–15.

Jovcevski, B. *et al.* (2015) "Phosphomimics destabilize Hsp27 oligomeric assemblies and enhance chaperone activity." *Chemistry and Biology*, 22(2), pp. 186–95.

Kang, L. *et al.* (2012) 唆-terminal acetylation of吝-synuclein induces increased transient helical propensity and decreased aggregation rates in the intrinsically disordered monomer志*Protein Science*, 21(7), pp. 911唾17.

Karpinar, D. P. *et al.* (2009) 唆re-fibrillar alpha-synuclein variants with impaired beta-structure increase neurotoxicity in Parkinson志disease models.志*The EMBO journal*, 28(20), pp. 3256唾268.

Keel, S. B. *et al.* (2008) 唆 heme export protein is required for red blood cell differentiation and iron homeostasis志*Science (New York, NY)*, 319(5864), pp. 825唾28.

Kim, D. S., Park, S. Y. and Kim, J. K. (2001) 唆urcuminoids from Curcuma longa L. (Zingiberaceae) that protect PC12 rat pheochromocytoma and normal human umbilical vein endothelial cells from betaA(1-42) insult.志*Neuroscience letters*, 303(1), pp. 57唾1.

Kim, W. S., Kūgedal, K. and Halliday, G. M. (2014) 唆lpha-synuclein biology in Lewy body diseases.志*Alzheimer志research & therapy*, 6(5), p. 73.

Knowles, T. P. J., Vendruscolo, M. and Dobson, C. M. (2014) 唆he amyloid state and its association with protein misfolding diseases.志*Nature reviews. Molecular cell biology*, 15(6), pp. 384唾6.

Kondo, K., Obitsu, S. and Teshima, R. (2011) 唆Synuclein aggregation and transmission are enhanced by leucine-rich repeat kinase 2 in human neuroblastoma SH-SY5Y cells.志*Biological & pharmaceutical bulletin*, 34(7), pp. 1078唾083.

Konermann, L. *et al.* (2013) 唳nraveling the mechanism of electrospray ionization壴*Analytical Chemistry*, 85(1), pp. 2唖.

Konno, T. *et al.* (2016) 唳utosomal dominant Parkinson壴 disease caused by SNCA duplications壴*Parkinsonism and Related Disorders*, 22, pp. S1唖6.

Kundu, P. *et al.* (2016) 唳elivery of Dual Drug Loaded Lipid Based Nanoparticles across the Blood唖Brain Barrier Impart Enhanced Neuroprotection in a Rotenone Induced Mouse Model of Parkinson壴 Disease壴*ACS Chemical Neuroscience*, 7(12), pp. 1658-1670.

Kuner, P., Schubenel, R. and Hertel, C. (1998) 唳amyloid binds to p75(ntr) and activates nf-┻b in human neuroblastoma cells壴*Journal of Neuroscience Research*, 54(6), pp. 798唖804.

Kuwahara, T. *et al.* (2012) 唳hosphorylation of ┳-synuclein protein at ser-129 reduces neuronal dysfunction by lowering its membrane binding property in Caenorhabditis elegans壴*Journal of Biological Chemistry*, 287(10), pp. 7098唖7109.

Lashuel, H. A. *et al.* (2013) 唳he many faces of alpha-synuclein: from structure and toxicity to therapeutic target壴*Nat Rev Neurosci*, 14(1), pp. 38唖8.

de Lau, L. M. L. *et al.* (2006) 唳pidemiology of Parkinson壴disease.壴*The Lancet. Neurology*, 5(6), pp. 525唖5.

Laurens, B. *et al.* (2017) 唳ultiple System Atrophy - State of the Art壴*Current Neurology and Neuroscience Reports*., 17(5), pp. 41

Lee, H.-J., Bae, E.-J. and Lee, S.-J. (2014) 唳xtracellular ┳--synuclein-a novel

and crucial factor in Lewy body diseases.〞*Nature reviews. Neurology*, 10(2), pp. 92–.

Leger, J. *et al.* (1997) ‟onversion of Serine to Aspartate Imitates Phosphorylation- induced Changes in the Structure and Function of Microtubule-associated Protein Tau *〞*The Journal of Biological Chemistry*, 272(13), pp. 8441–446.

Lhermitte, J., Kraus, W. M. and McAlpine, D. (1924) ‟he Occurence of abnormal deposits of iron in the brain in parkinsonism with special reference to its localisation〞*The Journal of Neurology and Psychopathology*, V(19), pp. 195–208.

Lill, C. M. (2016) ‟enetics of Parkinson〞 disease〞*Molecular and Cellular Probes*, pp. 386–96.

Lin, C.-F. *et al.* (2013) ‟urcumin reduces amyloid fibrillation of prion protein and decreases reactive oxidative stress.〞*Pathogens*, 2(3), pp. 506–19.

Liu, L. L. and Franz, K. J. (2007) ‟hosphorylation-dependent metal binding by alpha-synuclein peptide fragments.〞*Journal of biological inorganic chemistry*〞*JBIC*〞*a publication of the Society of Biological Inorganic Chemistry*, 12(2), pp. 234–7.

Liu, Y. *et al.* (2011) ‟n mobility mass spectrometry studies of the inhibition of alpha synuclein amyloid fibril formation by (-)-epigallocatechin-3-gallate〞in *Australian Journal of Chemistry*, pp. 36–0.

Lopresti, A. L. *et al.* (2015) ‟urcumin and major depression: A randomised,

double-blind, placebo-controlled trial investigating the potential of peripheral biomarkers to predict treatment response and antidepressant mechanisms of change㸼*European Neuropsychopharmacology*, 25(1), pp. 38㹼0.

Lovell, M. A. *et al.* (1998) 㹽opper, iron and zinc in Alzheimer㸼disease senile plaques㸼*J. Neurol. Sci.*, 158, p. 47.

Lozoff, B. and Georgieff, M. K. (2006) 㹽on deficiency and brain development㸼*Semin Pediatr Neurol*, 13(3), pp. 158㹼65.

Lu, Y. *et al.* (2011) 㹽hosphorylation of㺀-synuclein at Y125 and S129 alters its metal binding properties: Implications for understanding the role of㺀-synuclein in the pathogenesis of Parkinson㸼disease and related disorders㸼*ACS Chemical Neuroscience*, 2(11), pp. 667㹼675.

Lundblad, M. *et al.* (2012) 㹽mpaired neurotransmission caused by overexpression of ₸-synuclein in nigral dopamine neurons.㸼*Proceedings of the National Academy of Sciences of the United States of America*, 109(9), pp. 3213㹼9.

Machiya, Y. *et al.* (2010) 㹽hosphorylated㺀Synuclein at Ser-129 is targeted to the proteasome pathway in a ubiquitin-independent manner㸼*Journal of Biological Chemistry*, 285(52), pp. 40732㹼0744.

Mamyrin, B. A. *et al.* (1973) 㹽he mass-reflectron, a new nonmagnetic time-of-flight mass spectrometer with high resolution㸼*Sov. Phys. - JETP*, 37(1), pp. 45㹼48.

Del Mar, C. *et al.* (2005) 㹽tructure and properties of alpha-synuclein and other

amyloids determined at the amino acid level.㻌*Proceedings of the National Academy of Sciences of the United States of America*, 102(43), pp. 15477㻙82.

Marder, K. *et al.* (1996) 㻌isk of Parkinson㻌disease among first-degree relatives: A community-based study.㻌*Neurology*, 47(1), pp. 155㻙60.

Martin, Z. S. *et al.* (2012) 㻌-Synuclein oligomers oppose long-term potentiation and impair memory through a calcineurin-dependent mechanism: Relevance to human synucleopathic diseases㻌*Journal of Neurochemistry*, 120(3), pp. 440㻙452.

Martin Vabulas, R. and Ulrich Hartl, F. (2011) 㻌berrant protein interactions in amyloid disease㻌*Cell Cycle*, pp. 1512㻙513.

Mason, R. J. *et al.* (2016) 㻌opper Binding and Subsequent Aggregation of㻌-Synuclein Are Modulated by N-Terminal Acetylation and Ablated by the H50Q Missense Mutation㻌*Biochemistry*, 55(34), pp. 4737㻙741.

McCloy, R. A. *et al.* (2014) 㻌artial inhibition of Cdk1 in G2 phase overrides the SAC and decouples mitotic events㻌*Cell Cycle*, 13(9), pp. 1400㻙412.

McFarland, N. R. *et al.* (2009) 㻌lpha-synuclein S129 phosphorylation mutants do not alter nigrostriatal toxicity in a rat model of Parkinson disease.㻌*Journal of neuropathology and experimental neurology*, 68(5), pp. 515㻙24.

Menon, V. P. and Sudheer, A. R. (2007) 㻌ntioxidant and anti-inflammatory properties of curcumin㻌*Advances in Experimental Medicine and Biology*, pp. 105㻙25.

Meuvis, J. *et al.* (2010) 㻌he conformation and the aggregation kinetics of㻌-

synuclein depend on the proline residues in its C-terminal region〞*Biochemistry*, 49(43), pp. 9345–9352.

Miller, L. M. *et al.* (2006) 'Synchrotron-based infrared and X-ray imaging shows focalized accumulation of Cu and Zn co-localized with β-amyloid deposits in Alzheimer〞disease〞*Journal of Structural Biology*, 155(1), pp. 30–37.

Mishra, S. and Palanivelu, K. (2008) 'The effect of curcumin (turmeric) on Alzheimer〞 disease: An overview〞*Annals of Indian Academy of Neurology*, 11(1), pp. 13–9.

Modasiya, M. K. and Patel, V. M. (2012) 'Studies on solubility of curcumin〞*International Journal of Pharmacy & Life Sciences*, 3(3), pp. 2713–716.

Montes *et al*, (2014) 'Copper and copper proteins in Parkinson's disease'. *Oxidative Medicine and Cellular Longevity,* 147251 epub

Moree, B. *et al.* (2015) 'Small molecules detected by second-harmonic generation modulate the conformation of monomeric α-synuclein and reduce its aggregation in cells〞*Journal of Biological Chemistry*, 290(46), pp. 27582–27593.

Morita, A. *et al.* (2001) 'The effect of aging on the mineral status of female SAMP1 and SAMR1〞*Biol Trace Elem Res*, 80(1), pp. 53–65.

Morris, A. M. and Finke, R. G. (2009) 'α-Synuclein aggregation variable temperature and variable pH kinetic data: A re-analysis using the Finke-Watzky 2-step model of nucleation and autocatalytic growth〞*Biophysical Chemistry*, 140(1–3), pp. 9–15.

Mukherjee, A. *et al.* (2015) 'Type 2 diabetes as a protein misfolding disease〞

Trends in Molecular Medicine, pp. 439哑49.

Natalello, A. *et al.* (2011) 唉ompact conformations of酋-synuclein induced by alcohols and copper志*Proteins: Structure, Function and Bioinformatics*, 79(2), pp. 611哑21.

Nedumpully-Govindan, P. *et al.* (2016) 唉tabilizing Off-pathway Oligomers by Polyphenol Nanoassemblies for IAPP Aggregation Inhibition志*Scientific Reports*. Nature Publishing Group, 6, p. 19463.

Nemani, V. M. *et al.* (2010) 唉creased Expression of ₸-Synuclein Reduces Neurotransmitter Release by Inhibiting Synaptic Vesicle Reclustering after Endocytosis志*Neuron*, 65(1), pp. 66哑9.

Nilsson, M. R. (2004) 唉echniques to study amyloid fibril formation in vitro志*Methods*, 34(1), pp. 151哑60.

NΔbling, G. S. *et al.* (2014) 唉odelling Ser129 phosphorylation inhibits membrane binding of pore-forming alpha-synuclein oligomers志*PLoS ONE*, 9(6),e98906

Ono, K. *et al.* (2004) 唉urcumin Has Potent Anti-Amyloidogenic Effects for Alzheimer志酋Amyloid Fibrils In Vitro志*Journal of Neuroscience Research*, 75(6), pp. 742哑50.

Oueslati, A. (2016) 唉mplication of Alpha-Synuclein Phosphorylation at S129 in Synucleinopathies: What Have We Learned in the Last Decade?志*Journal of Parkinson志Disease*, pp. 39哑1.

Oueslati, a. *et al.* (2012) 唉imicking Phosphorylation at Serine 87 Inhibits the Aggregation of Human -Synuclein and Protects against Its Toxicity in a Rat

Model of Parkinson㸢Disease㸣*Journal of Neuroscience*, 32(5), pp. 1536㹼544.

Pagel *et al.* (2013) 'Intrinsically disordered p53 and its complexes populate compact conformations in the gas phase'. *Angew Chem Int Ed Engl,* 52(1), pp. 361-365.

Paik, S. R. *et al.* (1999) 㹻opper(Ⅱ)-induced self-oligomerization of alpha-synuclein.㸢*The Biochemical journal*, 340, pp. 821㹼28.

Pal, S. *et al.* (2016) 㹻urcumin inhibits the Al and Zn induced amyloid fibrillation of ㏇-lactoglobulin in vitro㸢*RSC Adv.* Royal Society of Chemistry, 6(112), pp. 111299㹼11307.

Paleologou, K. E. *et al.* (2008) 㹻hosphorylation at Ser-129 but not the phosphomimics S129E/D inhibits the fibrillation of㼀-synuclein㸢*Journal of Biological Chemistry*, 283(24), pp. 16895㹼6905.

Paleologou, K. E. *et al.* (2010) 㹻teractions㸢30(9), pp. 3184㹼198.

Pall, H. S. *et al.* (1987) 㹻AISED CEREBROSPINAL-FLUID COPPER CONCENTRATION IN PARKINSON㸢 DISEASE㸣*The Lancet*, 330(8553), pp. 238㹼41.

Panahi, Y. *et al.* (2014) 㹻pid-modifying effects of adjunctive therapy with curcuminoids-piperine combination in patients with metabolic syndrome: Results of a randomized controlled trial㸢*Complementary Therapies in Medicine*, 22(5), pp. 851㹼57.

Pandey, N. *et al.* (2008) 㹻urcumin inhibits aggregation of㼀-synuclein㸢*Acta Neuropathologica*, 115(4), pp. 479㹼89.

Pankratz, N. *et al.* (2007) 嗖enetics of Parkinson disease.壵*Genetics in medicine*牷*official journal of the American College of Medical Genetics*, 9(April), pp. 801嗵1.

Parkinson, J. (2002) 嗖n essay on the shaking palsy. 1817.壵*The Journal of neuropsychiatry and clinical neurosciences*, 14(2), p. 223嗵6

Peng, Y. *et al.* (2010) 嗖inding of㬎-synuclein with Fe(Ⅲ) and with Fe(Ⅱ) and biological implications of the resultant complexes壵*Journal of Inorganic Biochemistry*, 104(4), pp. 365嗵70.

Perfeito *et al.* (2014) 'Linking alpha-synuclein phosphorylation to reactive oxygen species formation and mitochondrial dysfunction in SHSY5Y cells', *Mol Cell Neurosci,* 62, pp.51-59.

Perez, R. G. *et al.* (2002) 嗖 role for alpha-synuclein in the regulation of dopamine biosynthesis.壵*The Journal of neuroscience*牷*the official journal of the Society for Neuroscience*, 22(8), pp. 3090嗵.

Perfeito, R. *et al.* (2014) 嗖nking alpha-synuclein phosphorylation to reactive oxygen species formation and mitochondrial dysfunction in SH-SY5Y cells壵*Molecular and Cellular Neuroscience*, 62, pp. 51嗵9.

Phillips, A. S. *et al.* (2015) 嗖onformational dynamics of㭎-synuclein: insights from mass spectrometry.壵*The Analyst*, 140(9), pp. 3070嗵1.

Popova, B., Kleinknecht, A. and Braus, G. H. (2015) 嗖osttranslational modifications and clearing of㭎-synuclein aggregates in yeast壵*Biomolecules*, pp. 617嗵34.

Prusiner, S. B. (2012) 嗖 Unifying Role for Prions in Neurodegenerative

Diseases‖*Science*, 336(June), pp. 1511–1513.

Rambaran, R & Serpell, L. (2008) 'Amyloid Fibrils', *Prion*, 2(3), pp. 112-117

Recchia, A. *et al.* (2004) ‖-Synuclein and Parkinson‖s disease‖*The FASEB Journal*, 18(6), pp. 617–626.

Riederer, P. *et al.* (1989) ‖ransition Metals, Ferritin, Glutathione, and Ascorbic Acid in Parkinsonian Brains‖*Journal of Neurochemistry*, 52(2), pp. 515–520.

Ringman, J. M. *et al.* (2005) ‖ potential role of the curry spice curcumin in Alzheimer‖s disease.‖*Current Alzheimer research*, 2(2), pp. 131–5.

Roberts, H. and Brown, D. (2015) ‖eeking a Mechanism for the Toxicity of Oligomeric -Synuclein‖*Biomolecules*, 5(2), pp. 282–305.

Rogers, J. T. *et al.* (2011) ‖he alpha-synuclein 5‖-untranslated region targeted translation blockers: anti-alpha synuclein efficacy of cardiac glycosides and Posiphen.‖*Journal of neural transmission (Vienna, Austria : 1996)*, 118(3), pp. 493–507.

Rose, F., Hodak, M. and Bernholc, J. (2011) ‖echanism of copper(II)-induced misfolding of Parkinson‖s disease protein‖*Scientific Reports*, 1, p. 11.

Ross, R. A. and Biedler, J. L. (1985) ‖resence and Regulation of Tyrosinase Activity in Human Neuroblastoma Cell Variants in Vitro Presence and Regulation of Tyrosinase Activity in Human Neuroblastoma Cell Variants in Vitro1‖ 45(APRIL), pp. 1628–1632.

Ruotolo, B. T. *et al.* (2008) ‖n mobility-mass spectrometry analysis of large protein complexes.‖*Nature protocols*, 3(7), pp. 1139–1152.

Sandur, S. *et al.* (2007) 'Curcumin, demethoxycurcumin, bisdemethoxycurcumin, tetrahydrocurcumin and tumerones differentially regulate anti-inflammatory and anti-proliferative reposnses through a ROS-independent mechanism.', *Carcinogenesis*, 28(8), pp. 1765-1773.

Sanmukhani, J. *et al.* (2014) 'Efficacy and safety of curcumin in major depressive disorder: a randomized controlled trial.', *Phytotherapy research : PTR*, 28(4), pp. 579–585.

Santner, A. and Uversky, V. N. (2010) 'Metalloproteomics and metal toxicology of α-synuclein.', *Metallomics : integrated biometal science*, 2(6), pp. 378–392.

Schenauer, M. R. and Leary, J. A. (2009) 'In ion mobility-mass spectrometry investigation of monocyte chemoattractant protein-1', *International Journal of Mass Spectrometry*, 287(1–3), pp. 70–76.

Sathasivam and Shaw, (2005) 'Apoptosis in amylotrophic lateral sclerosis - what is the evidence?', *Lancel Neurol,* 4, pp. 500-509.

Schildknecht, S. *et al.* (2013) 'Oxidative and nitrative alpha-synuclein modifications and proteostatic stress: Implications for disease mechanisms and interventions in synucleinopathies', *Journal of Neurochemistry*, pp. 491–511.

Schlachetzki, J. C. M., Saliba, S. W. and de Oliveira, A. C. P. (2013) 'Studying neurodegenerative diseases in culture models', *Revista Brasileira de Psiquiatria*, 35(SUPPL.2). s92-100.

Schmid, A. W. *et al.* (2013) 'Alpha-synuclein Post-translational Modifications as Potential Biomarkers for Parkinson Disease and Other Synucleinopathies',

Molecular & Cellular Proteomics, 12(12), pp. 3543–3558.

Scholz, S. W. *et al.* (2009) 'SNCA variants are associated with increased risk for multiple system atrophy', *Annals of Neurology*, 65(5), pp. 610–614.

Schreurs, S. *et al.* (2014) 'In vitro phosphorylation does not influence the aggregation kinetics of WT and -synuclein in contrast to its phosphorylation mutants', *International Journal of Molecular Sciences*, 15(1), pp. 1040–1067.

Seyyed Mehdi Mirhashemi (2012) 'Effect of two herbal polyphenol compounds on human amylin amyloid formation and destabilization', *Journal of Medicinal Plants Research*, 6(16), pp. 3207–3212.

Shelimov and Jarrold, (1997) 'Conformations, unfolding and refolding of apomyoglobin in vacuum: an activation barrier for gas-phase protein unfolding', *JACS*, 119(3), pp. 2987-2994.

Shoba, G. *et al.* (1998) 'Influence of piperine on the pharmacokinetics of curcumin in animals and human volunteers', *Planta Medica*, 64(4), pp. 353–56.

Shrivastava, P. *et al.* (2013) 'Anti-apoptotic and Anti-inflammatory effect of Piperine on 6-OHDA induced Parkinson' Rat model', *Journal of Nutritional Biochemistry*, 24(4), pp. 680–687.

Shvartsburg, A. A. and Smith, R. D. (2008) 'Fundamentals of traveling wave ion mobility spectrometry', *Analytical Chemistry*, 80(24), pp. 9689–9699.

da Silveira, S. A. *et al.* (2009) 'Phosphorylation does not prompt, nor prevent, the formation of -synuclein toxic species in a rat model of Parkinson' disease', *Human Molecular Genetics*, 18(5), pp. 872–887.

Singh, P. K. *et al.* (2013) 嗖urcumin modulates ┳-synuclein aggregation and toxicity悲*ACS Chemical Neuroscience*, 4(3), pp. 393嗵07.

Singh, S., Jamwal, S. and Kumar, P. (2015) 嗖iperine Enhances the Protective Effect of Curcumin Against 3-NP Induced Neurotoxicity: Possible Neurotransmitters Modulation Mechanism悲*Neurochemical Research*, 40(8), pp. 1758嗵766.

Smith, D. P. *et al.* (2009) 嗖eciphering drift time measurements from travelling wave ion mobility spectrometry-mass spectrometry studies.悲*European journal of mass spectrometry*, 15(2), pp. 113嗵30.

Snead, D. and Eliezer, D. (2014) 嗖lpha-synuclein function and dysfunction on cellular membranes.悲*Experimental neurobiology*, 23(4), pp. 292嗵13.

Sofic, E. *et al.* (1988) 嗖creased iron (Ⅲ) and total iron content in post mortem substantia nigra of parkinsonian brain悲*Journal of Neural Transmission*, 74(3), pp. 199嗵05.

Spillantini, M. G. and Goedert, M. (2000) 'The ┳-Synucleinopathies: Parkinson's Disease, Dementia with Lewy Bodies, and Multiple System Atrophy', *Annals of the New York Academy of Sciences*.', 920, pp. 16-27.

Spillantini, M. G. *et al.* (1997) 嗖lpha-synuclein in Lewy bodies.悲*Nature*, 388(6645), pp. 839嗵40.

Spinelli, K. J. *et al.* (2015) 嗖urcumin treatment improves motor behavior in酉-synuclein transgenic mice悲*PLoS ONE*, 10(6). doi: 10.1371/journal.pone.0128510.

Stefanis, L. (2012) 噴-Synuclein in Parkinson悲 disease悲*Cold Spring Harbor Perspectives in Medicine*, 10(6), e0128510.

Sweeney, P. *et al.* (2017) 噎rotein misfolding in neurodegenerative diseases: implications and strategies悲*Translational Neurodegeneration*, 6(1), p. 6.

Tenreiro, S. *et al.* (2014) 噎hosphorylation Modulates Clearance of Alpha-Synuclein Inclusions in a Yeast Model of Parkinson悲Disease悲*PLoS Genetics*, 10(5), e1004302.

Thalassinos, K. and Scrivens, J. H. (2009) 噎pplications of traveling wave ion mobility-mass spectrometry.悲*Pract. Aspects Trapped Ion Mass Spectrom.*, (Im), pp. 205唖36.

Todorich, B. *et al.* (2009) 噎ligodendrocytes and myelination: The role of iron悲*GLIA*, pp. 467唖78.

Toyama, B. H. and Weissman, J. S. (2011) 噎myloid structure: conformational diversity and consequences.悲*Annual review of biochemistry*, 80, pp. 557唖5.

Tsigelny, I. F *et al.* (2007) 'Dynamics of alpha-synuclein aggregation and inhibition of pore-like oligomer development by beta-synuclein.', *FEBS J*, 274(7), pp. 1862-77.

Ucisik, M. H. *et al.* (2013) 噎haracterization of CurcuEmulsomes: nanoformulation for enhanced solubility and delivery of curcumin悲*Journal of Nanobiotechnology*, 11, p. 37.

Uversky, V. N. *et al.* (2002) 噎ethionine oxidation inhibits fibrillation of human吾-synuclein in vitro悲*FEBS Letters*, 517(1唖), pp. 239唖44.

Uversky, V. N. (2008) 嗖myloidogenesis of natively unfolded proteins.悥*Current Alzheimer research*, 5(3), pp. 260唖87.

Uversky, V. N. and Eliezer, D. (2009) 嗖iophysics of Parkinson悥 disease: structure and aggregation of alpha-synuclein.悥*Current protein & peptide science*, 10(5), pp. 483唖9.

Uversky, V. N., Li, J. and Fink, A. L. (2001) 嗖etal-triggered structural transformations, aggregation, and fibrillation of human alpha-synuclein. A possible molecular NK between Parkinson悥disease and heavy metal exposure.悥*The Journal of biological chemistry*, 276(47), pp. 44284唖6.

Vargas, K. J. *et al.* (2017) 嗖ynucleins Have Multiple Effects on Presynaptic Architecture悥*Cell Reports*, 18(1), pp. 161唖73.

Vendruscolo, M., Knowles, T. P. J. and Dobson, C. M. (2011) 嗖rotein solubility and protein homeostasis: A generic view of protein misfolding disorders悥*Cold Spring Harbor Perspectives in Biology*, 3(12), a010454.

Venkateswarlu, S., Ramachandra, M. S. and Subbaraju, G. V (2005) 嗖ynthesis and biological evaluation of polyhydroxycurcuminoids.悥*Bioorganic & medicinal chemistry*, 13(23), pp. 6374唖380.

Vergouw LJM, van Steenoven I, van de Berg WDJ, Teunissen CE, van Swieten JC, Bonifati V, Lemstra AW, de J. F. (2017) 嗖n update on the genetics of dementia with Lewy bodies悥*Parkinsonism Related Disorders*, 43, pp. 1-8.

Vlad, C. *et al.* (2011) 嗖utoproteolytic fragments are intermediates in the oligomerization/aggregation of the Parkinson悥disease protein alpha-synuclein

as revealed by ion mobility mass spectrometry㸧*ChemBioChem*, 12(18), pp. 2740㹢744.

Waldron, K. J. *et al.* (2009) 㹣etalloproteins and metal sensing㸧*Nature*, 460(7257), pp. 823㹦30.

Walzthoeni, T. *et al.* (2013) 㹣ass spectrometry supported determination of protein complex structure㸧*Current Opinion in Structural Biology*, pp. 252㹢60.

Wang, J. and Pantopoulos, K. (2011) 㹥egulation of cellular iron metabolism㸧*Biochem J*, 434(3), pp. 365㹢81.

Wang, M. S. *et al.* (2010) 㹥urcumin reduces alpha-synuclein induced cytotoxicity in Parkinson㸧disease cell model.㸧*BMC Neuroscience*, 11(57), pp. 1㹢0.

Wang, X. *et al.* (2010) 㹥opper binding regulates intracellular alpha-synuclein localisation, aggregation and toxicity㸧*Journal of Neurochemistry*, 113(3), pp. 704㹢14.

Wilm, M. (2011) 㹥rinciples of electrospray ionization.㸧*Molecular & cellular proteomics㸦MCP*, 10(7), p. M111.009407.

Winkelhofer *et al*, (2008) 'The two faces of protein misfolding: gain- and loss-of-function in neurodegenerative diseases', *EMBO J*, 22(2), pp.336-349.

Winner, B. *et al.* (2011) 㹣 vivo demonstration that alpha-synuclein oligomers are toxic.㸧*Proceedings of the National Academy of Sciences of the United States of America*, 108(10), pp. 4194㹢.

Witkin, J. M. and Li, X. (2013) 㹥urcumin, an Active Constiuent of the Ancient Medicinal Herb Curcuma longa L.: Some Uses and the Establishment and

Biological Basis of Medical Efficacy. *Cns & Neurological Disorders-Drug Targets*, 12(4), pp. 487–97.

Wolfe, K. J. and Cyr, D. M. (2011) 'Amyloid in neurodegenerative diseases: Friend or foe?', *Seminars in Cell and Developmental Biology*, pp. 476–81.

Wong, Y. C. and Krainc, D. (2017) 'α-synuclein toxicity in neurodegeneration: mechanism and therapeutic strategies', *Nature Medicine*, 23(2), pp. 1–13.

Wright, J. a, Wang, X. and Brown, D. R. (2009) 'Unique copper-induced oligomers mediate alpha-synuclein toxicity.', *The FASEB journal : official publication of the Federation of American Societies for Experimental Biology*, 23(8), pp. 2384–2393.

Wright, P. E. and Dyson, H. J. (1999) 'Intrinsically unstructured proteins: re-assessing the protein structure-function paradigm.', *Journal of molecular biology*, 293(2), pp. 321–31.

Xicoy, H., Wieringa, B. and Martens, G. J. M. (2017) 'The SH-SY5Y cell line in Parkinson's disease research: a systematic review', *Molecular Neurodegeneration*. Molecular Neurodegeneration, 12(1), p. 10.

Yamin, G. *et al.* (2003) 'Certain metals trigger fibrillation of methionine-oxidized α-synuclein', *Journal of Biological Chemistry*, 278(30), pp. 27630–7635.

Yanagisawa, D. *et al.* (2011) 'Curcuminoid Binds to Amyloid-beta(1-42) Oligomer and Fibril', *Journal of Alzheimers Disease*, 24, pp. 33–42. doi: Doi 10.3233/Jad-2011-102100.

Yanagisawa, D. *et al.* (2015) 'Novel curcumin derivatives as potent inhibitors of

amyloid aggregation. *Biochemistry and Biophysics Reports*, 4, pp. 357–368.

Yang, F. *et al.* (2005) Curcumin inhibits formation of amyloid oligomers and fibrils, binds plaques, and reduces amyloid in vivo. *Journal of Biological Chemistry*, 280(7), pp. 5892–5901.

Yang, W. and Yu, S. (2017) Synucleinopathies: common features and hippocampal manifestations. *Cellular and Molecular Life Sciences*, pp. 1485–1501.

Yasamin DavatgaranTaghipour *et al.* (2017) Polyphenol nanoformulations for cancer therapy: experimental evidence and clinical perspective. pp. 2689–2702.

Young, L. M. *et al.* (2014) Ion mobility spectrometry-mass spectrometry defines the oligomeric intermediates in amylin amyloid formation and the mode of action of inhibitors. *Journal of the American Chemical Society*, 136(2), pp. 660–670.

Young, L. M., Saunders, J. C., Mahood, R. a, *et al.* (2015) SI-IMS-MS: A method for rapid analysis of protein aggregation and its inhibition by small molecules. *Methods*, pp. 9–14.

Young, L. M., Saunders, J. C., Mahood, R. A., *et al.* (2015) Screening and classifying small-molecule inhibitors of amyloid formation using ion mobility spectrometry-mass spectrometry. *Nature chemistry*, 7(1), pp. 73–81.

Zhou, W. *et al.* (2010) Methionine oxidation stabilizes non-toxic oligomers of -synuclein through strengthening the auto-inhibitory intra-molecular long-range interactions. *Biochimica et Biophysica Acta - Molecular Basis of Disease*, 1802(3), pp. 322–30.

Zilch *et al.* (2007) 'Folding and unfolding of helix-turn-helix motifs in the gas phase', *J Am Soc Mass Spectrom*, 18(7), pp. 1239-1248.

Appendices

Appendix 2A:

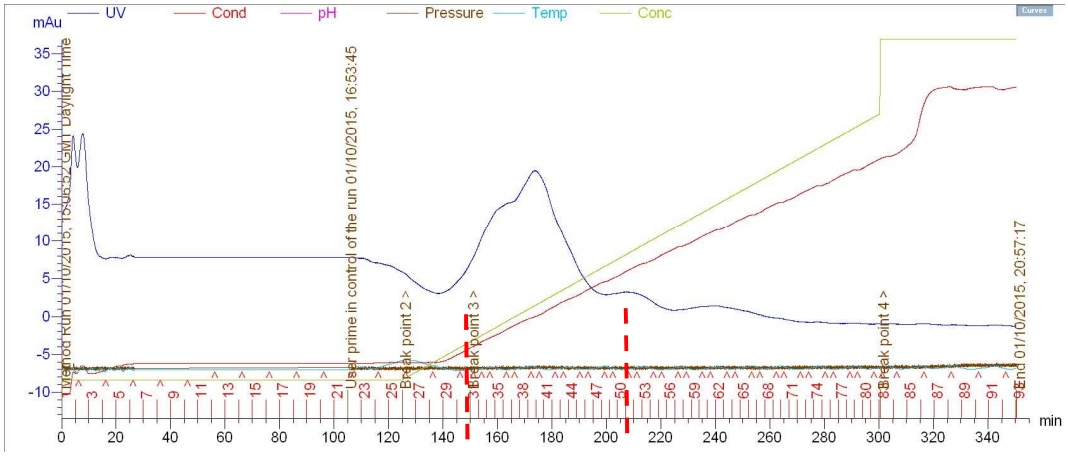

Appendix 2A: Anion exchange chromatograph of TSyn. Fractions were collected for SDS-PAGE within the region marked by the red dashes.

Appendix 2B:

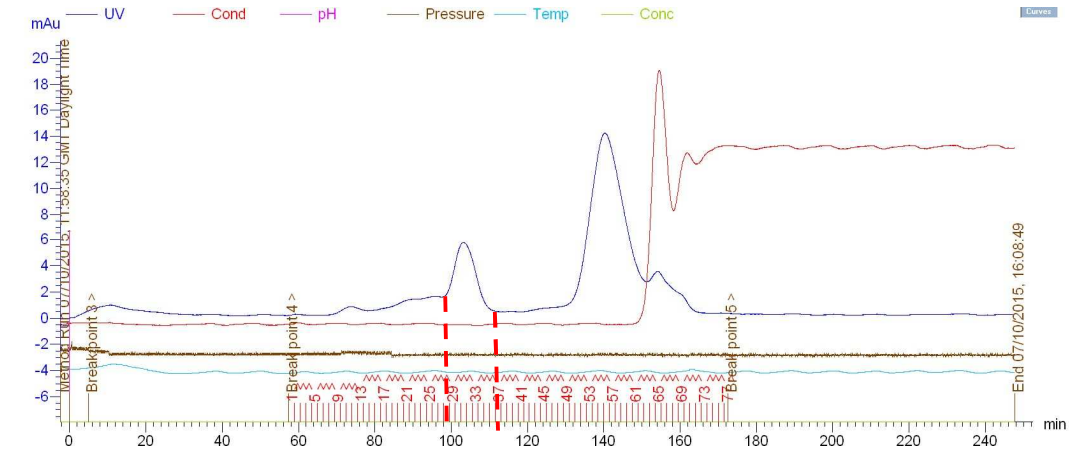

Appendix 2B: Size exclusion chromatograph of TSyn. Fractions were collected for SDS-PAGE within the marked region.

Appendix 3A:

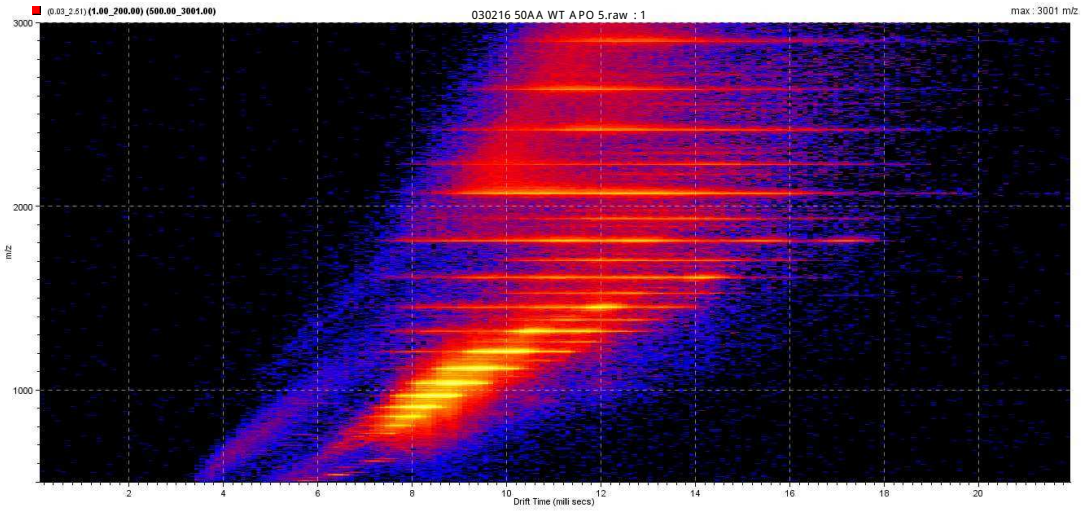

Appendix 3A: Drift scope plot of WT α-syn acquired in 50mM ammonium acetate using ESI-IMS-MS in positive ion mode.

Appendix 3B:

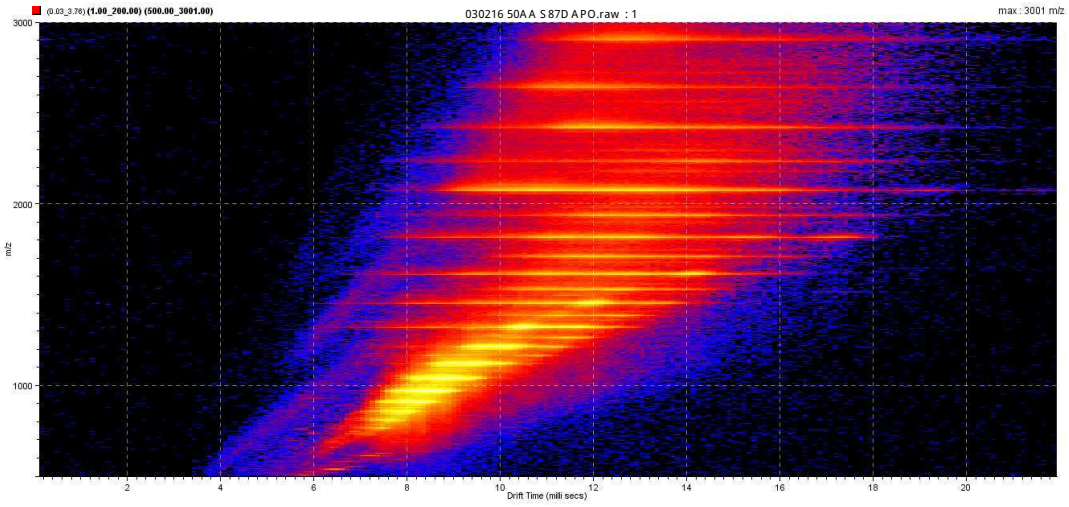

Appendix 3B: Drift scope plot of S87D mutant α-syn acquired in 50mM ammonium acetate using ESI-IMS-MS in positive ion mode.

Appendix 3C:

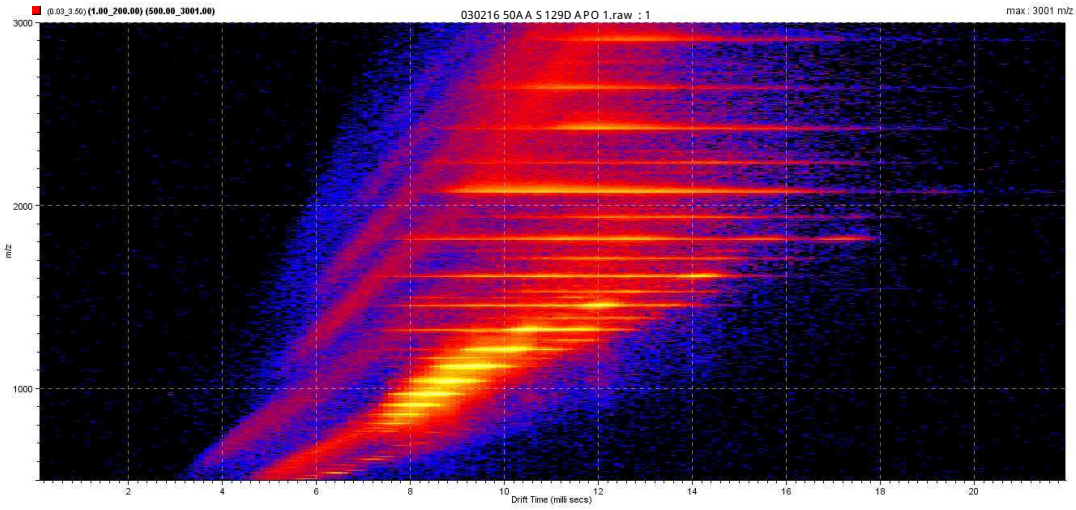

Appendix 3C: Drift scope plot of S129D mutant T-syn acquired in 50mM ammonium acetate using ESI-IMS-MS in positive ion mode.

Appendix 3D:

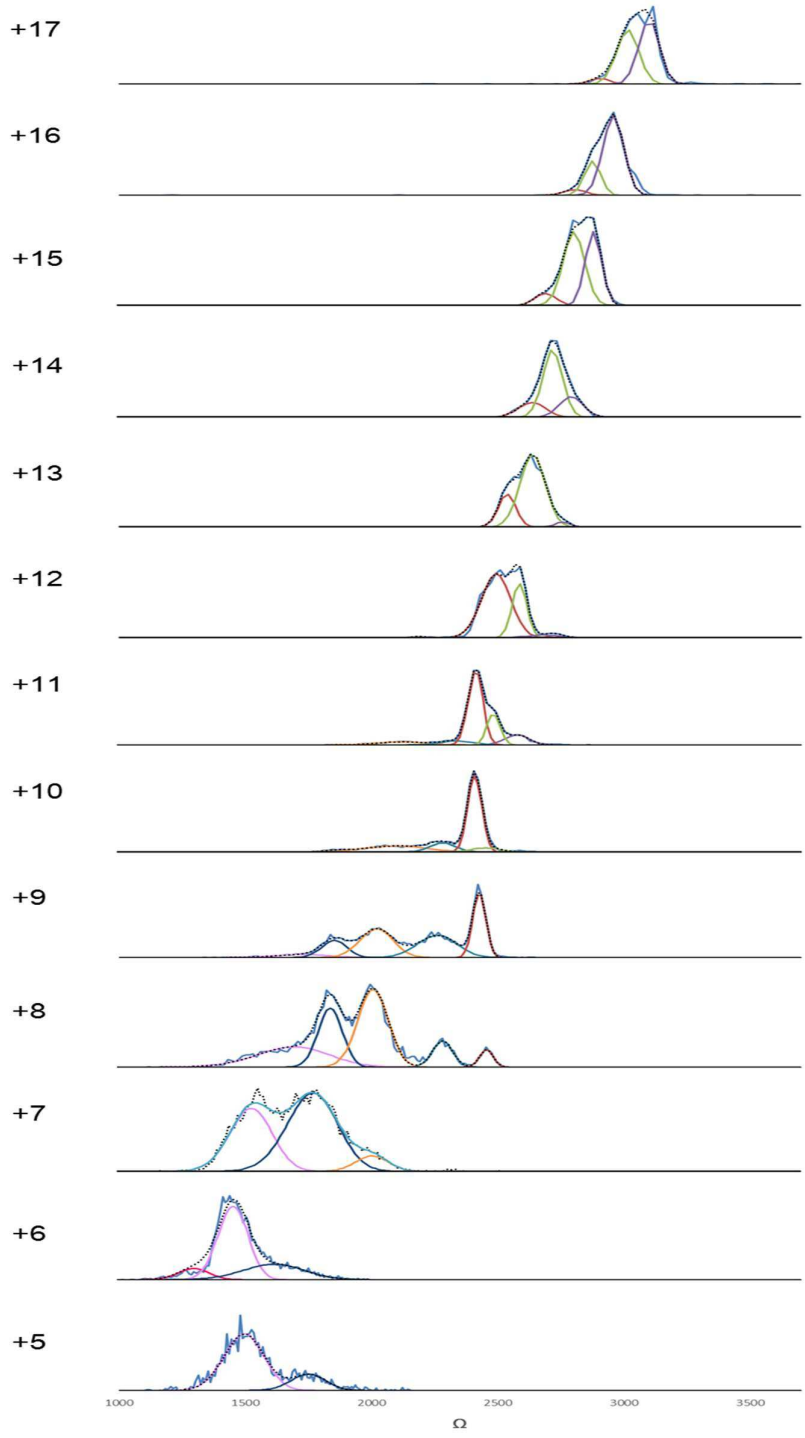

Appendix 3D: ATD of each charge state ion of S87D mutant-syn acquired by IST-IMS-MS in 50mM ammonium acetate under previously described conditions.

Appendix 3E:

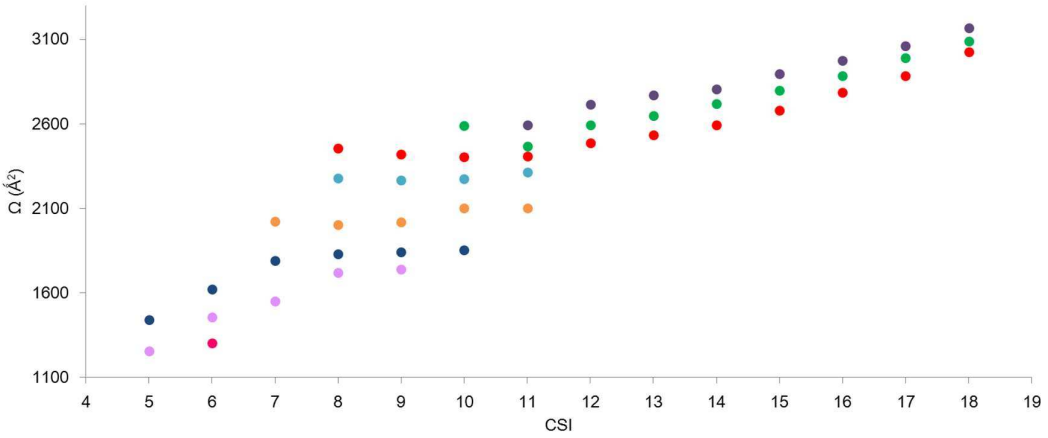

Appendix 3E: Conformational arrangement of S67D mutant γ-syn acquired in 50mM ammonium acetate using ESI-IMS-MS in positive ion mode. S67D γ-syn occupies the same 7 distinct conformational families as WT γ-syn.

Appendix 3F:

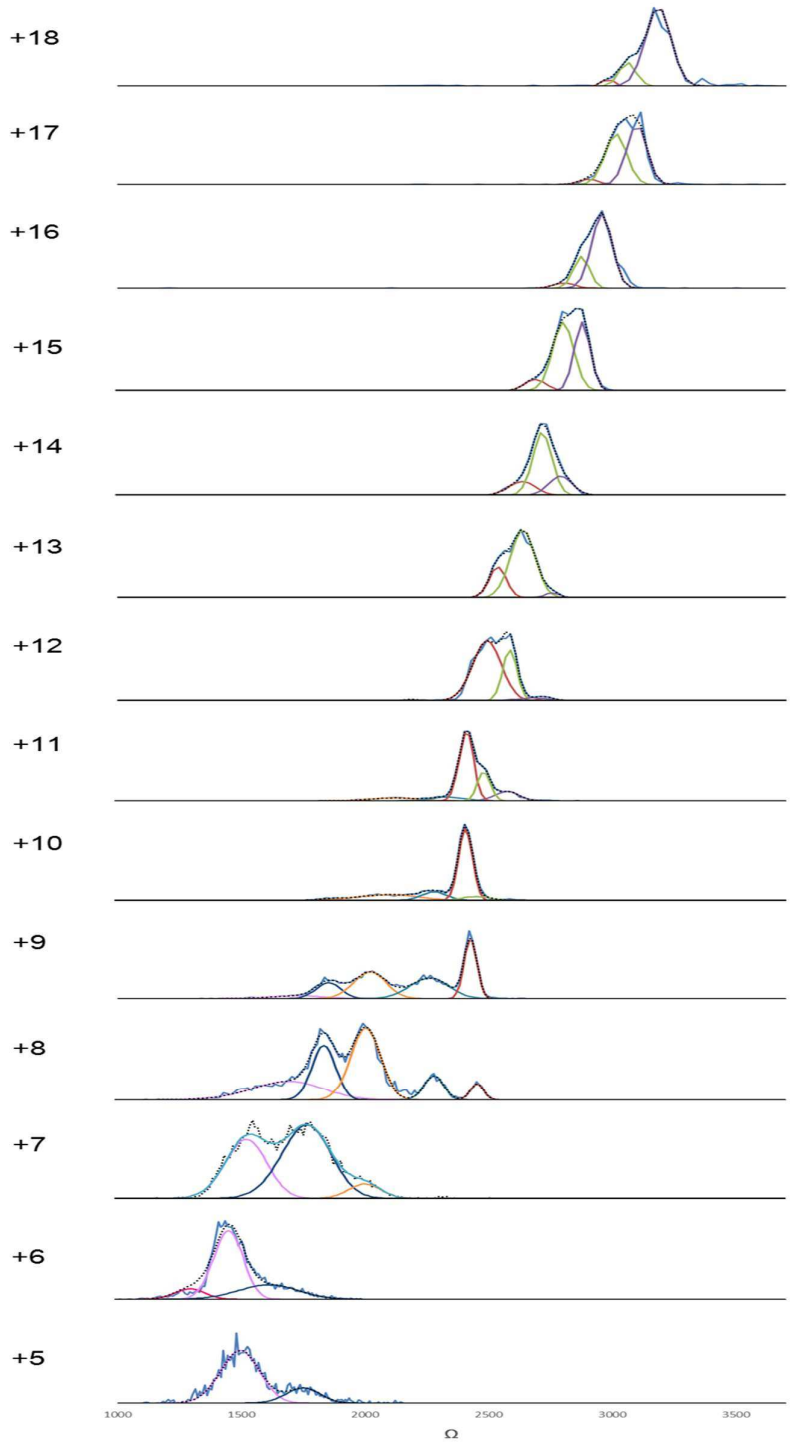

Appendix 3F: ATD of each charge state ion of S128D mutant-pyn acquired by IST-IMS-MS in 50mM ammonium acetate under previously described conditions.

Appendix 3G:

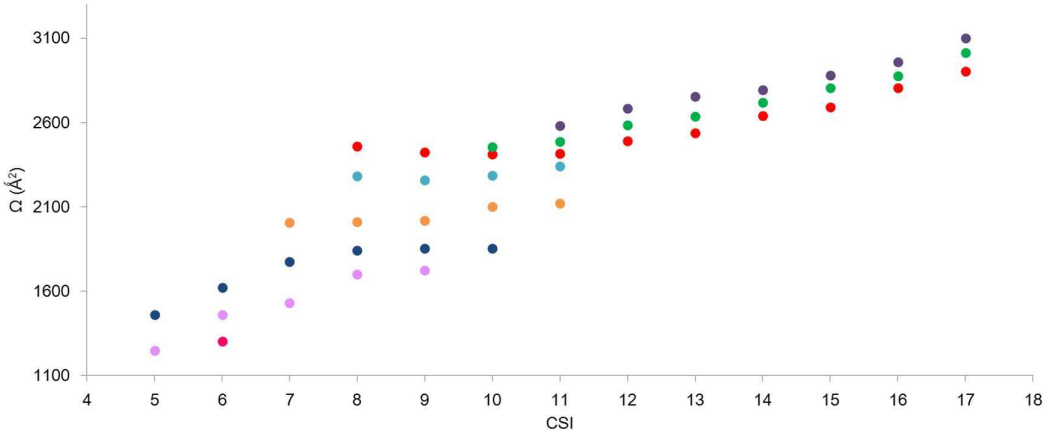

Appendix 3G: Conformational arrangement of S129D mutant-pyn acquired in 150mM ammonium acetate using ESI-IMS-MS in positive ion mode. S129D-pyn occupies the same 7 distinct conformational families as WT and S87D-pyn.

Appendix 3H:

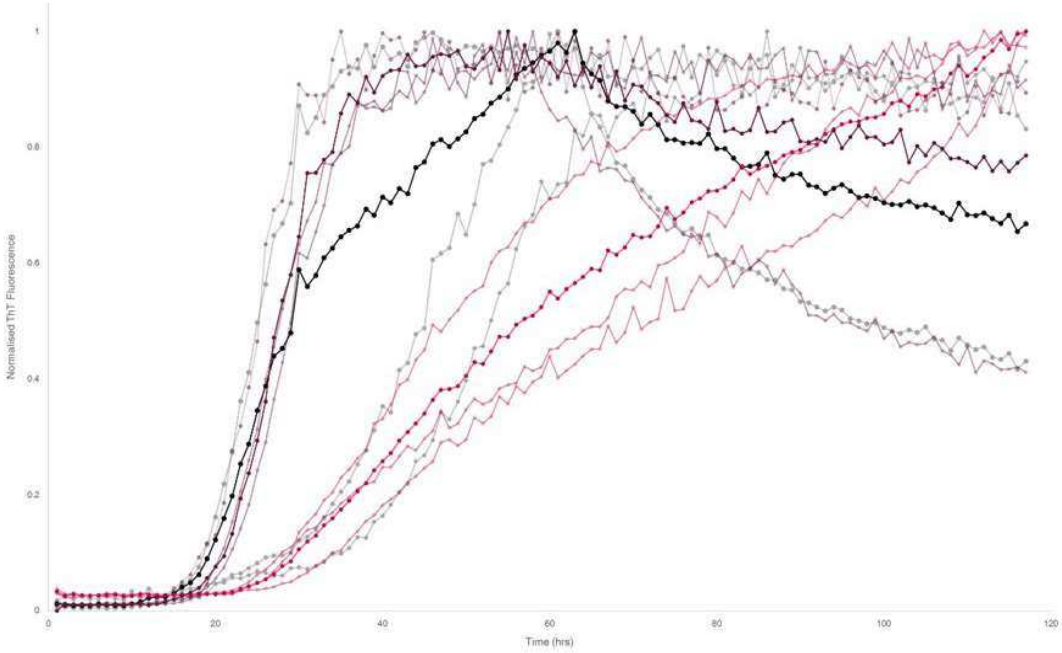

Appendix 3H: Normalised thioflavin-t fluorescence data with WT αsyn with repeats shown in grey and mean fluorescence from three separate experiments in black, S87D repeats in light pink and mean fluorescence from three separate experiments in dark pink, and S129D repeats in light purple and mean fluorescence from three separate experiments in dark purple.

Appendix 3I:

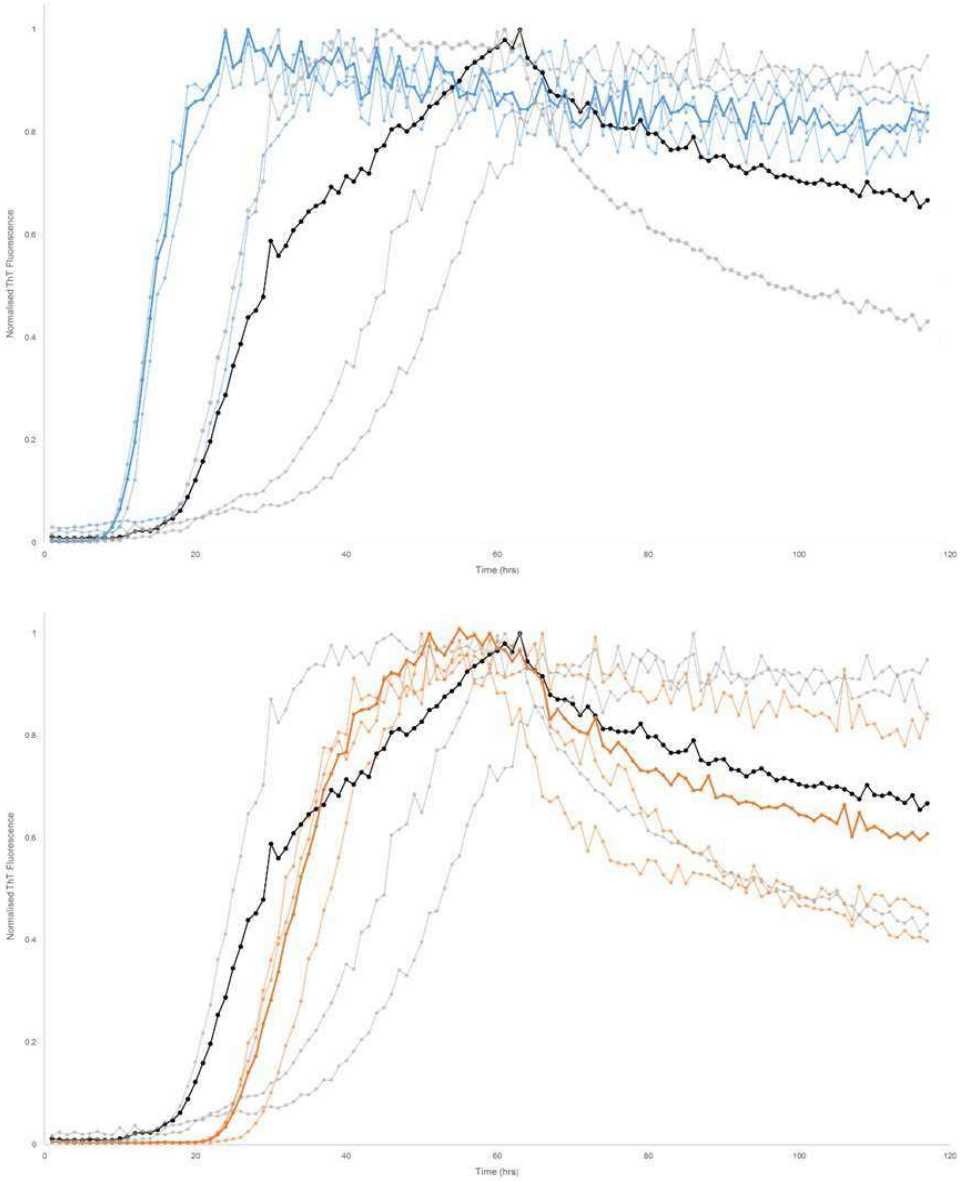

Appendix 3I: Normalised thioflavin-t fluorescence data with WT αsyn repeats shown in grey and mean fluorescence from three separate experiments normalized in black. WT αsyn + equimolar $CuCl_2$ repeats in light blue, mean from three independent experiments in darker blue. WT αsyn + equimolar $FeCl_2$ repeats in yellow, mean from three independent experiments in orange.

Appendix 3J :

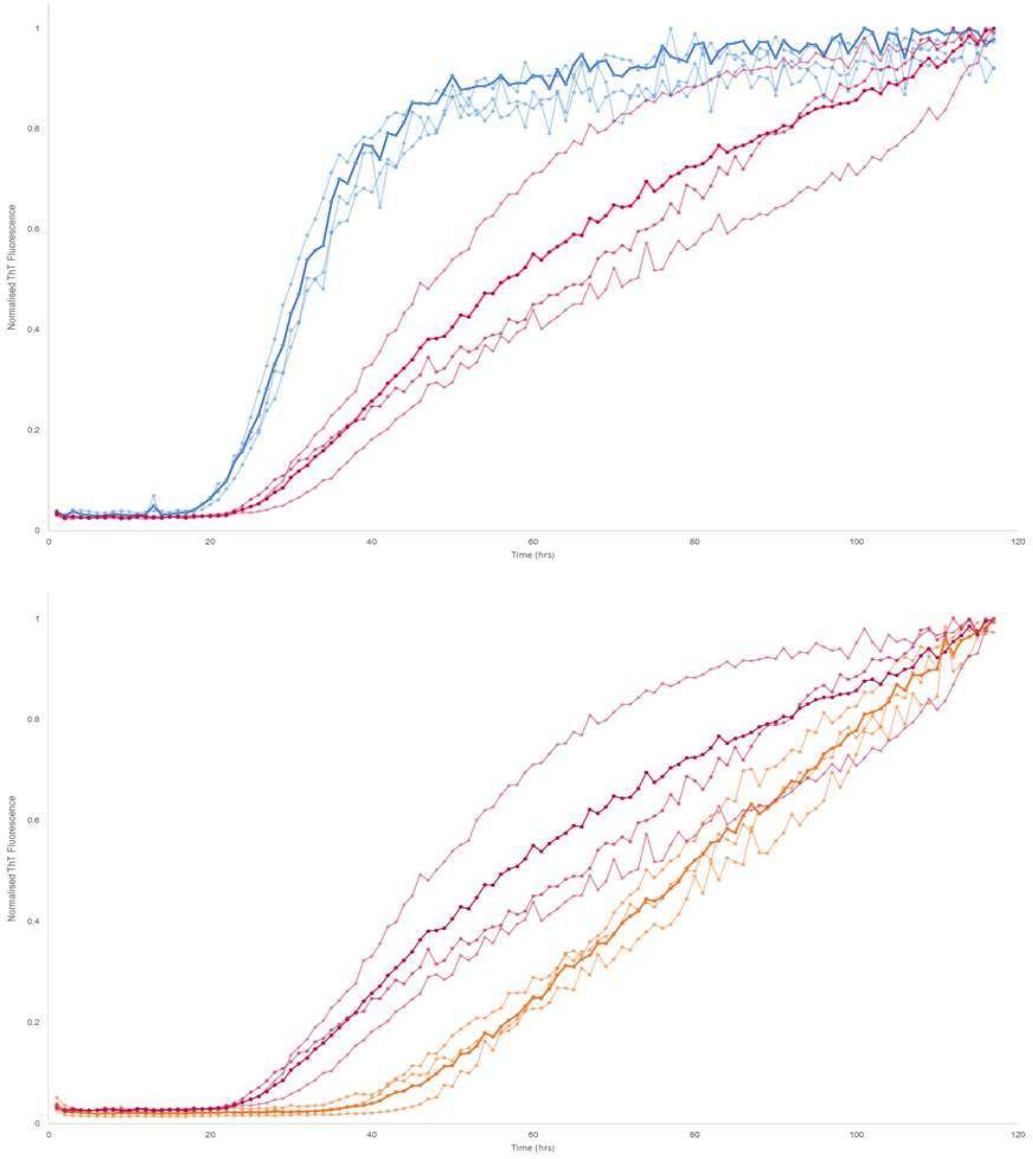

Appendix 3J : Normalised thioflavin-t fluorescence data with S87D α-syn repeats shown in pink and mean fluorescence from three separate experiments normalized in darker pink. S87D α-syn + equimolar $CuCl_2$ repeats in light blue, mean from the three independent experiments in darker blue. S87D α-syn + equimolar $FeCl_2$ repeats in yellow, mean from the three independent experiments in orange.

Appendix 3K:

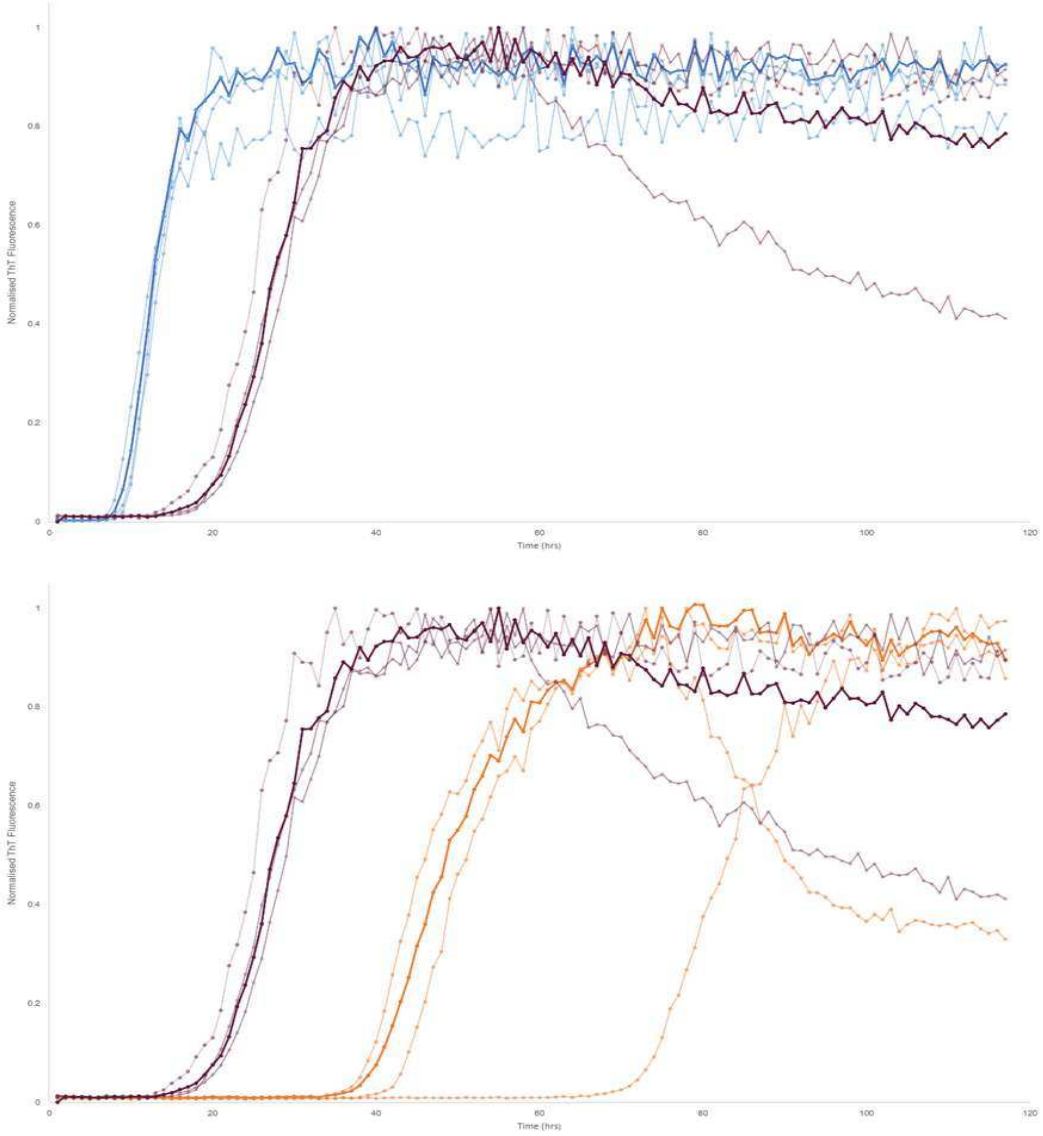

Appendix 3K: Normalised thioflavin-t fluorescence data with S128D α-syn repeats shown in purple and mean fluorescence from three separate experiments normalized in darker purple. S129D α-syn + equimolar $CuCl_2$ repeats in light blue, mean from the three independent experiments in darker blue. S129D α-syn + equimolar $FeCl_2$ repeats in yellow, mean from the three independent experiments in orange.

Appendix 3L:

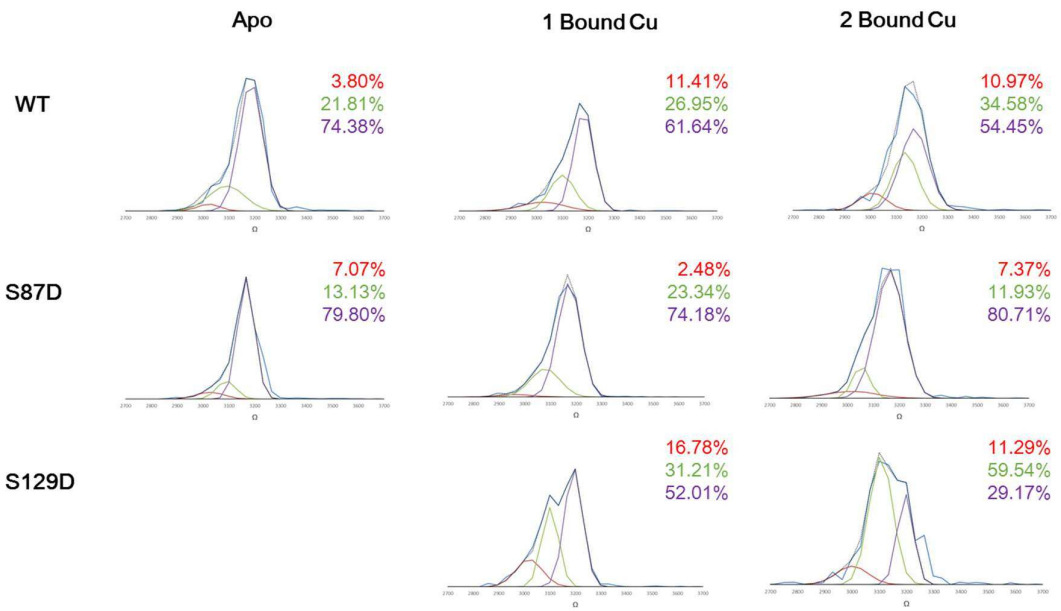

Appendix 3L: +13 charge state ion of WT, S87D and S129D in the presence of equimolar $CuCl_2$ with Gaussian fitting applied to show relative proportions of conformations A, B & C.

Appendix 3M:

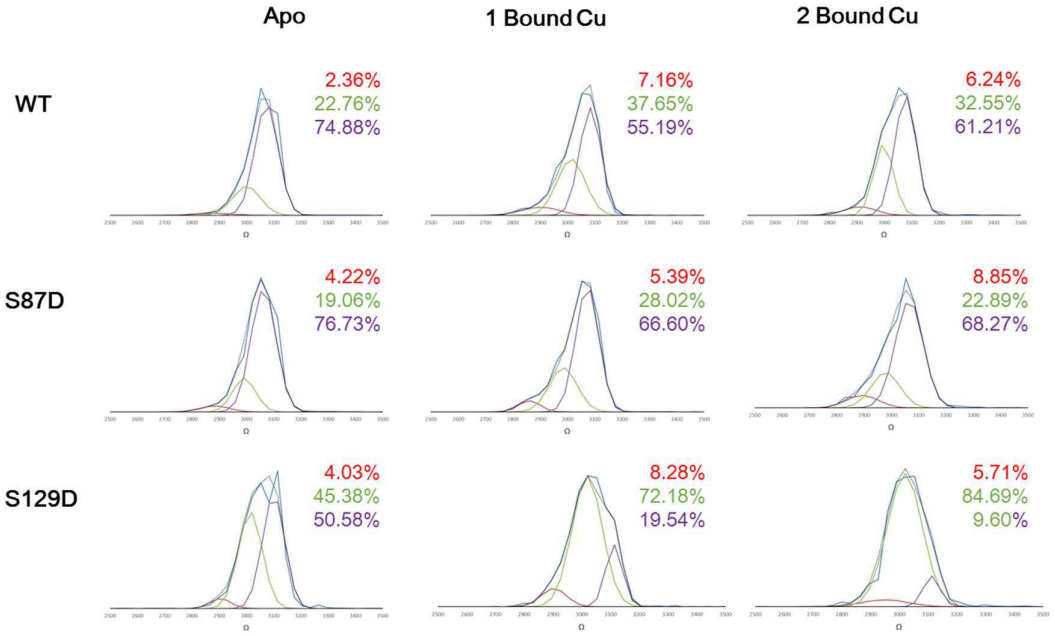

Appendix 3M: +17 charge state ion of WT, S87D and S129D in the presence of equimolar $CuCl_2$ with Gaussian fitting applied to show relative proportions of conformations A, B & C.

Key Findings:

No notable changes observed with S87D α-syn. WT and S129D both demonstrate an increase in conformation B via a decrease in the most extended conformation, A. S129D had the highest proportion of conformation B of all the apo proteins.

Appendix 3N:

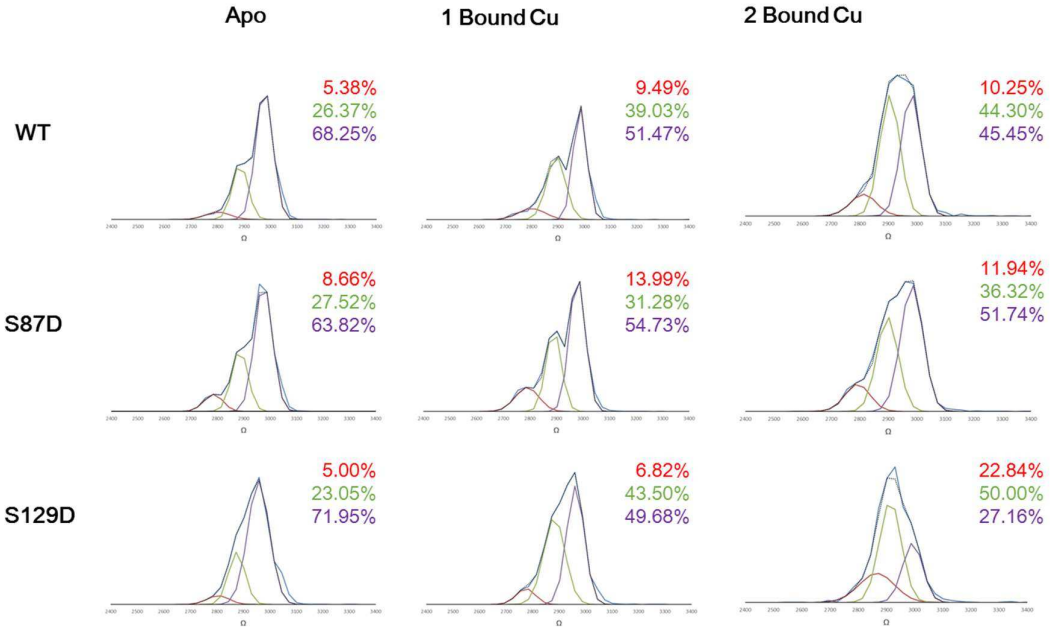

Appendix 3N: +16 charge state ion of WT, S87D and S129D in the presence of equimolar $CuCl_2$ with Gaussian fitting applied to show relative proportions of conformations A, B & C.

Key Findings:

No notable differences in apo samples. No notable changes observed with S87D upon addition of $CuCl_2$. WT & S129D again show an increase in B via reduction in A. S129D when bound to two $CuCl_2$ ions also shows notable increase in the most compact conformation, conformation A.

Appendix 3O:

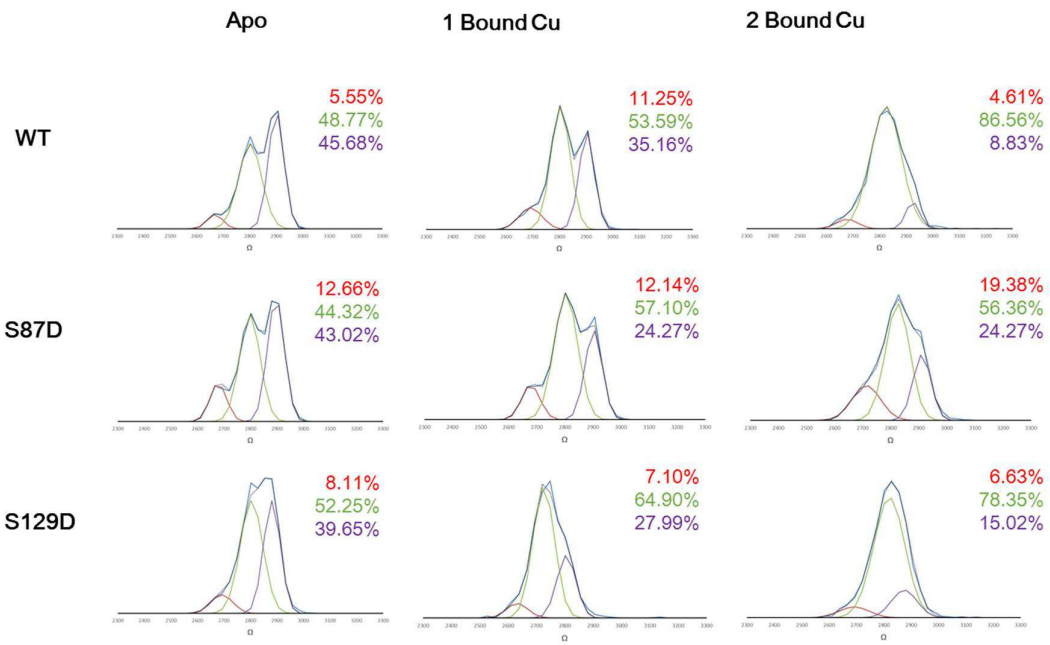

Appendix 3O: +15 charge state ion of WT, S87D and S129D in the presence of equimolar $CuCl_2$ with Gaussian fitting applied to show relative proportions of conformations A, B & C.

Key Findings:

S87D has the highest proportion of conformation C of the apo samples. All protein variants show an increase in conformation B via a reduction in A. The most pronounced difference is seen with WT αsyn bound to two copper ions.

Appendix 3P:

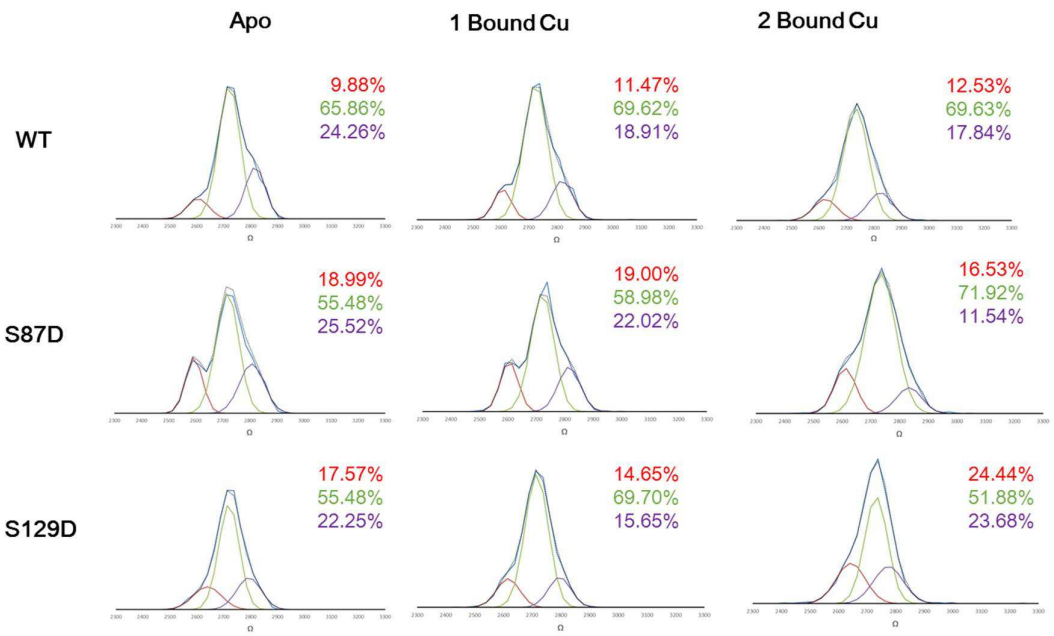

Appendix 3P: +14 charge state ion of WT, S87D and S129D in the presence of equimolar $CuCl_2$ with Gaussian fitting applied to show relative proportions of conformations A, B & C.

Key Findings:

No real alterations. WT and S129D α-syn both have an increased proportion of conformation C in the apo samples.

Appendix 3Q:

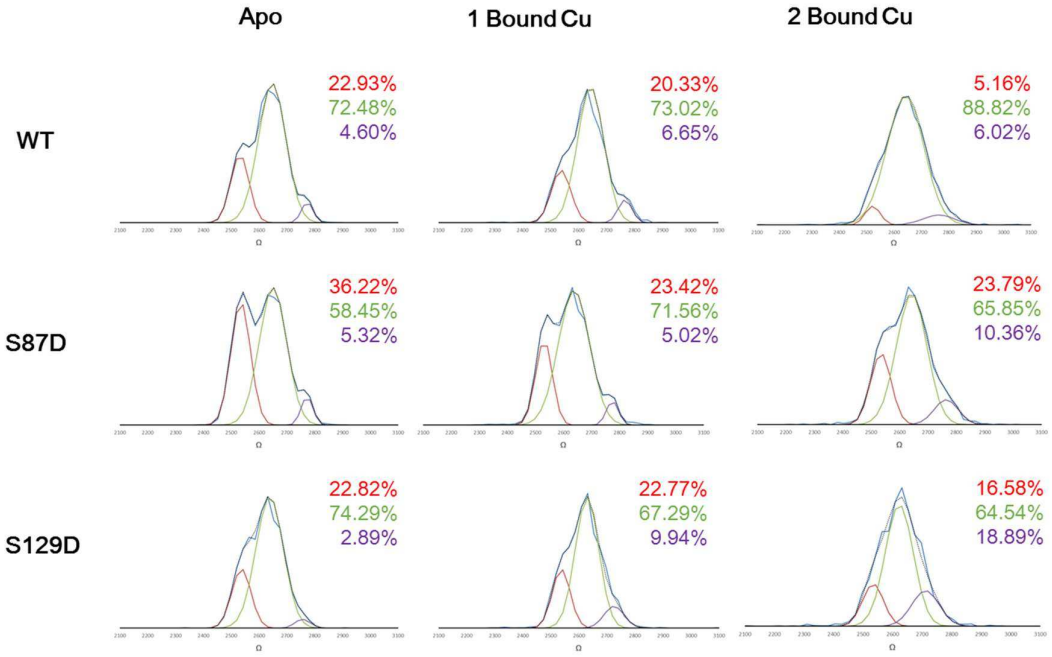

Appendix 3Q: +13 charge state ion of WT, S87D and S129D in the presence of equimolar $CuCl_2$ with Gaussian fitting applied to show relative proportions of conformations A, B & C.

Key Findings:

No notable alterations to WT or S129D. S87D shows slight increase in conformation B via a reduction in C.

Appendix 3R:

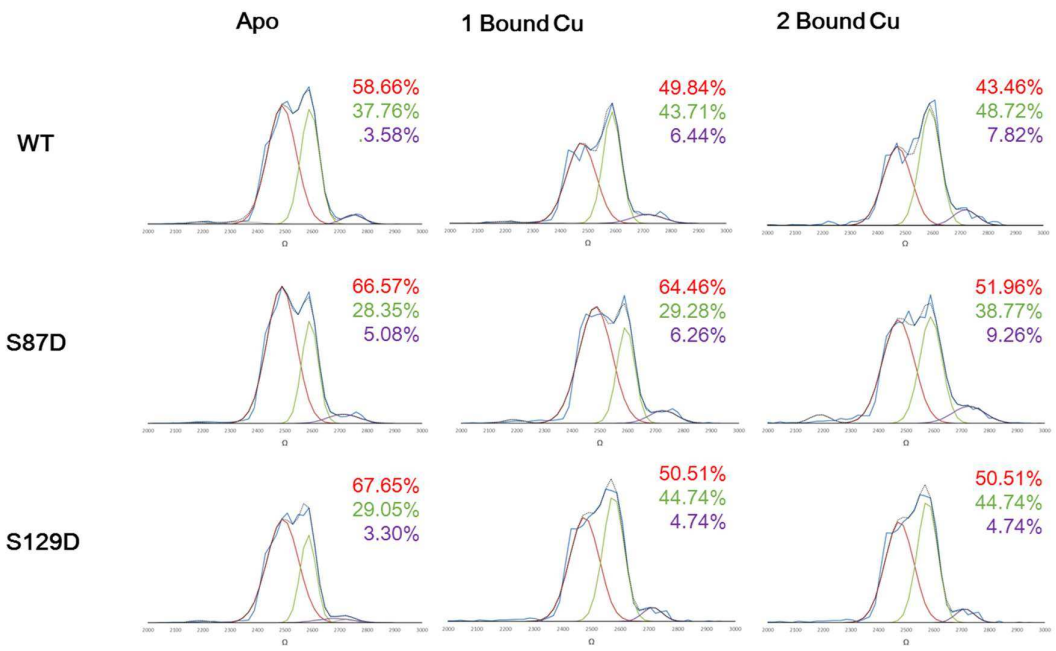

Appendix 3R: +12 charge state ion of WT, S87D and S129D in the presence of equimolar $CuCl_2$ with Gaussian fitting applied to show relative proportions of conformations A, B & C.

Key Findings:

No Notable alterations to S87D α-syn. WT & S129D show slight decrease in most compact conformation, conformation C.

Appendix 3S:

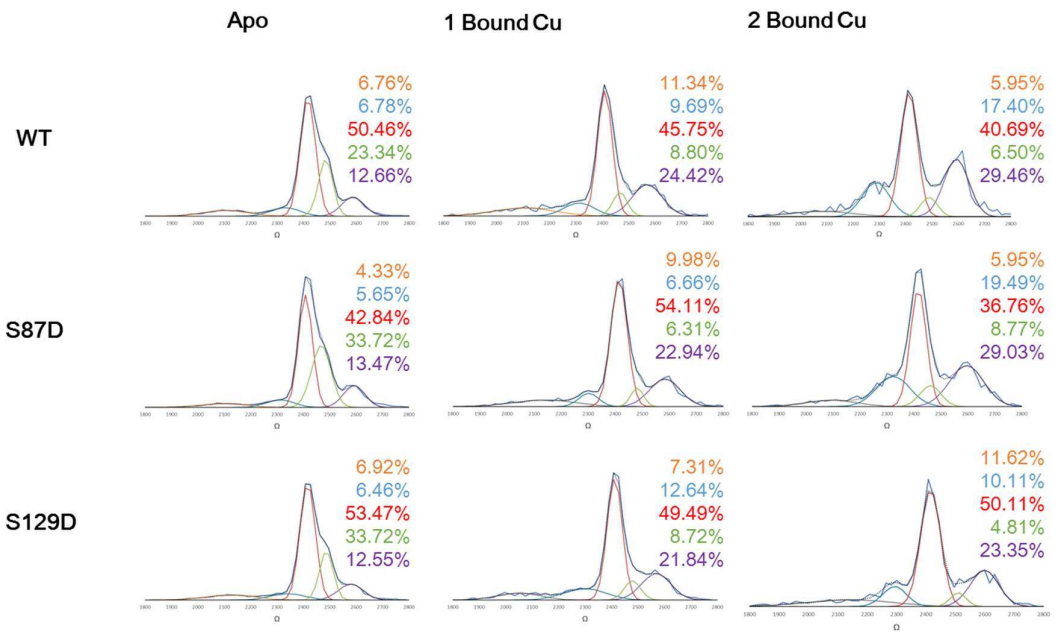

Appendix 3S: +11 charge state ion of WT, S87D and S129D in the presence of equimolar $CuCl_2$ with Gaussian fitting applied to show relative proportions of conformations A, B, C, D & E.

Key Findings:

All protein variants show an increase in conformations A & D via a reduction in conformations B & C.

Appendix 3T:

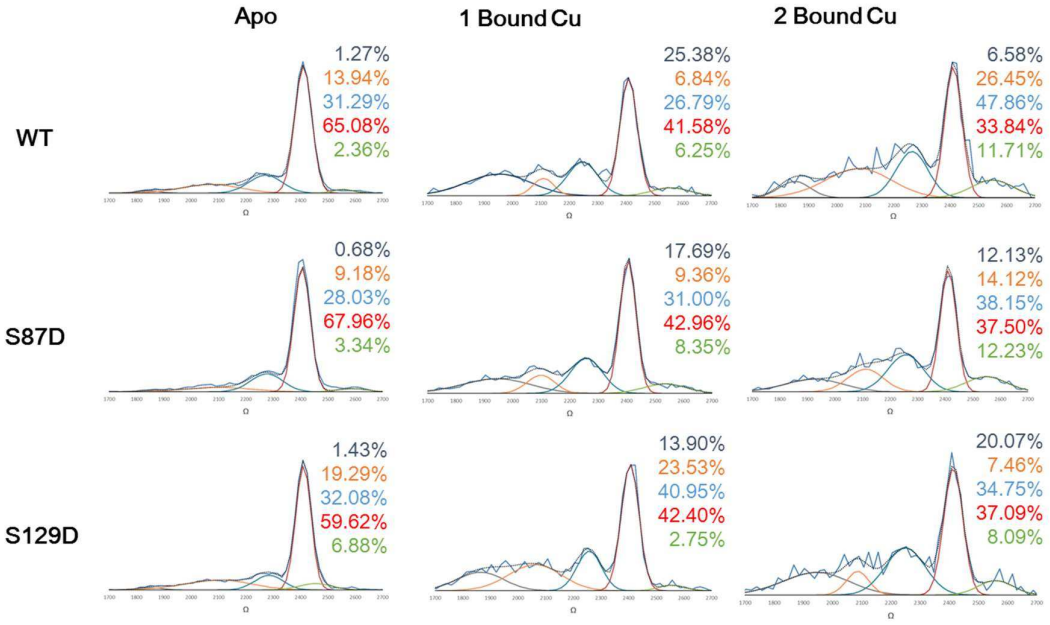

Appendix 3T: +10 charge state ion of WT, S87D and S129D in the presence of equimolar $CuCl_2$ with Gaussian fitting applied to show relative proportions of conformations B, C, D, E & F.

Key Findings:

All protein variants show an increase in conformations C, D, E, & F, via a reduction in conformation B.

Appendix 3U:

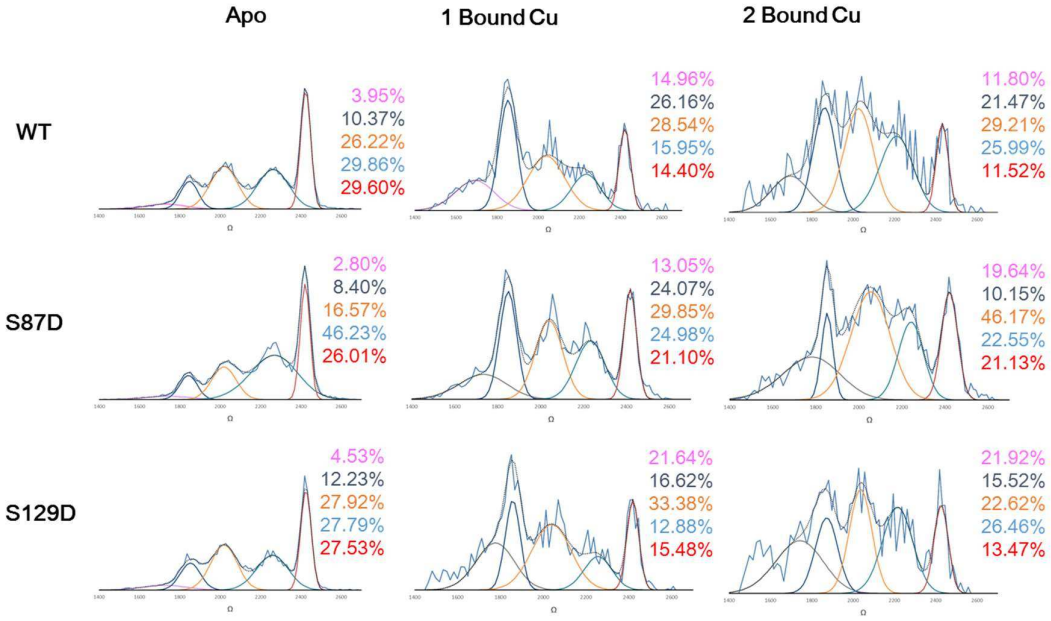

Appendix 3U: +9 charge state ion of WT, S87D and S129D in the presence of equimolar $CuCl_2$ with Gaussian fitting applied to show relative proportions of conformations C, D, E, F & G.

Key Findings:

All protein variants show an increase in conformations E, F & G via a reduction in C and/or D.

Appendix 3V:

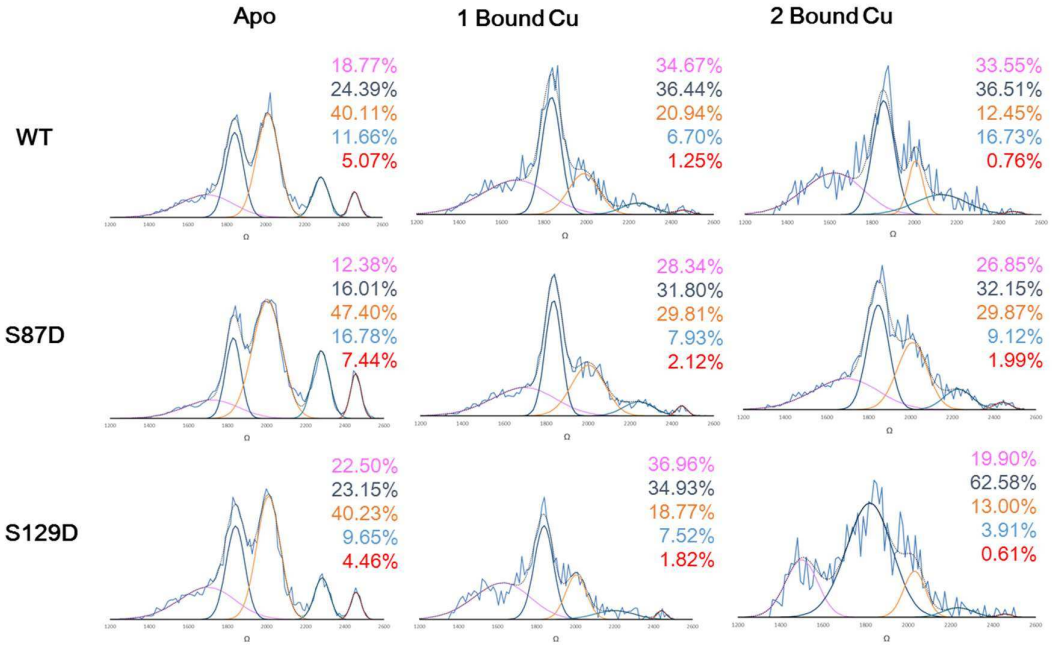

Appendix 3V: +3 charge state ion of WT, S87D and S129D in the presence of equimolar $CuCl_2$ with Gaussian fitting applied to show relative proportions of conformations C, D, E, F & G.

Key Findings:

All protein variants demonstrate an increase in conformations F & G via a reduction in conformations C, D & E.

Appendix 3W:

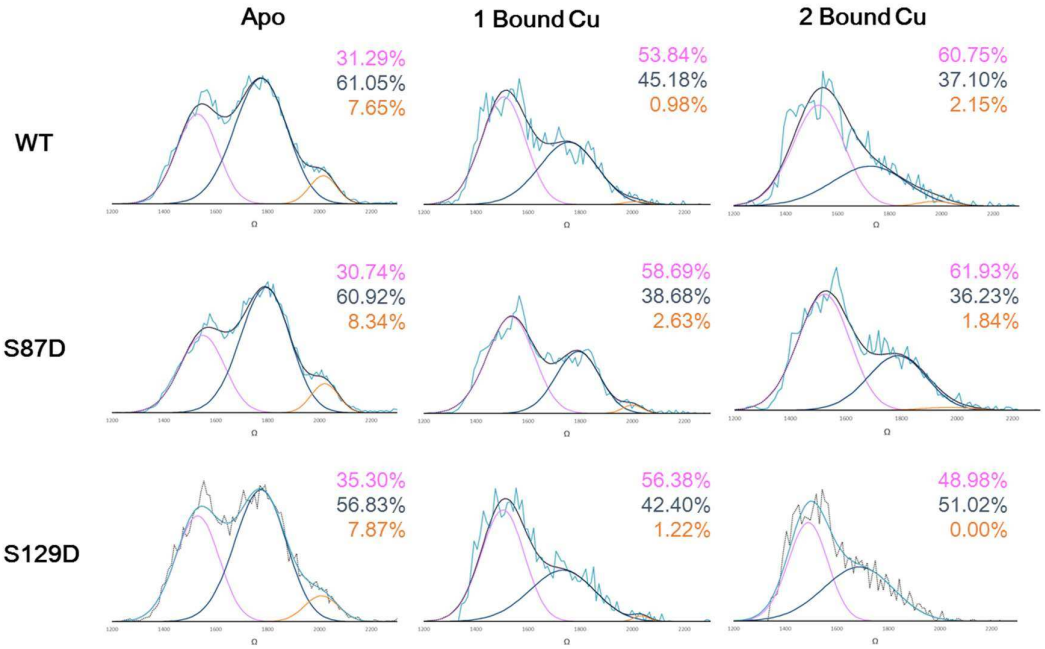

Appendix 3W: +7 charge state ion of WT, S87D and S129D in the presence of equimolar $CuCl_2$ with Gaussian fitting applied to show relative proportions of conformations E, F & G.

Key Findings:

All proteins show an increase in conformation G via a reduction in conformations F & E.

Appendix 3X:

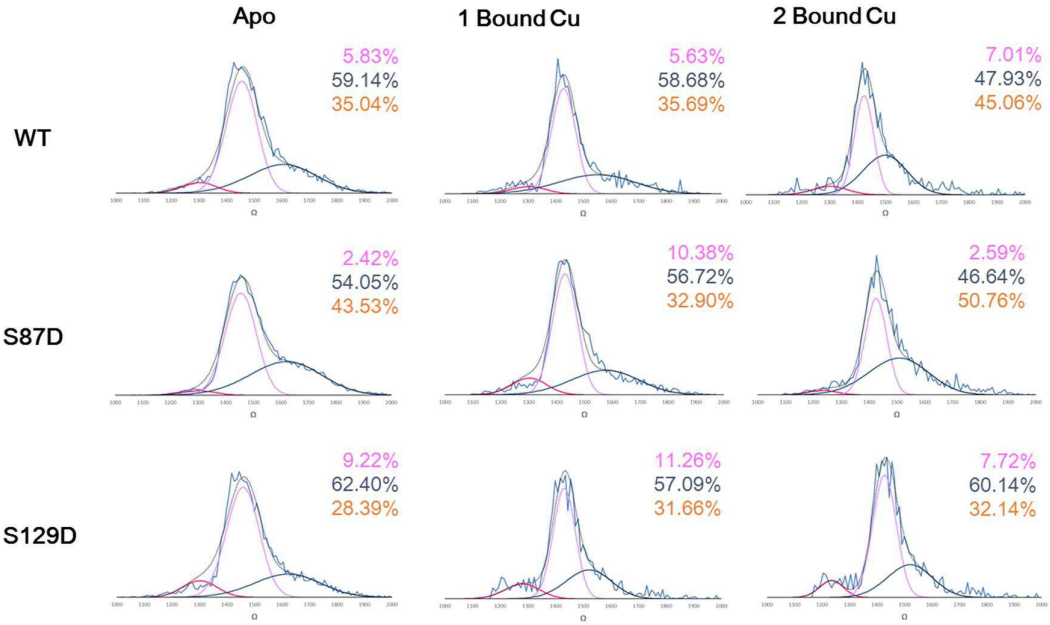

Appendix 3X: +6 charge state ion of WT, S87D and S129D in the presence of equimolar $CuCl_2$ with Gaussian fitting applied to show relative proportions of conformations F, G & H.

Key Findings:

No notable changes observed with any protein variants.

Appendix 4A:

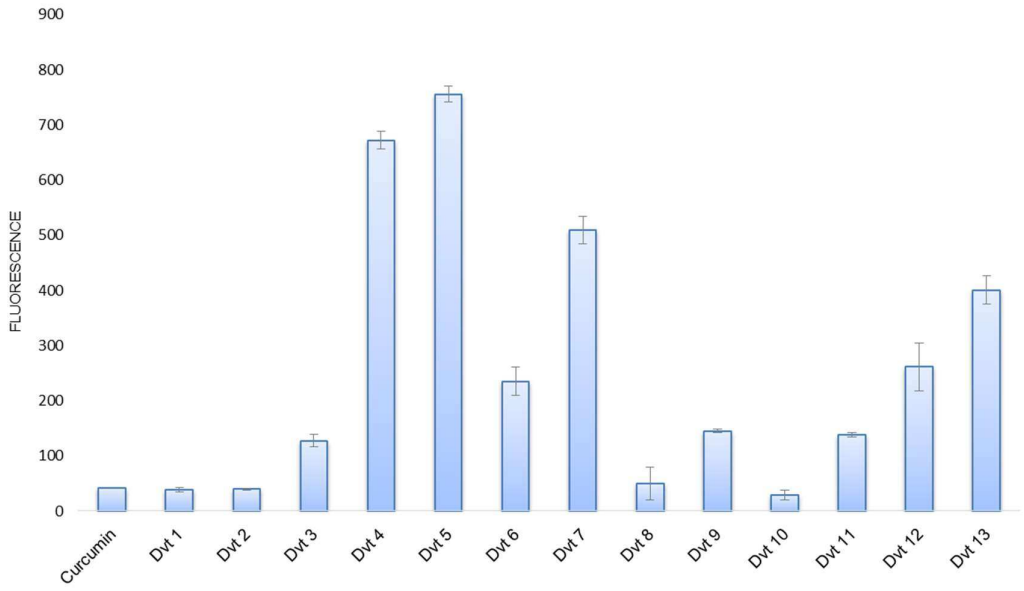

Appendix 4A: Initial ThT fluorescence readings of 70µM natural curcumin and the thiben derivatives, upon immediate addition to equimolar WT-tau in 50mM ammonium acetate containing 100µM thioflavin-T. n=3

Appendix 4B:

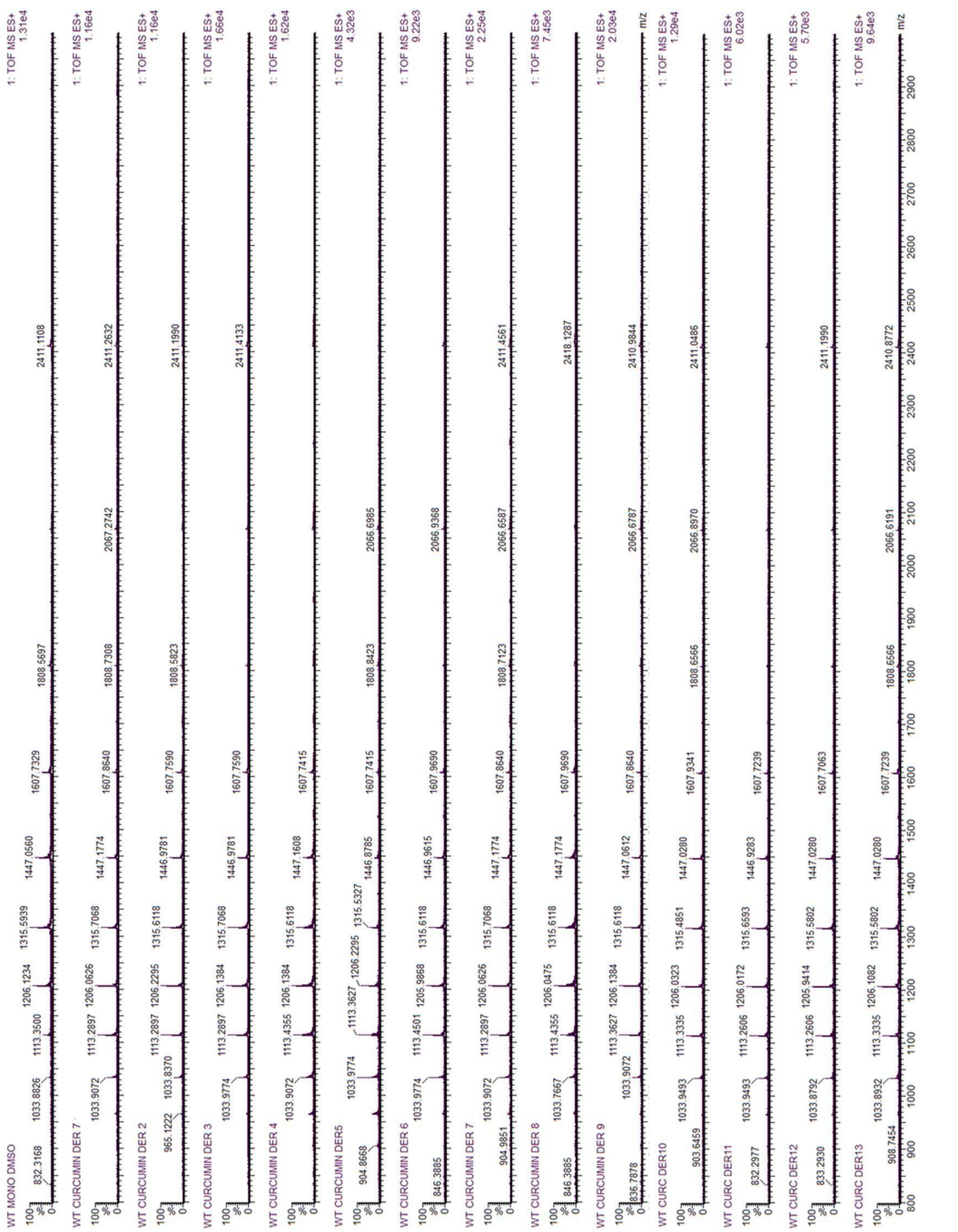

Appendix 4B: No binding was observed during ESI-MS experiments with any of the curcumin derivatives after immediate addition to equilibrated pyr.

Appendix 4C

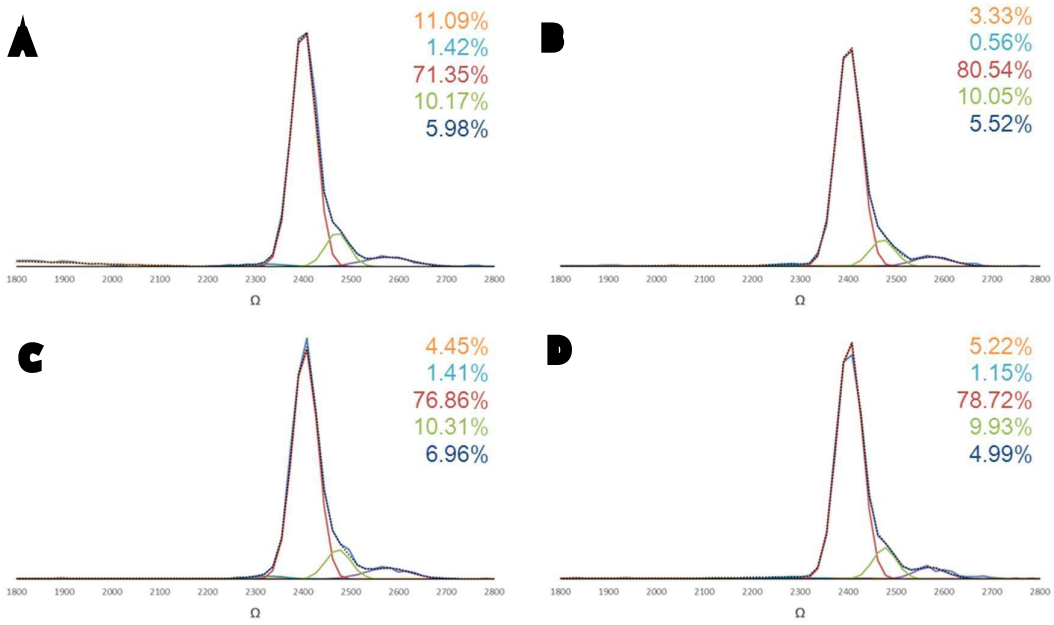

Appendix 4C: Gaussian fitting was performed on the +11 charge state ion of WT -syn after immediate addition of A) 1% DMSO, B) 1% DMSO + equimolar natural curcumin, C) 1% DMSO + equimolar derivative 5, and D) 1% DMSO + equimolar derivative 7. No alterations to the protein conformations were observed.

Appendix 4D:

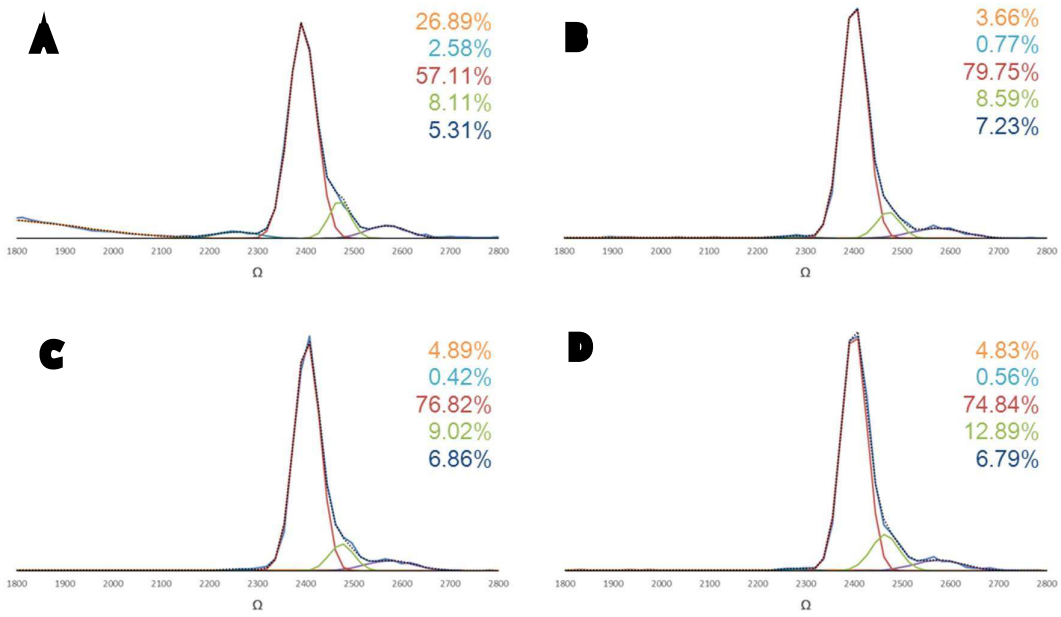

Appendix 4D: Gaussian fitting was performed on the +11 charge state ion of WT ataxin-3 after 48hours incubation with of A) 1% DMSO, B) 1% DMSO + equimolar natural curcumin, C) 1% DMSO + equimolar derivative 5, and D) 1% DMSO + equimolar derivative 7. Curcumin and the derivatives appear to reduce the proportion of the most compact conformation observed within this charge state ion.

Appendix 4E:

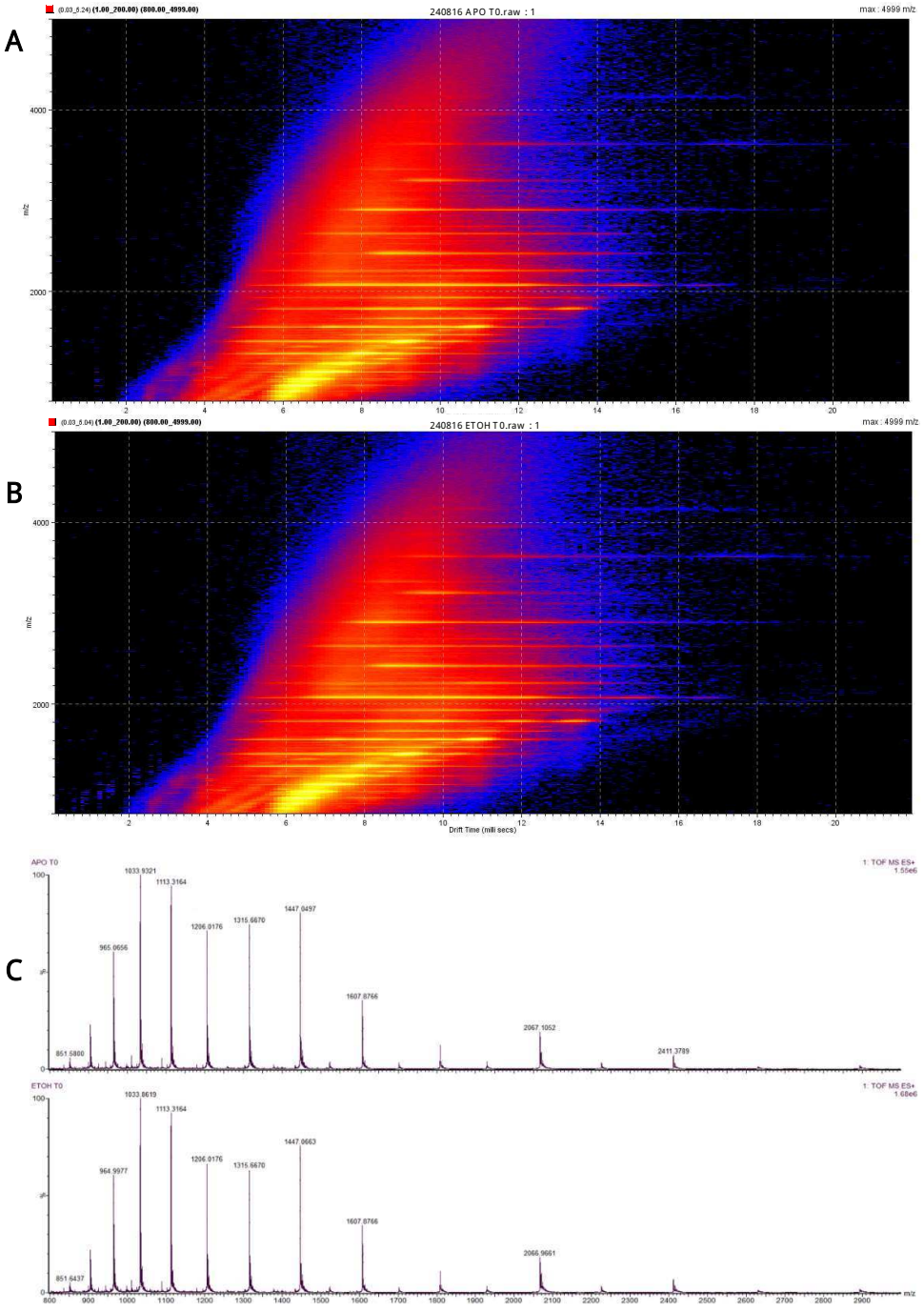

Appendix 4E: A) Drift scope plot of 70¾M ₸syn in 50mM ammonium acetate acquired by ESI-IMS-MS, B) 70¾M ₸syn + 10% EtOH, and C) Corresponding mass spectra of 70¾M ₸syn +/- 10% EtOH.

Appendix 4F:

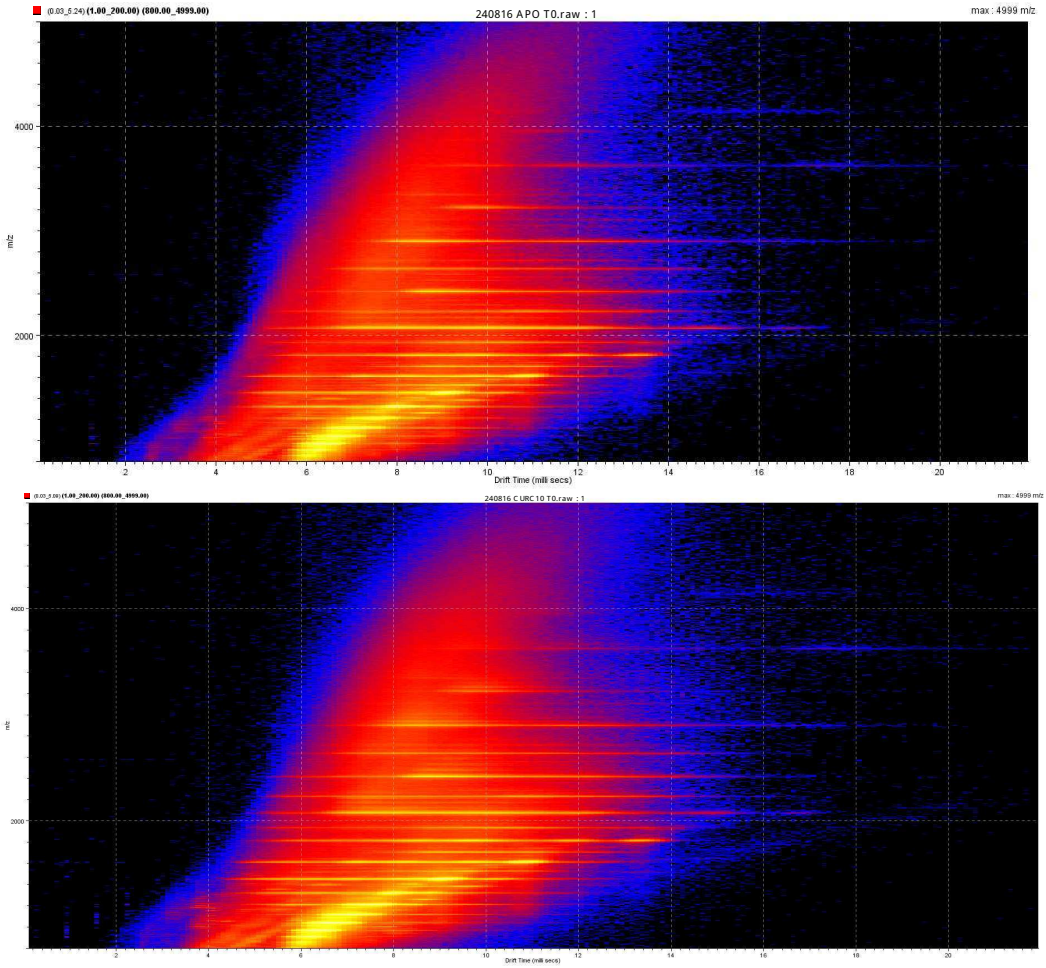

Appendix 4F: Upon immediate addition of 10¾M curcumin to 70¾M T-syn, a reduction in oligomeric species is observed, akin to that seen with addition of equimolar curcumin.

Appendix 4G:

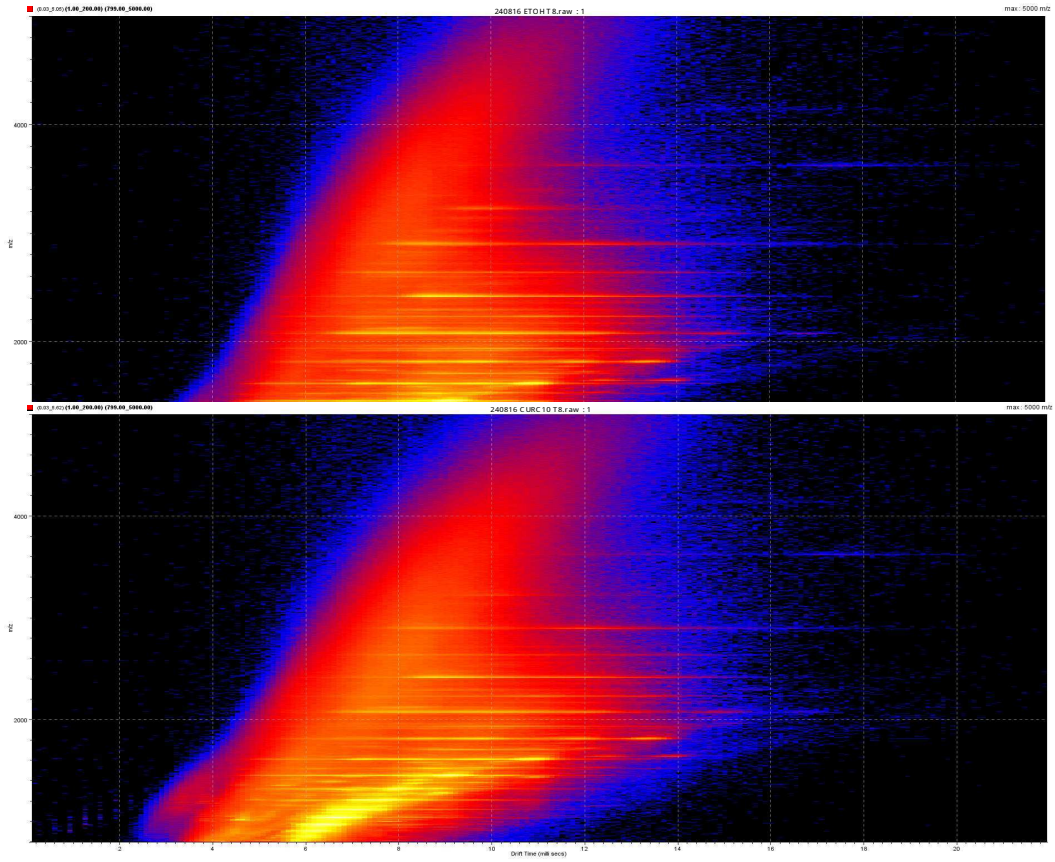

Appendix 4G: After 8hrs incubation of 10¾M curcumin with 70¾M T-syn, a further reduction in oligomeric species is observed, akin to that seen with addition of equimolar curcumin.

Appendix 4H:

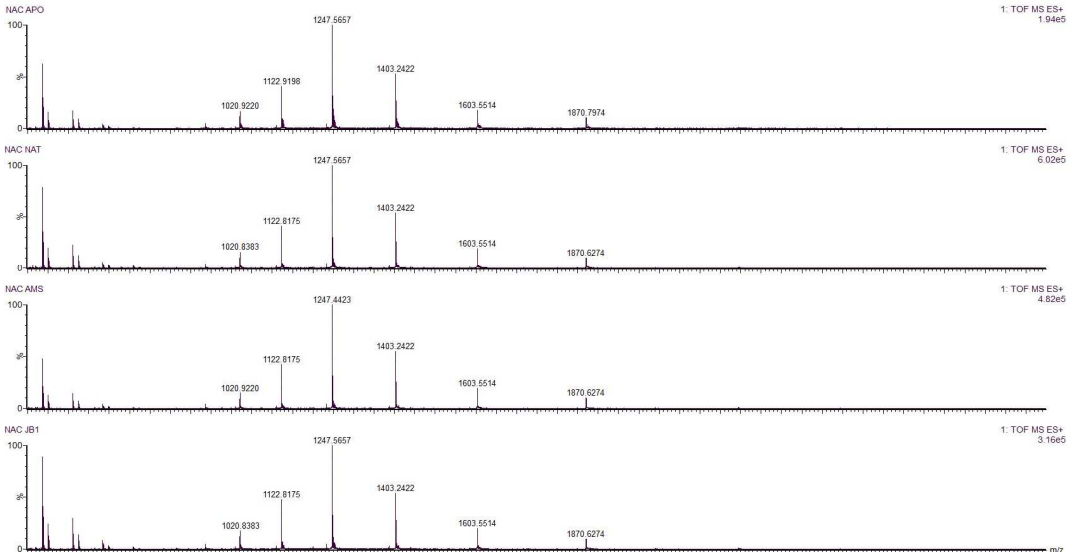

Appendix 4H: None of the curcumin derivatives investigated were observed to bind to ᵀsyn with the NAC region removed.

Appendix 5A:

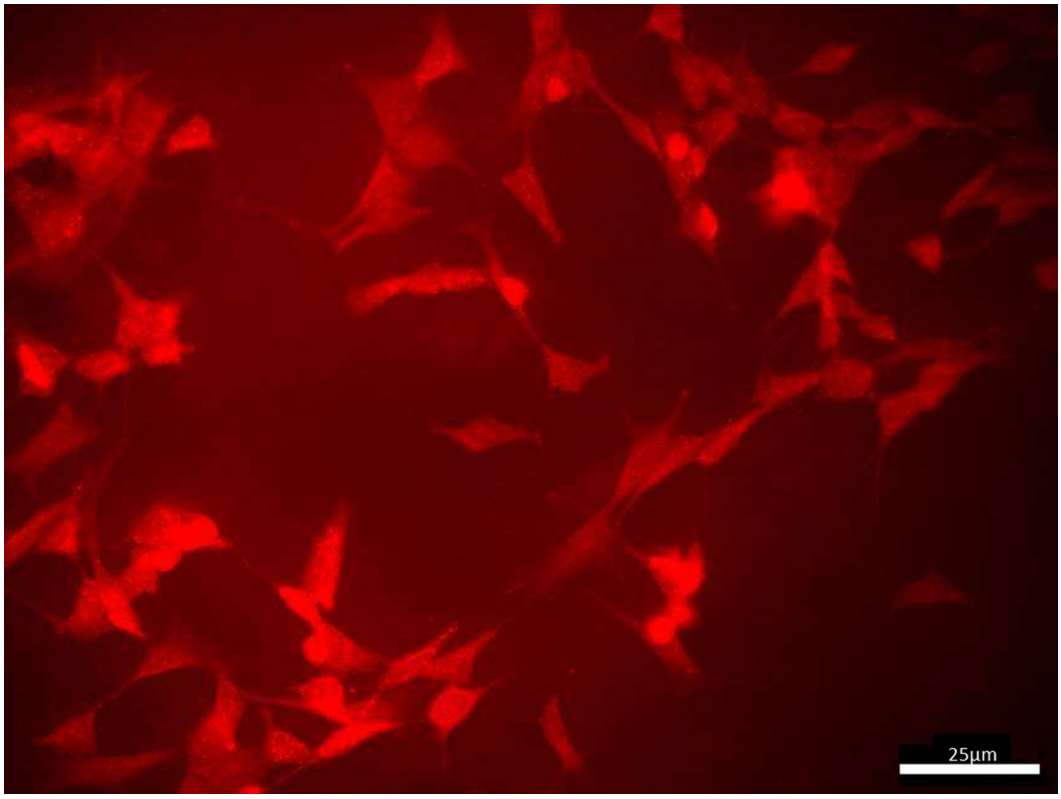

Appendix 5A: Example ICC image of SHSY5Y cells utilised for grading of aggregate counts in chapter 5. Untreated cells stained for Syn211.

Appendix 5B:

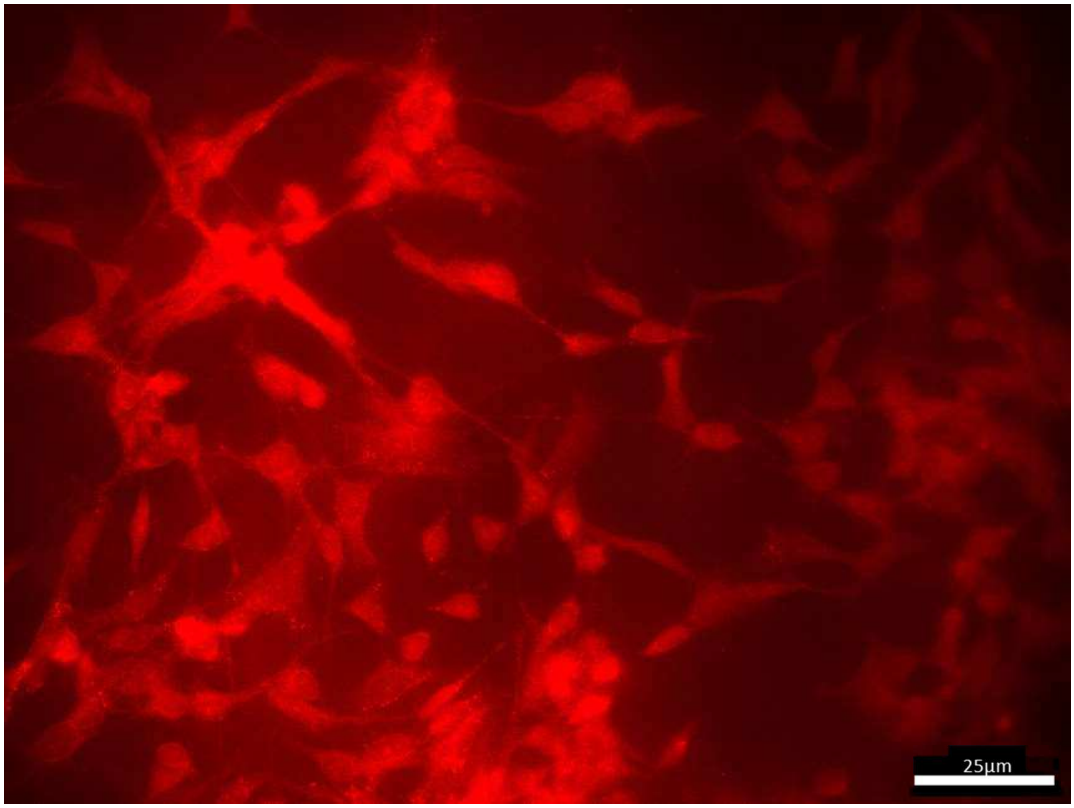

Appendix 5B: Example ICC image utilised for grading of aggregate counts in chapter 5. 100µM $CuCl_2$ treatment of SHSY5Y cells stained for Syn211.

Appendix 5C:

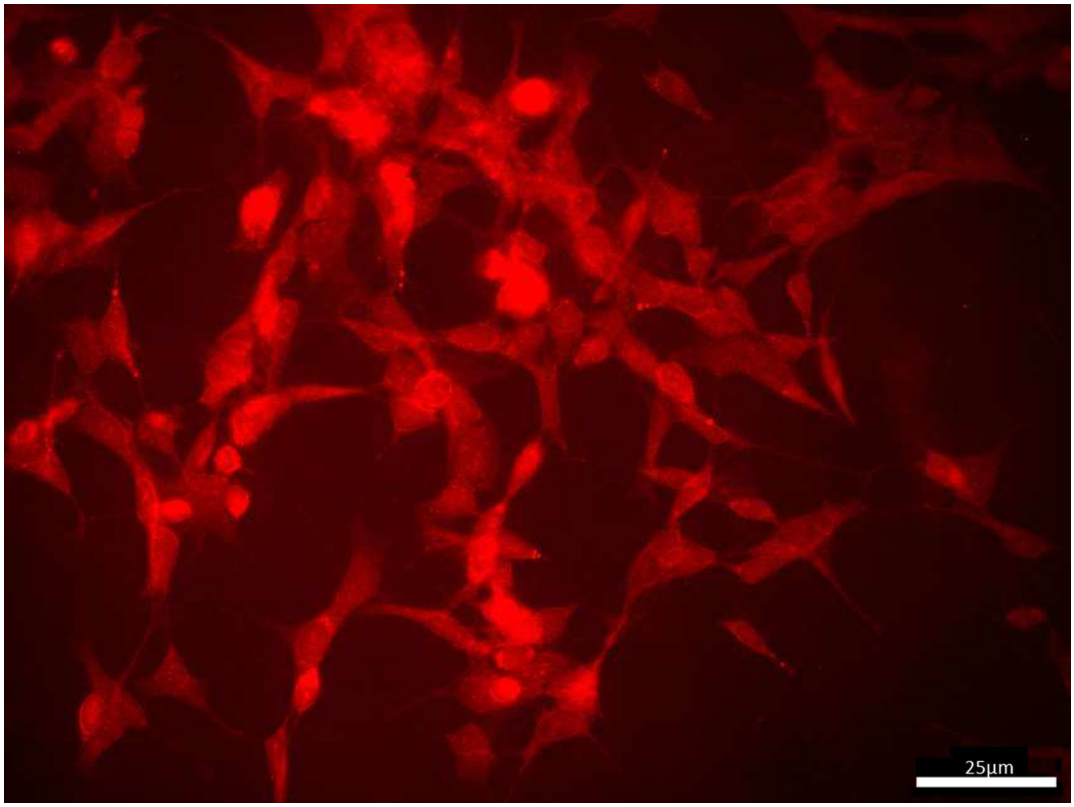

Appendix 5C: Example ICC image of SHSY5Y cells utilised for grading of aggregate counts in chapter 5. Treatment with 300µM $CoCl_2$ and stained for Syn211.

Appendix 5D:

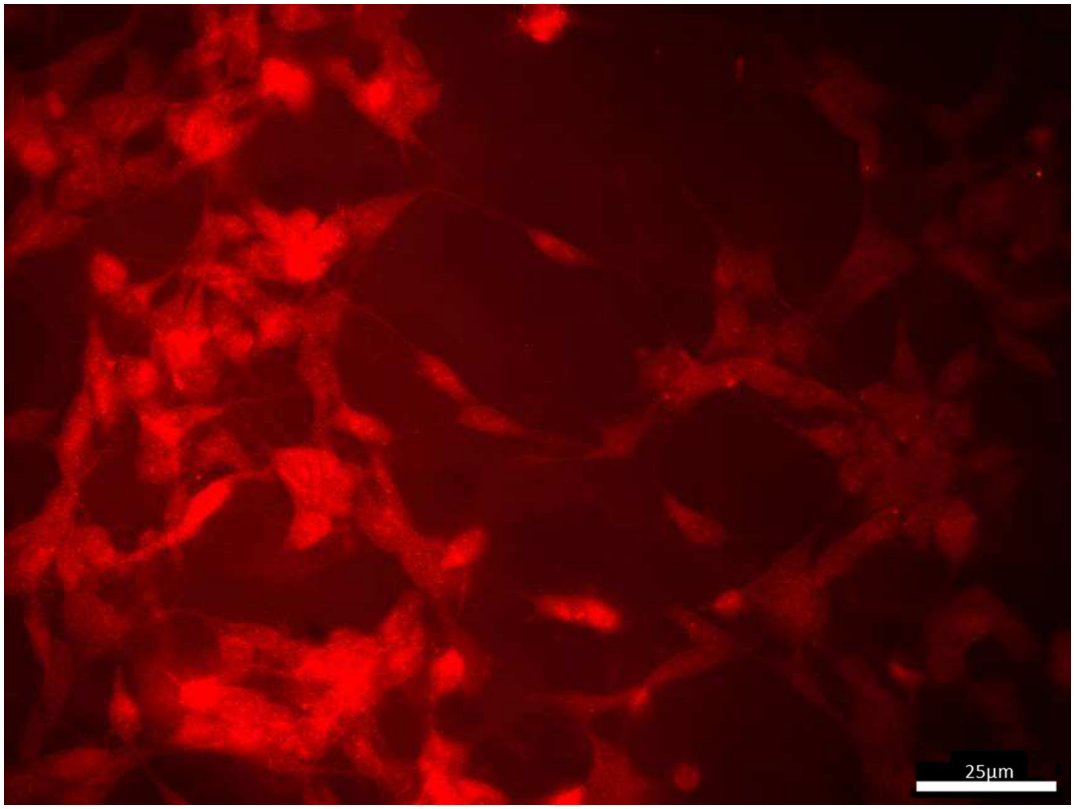

Appendix 5D: Example ICC image of SHSY5Y cells utilised for grading of aggregate counts in chapter 5. Cells treated with 500µM $CuCl_2$ and stained for Syn211.

Appendix 5E:

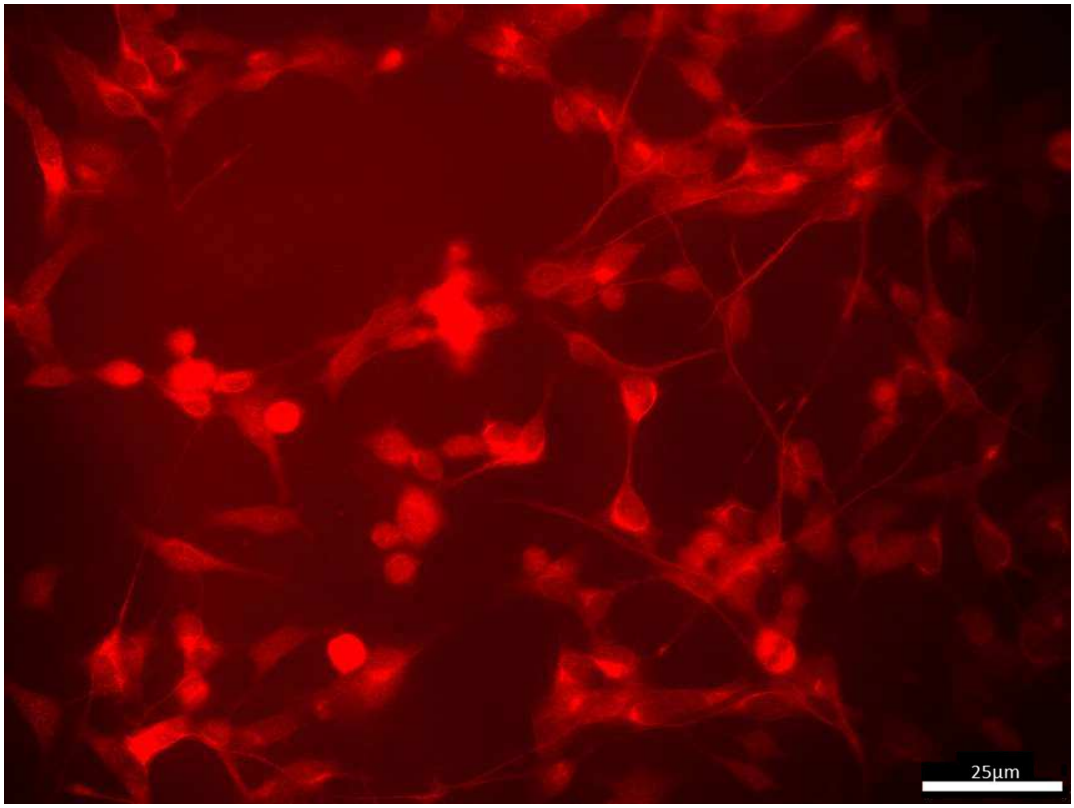

Appendix 5E: Example ICC image of SHSY5Y cells utilised for grading of aggregate counts in chapter 5. Untreated cells stained for Phos129.

Appendix 5F:

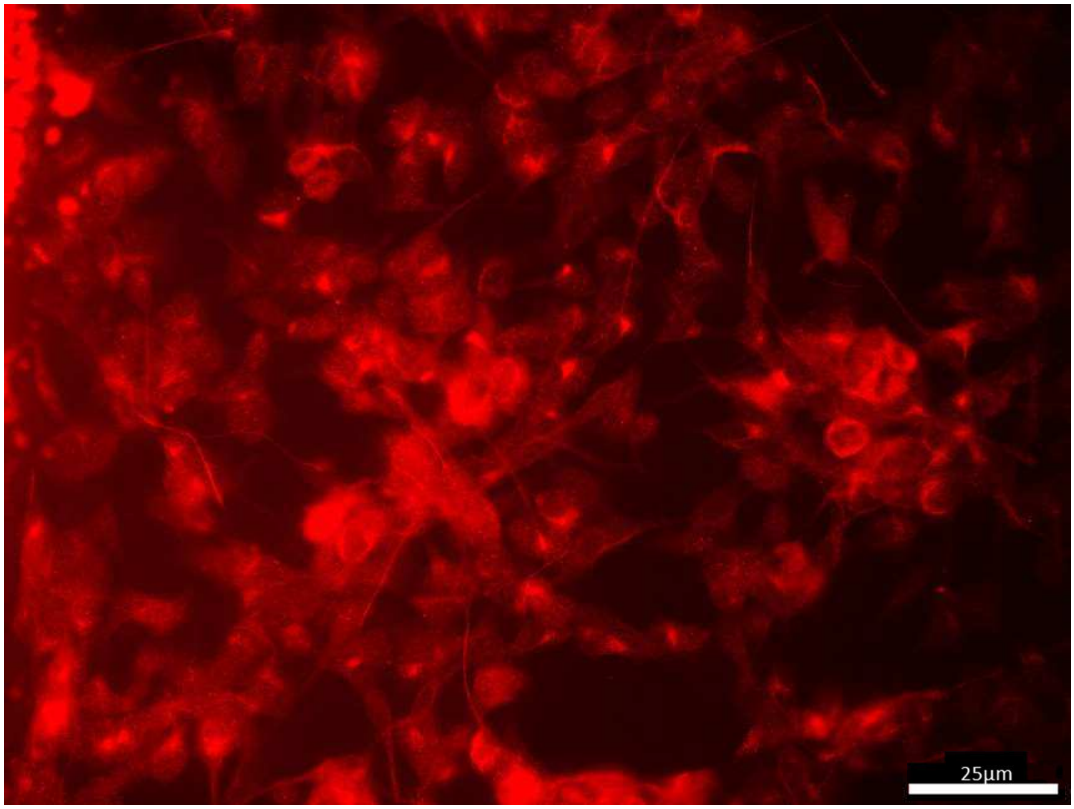

Appendix 5F: Example ICC image of SHSY5Y cells utilised for grading of aggregate counts in chapter 5. Cells treated with 100µM $CaCl_2$ stained for Phos129.

Appendix 5G:

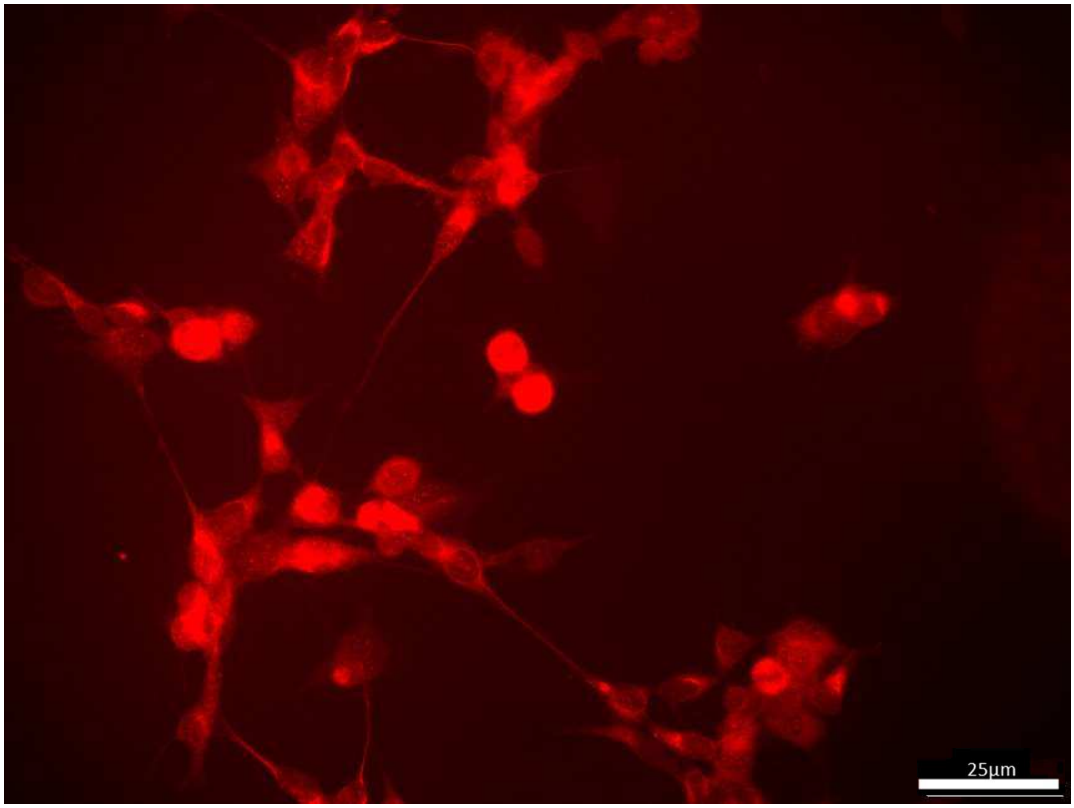

Appendix 5G: Example ICC image of SHSY5Y cells utilised for grading of aggregate counts in chapter 5. Cells were treated with 300µM $CuCl_2$ and stained for Phos129.

Appendix 5H:

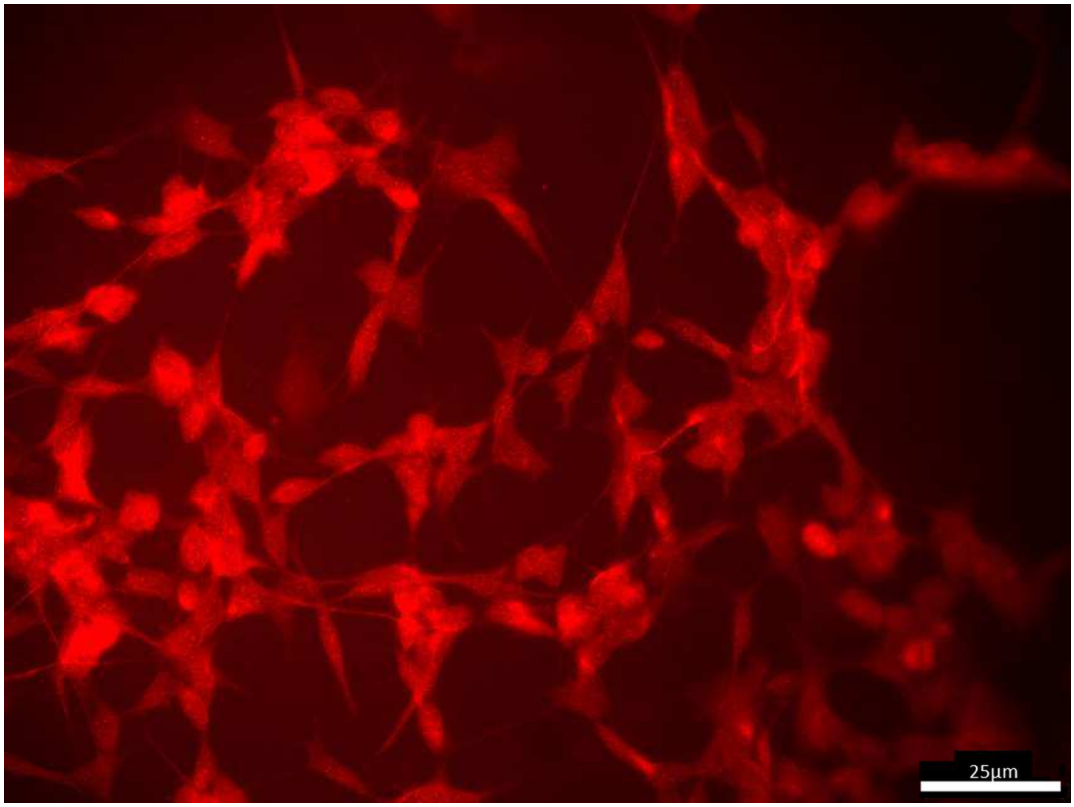

Appendix 5H: Example ICC image of SHSY5Y cells utilised for grading of aggregate counts in chapter 5. Cells were treated with 500µM $CuCl_2$ and stained for Pless129.

Appendix 5I:

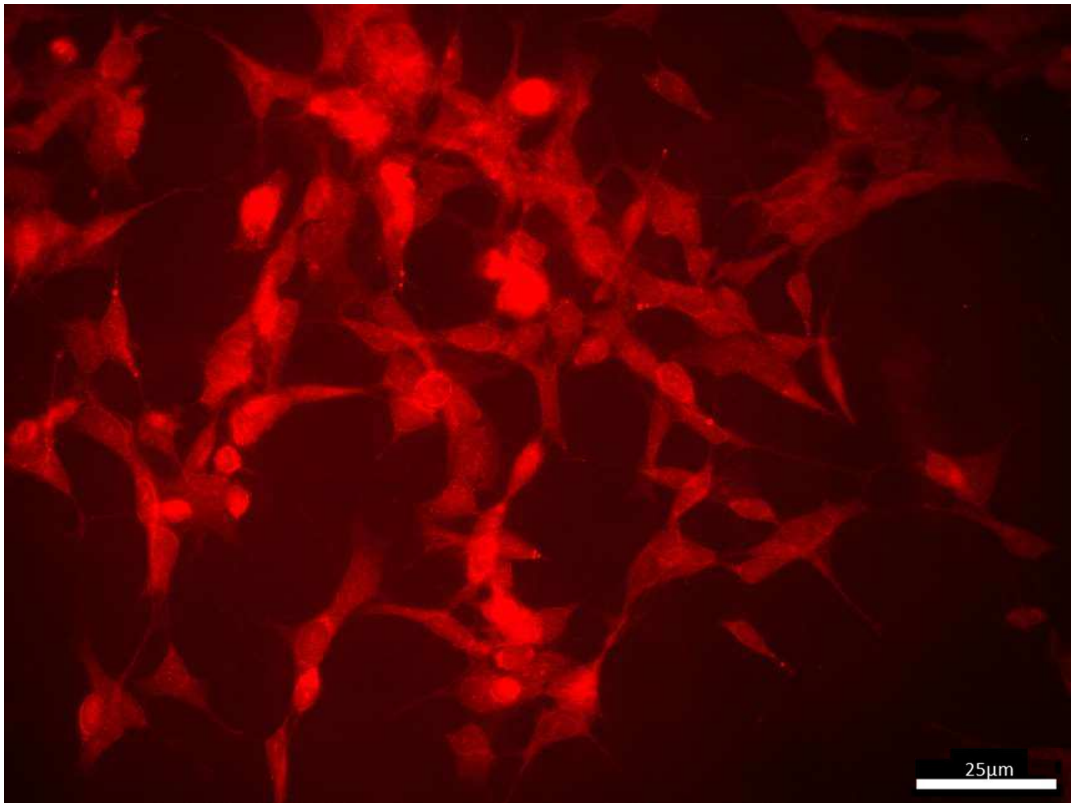

Appendix 5I: Example ICC image of SHSY5Y cells utilised for grading of aggregate counts in chapter 5. Cells were treated with 300µM $CuCl_2$ and stained for Syn211.

Appendix 5J :

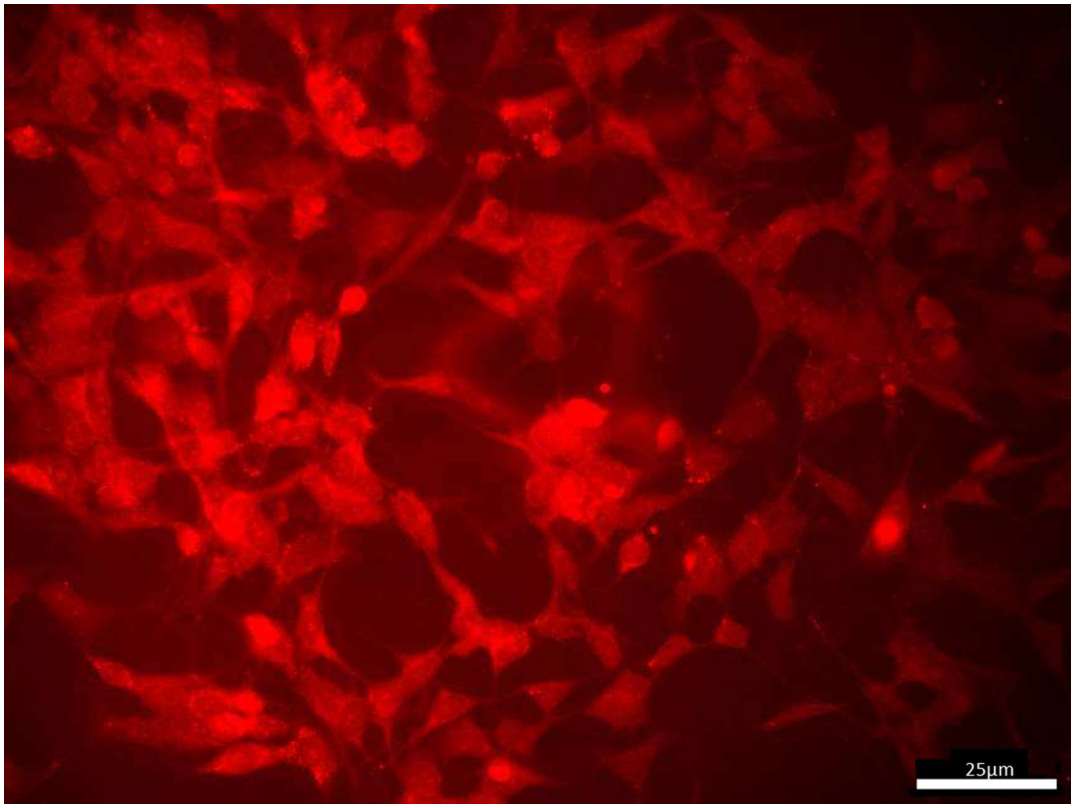

Appendix 5J: Example ICC image of SHSY5Y cells utilised for grading of aggregate counts in chapter 5. Cells were treated with 300µM $CaCl_2$ + 40µM curcumin and then stained for Syn211.

Appendix 5K:

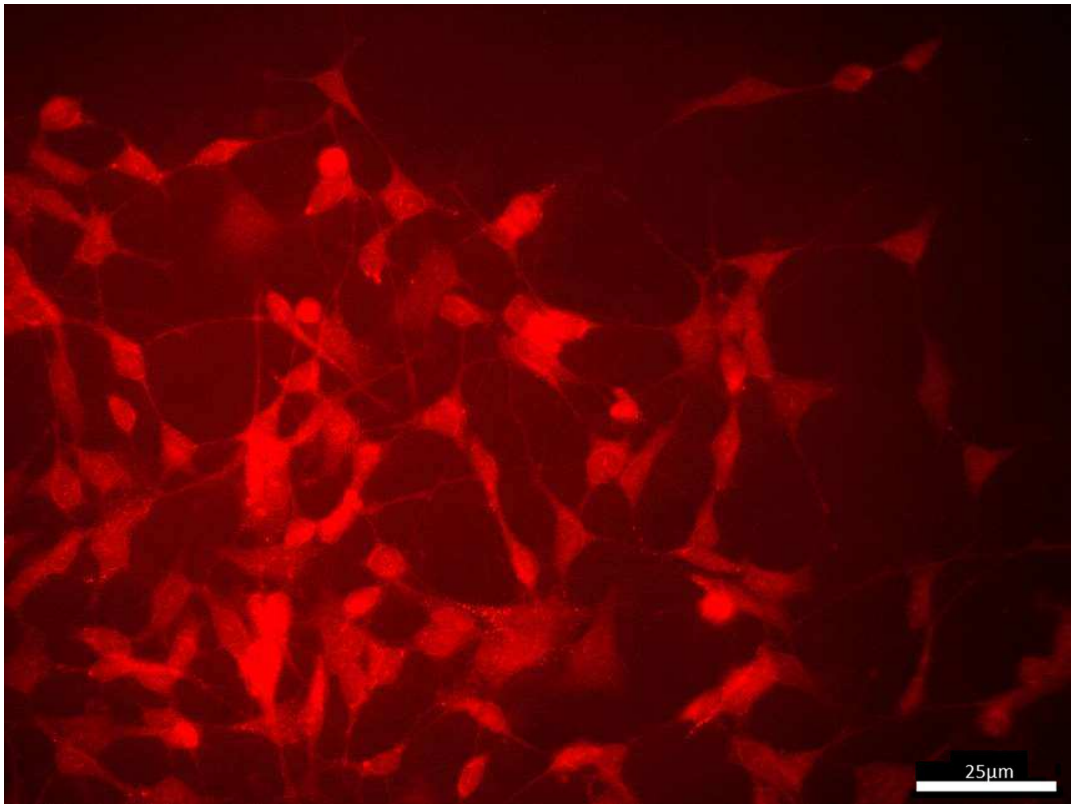

Appendix 5K: Example ICC image of SHSY5Y cells utilised for grading of aggregate counts in chapter 5. Cells were treated with 300µM $CaCl_2$ + 7µM curcumin and stained for Syn211.

Appendix 5L:

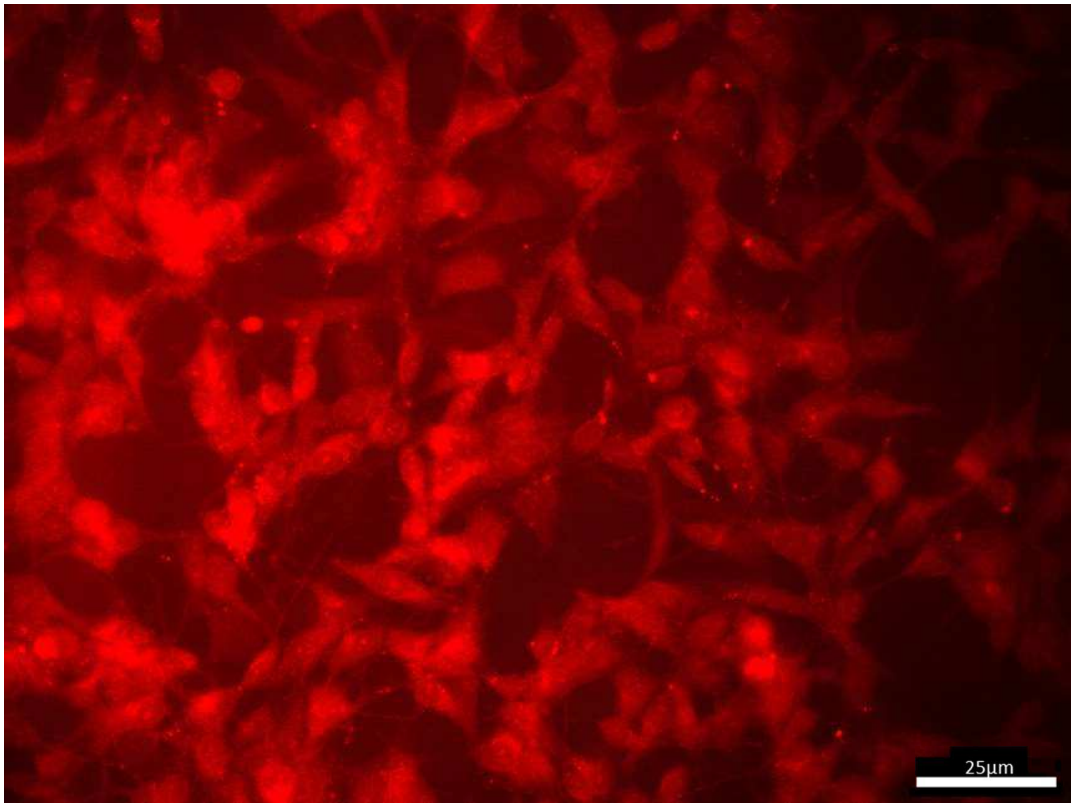

Appendix 5L: Example ICC image of SH5YSY cells utilised for grading of aggregate counts in chapter 5. Cells were treated with 300µM $CuCl_2$ + 10µM curcumin and stained for Syn211.

Appendix 6:

Publications

Mason RJ, Paskins AR, Dalton CF & Smith DP (2016) "Copper binding and subsequent aggregation of alpha-synuclein is modulated by N-terminal acetylation and is ablated by the H50Q missense mutation." *Biochemistry*. 55(34):4737-41. doi: 10.1021/acs.biochem.6b00708

Publication is included at the end of the appendices.

Appendix 7:

Conference Dissemination

13-15/09/2016: **BMSS Annual Meeting** (Eastbourne, UK) - Oral

17/12/2015: **BMRC/MERI Christmas Poster Event** (Sheffield, UK) - Poster

22/09/2015: **Sheffield Glia Symposium** (Sheffield, UK)

7-8/07/2015: **BMSS IM-MS SIG Annual Meeting** (Liverpool, UK)

27-30/06/2015: **27th International Symposium on Cerebral Blood Flow, Metabolism and Function / 12th International Conference on Quantification of Brain Function with PET** (Vancouver, Canada) - Poster

Paskins *et al.*, (2016) 唀vestigating metal binding and the resulting conformational changes and aggregation of monomeric wild-type alpha-synuclein and a phosphorylation mimic昀*ournal of Cerebral Blood Flow and Metabolism.* 36:594-595

11/12/2014: **BMRC/MERI Christmas Poster Event** (Sheffield, UK) - Poster

24-29/08/2014: **IMSC** (Geneva, Switzerland) - Poster

01-02/07/2014: **BMSS IM-MS SIG Annual Meeting** (Manchester, UK)

31/03/2014 - 02/04/2014: **BMSS Annual Meeting** (Manchester, UK) - Poster

17/12/2013: **BMRC/MERI Christmas Poster Event** (Sheffield, UK) - Poster

Appendix 8:

Teaching and Public Engagement

Undergraduate Laboratory Demonstrating –Oct 2014 –April 2017 (Sheffield Hallam University)

Work experience Supervision - July 2013, 2014 & 2015 (Sheffield Hallam University)

Science and Engineering Week Event - March 2014, 2015 & 2016 (Sheffield Hallam University)

FameLab –February 2017 (Sheffield)

PubHD –March 2017 (Sheffield)

The Big Bang Yorkshire - June 2016 (Doncaster)

230th Gleadless Scouts Science Fair - April 2016 (Sheffield)

Biotechnology YES Competition - October 2015 (GSK, Stevenage)

3 Minute Thesis Competition - June 2015 (Sheffield Hallam University)

Multidisciplinary Research Cafǔ –March 2015 (Sheffield Hallam University)

Appendix 9:

Training Courses

09/07/2016: **Mass Spectrometry Imaging Symposium** (Sheffield, UK)

18/04/2016: **Royal Society of Biology Science Communication Workshop** (London, UK)

28/04/2015 - 01/05/2015: **Common Purpose Leadership Award** (Sheffield, UK)

01-02/07/2014: **BMSS Ion Mobility-Mass Spectrometry Special Interest Group Training Course** (Manchester, UK)

31/03/2014 - 02/04/2014: **BMSS Introduction to Mass Spectrometry Course** (Manchester, UK)